An *In-vitro* Medium Term Simulation of Hip Hemiarthroplasty

Simon D. Taylor (MEng, Hons)

Submitted in accordance with the requirements for the degree of

Doctor of Philosophy.

The University of Leeds

School of Mechanical Engineering

April 2012

The candidate confirms that the work submitted is his/her own, except where work which has formed part of jointly-authored publications has been included. The contribution of the candidate and the other authors to this work has been explicitly indicated below. The candidate confirms that appropriate credit has been given within the thesis where reference has been made to the work of others.

Chapter 3 was published as a jointly-authored journal publication:

S. Taylor, E. Tsiridis, E. Ingham, Z. Jin, J. Fisher and S. Williams. Comparison of human and animal femoral head chondral properties and geometries. *Proceedings of the Institution of Mechanical Engineers, Part H: Journal of Engineering in Medicine*. 2012, 226:55-62

Mr. Tsiridis supplied the femoral heads and all the authors reviewed the paper before submitting. All the work in this paper and the current thesis was performed by Simon David Taylor.

Acknowledgements

"In theory, there is no difference between theory and practice, but in practice there is."
--Lawrence Peter "Yogi" Berra

This PhD was funded by EPSRC case studentship and in kind support from DePuy International Ltd. I was supervised by Prof. Zhongmin Jin, Prof. Eileen Ingham, Prof. John Fisher and Dr. Sophie Williams (primary supervisor).

A PhD may be an individual project, but you are not alone whilst conducting it. If there is one piece of advice I can give to new PhD students is that the people around you; the colleagues in your group and also in other groups all have valuable knowledge and experiences. So use that to not only help you during difficult times (which I can almost ensure you will be, many times throughout your PhD), but also to push your research further than you could do by yourself. There are many people I would like to thank. Some for helping me through difficult times; but others that provided the help and advice I sorely needed to complete a truly multidisciplinary PhD project.

First and foremost, I would like to thank my supervisor Dr. Sophie Williams. You have not only been a first class supervisor but a brilliant friend. In times of PhD trouble you have always come through for me. I would also like to thank my other supervisors, Prof. John Fisher, Prof. Eileen Ingham and Prof. Zhongmin Jin who have provided fantastic support. To Phil Wood, Irvin Homan, Lee Wetherill, Amisha Desai and Keith Dyer who without their technical support, this PhD project simply couldn't work and also for fixing all the machines that I have broken! Thank you to Dr. Joanne Ingham, whom I have really enjoyed working with, trying to dissect acetabulae aseptically! I couldn't have done any of my PhD without your help! Thank you to Miss Fermor who is really down with the trumpets. You have not only made histology fun (which is really hard to do), but you have also been a truly great friend.

Thank you to all my other friends from Micro (sorry, Garstang) for taking me in like one of your own. My friends here in Mech Eng, specifically Adam, Stew and Niki who I have enjoyed spending the last 7-8 years with (even though I severely doubt that feeling will be reciprocated!). Thank you to Dr. Sainath Pawaskar for allowing me to ask for FE help over and over and over again! Thank you to the entire room 442c for putting up with my endless chatting, especially Phil, Raman, Mazen and Dawn. I sincerely like to thank my parents and grandparents who have been a cornerstone throughout my life and have pushed me to achieve greater things. My sister, Nicole, who I have always been very proud of, even though I don't say it nearly enough. And last but not least, my absolutely gorgeous wife Rachel who deserves a medal just for vowing to be with me until death do us part!

Dedicated to my Grandpa Rabee

That £50 really helped.

Abstract

Hemiarthroplasty of the hip is a common procedure to treat fracture of the neck of femur, which commonly affects the elderly. The treatment involves replacing the femoral head with a metallic component, leaving it to articulate against the cartilage of the acetabulum. This can commonly lead to rapid cartilage erosion. There have been several studies that examined the tribology of cartilage under a variety of contact mechanics conditions, the majority of these studies use simple geometrical models and none of the current *in-vitro* studies have examined cartilage tribology for longer than a two hour period. This is a relatively short period which is a limitation with regards to drawing conclusions that might affect clinical practice. Therefore, the overall aim of this thesis was to investigate the *in-vitro* tribological effect of varying clearance of hip hemiarthroplasty over a four day period. This involved developing a medium term *in-vitro* simulation system, which needed to be validated.

There were five areas that required development and validation for the proposed *in-vitro* tribological simulation system. Firstly, the animal acetabulum that was used to represent human tissue needed to be chosen. This was performed by comparing the mechanical and geometrical properties of the hip joint and femoral head cartilage between human and a variety of animals. Secondly, the lubricant which was based on previous literature was validated in terms of maintaining sterility, preventing tissue degradation and its ability to mimic synovial fluid. Through performing this validation, it was found that contamination significantly decreases friction coefficient and hence, needed to be eliminated. Therefore, the third area of validation was the aseptic dissection technique. The fourth area that needed to be addressed was to design, develop and validate the “vessel” that will house the *in-vitro* simulation system. The final area of validation was the contact mechanics of the hemiarthroplasty simulation system, which needed to be similar to that seen *in-vivo*.

During hemiarthroplasty surgery, the size of the metallic femoral head is chosen with the aim to best match the geometry of the natural femoral head. The diameter of the natural femoral head is commonly measured using either callipers or circular templates. However, 2 mm diameter sizing increments are commonly used in clinical practice; which could potentially lead to increasing the radial clearance between the femoral head and acetabulum by 1 mm. Therefore, the effect of mismatching the femoral head geometry with the acetabulum by 1 mm radial clearance was investigated tribologically in the medium term using the validated system.

It was found that by mismatching the hip hemiarthroplasty geometry by an extra 1 mm radial clearance; friction coefficient, frictional shear stress and bone exposure significantly increased. There was no significant difference in cartilage thickness. However, through histological assessment, the cartilage exhibited large undulations with fractures to the cartilage surface. Biochemical assessment also showed that there was a significant decrease in glycosaminoglycan concentration compared to fresh cartilage when the geometries were mismatched.

In conclusion, increasing the radial clearance between the femoral head and acetabulum by an extra 1 mm could have a significant effect on the longevity of the hemiarthroplasty implant. This could have clinical implications due to 2 mm diameter sizing increments that are commonly used in clinical practice. Therefore, tighter control over sizing the correct hemiarthroplasty implant must be performed to improve clinical outcomes. It was also found by allowing the cartilage to recover, the friction coefficient and frictional shear stress significantly decreased, which could have a major factor in the wear. Therefore, for future longer term *in-vitro* tribological studies, the effect of cartilage recovery must be taken into consideration.

Contents

Figures

Tables

Chapter 1: Literature Review

1.1 Introduction

Femoral neck fractures are extremely common with approximately 70,000 reported cases in the UK in 2009/2010. This is a rise of nearly 20,000 cases since 1999/2000 (The Information Centre for Health and Social Care, 2011). This has large economic implications with annual costs of £380 million on pharmaceutical drugs, consultations and surgery in Britain alone (NHS Institute for Innovation and Improvement, 2011). For younger, more active patients, total hip replacements are commonly used to treat femoral neck fractures. However, this procedure involves removal of bone and healthy tissue, which is not desirable in all patients. For patients with low demand, a hemiarthroplasty of the hip is a common procedure to treat a fractured neck of femur. The procedure involves replacing the femoral head with a metallic component, leaving the acetabulum untouched. The benefits of this procedure are that surgery time and blood loss during surgery are lower than in total hip replacement surgery (van den Bekerom *et al.*, 2011). This is integral to the recovery of patients by reducing the occurrence of post-surgical trauma. There are also economic benefits to using hemiarthroplasty as an alternative to total hip replacement due to shorter surgical times and only implanting a femoral component.

However, hip hemiarthroplasty has a significantly lower success rate compared to total hip replacement. A major complication resulting from hemiarthroplasty is rapid cartilage erosion. This is because by only replacing the femoral head with a metallic ball, it is allowed to articulate against the acetabular cartilage. Although the failure of hemiarthroplasties due to cartilage erosion has been reported in clinical studies, *in-vitro* studies, examining the factors that affect cartilage erosion after hemiarthroplasty of the hip are not common. Most studies have used a simple geometrical *in-vitro* model such as a pin-on-plate or pin-on-disc to study tribology of acetabular cartilage against different materials or under different stresses. All studies have only studied cartilage tribology in the short term (a maximum of several thousand cycles); longer term assessment has not been

reported. This could be a primary reason for the lower success rate of hemiarthroplasty compared to the gold standard total hip replacements which have been studied in the long term (several million cycles).

1.2 The Synovial Joint

The synovial joint is the most common type of joint in the human body (Moore and Agur, 2002). Enclosed by a fibrous capsule (synovial membrane), the synovial joint contains synovial fluid that separates and lubricates the articulating surfaces. Articular (hyaline) cartilage is integrated with the underlying bone, providing a surface with low coefficient of friction, allowing smooth motion (Figure 1-1) (Stockley, 1986; Hamill and Knutzen, 1995). Movement of the joint is controlled by the action of the muscles, which are connected to the bone via tendons. Ligaments stabilises the synovial joint by eliminating excessive movement without restricting motion (Stockley, 1986; Moore and Agur, 2002).

1.2.1 The Anatomy of the Hip Joint

The hip joint connects the lower extremities of the body to the pelvis and axial skeleton of the trunk. Commonly referred to as a “ball and socket joint”, the human hip consists of a femoral head (ball) and an acetabulum (socket) (Figure 1-1). This configuration allows relatively free articulation with extremely low friction attributed to the articular cartilage, which covers the ends of the femoral head and acetabulum. Five predominant ligaments stabilise the joint and prevent excessive motions: pubofemoral ligament (attaches the pubis bone of the pelvis to the femur), iliofemoral ligament (attaches the from of the pelvis to the femur), ischiofemoral ligament reinforces the joint capsule (attaches the acetabular rim to the femur), transverse acetabular ligament (prevents inferior dislocation of the femoral head) and ligamentum teres, a small ligament attached to the centre of the femoral head and the centre of the cup within the joint cavity.

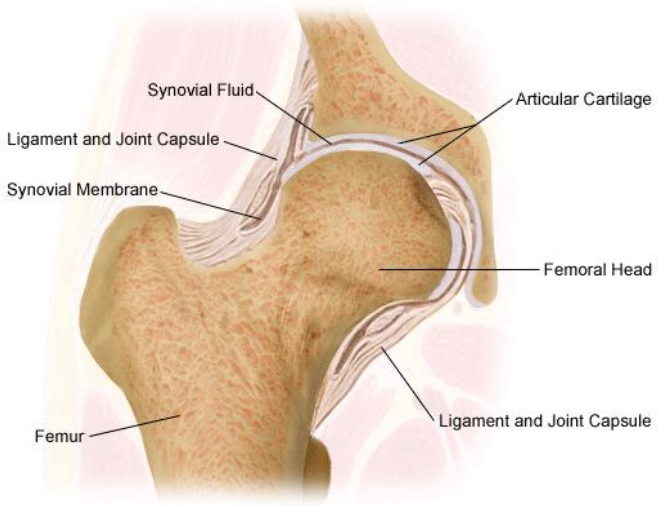

Figure 1-1: The hip joint (Orthopaedics, 2007).

1.2.2 The Motions of the Hip Joint

The motion of the hip joint occurs in three planes: sagittal (flexion – extension), frontal (abduction – adduction), and transverse (internal – external rotation). The full range of motion (ROM) of the hip is largest in the sagittal plane, where the flexion/extension ranges from +140^{o} to -15^{o} (Nordin and Frankel, 2001). The ranges of abduction/adduction is +30^{o} to -25^{o}. When the hip joint is flexed, the outer/inner rotation is ±40^{o}. However, these angles are lower in patients suffering from osteoarthritis (Figure 1-2) (Nordin and Frankel, 2001).

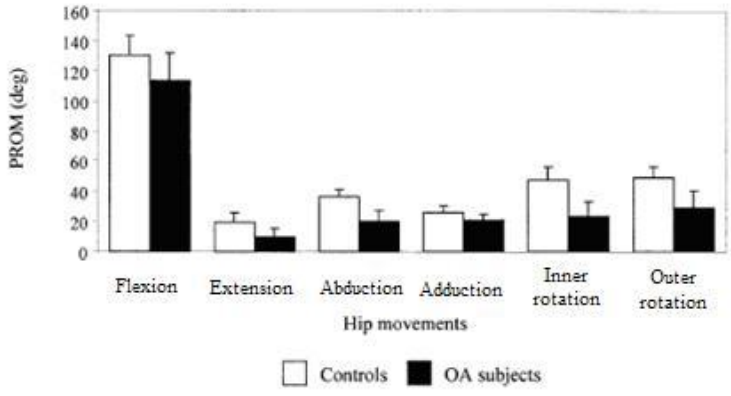

Figure 1-2: Passive ROM of the natural hip (Nordin and Frankel, 2001)

During activities of daily living (ADL), such as tying shoe laces and ascending stairs, the maximum range of motion is not reached. However, results from a study carried out by Johnston and Smidt (1970) indicate that hip flexion of at least 120^{o} and abduction/external rotation of 20^{o} are paramount to enable ADL. The ranges of

motion of 33 men carrying out various ADL measured via an electrogoniometer are tabulated below (Table 1-1).

Table 1-1: Maximum hip motion in three planes during common activities (Johnston and Smidt, 1970).

Activity	**Plane of Motion**	**Recorded Value* (Degrees)**
Tying shoe with foot on floor	Sagittal Frontal Transverse	124 19 15
Tying shoe with foot across opposite thigh	Sagittal Frontal Transverse	110 23 33
Sitting down on chair and rising from sitting	Sagittal Frontal Transverse	104 20 17
Stooping to obtain object from floor	Sagittal Frontal Transverse	117 21 18
Squatting	Sagittal Frontal Transverse	122 28 26
Ascending stairs	Sagittal Frontal Transverse	67 16 18
Descending stairs	Sagittal	36

*Mean value for 33 asymptomatic men

For normal level walking (gait) the hip joint moves from flexion to extension, adduction to abduction and internal rotation to external rotation in a cyclic pattern. Just prior to heel strike the leg is at 35 - 40^{o} flexion and is slightly adducted and internally rotated at 0 – 5^{o} (Nordin and Frankel, 2001). During the stance phase the leg extends, abducts and externally rotates to approximately 5^{o} and the reverse occurs during the swing phase. This is represented graphically in Figure 1-3a and Figure 1-3b which were originally adapted from Murray (1967) and Johnston and Smidt (1969) studies respectively.

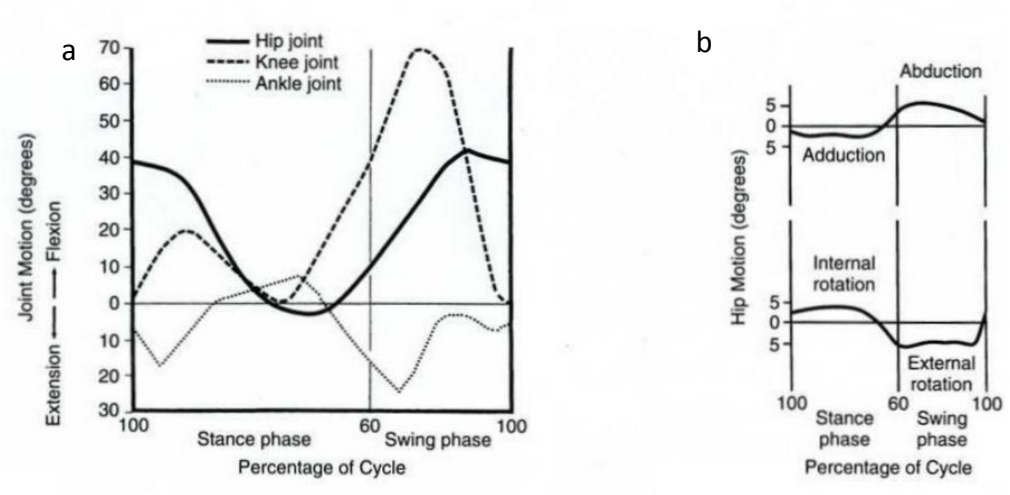

Figure 1-3: a) Joint motion of normal hip during level walking gait taken in the sagittal plane. The knee and ankle motion is also displayed. b) Range of adduction/abduction and internal/external rotation during normal level gait (Nordin and Frankel, 2001).

1.2.3 Hip Joint Forces

If the subject is in a single-leg stance, the centre of gravity shifts in all three planes, producing a torque around the hip joint. To counter this, muscles contract to keep the moments in equilibrium. Hence, there are two types of moments involved (Figure 1-4); 1) the moment arising from the gravitational force produced by the weight of the upper extremities including the raised leg (5/6 BW) times the gravitational force lever arm (b); and 2) the moments arising from the force produced by the abductor muscle (A), times the abductor lever arm (c). All lever arms are measured from the centre of rotation (Q) of the hip to the line of action.

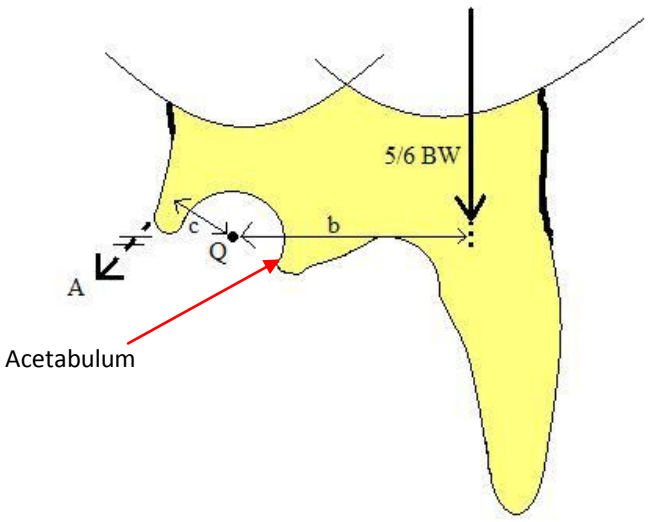

Figure 1-4: A Free body diagram of the forces and moments subjected to the hip.

A study of hip joint reaction forces produced during a single gait cycle was carried out to compare the results for men and women (Nordin and Frankel, 2001). When studying the men, two peak forces were produced during the stance phase, due to the contraction of the abductor muscle to stabilise the pelvis (Figure 1-5a). One peak of approximately four times BW was observed just after heel strike and another peak occurred of around seven times BW just prior to toe off. These values correlate well with the results stated by Kuster (2002).

The gait pattern for the women was similar but with a smaller magnitude of force (reaching a maximum of four times BW just prior to toe off) (Figure 1-5b) (Nordin and Frankel, 2001). This could be due to the wider female pelvis or dissimilarity in foot wear.

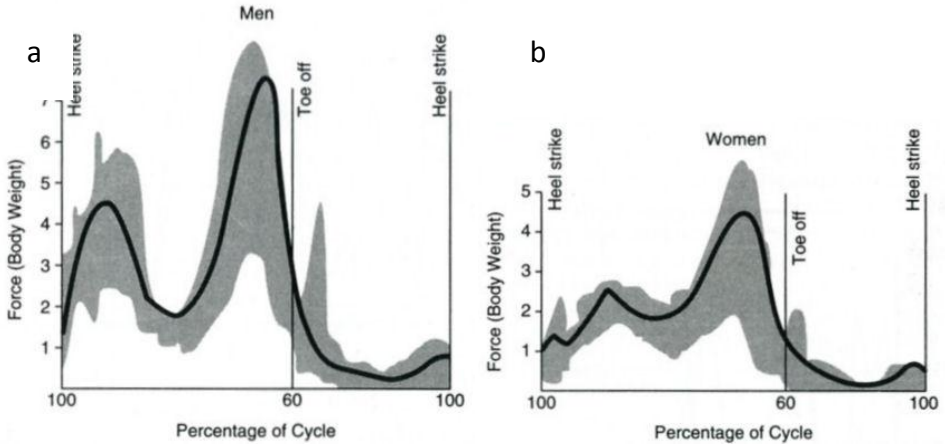

Figure 1-5: Hip reaction force in percentage body weight for a) normal men and b) normal woman. The shaded areas indicate the variations among subjects. Adapted from Nordin and Frankel (2001).

1.2.4 Contact Mechanics of the Hip Joint

Contact mechanics, specifically contact stress and cartilage strain and how they change over time, play a crucial role in the tribology of natural joints. For this reason, contact stress of the hip joint during gait and other activities has been a subject of interest. Studies that examined contact stress in the hip joint used theoretical models, finite element models, *in-vivo* and *in-vitro* analysis. Examples of these studies are discussed below.

An example of a simple theoretical model is a study by Brinckmann *et al.* (1981) who created a mathematical model from anterior-posterior radiograph images of hip joints taken from 304 healthy human subjects. The radiographs

allowed the three-dimensional geometry of the contact area of the femoral head and the acetabulum to be reconstructed. It was found that the average peak contact stress was 3.72 MPa just prior to toe-off, where the load was approximately five times body weight. Another simple theoretical model was conducted by Ipavec *et al.* (1999), who assumed the acetabulum was perfectly spherical. It was found that during gait, the peak stress in the stance period was around 3 MPa.

Finite element models are useful for looking at parameters that cannot be examined *in-vitro*, such as fluid load support. Finite element modelling also can include other more complex factors such as the intrinsic mechanical properties of cartilage compared to simple theoretical models. Anderson *et al.* (2008) modelled the cartilage of the hip as homogeneous, isotropic, incompressible and neo-Hookean hyperelastic. They were able to predict a contact stress of 10.78 MPa during normal gait. It was also found that during ascending and descending stairs, the peak contact stress in the hip was 11.61 MPa and 12.73 MPa respectively. Another study that utilised finite element analysis to predict hip joint contact stress during gait and other activities of daily living was Harris *et al.* (2012) who modelled the cartilage as hyperelastic. A peak contact stress of 8.66 MPa was calculated during walking gait.

The majority of these studies and finite element models were used to predict hip contact stress in the natural joint due to the difficulties in examining the contact stress in the natural joint *in-vivo* and *in-vitro* during gait. The vast majority of *in-vivo* studies use instrumented prosthesis (endoprosthesis) that directly records joint forces to predict contact stresses (Rydell, 1965; Bergmann *et al.*, 1984; Hodge *et al.*, 1989; Bergmann *et al.*, 1993; Catani *et al.*, 1995; Krebs *et al.*, 1998; Bergmann *et al.*, 2004). *In-vivo* studies have only concentrated on the contact stress in hemiarthroplasties or total joint replacements due to needing an endoprosthetic femoral head.

In-vitro studies that have measured contact stress during gait in the natural joint are rare. Adams and Swanson (1985) placed piezoelectric pressure transducers in the acetabulum through holes drilled in the cancellous bone. A

loading cycle originally discussed in a previous study (Paul, 1967) was applied to the cartilage and the pressures were obtained. The peak pressure ranged from 5.26 to 8.57 MPa during heel strike, which was approximately 4.17 times body weight. This, although novel, is not a true representation of a true gait cycle as only axial force was applied (with no motion).

Examples of the studies that investigated contact stress in the hip during gait are summarised in Table 1-2. The values obtained for contact stress in the hip joints covers a large range, from 3.0 MPa to 10.78 MPa. This is possibly due to the method in which the contact stress was calculated, what conditions were applied to the cartilage, and the assumptions that were made.

Table 1-2: Contact stress values during gait from previous studies using either theoretical calculations, finite element modelling, *in-vivo* or *in-vitro* models

Reference	**Hip Joint Contact Stress During Walking (MPa)**		**Load (N)**	**Type of Model**
	Average	**Peak**		
Brinckmann *et al.*, 1981	3.72	-	5 × BW	Theoretical model
Ipavec *et al.*, 1999	-	3.0	2000	Theoretical model
Anderson *et al.*, 2008	-	10.78	1949	Finite Element Model
Harris et al., 2011	-	8.66	2.6 x BW	Finite Element Model
Hodge *et al.*, 1989	-	5.5	667	*In-Vivo* Model (endoprothesis)
McGibbon *et al.*, 1999)	-	6.5	-	*In-Vivo* Model (endoprothesis)
Adams and Swanson, (1985)	-	8.57	2380	*In-vitro* Model

Most *in-vitro* studies that examined contact stresses in the hip joint used a static load due to complexities of applying a dynamic load (Rushfeldt *et al.*, 1981; Macirowski *et al.*, 1994; von Eisenhart-Rothe *et al.*, 1997; Lizhang, 2010). Lizhang (2010) used a pressure sensitive film to measure contact area and stress in an *in-vitro* hemiarthroplasty model. A pendulum friction simulator was used to apply a contact load of 800 N through a CoCr femoral head to a porcine acetabular cup with different radial clearances. The average contact stress ranged from 3.4 MPa to

6.3 MPa and peak contact stress ranged from 5.6 MPa to 10.6 MPa for small (<0.6 mm) to extra large clearances (>1.8 mm) respectively.

1.2.5 The Role of Synovial Fluid

Synovial fluid is a clear yellowish, highly viscous fluid that lubricates the synovial joint, aiding smooth motion between articulating surfaces. It possesses non-Newtonian flow properties such as a shear thinning effect, normal shear stress effect and elastic effect; typical to that seen in all polymeric fluids. For example, it has been shown that as the shear rate of bovine synovial fluid increased from 0.1 to 1000 s^{-1}, viscosity decreased nonlinearly from 10 to 0.02 N-sec/m^2 (King, 1966). As well as lubricating the synovial joint, another role for synovial fluid is to act as a medium for osmosis between the blood supply and the joint (Mow *et al.*, 2005). Synovial fluid is essentially a dialysis of blood, but without clotting factors, erythrocytes, or haemoglobins. Instead it contains hyaluronate (an extended GAG chain), lubricating glycoprotein and wear-retarding phospholipids (Mow *et al.*, 2005). As well as mixed and fluid film lubrication, synovial fluid aids the superior boundary lubrication of articular cartilage. However, the precise constituents of synovial fluid responsible for the boundary lubrication regime are subject of much debate. These are discussed in the following sections.

<u>Hyaluronic Acid (HA)</u>

The effect hyaluronic acid (HA) has on the boundary lubrication of articular cartilage is debated. Bell *et al.* (2006) used a simple pin-on-plate simulator to measure the effect HA has on the friction between cartilage samples. Three different cartilage models were used: healthy bovine cartilage, deliberately damaged bovine cartilage (by rubbing emery paper on the cartilage surface) and osteoarthritic human cartilage. It was shown that HA reduced friction compared to Ringers solution in all three models under static conditions. However, HA was less effective under dynamic conditions. Other studies suggest HA plays a negligible role in the boundary lubrication of articular cartilage (Radin *et al.*, 1970; Swann *et al.*, 1974) however, these studies also used dynamic conditions. In summary, the role

of HA in the tribology of cartilage depends on the lubrication conditions of the contact.

Lubricin

A study by Radin *et al.* (1970) found that the boundary lubricant was either a protein or a glycoprotein whilst attempting to explore the effectiveness of HA as a boundary lubricant. Further research carried out by Swann *et al.* (1981) confirmed that these glycoproteins reduce friction to a similar level as normal synovial fluid and termed it lubricin. Jay (1992) and Jay and Hong (1992) shown the gene Prg4 was the regulator for both lubricin and another protein called superficial zone protein (SZP), which are both found on the cartilage's surface. It was also concluded that lubricin acts in synergy with HA as an effective boundary lubricant. Now, it is thought that lubricin is not only a lubricating glycoprotein present in synovial fluid but also plays an essential part in preventing cartilage wear, synovial cell adhesion and proliferation (Rhee *et al.*, 2005). Since these studies, the use of lubricin based biotherapeutic approaches to treat osteoarthritis have been explored with success (Flannery *et al.*, 2009).

Surface-active Phospholipids

More recent reports suggest that surface active phospholipids (SAPL) are components of lubricin and that these act as the main boundary lubricant. However, the insoluble nature of SAPL would hinder its absorption into synovial fluid. Hence, lubricin, which is a large water-soluble molecule, acts as a carrier for SAPL (Hills and Butler, 1984). Therefore, this has led to idea that synovial fluid does not directly lubricate the joint, but could act as the transport mechanism between the synovium and the articular cartilage surface (Hills and Butler, 1984).

Previous studies have shown that SAPL reduces friction under boundary lubricating conditions *in-vitro* (Higaki *et al.*, 1998; Foy *et al.*, 1999). A study that involved removing lipids from the surface of articular cartilage increased the coefficient of friction in a cartilage pin on cobalt chrome plate model.

1.3 Articular Cartilage

Articular cartilage is a highly specialised connective tissue that reduces friction and dampens compressive, tensile, and shear forces experienced in the joint (Lee *et al.*, 2006). Articular cartilage is a multiphasic material, consisting of two predominant phases: a solid and a fluid phase. The constituents of both of these phases are described in Table 1-3. A third phase has been described as the dissolved electrolytes which accounts for the osmotic swelling of the cartilage. The composition of these phases and the synergy between them are integral to the mechanical behaviour and hence, physiological function of articular cartilage.

Table 1-3: The solid and fluid constituents of articular cartilage (Mow *et al.*, 2005).

Phase	Constituents	Percent Wet Weight
Solid Phase	Collagen	10% - 20%
	Proteoglycans	5% - 10%
	Chondrocytes	< 1%
Fluid Phase	Water	60% - 85%
	Inorganic Salts	Minute quantity

In-silico Modelling of articular cartilage has evolved of the past century from basic isotropic and linearly elastic models to more sophisticated viscoelastic models. However, these early viscoelastic models failed to explain the direct role of the fluid phase. Mow *et al.* (1984) described a viscoelastic model that involves both the solid and fluid phases; which were both taken as separate and immiscible. This theory was then developed to include the electrolyte phase that accounts for the osmotic swelling pressure of articular cartilage. This is known as the triphasic theory (Lai *et al.*, 1989a; Lai *et al.*, 1989b).

1.3.1 Articular Cartilage Macrostructure

Articular cartilage contains four major zones; deep zone (1), radial zone (2), transitional (middle) zone (3) and superficial (surface) zone (4) (Figure 1-6). The orientation and nano-architecture of the extracellular matrix (ECM) components, and hence, the unique viscoelastic/anisotropic properties of articular cartilage is zone dependent (Peterfy and Genant, 1996). The deepest zone is a calcified layer that anchors the radially orientated parallel collagen fibrils found in the radial zone.

The arrangement of the collagen fibrils are more disorganised in the transitional zone, resisting the shear forces that occur in this region. The superficial zone contains a large proportion of tangentially orientated collagen fibrils (Peterfy and Genant, 1996).

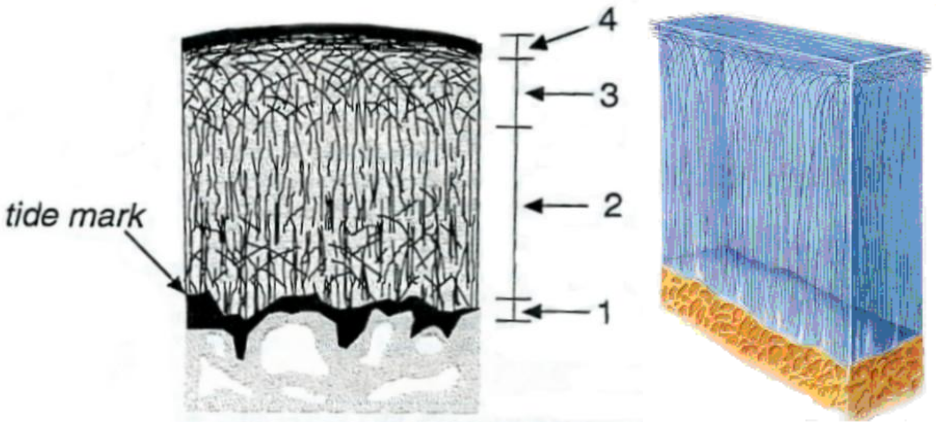

Figure 1-6: The four zoned composition of articular cartilage: deep zone (1), radial zone (2), transitional (middle) zone (3) and superficial (surface) zone (4). Left: Peterfy and Genant (1996). Right: Waldschmidt *et al.* (1997).

1.3.2 Articular Cartilage Microstructure

The main components of articular cartilage (Table 1-3) will be discussed in more detail in the following sections. However, other constituents of minute quantity are also found in articular cartilage but not discussed include other smaller proteoglycans and hyaluronans. It is important to mention these components because they may still play a vital mechanical and biological role.

Interstitial Water

Interstitial water makes up 65% of cartilage wet weight in the deep zone and 80% at the surface, making it the most abundant component. The majority of the water molecules are in the form of a proteoglycan-collagen gel, which can freely efflux and influx the cartilage.

Approximately 30% of water resides within the collagen intrafibrillar space, and is modulated by the swelling pressure of the fixed charge density (FCD) of the surrounding proteoglycans. Unlike the water molecules discussed in the previous paragraph, these water molecules are not available for transport under mechanical loading and are exuded from the proteoglycans, raising the density of the fixed

charges. This in turn raises the interstitial osmotic pressure in accordance to Donnan osmotic pressure law, which is integral to the cartilage structure (Mow and Hayes, 1997).

The amount of water that resides in cartilage depends on (1) the concentration of proteoglycans and hence the fixed charged densities, (2) the microarchitecture of the collagen fibres, and (3) stiffness and strength of these fibrous networks which resist swelling pressure. There is a significant increase of water content in articular cartilage after degradation occurs. This is thought to be due to the destruction of the collagen matrix, allowing increased water uptake and hence, swelling (Mankin and Thrasher, 1975). This is known as hyperhydration.

Collagen

Collagen is the most abundant component of the ECM. Cartilage mainly comprises of collagen type II, with lower amounts of collagen type V, VI, IX and XI. The fundamental structure of type II collagen comprises a right-handed triple helix of three *α1* polypeptide chains. Each of the *α1* polypeptide chain consists of segments of the structural motive Gly-X-Y, tightly bound to form a left-handed helix. The triple helix further polymerises into larger collagen fibrils (Ø = 10 – 200 nm) which are stabilised with the use of intermolecular and intramolecular covalent crosslinks. These crosslinks allow collagen to resist the swelling pressure produced by the FCD of the proteoglycans coupled with the *in-situ* loads during activities of daily living (Mow and Huiskes, 2005).

Proteoglycans and Glycosaminoglycans

Proteoglycans are large molecules formed by several glycosaminoglycan (GAGs) chains covalently bonded to a core protein. One of the main constituents of articular cartilage are large aggregating proteoglycan known as aggrecans; which exhibit the mechanical properties essential to withstand the large compressive stresses in the joint. Aggrecans can be split up into distinct regions: an N-terminal region consisting of two globular domains G1 and G2, keratan sulphate rich region, a chondroitin sulphate rich domain and a C-terminal globular domain G3 (Mow and Ateshian, 1997).

Chondroitin sulphate is the most abundant GAG in articular cartilage; however, other GAGs include keratan sulphate, heparin, heparin sulphate and dermatan sulphate. All the GAGs contain sulphate and carboxyl groups which are negatively charged. This high negative charge serves three purposes: 1) to resist compression loads in the joint due to its rigidity, 2) to attract counterions which enable cartilage hydration through Donnan osmotic pressure, and 3) resist interstitial fluid flow, lowering the permeability of the cartilage (Mow and Ateshian, 1997).

Chondrocytes

Chondrocytes are the only cell type found in articular cartilage. Even though they make up just 5-10% of cartilage volume, they are responsible for synthesising and maintaining the proteoglycans and collagen found in cartilage. Chondrocytes are surrounded by a 2 µm thick layer known as pericellular matrix; which both work as a functional unit, named the chondron (Poole *et al.*, 1987).

Depending on the location within the cartilage, chondrocytes vary in size, shape, orientation and formation. In the superficial zone chondrocytes are flat, orientated parallel to the surface. These chondrocytes make large amounts of collagen and smaller amounts of proteoglycans. In the transitional and deep zones, chondrocytes are sparser. In the transitional zone, the chondrocytes are more spherical creating a large concentration of proteoglycans and large diameter collagen fibrils. In the deep zone, chondrocytes are aligned in columns perpendicular to the cartilage surface (Mow *et al.*, 2005).

Cartilage is avascular; therefore, receives most of its nutrition through the synovial fluid. In the past researchers thought that nutrition from the blood supply in the subchondral bone was impossible due to the densely calcified basal zone which would act as an impenetrable barrier. However, in a more recent study, the possibility of nutrients crossing from the subchondral bone was eliminated by coating the bottom of autologous osteochondral transplants with methylmethacrylate before transplanting into baboons (Malinin and Ouellette, 2000). After three years, the transplants with the coating exhibited degeneration whilst the transplants without the coating were similar to that of normal healthy

cartilage. Hence, it was concluded that chondrocytes do not only receive nutrients from the subchondral bone, but that this nutrient pathway is essential for cartilage homeostasis.

Collagen-Proteoglycan Interactions

The interaction between collagen and proteoglycans is extremely important yet poorly understood. It is believed collagen and proteoglycans work in synergy to aid the cartilage mechanical properties. As mentioned previously, a high FCD (creating Donnan osmotic pressure) draws in water creating a swelling pressure. This inflates the collagen network and maintains the cartilage structure (Mow *et al.*, 1992). Zhu *et al.* (1993) suggested that the proteoglycans enmeshed in the collagen matrix causes the collagen to exhibit pre-stress. This is due to the repulsive force of the negatively charged groups along the proteoglycan molecules.

The physical restraint proteoglycans have on collagen inhibits sudden extension of the collagen network. This has been thought to protect the cartilage from sudden impacts under certain physiological situations (Schmidt *et al.*, 1990).

1.4 Mechanical Properties of Articular Cartilage

The zone dependent structural organisation of the collagen and proteoglycans give articular cartilage its inhomogeneous and anisotropic mechanical behaviour. As discussed in Section 1.2.3, the forces in the hip can reach up to several times body weight. Therefore, this inhomogeneous and anisotropic mechanical behaviour is vital to resist these loads over many millions of cycles. To understand how cartilage performs *in-vitro*, its compressive, tensile and shear properties must be understood.

1.4.1 Compressive Properties

Time dependent compressive properties are primarily governed by the fluid pressure, proteoglycans and fluid concentration. These, as described in Section 1.3.1, vary greatly between zones, throughout the thickness of cartilage. Therefore, the compressive properties of cartilage are also depth dependent, where the

deeper zone exhibits stiffer properties. The highly electronegative charge of the proteoglycans repel each other expanding the network, resisting the free flow of interstitial fluid. The collagen network limits the expansion of the extra cellular matrix causing residual Donnon osmotic pressure within the tissue. This is the primary mechanism that cartilage utilises to resist large compressive loads (Mow and Huiskes, 2005).

The compressibility of cartilage is usually measured using a simple geometrical model such as an osteochondral plug. Aggregate modulus is commonly used to describe the compressibility of the entire biphasic cartilage. In initial studies, shape change of the cartilage during creep compression was simplified, allowing modelling to be conducted with relative ease. This involved compressing the cartilage with a rigid semi-permeable disk. Lateral fluid and shape change were eliminated by constraining the osteochondral plug in a non-permeable tube. One of the earliest examples of confined compression and articular cartilage mechanical property derivation was conducted by Mow *et al.*(1980). In this study, Mow and colleagues described a methodology and constitutive equations to derive aggregate modulus and permeability constant. The aggregate modulus takes into account the whole biphasic tissue (solid and fluid phases). The solid matrix was assumed to be intrinsically incompressible, linearly elastic and nondissipative, and the interstitial fluid was assumed to be also incompressible and nondissipative. It was shown that there was a linear relationship between equilibrium stress and equilibrium strain up to approximately 22% strain. After which, the equilibrium strain increases at a slower rate with an increase in equilibrium stress. Therefore, after 22% strain it was found that the aggregate modulus was strain dependant, whereby at larger strains, the cartilage becomes more stiff. By restricting radial deformation, other values such as Poisson's ratio could not be determined.

In later studies, more complex models were used allowing Poisson's ratio of the entire biphasic tissue, as well as permeability and aggregate modulus to be calculated. For this, creep indentation was performed which allowed lateral shape change. Athanasiou and colleagues studied the aggregate modulus of femoral head articular cartilage (Athanasiou *et al.*, 1995). Depending on location, these values

varied between 0.82 MPa to 1.44 MPa; where the primary weight bearing region of the femoral head exhibited the stiffest properties.

Other studies have calculated equilibrium elastic modulus. This takes into account the solid component after maximum deformation of tissue has occurred and fluid exudation has reached equilibrium. The Poisson's ratio of the solid component in this model was assumed to be zero for simplicity. This also involves indentation and hence, lateral shape change was allowed to occur.

However, the compressive properties of the tissue can vary with age, pathology, and type of joint. It is commonly accepted that when osteoarthritis occurs, cartilage swells and the compressive modulus drops. However, it has been reported that in the absence of joint disease, cartilage becomes stiffer with increasing age. This is due to the reaction of nonenzymatic glycation of proteins initiated by the reaction of protein residual sugars such as lysine and arginine that eventually leads to the accumulation of advanced glycation end products (AGEs) over time. This reaction is known as Maillard or browning reactions due to the discoloring of the cartilage from a white/blue to a yellow/brown. This causes large amounts of crosslinking between collagen which has shown to be sufficient to change the cartilage mechanical properties by the stiffening of the articular cartilage collagen network (Verzijl *et al.*, 2000).

1.4.2 Tensile Properties

Under a constant uniaxial load in tension, the solid phase of cartilage exhibits nonlinear stress-strain behaviour (Figure 1-7A). When cartilage is initially placed in tension, the coiled collagen fibres straighten. This requires a relatively small load and is represented by the toe region on the stress-strain curve. After which, there is a linear region caused by stretching of the straightened collagen fibres. Failure occurs when the collagen fibres rupture (Ozkaya and Nordin, 1998; Nordin and Frankel, 2001).

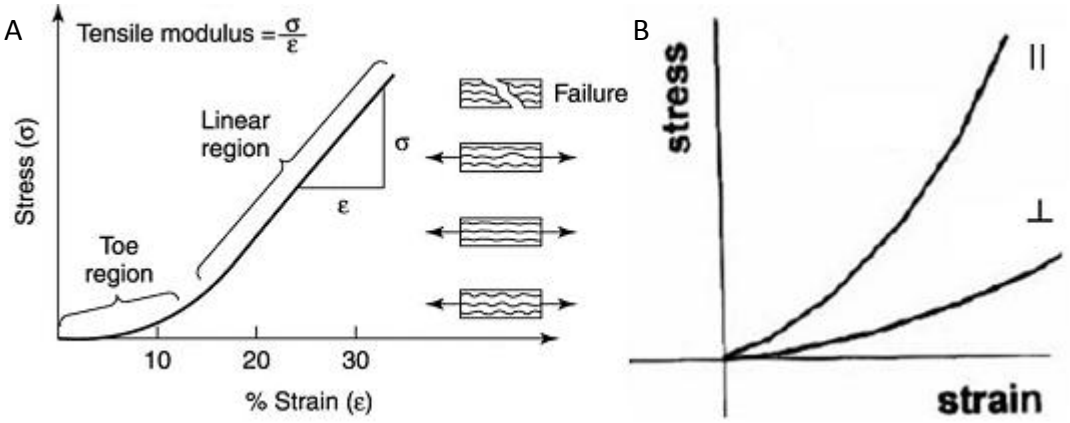

Figure 1-7: Articular cartilage in tension. A: Typical stress-strain curve when a constant strain rate is applied to cartilage. B: The anisotropic properties of cartilage causes a difference in the stress-strain curve when the load is applied parallel (||) and perpendicular (⊥) to the split lines (Mow *et al.*, 1992).

Cartilage is also anisotropic; therefore, the ultimate tensile strength differs depending on whether the line of action in perpendicular or parallel to the collagen fibrils at the cartilage surface (split line direction) as seen in Figure 1-7B (Mow *et al.*, 1992). This is also true for the gradient of the linear region, and hence the tensile modulus. This shows not only that there is an optimum alignment to resist tensile forces, but also indicates that tensile properties are independent of proteoglycan content. Kempson studied the tensile modulus of human femoral head cartilage and found a large variation between 2 MPa and 32 MPa (Kempson, 1991). As is the case with compressive modulus of the solid phase, tensile modulus of the solid phase varies with age, pathology, type of joint, and the location in the joint.

1.4.3 Viscoelasticity

The time dependent response of articular cartilage is primarily associated with the frictional drag of fluid through the solid matrix and within the tissue and the viscoelastic response of the solid matrix itself. This is known as the 'flow-dependent' viscoelastic behaviour of cartilage.

As well as the frictional drag of fluid through the solid matrix, the property of the solid matrix itself can also be considered as viscoelastic. This is known as 'flow-independent' viscoelastic behaviour. One method to examine the viscoelastic response of the solid matrix is to perform pure shear tests under small strain

conditions. By not altering the overall volume of cartilage, the fluid flow can be eliminated and hence, the viscoelastic response of just the solid matrix can be determined. Mow and colleagues found the shear modulus of the solid matrix to be approximately 0.20 to 0.40 MPa and hence the cartilage has a high tolerance to deformation (Mow *et al.*, 1992).

Dynamic shear properties have also been examined in previous studies. Zhu and colleagues used a sinusoidal torsional strain with a physiological range of frequencies (0.01-20 Hz) to measure the dynamic shear modulus of the solid matrix (Zhu *et al.*, 1993). It was found that the shear modulus increased from 0.2 to 2.5 MPa with increasing frequency. Zhu and others also found a correlation between collagen/proteoglycan content and shear modulus. Therefore, it was concluded that collagen has the ability to resist tension elastically, whilst proteoglycans inflate the collagen network, pretensioning the collagen fibrils via Donnan osmotic pressure (Zhu *et al.*, 1993).

1.4.4 Biphasic Stress Relaxation and Creep

As mentioned previously, articular cartilage is made up of two phases, a solid phase (proteoglycans and collagen type II) and a fluid phase (water and electrolytes); hence it is known as biphasic. The biphasic theory was developed by Mow and colleagues (Mow *et al.*, 1980) to describe the deformational behaviour of articular cartilage under a prescribed load. The theory assumes that the solid and fluid phases are incompressible and hence, the deformation of cartilage is solely due to the extradition of fluid through the permeable solid matrix. Therefore, permeability is a primary factor when determining the deformation and viscoelastic properties of cartilage. Previous studies that have looked at the permeability of cartilage have shown a wide range of values on a very low scale (in the order of 10^{-15} to 10^{-16} $m^4N^{-1}s$) (Lai and Mow, 1980). The porosity of cartilage is very high, (20-30% solid content and 70-80% water content), therefore the low permeability and strong resistance to fluid flow is primarily due to the proteoglycan network's strong affinity to the water molecules. The frictional drag between the fluid and solid phase compacts the solid matrix, leading to a further reduction in porosity and thus permeability. The strain dependent permeability property helps the

cartilage retain more fluid under excessive loads and also dissipates energy (Mow and Ateshian, 1997). The following will describe a number of tests that have been used to examine this biphasic behaviour.

Creep

Creep is the time dependent deformation under a constant load. The compressive creep properties of articular cartilage have been extensively investigated in previous studies (Mow *et al.*, 1980; Lai *et al.*, 1981; Mow *et al.*, 1984; Holmes *et al.*, 1985). These studies involve applying a constant load to the cartilage surface and monitoring the deformation. The cartilage samples are loaded through a porous plate to ensure that the fluid can flow unimpeded through the surface. The cartilage is also housed in a non-porous container to eliminate lateral flow of fluid and radial deformation. When a constant load is applied to the cartilage, fluid immediately starts flowing out of the superficial layer, and gradual deformation occurs. This is known as creep.

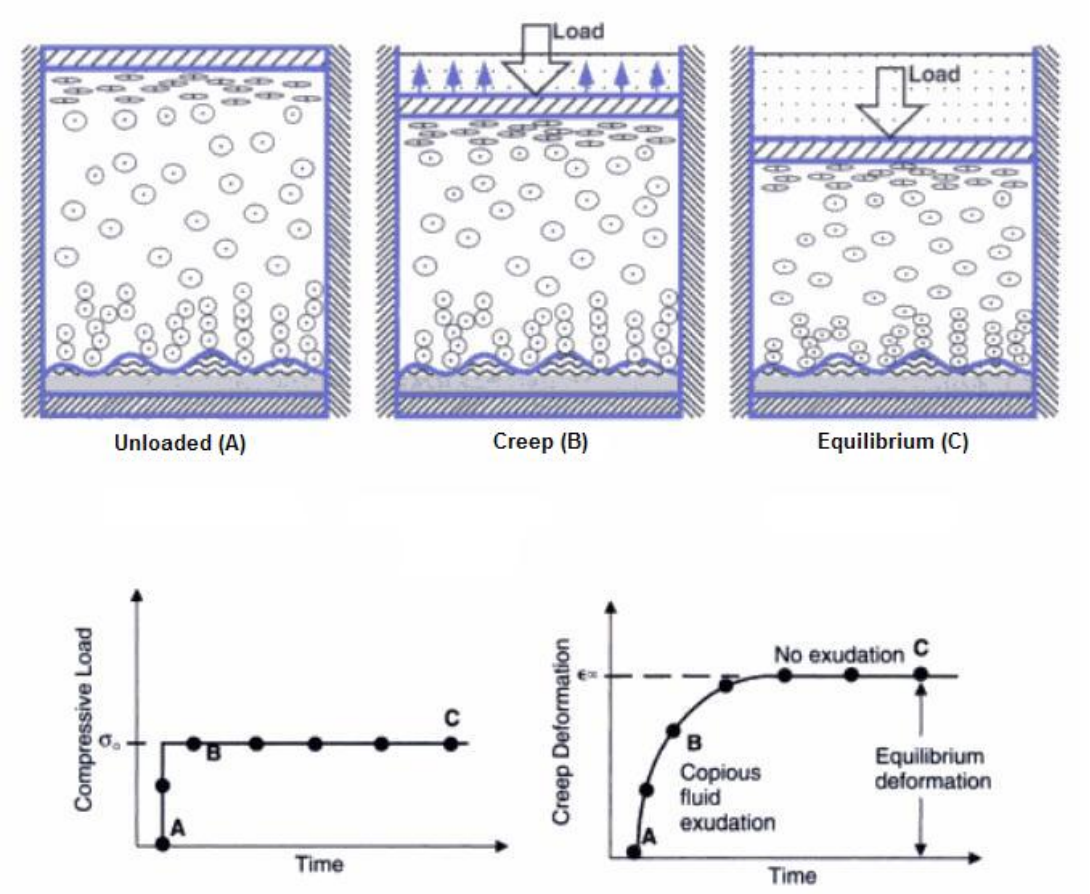

Figure 1-8: Creep response of articular cartilage under constant load Top: A) The cartilage is unloaded, B) fluid flows out of the cartilage under constant load, C) Equilibrium eventually occurs and fluid ceases to flow out of the cartilage (Nordin and Frankel, 2001). Bottom: Under constant load, deformation occurs due to fluid exuding out of the cartilage until equilibrium is reached where no further fluid exudation occurs (Mow *et al.*, 1980)

Initially, fluid exudes at a rapid rate. This gradually slows down as water content within the cartilage decreases until the load is fully supported by the solid ECM (Mow *et al.*, 1980). This is represented in the creep deformation/time curve in Figure 1-8. The creep response is primarily attributed to the fluid exudation and thus, permeability of the cartilage surface. Hence, permeability can be calculated via the initial part of the creep deformation/time curve.

Unconfined creep tests (including indentation) experiments have also been used in the past to establish other compressive properties of cartilage; such as equilibrium elastic modulus, aggregate modulus, Poisson's ratio as well as permeability. Lu and colleagues also used indentation to explore the electrochemical properties of cartilage using Donnan osmotic pressure theory (Lu *et al.*, 2004).

Stress Relaxation

Using the same set up described in the section detailing creep (Section 1.4.4), stress relaxation of cartilage can also be measured. However, instead of using a constant load whilst measuring cartilage deformation; a constant displacement is applied whilst the internal stress is measured (calculated using the force required to maintain constant displacement). The cartilage is compressed (under a constant rate of displacement) and then strain is maintained (Mow *et al.*, 1989). During compression, internal stress increases rapidly due to the large frictional drag between the solid and fluid phase. However, when the strain is left constant, fluid ceases to exude and instead redistributes within the cartilage until equilibrium is reached (Mow *et al.*, 1989). This reduces the internal stress of the cartilage and is hence known as stress relaxation. A typical stress time graph of this experiment is shown in Figure 1-9.

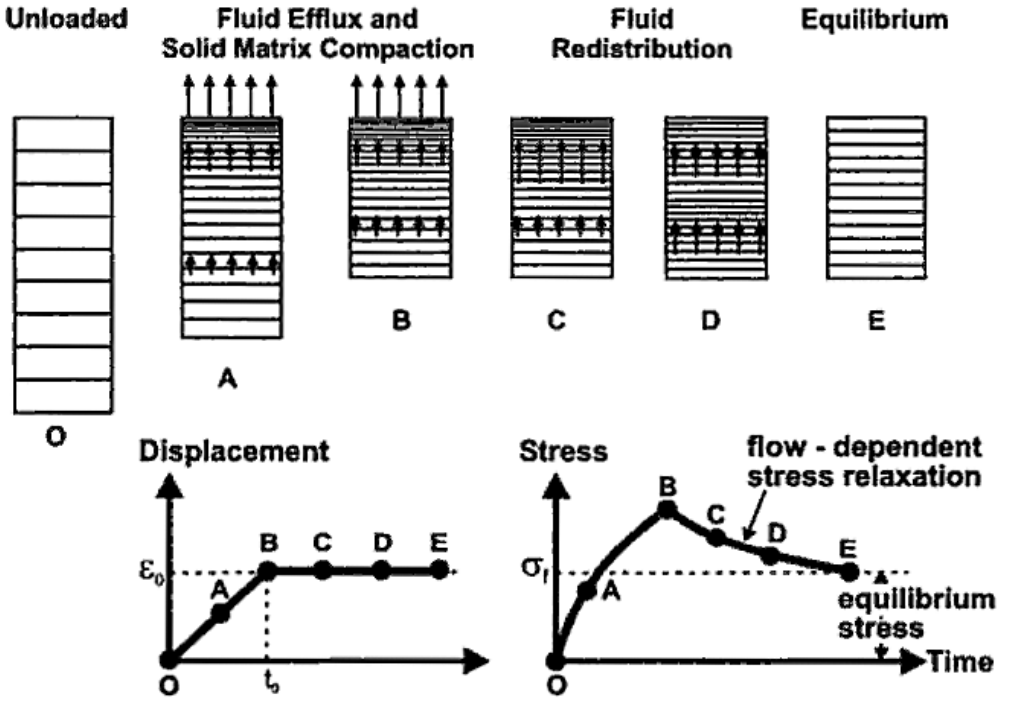

Figure 1-9: Top: When cartilage is deformed, fluid flows out the cartilage and the stress increases. When the deformation is constant, the fluid redistributes which reduces the stress. This is known as stress relaxation (Mow *et al.*, 1989)

1.5 Conditions and Diseases of the Hip

There are many conditions of the hip joint. The following section will discuss the three most common conditions and diseases of the hip.

1.5.1 Arthritis

There are more than 100 types of arthritis such as rheumatoid arthritis, psoriatic arthritis and gout. However, the most common type of arthritis is osteoarthritis (OA), affecting 10 – 20% of people over the age of 65, causing pain and discomfort. Approximately eight million people exhibit OA in Great Britain; one million of which receive treatment (Arthritis Research Campaign, 2005). It is generally accepted that there are two main categories of OA based on the cause: primary and secondary. Primary OA has no apparent initiating factor and is more prevalent with the age of the patient. If there is an underlying cause for OA such as congenital or hormonal disorders, joint injury, and other factors such as obesity or pregnancy; OA is dubbed secondary.

The pathology of OA is a subject of great interest yet poorly understood. It is thought that in the early stages of OA, cartilage can be graded as matrix disruption, partial thickness defects, and full thickness defects. This is similar to the macroscopic grading system used in arthroscopy. Matrix disruption occurs in the very early stages of OA, when proteoglycan content decreases. This could be caused by degradation of the molecules or/and decreased synthesis. Due to the importance of the proteoglycans in the mechanics of cartilage (Section 1.4), the cartilage becomes softer and more prone to damage after impact or cyclic loading (Buckwalter and Mow, 1992). This can disrupt the proteoglycan/collagen relationship and further damage the cartilage.

1.5.2 Femoroacetabulum Impingement (FAI)

Femoroacetabulum impingement (FAI) is bone to bone contact between the femoral neck and acetabulum cup, reducing the range of motion of the hip joint. There are two forms of FAI: cam form and pincer form. Cam form FAI is caused by the deformation of the femoral neck so that the femoral head is not perfectly

round and the head/neck ratio is asymmetrical. Pincer form FAI is caused by excessive coverage of the femoral head, due to the deformation of the acetabulum cup (Coleman, 2007). It has been proposed that FAI is a mechanism for the development of early osteoarthritis (Ganz *et al.*, 2003).

1.5.3 Avascular Necrosis (AVN)

Avascular necrosis (AVN) of the hip occurs when there is interruption of blood flow to the femoral head leading to death of cells (necrosis).. This interruption can be the result of embolism, obstruction of the venous system or arterial disease. Local cell death of the subchondral bone can lead to inferior mechanical properties, causing the bone to collapse. This can alter stress distribution over the femoral head, leading to articular cartilage damage. AVN can also affect the femoral neck, which can lead to dislocation or neck fracture (Bullough and DiCarlo, 1990). In the United States of America, approximately 12% of patients who undergo a total hip replacement were diagnosed with AVN (Mont and Hungerford, 1995).

1.5.4 Fracture of the Proximal Femur

One of the major socioeconomic problems to date is an age related bone deteriorating disease known as osteoporosis. Osteoporosis involves symptomatic bone loss; reducing its strength and hence becoming more prone to fracture. There are two types of osteoporosis, categorised in a similar way to osteoarthritis (Al-Tubaikh, 2010). Primary osteoporosis occurs when there is no trace to an underlying disease. This is further divided into juvenile, idiopathic and post-menopausal. Juvenile osteoporosis often affects children and young adults before puberty is reached. Idiopathic osteoporosis has similar clinical features as juvenile osteoporosis, however, typically affecting patients between 20 to 45 years of age. Post-menopausal osteoporosis is observed in women after menopause or oophorectomy (a surgical procedure which involves the removal of one or both ovaries). Secondary osteoporosis occurs when there is an underlying disease or a side effect by certain drugs (Al-Tubaikh, 2010).

A relatively common location of fracture is the femoral neck, known as fracture of the proximal femur. Femoral neck fractures are extremely common with

approximately 70,000 reported cases in the UK in 2009/2010. This is a rise of nearly 20,000 cases since 1999/2000 (The Information Centre for Health and Social Care, 2011). These fractures are due to bone fragility commonly and usually occur after a low-impact trauma, such as a fall (Abrahamsen *et al.*, 2009). Hip fractures can be split up into two categories, intracapsular and extracapsular which are determined by the location of the fracture line with respect to the joint capsule (Yochum *et al.*, 2005). Women over the age of 50 years are most likely to obtain a hip fracture and the mean age at which hip fractures occur is 80 years (Melton, 2003; Dennison *et al.*, 2006). It has been estimated that there were 1.6 million hip fractures attributed to osteoporosis for patients over the age of 50 since in year 2000, where approximately 70% were women (Johnell and Kanis, 2006).

1.6 Current Treatments for Hip Disorders

There are many different approaches to treat the pain of hip disease and modify its progression. This section of the literature review will explore the current nonsurgical and surgical interventions in order of least to most invasive. The relatively new concept of tissue engineering of cartilage will be discussed at the end of this section.

1.6.1 Non-invasive Interventions

Even though nonsteroidal anti-inflammatory drugs (NSAIDs) are one of the most frequently prescribed medications to relieve pain for arthritic patients, there is little evidence to suggest these drugs suspend or slow down arthritis (Schurman and Smith, 2004). Other drugs such as acetaminophen and Celecoxib also act as a pain reliever with fewer side effects than NSAIDs (Schurman and Smith, 2004).

Food supplements such as chondroitin sulfate and glucosamine are commonly used for self-treatment of articular cartilage (Reginster *et al.*, 2005; Bruyere and Reginster, 2007; Reginster *et al.*, 2007). This area has been studied in great depth and has been shown to reduce the pain experienced by osteoarthritis patients. A study by Reginster *et al.* (2007) found a significant reduction in joint space loss after three years for patients who took glucosamine (-0.06 mm)

compared to placebos (-0.31 mm). However, other reports suggest that these food supplements are not disease modifying and do not show any significant difference from placebos (Pavelka *et al.*, 2002).

Short term pain relief drugs such as NSAIDs are the first treatment response when dealing with osteoarthritis (Leopold *et al.*, 2003; Frampton and Keating, 2007; Scanzello *et al.*, 2008). With carefully controlled prescriptions, more invasive approaches can be postponed. However, other injectable medicines for palliative treatment can be used for long term pain relief, such as corticosteroids or sodium versions of hyaluronic acid (hyaluronan) (Gossec and Dougados, 2006). The ability to give long term pain relief is a subject of great controversy; however, it is presumed that it is due to the elimination of an inflammatory feedback loop of inflammation. However, like the NSAIDs, there is little or no proof that steroid injections modify the path of osteoarthritis (Karlsson *et al.*, 2002; Jubb *et al.*, 2003).

1.6.2 Joint Perseveration Surgery

Femoroacetabulum impingement (FAI) has proven to reduce the functional ranges of motion in the hip joint and can lead to excessive articular cartilage degeneration (Section 1.5.2). A common treatment is to “trim” the overgrowth of bone tissue (osteophytes), restoring the correct anatomical morphology. By only trimming the excess bone, the proximal joint including the articular cartilage is preserved; hence, this type of treatment is dubbed “joint preservation” surgery (Trousdale and Wenger, 2007). Previous reports have shown 65% to 94% good to excellent outcomes after a mean follow up of 40 months (n=194) for open surgery and a similar results for arthroscopic techniques (Bedi *et al.*, 2008).

1.6.3 Osteotomies

The aim of hip osteotomy is simply to re-orientate of the hip so healthy articular cartilage is placed in the weight bearing location of the joint. For this to be achieved, the bones are resected, moved and fixed in a new orientation (Trousdale and Wenger, 2007). This procedure can be performed on the pelvis (pelvic osteotomy) and/or the femoral neck (varus rotational osteotomy). The surgeon can also choose to insert a section of bone, obtained from a different location (known

as opening wedge osteotomy); or remove a section of bone (known as closing wedge osteotomy) (Trousdale and Wenger, 2007). Leunig and Ganz, (2011) achieved a good-to-excellent result in 88% of patients (n=75) who underwent a periacetabular osteotomy with a minimum of a 10 year follow up (Leunig and Ganz).

1.6.4 Hemiarthroplasty

Hemiarthroplasty is commonly used to treat low demand patients who have suffered a femoral neck fracture. As its name suggests; hemiarthroplasty is similar to THR; however it, only replaces one half of the hip (the femoral head). It is commonly performed to treat femoral neck fractures; however, it can also be used to treat AVN (Section 1.5.3). There are two types of hemiarthroplasty: unipolar and bipolar (Levine *et al.*, 2007).

Unipolar Hemiarthroplasty

First developed in the 1940s, the original unipolar design consisted of a solid, polished, unipolar head with a straight, collared, fenestrated stem suitable for noncemented use. The best known design was the Austin-Moore prosthesis (Figure 1-10A) (Levine *et al.*, 2007).

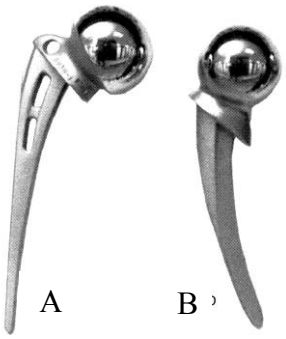

Figure 1-10: A) The Austin-Moore unipolar hemiarthroplasty. B) The Thompson and Moore unipolar hemiarthroplasty (Peltier, 2007).

The performance and success of the unipolar prostheses has been extensively studied clinically. Isotalo *et al.* (2002) used Kaplan-Meier analysis (Kaplan, 1958) to predict the life span of 228 displaced femoral neck fractures treated with the

Thompson and Moore prosthesis (Figure 1-10B). A 93% 3-year survival and 88% 6-year survival were calculated. However, the Kaplan-Meier only provides an estimate, predicting the lifespan of the prosthesis. Long term clinical studies into unipolar hemiarthroplasty are rare due to the relatively short life expectancy of patients. However, a study by Norrish et al. (2006) recorded the success rates of the Austin Moore hemiarthroplasty prosthesis with a cohort of 500 patients and found a 94% survival at 5 years and an 83% survival at 12 years (Norrish *et al.*, 2006).

Several complications are associated with the unipolar design. If the femoral head was too small, pain occurred and subsequent revision was required. Therefore, using the correct prosthetic circular templates to select the appropriate femoral head size should eliminate this pain (Sharif and Parker, 2002). Inadequate reaming of the femur for fear of fracturing the long bone could also lead to failure. If the femoral neck was cut too proximal or distally, this could result in premature failure as well (Sharif and Parker, 2002).

Rapid cartilage wear and degradation after bipolar implantation is also of a great concern. The severity and progression of articular cartilage wear was correlated with the age of the implant, and after five years post-implantation of the Austin-Moore prosthesis with a stable femoral component, caused nearly full thickness cartilage degeneration (Dalldorf *et al.*, 1995). There are also reports of the femoral head penetrating into the pelvis (protrusio acetabuli) (Dalldorf *et al.*, 1995).

Bipolar Hemiarthroplasty

The development of the bipolar hemiarthroplasty was driven by the poor clinical experiences associated with the unipolar hemiarthroplasty. A bipolar hemiarthroplasty consists of three parts (Figure 1-11): 1) A metallic femoral stem with a femoral head. The more recent hemiarthroplasties have interchangeable femoral heads, allowing easier conversion from hemiarthroplasty to THR if required. This eliminates the need to replace the entire stem, thus, less surrounding bone is affected. 2) An ultra high molecular weight polyethylene (UHMWPE) bearing insert. This provides an intermediate articulating layer; and 3)

an outer metallic head that articulates against both the bearing insert and the acetabulum articular cartilage.

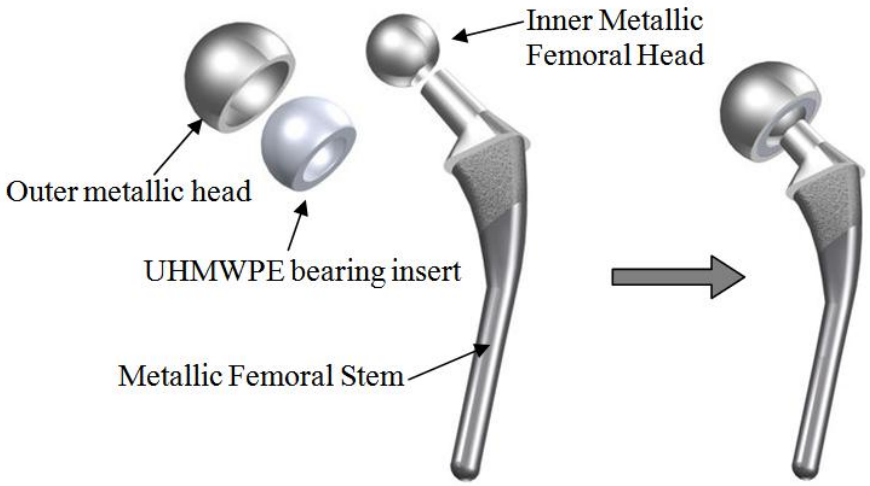

Figure 1-11: A schematic of the different components associated with a typical bipolar hemiarthroplasty (Orthopod, 2002).

The original bipolar implants were of a concentric design, where the outer metallic head and the bearing insert centres of rotation coincided (Levine *et al.*, 2007). However, the outer metallic head often became fixed in varus, causing increased amounts of wear, leading to prosthesis failure due to dislocation or fracture (Levine *et al.*, 2007). Therefore, the modern bipolar hemiarthroplasties are eccentric, so that the bearing surfaces "self centres" when load is applied.

Many complications have been reported in previous studies, where the most common is dislocation; occurring in approximately 10% of cases on average (Lee *et al.*, 2008). Dislocation can occur between the outer metallic head and the natural acetabulum cup, however in a minority of cases, the bearing insert and the inner femoral head becomes disassembled (Lee *et al.*, 2008). This type of disassembly is due to the excessive wear of articular cartilage, increasing the friction between the outer head and acetabulum articular cartilage. This restricts the movement of the outer head, increasing the risk of impingement between the femoral neck and UHMWPE rim. The impingement causes deformity and eventual detachment of the locking ring and thus dislocating the inner head from the outer head (Hasegawa *et al.*, 2004).

A study by Pickard *et al.* (2000) examined the condition of the cartilage after the implantation of a bipolar hemiarthroplasty in terms of frictional coefficient and compression creep tests. Pickard *et al*. found that cartilage friction was significantly larger from bipolar patients; compared to relatively healthier cartilage taken from patients who were undergoing total hip replacements after fracture of the femoral neck (control group). It was also shown that the rate of deformation was larger for cartilage taken from bipolar patients compared to the control group. Pickard *et al*. also performed histological assessment on both the bipolar and control groups. The details surrounding histological assessment are discussed further in Sections 1.8.1 and 1.9.4. It was found that the majority of the bipolar group showed intact cartilage with a distribution of collagen, however with little proteoglycan present. The rest of the bipolar group showed degeneration of the tissue's architecture and was described as fibrous with fibroblasts present.

1.6.5 Total Hip Replacement

Total hip replacement (THR) is the gold standard surgical treatment for osteoarthritis of the hip, with a recorded success rate as high as 81% after 25 years (Berry *et al.*, 2002). Initially THR was limited to the elderly and infirm; however, with the incremental improvement over the second half of the twentieth century, the life expectancy of these artificial joints has increased considerably and indications have expanded to younger and more active patients.

A variety of biomaterials are currently used in total hip replacements including metal-on-metal (MOM), ceramic-on-ceramic (COC) and metal-on-ultra high molecular weight polyethylene (UHMWPE) (Black *et al.*, 2007). THR can also be cemented or cementless; the decision of which will be based on the age and level of activity of the patient as well as the bone quality in the femur and cost of procedure. For instance, cementless designs will need good quality surrounding bone to support the implant, therefore is suitable for younger patients with no signs of osteoporosis (bone degenerate disease) (Black *et al.*, 2007).

One of the most common modes of failure is aseptic loosening of the femoral stem, initiated by the release of polyethylene wear particles. It is well documented that these particles can cause rapid bone loss, known as osteolysis. This occurs over

a sequence of metabolic activities involving phagocytic cells and macrophages (Shanbhag *et al.*, 2007).

1.6.6 New and Future Therapies

Recently, new therapies have been developed with the aim to delay the implantation of total joint replacement. Microfracture is a relatively new technique where the surgeon creates a perforation in the subchondral bone to stimulate the marrow; promoting cartilage re-growth around the defect (McGill *et al.*, 2010). Osteochondral graphs can be used to replace the affected part of the joint. When many osteochondral graphs are needed due to the large size of the defect, it is known as mosaicplasty (Bentley *et al.*, 2003). This is commonly performed on the knee, however can be used for the hip.

Tissue engineering (also known as regenerative medicine) is a growing area that incorporates the principles of engineering and biological sciences to repair tissue. It generally involves either the *in-situ* mobilisation or the implantation of cells to eventually restore the micro-architecture of tissue. The stereotypical process of tissue engineering is to attach the selected cells onto a scaffold (known as seeding), supply the scaffold with nutrients and mechanical stimuli that aids tissue growth, and then finally implantation.

Studies that have examined the use of tissue engineered cartilage as a replacement for degraded cartilage have shown inferior friction and wear characteristics when compared to native cartilage (Morita *et al.*, 2006; Plainfosse *et al.*, 2007). However, the use of tissue engineering in the repair of articular cartilage is still in its infancy and the hope is that eventually this extremely low invasive technique can restore the function of the joint by replacing the damaged parts with a material that will grow and adapt in unison with the patient's body.

1.7 Lubrication of the Synovial Joint

Cartilage is an exceptional material. It is able to resist large cyclic loads in excess of 10,000 times a day and yet still provide smooth motion. The friction coefficient has been measured to be as low as 0.005 (Dowson and Wright, 1981).

The tribological mechanism of cartilage is still an area of great controversy; however, it is commonly understood that due to the complex nature of synovial fluid, it is not possible to describe the tribology of the natural joint with a single lubrication theory, boundary, fluid film, and biphasic lubrication should be considered. Specific wear mechanism and studies that investigate the tribology of cartilage will be discussed in subsequent sections.

1.7.1 Boundary Lubrication

Boundary lubrication is present when the fluid film thickness is smaller than the average surface roughness; hence, surface to surface contact occurs. Boundary lubrication is more likely to occur during low speeds such as walking after standing still for a finite period of time (Unsworth, 1991). In this scenario, the interaction of lubricant molecules within the film or surface layer determines the load bearing properties of articular cartilage. This interaction of molecules is important for the maintenance and protection of articular cartilage. The main molecules involved with the protection of articular cartilage are hyaluronic acid (HA), proteoglycan 4 (PRG4), and surface-active phospholipids (SAPL) which are all found in the synovial fluid. The details of these molecules are described in Section 1.2.4. Each molecule is ideally positioned to interact with and adsorb to the articular surface, giving articular cartilage its unique and exceptional tribological properties (Schmidt *et al.*, 2007).

1.7.2 Fluid Film Lubrication

Fluid film lubrication occurs when there is complete separation of the two bearing surfaces, allowing low frictional motion. Fluid film lubrication can be split up into diverse mechanisms depending on the load applied, type of motion and the properties of the fluid. The different mechanisms are discussed below.

<u>Hydrodynamic Lubrication</u>

Hydrodynamic lubrication occurs when the lubricant generates lifting forces, as the soft bearing surfaces form a wedge shaped gap (Figure 1-12). In order to

generate enough lifting force, the lubricant (synovial fluid) must be viscous and the relative speed of the articulating surfaces must be large and continuous.

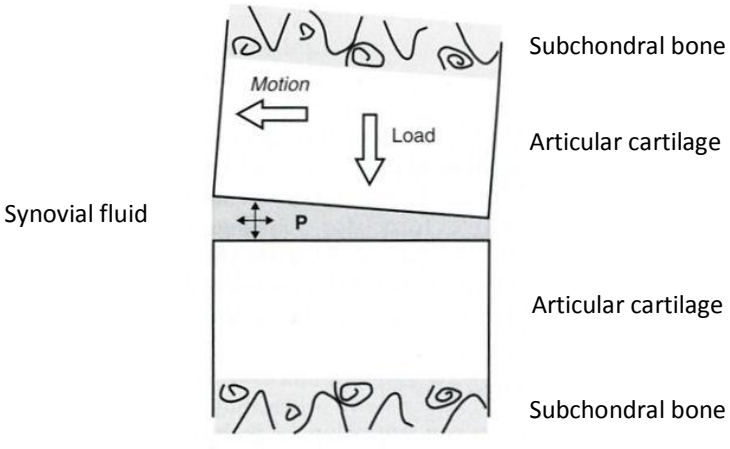

Figure 1-12: The wedge effect of hydrodynamic lubrication. (Nordin and Frankel, 2001).

Elastic-hydrodynamic Lubrication (EHL)

Similar to hydrodynamic lubrication, elastic-hydrodynamic lubrication (EHL) assumes complete separation of the two bearing surfaces. However, due to the elastic nature of articular cartilage, EHL suggests that the pressure generated during compression of the joint could deform the surface (Wright and Dowson, 1976). This would reduce the roughness of the articular cartilage surface and hence less relative speed and separation of the articulating surfaces is needed to allow hydrodynamic lubrication.

Squeeze-film Lubrication

It was suggested by Fein (1967) that hydrodynamic lubrication would occur to overcome the viscous resistance of the flowing synovial fluid, even without any relative motions. This phenomenon was named “squeeze-film” lubrication. Squeeze-film lubrication occurs when the two opposing surfaces move normally, closing the gap which separates them (Lo *et al.*, 2002). This increases internal pressure which forces the fluid to flow out of the gap tangentially (Figure 1-13) (Lo *et al.*, 2002). Squeeze-film lubrication is highly dependent on the viscosity of the synovial fluid and is limited to high loads subjected normally through the centre of the hip joint over a short period of time (Fein, 1967).

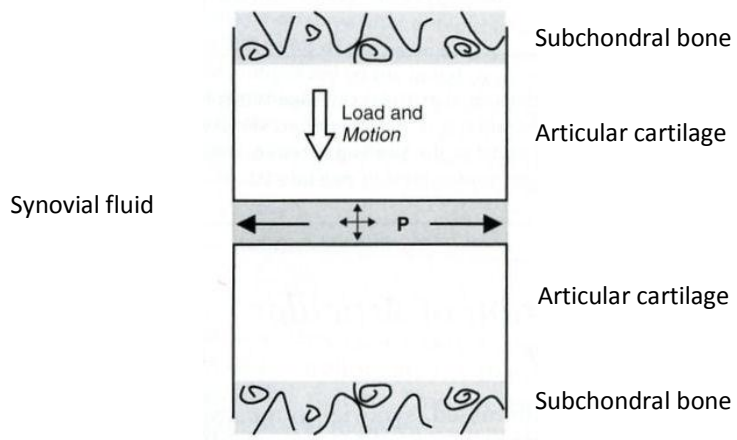

Figure 1-13: Squeeze-film lubrication theory. (Nordin and Frankel, 2001).

Boosted Lubrication

Boosted lubrication is thought to act in conjunction with squeeze-film lubrication (Walker *et al.*, 1968a; Walker *et al.*, 1970; Lo *et al.*, 2002). Due to the permeability of articular cartilage; as the joint is loaded, the increased pressure of the synovial fluid forces small molecules (such as water and electrolytes) into the cartilage matrix (Figure 1-14). This leaves a more viscous fluid, with an increase in hyaluronic acid and protein concentration, which acts as a more efficient lubricant. Boosted lubrication could also increase the effect of squeeze-film lubrication due to being a lubricant viscosity dependant theory.

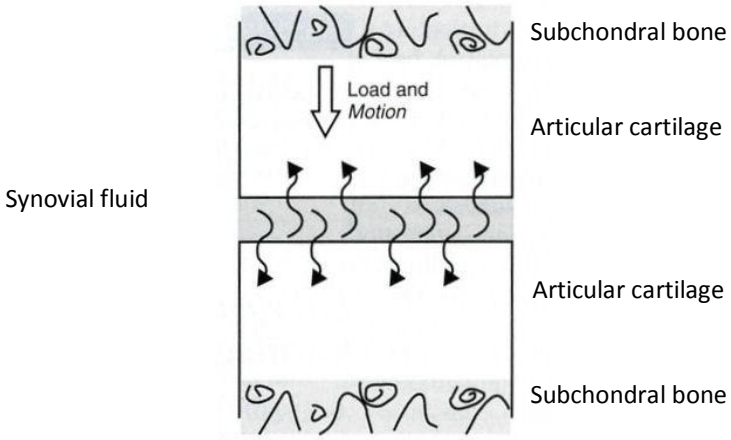

Figure 1-14: Boosted lubrication. The black arrows indicate the flow of the smaller molecules such as water and electrolytes. (Nordin and Frankel, 2001).

Weeping Lubrication

Lewis and McCutchen (1959) were the first to suggest self pressurised hydrostatic “weeping lubrication” occurs in the synovial joint, often in conjunction with EHL. As the bearing surfaces move closer together in the normal axis, pressure

within the cartilage matrix increases. This expels fluid contained within the ECM of the articular cartilage, which then acts as a thin layer of lubricant (Figure 1-15) (Lewis and McCutchen, 1959). This theory was examined by Mow and Lai (1980) using a thin layer of biphasic medium supported by a hard bony substrate as a model. A constant-width, parabolically distributed normal load sliding over the opposing surface at a constant speed was used to simulate the hydrostatic pressure of the synovial fluid. This experiment aimed to find out whether, under prescribed traction, articular cartilage could yield its interstitial fluid so it can act as a fluid film lubricant (Mow and Ateshian, 1997).

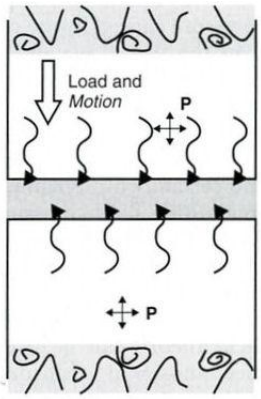

Figure 1-15: Weeping Lubrication. The black arrows represent the influx of interstitial fluid from the cartilage matrix to the joint cavity. (Nordin and Frankel, 2001).

It was shown that the fluid exuded under the leading and trailing edges of the load area, whilst the fluid in the centre resorbed back into the articular cartilage (Figure 1-16). It was suggested that the fluid exuded under the leading edge provided a sufficient amount of lubrication to lower the frictional coefficient and was termed “self-generating mechanism” (Mow and Ateshian, 1997).

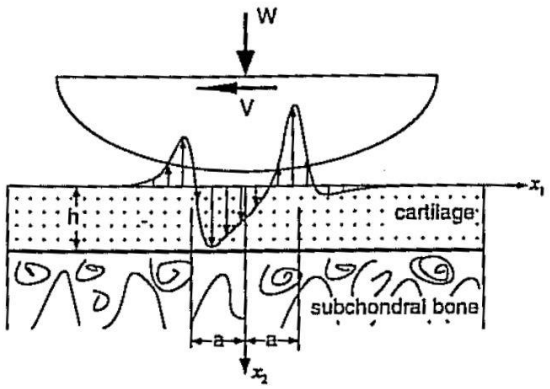

Figure 1-16: Combination of weeping lubrication (under the leading and trailing edges of the applied load) and boosted lubrication (under the centre of the applied load). (Mow and Ateshian, 1997).

1.7.3 Biphasic Lubrication

Biphasic lubrication is the most important form of lubrication. As discussed previously in Section 1.3.1, articular cartilage consists of both a solid and fluid phase, which is important for the load bearing properties of articular cartilage (Section 1.4.1). The exudation of fluid also helps to explain the "self generated mechanism" (Section 1.7.2). It is generally accepted with regards to the biphasic theory, both the solid and fluid phases are immiscible, separate and incompressible (Mow and Hung, 2001). These biphasic properties and the elastic properties of articular cartilage suggest that for many loading conditions, friction and lubrication is controlled by the proportion of the load carried by the fluid phase of the biphasic cartilage.

Forster and Fisher (1996) used a linear reciprocating motion rig and concluded that the major factor that influences the friction coefficient is the loading time/pattern. Load carried by the fluid phase reduces friction, as opposed to the solid phase. The load support by the fluid phase is time dependent and hence, prolonged loading may decrease fluid load support, increasing friction. Krishnan *et al.* (2004) also used a linear reciprocating motion rig to measure the friction coefficient and the interstitial fluid load support in bovine articular cartilage. It was hypothesised that mixed lubrication is the most common type of lubrication found in the joint. However, this was subject to factors such as sliding velocity, magnitude of load and testing configuration (Krishnan *et al.*, 2004).

1.8 Wear of Articular Cartilage

Mow and Hung (2001) define wear as the unwanted removal of material from solid surfaces by a mechanical action. Even though this is correct for most engineering situations, with regards to articular cartilage, biochemical degradation also takes place. Therefore, wear of articular cartilage can be split into two categories: mechanical wear and biochemical degradation (Mow and Ateshian, 1997).

1.8.1 Mechanical Wear

There are two types of mechanical wear: interfacial wear resulting from the interaction between bearing surfaces and/or particles and fatigue wear resulting from bearing deformation under cyclic load.

Interfacial Wear

There are two types of interfacial wear: adhesion and abrasion, both of which only occur when there is no lubricant film separating the surfaces. Adhesive wear arises when two asperities (peaks on the bearing surface) from adjacent surfaces adhere to each other. During sliding, one or both of the asperities are torn off (Mow and Ateshian, 1997; Mow and Ratcliffe, 1997; Mow and Hung, 2001).

Abrasive wear arises when a softer material is scraped away by a harder one (Mow and Ateshian, 1997; Mow and Ratcliffe, 1997; Mow and Hung, 2001). The harder material can be in the form of the opposing surface such as the artificial bearing surface in hemiarthroplasty (known as two bodied abrasion) or by a loose particle between the two surfaces such as a piece of bone, cement or bearing material (known as three body abrasion).

A study by Lipshitz and Glimcher (1979) suggests that direct contact between cartilage bearing surfaces with no intermediate lubricant film are extremely rare. This is due to the articular cartilage lubrication mechanisms, such as boosted and weeping lubrication (Section 1.7.2). However, these mechanisms are highly dependent on the impermeability of the superficial layer. Previous studies have investigated the porosity of osteoarthritic articular cartilage and found that articular cartilage with structural defects is more permeable than healthy articular cartilage. This could reduce the effectiveness of such lubrication mechanisms, increasing the probability of cartilage/cartilage contact (Akizuki *et al.*, 1986; Setton *et al.*, 1994).

Fatigue Wear

Unlike interfacial wear, fatigue wear does not occur from the surface-to-surface contact and is independent from the lubrication mechanisms. Instead, it is the result of cyclic stresses and strains generated within the cartilage, due to the

load produced during joint motion (Section 1.2.3). As mentioned previously, structural support of articular cartilage is provided by both the collagen-proteoglycan matrix and the outflow of fluid from inside the matrix (Mow and Ateshian, 1997). So therefore, repetitive loading will cause repetitive stressing/straining of the matrix and repetitive outflow/inflow of fluid. Hence, there are two methods of disruption caused by fatigue: collagen- proteoglycan solid matrix disruption and proteoglycan "washout" (Mow and Hung, 2001).

Collagen-proteoglycan solid matrix disruption occurs over a period of time. Collagen and proteoglycan molecules and/or the interface between them become damaged due to the repetitive straining. It is generally accepted that the cumulative failure of the collagen fibres is the main cause of articular cartilage fatigue (Freeman, 1975). Other reports suggest that proteoglycan population alters with age and disease, enhancing articular damage. This correlates well with certain biochemical degradation (Mow and Hung, 2001).

Loss of proteoglycan can also be the result of proteoglycan "washout". This is where the continuous and repetitive exudation and imbibing of interstitial fluid leads to proteoglycan degradation and eventually "wash out" of the matrix into the joint cavity (Mow and Hung, 2001). This decreases the stiffness of articular cartilage and hence, reduces the load bearing capacity of the tissue.

Two specific visual defects of articular cartilage have been documented by Mow and Hung (2001) (Figure 1-17). 1) Erosion of the cartilage surface; also known as smooth-surface destructive thinning. 2) Splitting of the cartilage surface, also known as fibrillations, this can propagate through the full thickness of articular cartilage.

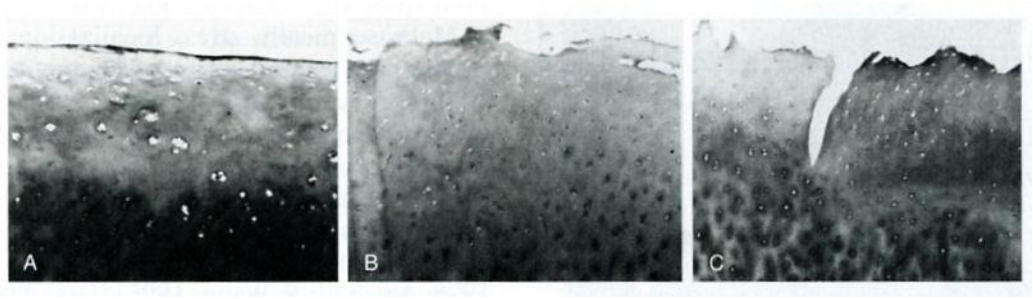

Figure 1-17: Photomicrographs displaying cross sections of A) Healthy articular cartilage, B) Articular cartilage with eroded surface, and C) Articular cartilage with a vertical split through the surface (Mow and Hung, 2001).

1.8.2 Biochemical Degradation

Mechanical wear of articular cartilage has been studied in detail; however, understanding research into biochemical degradation is still at an early stage. The complex nature of articular cartilage and its delicate equilibrium state with the surrounding chemical environment means that any small alteration to this balance can cause major changes in response to stress and strain.

Effect of Matrix Metalloproteinase and Pro-inflammatory Cytokines

Matrix metalloproteinases (MMPs) are a selection of enzymes that are designed to break down proteins found in the ECM, such as collagen and proteoglycan. As suggested by the name “metallo”, MMPs need metallic elements to fulfil their function, for example zinc or calcium atoms. Even though MMPs are usually associated with beneficial functions such as growth of new blood vessels (angiogenesis) and wound healing, there have been numerous studies suggesting that MMPs have a significant role in the degradation of articular cartilage during OA (Sandell and Aigner, 2001).

The synthesis of MMPs is regulated by chondrocytes. There is a general acceptance amongst researchers that the response to pro-inflammatory cytokines (a signalling protein), such as tumour necrosis factors (TNFs) and interleukin-1 (IL-1), causes the regulation of MMPs (Shlopov *et al.*, 2000).

The first study that suggested collagenase (a type of MMP) may be related to the degradation of articular cartilage was conducted by Ehrlich *et al.* (1977). OA and healthy human cartilage were cultured for seven days and the medium was

histologically assessed for the presence of collagenase. Even though no collagenase was found in either OA or healthy human articular cartilage, activity occurred when the specimens were pre-incubated with tripsin. So therefore, it was hypothesised that tripsin halted the activity of a potent inhibitor present in the culture media, thus allowing the collagenase activity to occur. Ehrlich *et al.* (1978) continued to examine the effect of collagenase on the degradation of articular cartilage and found that healthy cartilage contained very low levels of collagenase compared to cartilage with severe OA.

Since then other studies have also studied the correlation between MMPs and OA degradation. Tetlow *et al.* (2001) examined the effect of six MMPs (1, 2, 3, 8, 9, and 13), and two pro-inflammatory cytokines (IL-1β and TNFα) with the use of immunohistochemistry. MMPs 1, 3, 8, 13, IL-1β and TNFα were found to be most predominant in the superficial zone of cartilage with either some surface erosion or deeper surface erosions, when compared to the healthy articular cartilage; especially in areas of degradation, wear and high chondrocyte density. However, this diversity was reduced when comparing the deeper zones, where the articular cartilage was found to be unaltered and healthy. It was further suggested that this result supports the theory that the MMP-cytokine relationship is associated with an altered chondrocyte phenotype and advancing articular cartilage degradation during OA.

Changes in Structure and Orientation of Proteoglycan

Due to a positive correlation between the reduction of proteoglycan content and severity of disease, aggrecan constituents are the first to be affected (Martel-Pelletier *et al.*, 2008). As mentioned previously, proteoglycan breaks down along with collagen due to the degrading action of MMPs. However, the structure and orientation of proteoglycan also becomes altered in a variety of ways (Martel-Pelletier *et al.*, 2008).

Dunham *et al.* (1990) examined the changes in the orientation of proteoglycan during early OA. Polarised light microscopy of the birefringence brought on by Alcian blue staining was used to examine proteoglycan in healthy and OA murine (mouse) articular cartilage. Even though there is little change in

proteoglycan content of mice under the age of 30 weeks, disorientation of proteoglycan occurred more readily in the OA cartilage. Dunham *et al.* (1990) hypothesised that this disorientation can lead to increased free water content characteristics, which can alter the biomechanical properties of osteoarthritic articular cartilage. However, Dunham *et al.* (1990) only compared the articular cartilage of the lateral condoyle with that of the medial condoyle. This method was chosen because the lateral side of the joint "appeared" to remain unaffected by the disease. This presumably was decided upon visually, with no histological assessment performed. Also, Dunham et al. could only look at the medial zone of the articular cartilage due to the thin murine articular cartilage. As discussed in Section 1.3.1, proteoglycan orientation varies throughout the whole thickness of articular cartilage, so therefore this is another limitation of the Dunham *et al.* (1990) study. Nevertheless, this theory of proteoglycan disorientation is in agreement with other studies such as Wells *et al.* (2003) who suggested proteoglycan disorientation alters osmotic swelling and other interactions associated with the biomechanical properties of articular cartilage.

A review article by Freemont and Hoyland (2007) explored the morphological and histological changes of the musculoskeletal system due to age. It was suggested that as articular cartilage increases in age, the hyaluronan filament and aggrecans becomes shorter and lengths of the aggrecans become more varied (Figure 1-18). It was also concluded that the structural alteration of proteoglycans is the most predominant age related change observed in articular cartilage.

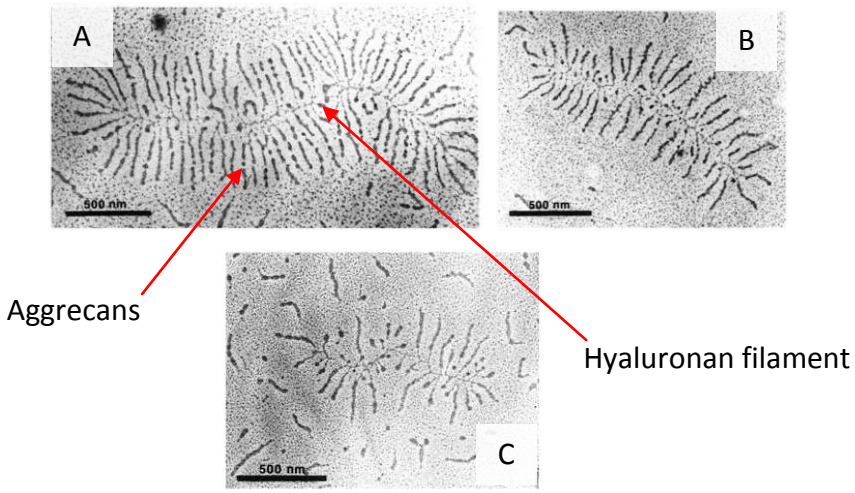

Figure 1-18: Changes of the proteoglycan in bovine articular cartilage due to age visually captured using SEM. A) A young fetal proteoglycan aggregate. B) A "skeletally immature" cow. C) A "skeletally mature" cow (Martin and Buckwalter, 2002).

This has been linked to age related changes to link proteins that facilitate a connection between the aggrecans and hyaluronan filaments (Martin and Buckwalter, 2002). An alteration such as this could reduce the tensile stiffness and strength of articular cartilage, leading to degeneration and increased risk of injury.

1.9 *In-vitro* Methods of Measuring Cartilage Tribology

Tribology is a collective term associated with the measurement of wear, friction and lubrication of two articulating surfaces. *In-vitro* analysis of cartilage tribology is extremely common. The following describes the parameters that are commonly measured and techniques that are used in cartilage tribological studies.

1.9.1 Friction

Friction Coefficient and Frictional Force

It is commonly accepted that "friction is the resistance to motion during sliding or rolling that is experienced when one solid body moves tangentially over another with which it is in contact" (Bhushan, 2002). Frictional force (F) is the force that resists the motion, acting in the opposite direction to the motion. The relationship between frictional force and normal load applied to the articulating bearing (W) is the coefficient of friction (μ).

$$\mu = \frac{F}{W} \tag{1.1}$$

Friction coefficient of cartilage has been a subject of interest since the 1930's (Jones, 1936). The majority of studies that examined friction of cartilage used a simple geometrical model such as a pin-on-plate where a cartilage plug articulates against a counter face; either cartilage or synthetic material such as glass or metal. Forster and Fisher (1999) examined the friction coefficient of cartilage against metal during continuous sliding. Cartilage pins were reciprocated against surgical grade stainless steel plate for up to 120 minutes and the real time friction was recorded. It was shown that the friction coefficient increased over time from 0.1 after 5 minutes to 0.6 after 2 hours (Figure 1-19). This gradual increase in friction was later correlated with interstitial load support using a similar setup to Forster and Fisher (Krishnan *et al.*, 2004). During continuous sliding, fluid is expelled from the cartilage and hence, fluid load support reduces. This increases the friction between the surfaces. Therefore, the friction of cartilage is governed by the biphasic nature of the cartilage tying together the theories of biphasic mechanical properties (such as stress relaxation and creep) presented in Section 1.4.4 and biphasic lubrication presented in Section 1.7.3.

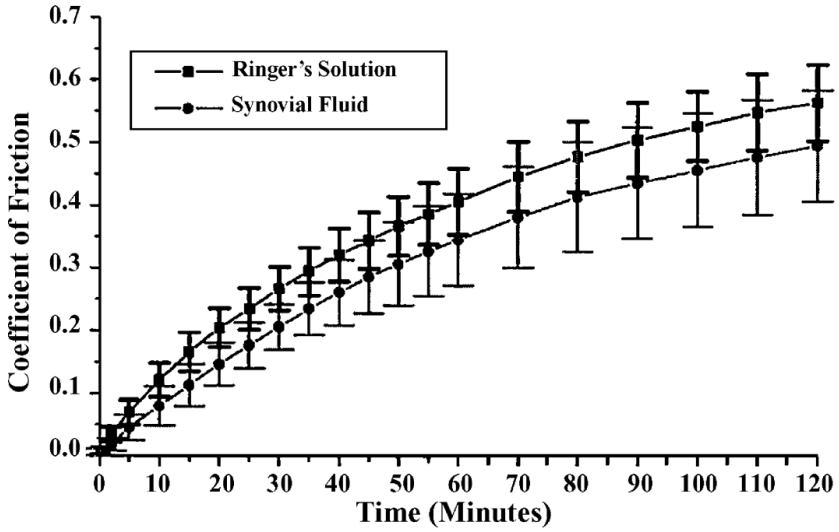

Figure 1-19: Friction of articular cartilage plug against a metal plate counter-face with Ringer's solution and synovial fluid at the lubricant (n=9) (Forster and Fisher, 1999).

Frictional Shear Stress

Frictional shear stress is an important factor in cartilage tribology; as it governs cartilage wear (Lizhang, 2010). Frictional shear stress (S_μ) is the shear stress created within the bearing material during articulation and is calculated by the following equation:

$$S_\mu = \frac{\mu \times W}{A} = \frac{F}{A} \tag{1.2}$$

Where W is the applied load and A is the contact area. There are a few studies that examined the relationship between frictional shear stress and contact stress. Walker *et al.* (1968) was one of the first to examine this relationship using a cartilage pin on glass model. The cartilage plugs were extracted from a variety of cadaveric joints from a wide range of age groups. A boundary lubrication regime was assured by preloading the cartilage pins for 30 minutes prior to friction testing. It was found that the relationship between contact stress and frictional shear stress was not linear. Instead, the gradient was large at lower contact stresses and gradually decreased with increasing contact stress (Figure 1-20).

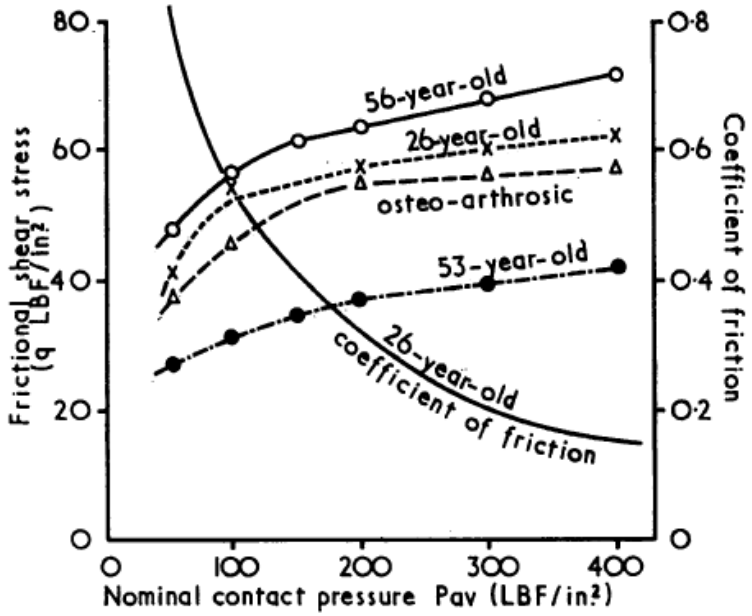

Figure 1-20: Correlation between frictional shear stress and contact stress on cartilage samples taken from cadaveric joint with a variety of ages (Walker *et al.*, 1968b).

Both frictional shear stress and contact stress are proportional to the frictional force and the normal load respectively. Therefore, the gradient of the

lines shown in Figure 1-20 is proportional to the friction coefficient. Hence, the change in gradient confers with the results found when comparing coefficient of friction and contact stress.

1.9.2 Radiographic Imaging

Magnetic resonance imaging (MRI) has increasingly been used to examine patients with hip pain clinically. However, as well as clinical *in-vivo* examinations, MRI has also recently been used to assess the *in-vitro* wear and degradation of articular cartilage. Using a delineation technique, Wang *et al.* (2008) investigated the capability of a 9.4 Tesla MRI machine to detect subtle wear or lesions (Figure 1-21).

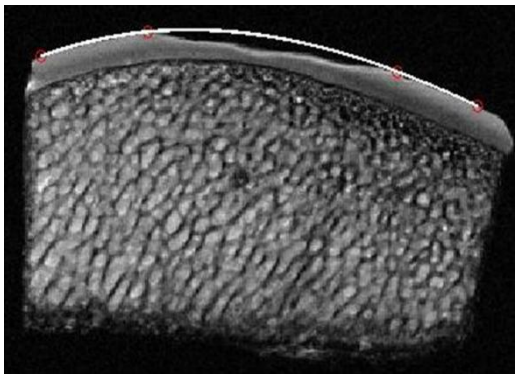

Figure 1-21: The curve fit on the MR image produced by the MATLAB™ code (Wang *et al.*, 2008).

It was concluded that high field MRI is capable of detecting volume of material lost during wear for *in-vitro* tribological studies (Wang *et al.*, 2008). However, due to the power of the MRI machine, there is a limit to the size of the sample which can be tested.

1.9.3 Surface Topography

It is generally accepted that an important factor in wear is surface structure. Surface topography aims to describe the surface in terms of its features. There are many different techniques used to measure surface topography such as scanning electron microscopy, transition electron microscopy (Forster and Fisher, 1999), atomic force microscopy (Park *et al.*, 2004) and non-contacting white light interferometry (Graindorge *et al.*, 2006). These studies aimed to observe and in

some cases quantify the changes in surface topography after tribological testing. However, due to the high water content of cartilage, use of characterising the surface as a measure of wear is extremely limited and hence used in conjunction with other wear measuring techniques.

Lizhang (2010) used stylus profilometry to measure wear volume. A mould replica was created of the cartilage surface after a tribological test. The stylus profilometry used a diamond tipped stylus to trace across the wear scars on the replica. Approximately 20 traces were performed (0.5 mm apart) perpendicular to the wear scars' direction. By removing the "form" and hence flattening the surface and creating a line of best fit between the unworn surfaces either side of the wear scars; the area under this line was taken as the cross-sectional wear area. Multiplying each cross-sectional wear area with the distance between each trace allows the wear volume to be calculated. It has been previously reported that the average roughness of native cartilage is between 1 – 2 µm (Katta, 2007; Northwood *et al.*, 2007; McCann, 2009). However after tribological testing the cartilage Lizhang (2010) measured the average roughness to be 5.59 – 7.85 µm.

1.9.4 Histological Assessment

As discussed previously, wear of articular cartilage involves both mechanical wear and biochemical degradation. Histology is specifically used to examine the microscopic components of biological tissue and can be used to identify the occurrence of biochemical degradation.

The stereotypical process of histological assessment is common throughout many studies and generally involves fixation, dehydration, paraffin embedding, sectioning and staining (An and Martin, 2003). The choice of stain will primarily depend on the tissue component in question. Histological stains can be categorised into acidic or basic compounds each attracted to a specific type of tissue. For example; a tissue that attracts a basic stain is labelled "basophilic", and "acidophilic" for tissues components that attract acidic stains (Junqueira and Carneiro, 2005).

Hematoxylin is a common basic stain, staining basophilic tissue components such as GAGs. This is because GAGs have an acidic composition so react and ionise

well with hematoxylin. Eosin is a common acid dye, staining acidophilic tissue components such as collagen. The combination of hematoxylin and eosin (H&E) has the ability to stain both GAGs blue and collagen pink allowing easy differentiation between the two. This large advantage makes H&E the most commonly used stain in histological assessment to show the general architecture of a tissue (Junqueira and Carneiro, 2005).

Since the late 19th century, histology has been used as a qualitative method, providing visual representation of the microstructure of the tissue. However, the development of a histological grading system to assess OA progression in relation to the tissue's matrix was initiated in the mid 20th century (Bennett, 1942). The most commonly used grading system is the Mankin score (Mankin *et al.*, 1971). Developed in the early seventies, the Mankin score was used to classify the degree of cartilage degradation of certain small areas of the femoral head with respect to the tissue's microstructure. Both H&E and safranin-O green-iron hematoxylin stains were used to study matrix structure, cell population and proteoglycan density (safranin-O stain distribution). The integrity of the tide mark was also examined (Table 1-4). The total of all the criteria's scores was calculated, resulting in a score out of 14; where 0 was healthy and 14 was the most severely degraded.

Table 1-4: The histological-histochemical grading system (Mankin *et al.*, 1971)

	Grade		Grade
I. Structure		III. Safranin-O staining	
a. Normal	0	a. Normal	0
b. Surface irregularities	1	b. Slight reduction	1
c. Pannus and surface irregularities	2	c. Moderate reduction	2
d. Clefts to transitional zone	3	d. Severe reduction	3
e. Clefts to radial zone	4	e. No dye noted	4
f. Clefts to calcified zone	5		
g. Complete degradation	6		
II. Cells			
a. Normal	0		
b. Diffuse hypercellularity	1	IV. Tidemark	
c. Cloning	2	a. Intact	0
d. Hypocellularity	3	b. Crossed by blood vessels	1

Similar to all grading systems (histological, arthroscopic, etc), the inter- and intra-observer reliability of the Mankin grading system is a concern. A study that investigated the inter- and intra-observer variability of the Mankin grading system

concluded that even though there was more variability than expected, it still produced adequate results (van der Sluijs *et al.*, 1992). Another limitation is that it does not include other defects such as osteophyte formation and tidemark reduplication. Therefore, other studies have attempted to modify this scoring system (Gahunia *et al.*, 1995).

1.9.5 Macroscopic Observations/Grading

Macroscopic observations are commonly used in clinical arthroscopy of the hip, because they are relatively low invasive methods of examining the severity of osteoarthritis *in-situ* compared to open surgery, without causing damage to the cartilage. Many grading systems have been developed to semi-quantify the observations including Société Française d'Arthroscopie (SFA) scoring system (Dougados *et al.*, 1993), American College of Rheumatology/Knee Arthroscopy Scale (ACR/KAOS) (Klashman *et al.*, 1995), International Cartilage Repair Society (ICRS) wear grade system (Peterson *et al.*, 2000), and the Oswestry Arthroscopy Score (OAS) (Smith *et al.*, 2005). The common connection between all the scoring systems is that they all multiply the degree of cartilage damage with the size of the defect. Where they differ is how the different defects are characterised and quantified. Recently, grading systems such as these have been adapted in the evaluation of cartilage wear after *in-vitro* tribological test (Lizhang, 2010).

1.9.6 Biochemical and Wear Debris Characterisation

In 1975, Lipshitz attempted to find an accurate "chemical index" to assess the *in-vitro* wear of cartilage (Lipshitz *et al.*, 1975). The method proposed was to assess the hydroxyproline content in the serum after testing due to being almost an exclusive constituent of collagen. There was a concern that there is a higher population of collagen on the articular cartilage surface compared to the deeper zones which could affect the wear analysis (overestimating the initial wear). Therefore, Lipshitz also assessed the collagen concentration through the entire thickness of articular cartilage to assess the collagen concentration gradient. Over 10% of hydroxyproline and 50-60% of GAGs was dissolved in the lubricating fluid.

Thus, both the solid wear debris and the lubricant solvent must be analysed to calculate the articular cartilage wear.

It was concluded that, except for the top of superficial zone, the collagen concentration (unlike previous studies) was uniform throughout the cartilage thickness. This coupled with the virtual insolubility of the solid articular cartilage wear debris allows the measurement of hydroxyproline to be a suitable method of determining articular cartilage wear (Lipshitz *et al.*, 1975). This is true as long as both the solid and fluid (lubricant) were analysed for reasons described above (Lipshitz *et al.*, 1975).

1.10 Current Studies on the Effect of Contact Mechanics on Cartilage Tribology

It has been suggested that frictional shear stress is a major factor in the mechanical degradation and fibrillation of cartilage. This has been attributed to microstructure of cartilage which has low resistance to shear stress due to its biphasic nature. Contact stress is directly related to frictional shear stress (Section 1.9.1) and hence, the relationship between contact stress and cartilage tribology has been as subject of great interest (Malcom, 1976; Forster and Fisher, 1996; Wang and Ateshian, 1997; Pickard *et al.*, 1998; Ateshian *et al.*, 2003; Katta *et al.*, 2007).

1.10.1 Simple Geometrical *In-vitro* Models

Earlier simple geometrical models such as the study conducted by Malcom (1976) varied the contact stress from 0.05 to 0.1 MPa in saline lubricant by counter-rotating cartilage surfaces under constant load with known contact areas. A slight decrease in the equilibrium frictional shear stress was found. However, by increasing the contact stress further from 0.1 to 0.5 MPa, an increase in frictional shear stress was observed.

Forster and Fisher (1996) articulated an osteochondral pin on a metal plate to compare friction of cartilage under a contact stress of 4 MPa and 0.5 MPa, using 3 mm and 9 mm pins respectively. By preloading the cartilage plug with a static load

for various lengths of time, the mixed or boundary lubrication regime of cartilage could be simulated (Section 1.7). For instance, by extending the period of preload from five minutes to 45 minutes, most of the fluid was exuded from the cartilage matrix and hence, the majority of the load was supported by the solid phase; promoting boundary lubrication. No difference was seen in the equilibrium coefficient of friction after five minutes of preloading between 4 MPa and 0.5 MPa contact stresses. However, a slight decrease in equilibrium coefficient of friction was observed when the contact stress increased from 0.5 MPa to 4 MPa after 45 minutes of preload. This suggests that the effect of contact mechanics on the coefficient of friction depends on the lubrication regime. A similar result was found in a study by Pickard et al. (1998), who also used a 3 mm diameter cartilage pins articulating against polished CoCr plates to examine the effect of different contact stresses on cartilage friction. Three different contact stresses were used 0.5, 2 and, 4 MPa with comparable articulating conditions as Forster and Fisher.

Katta *et al.* (2007) articulated a cartilage pin on a cartilage plate under a constant load and measured the resulting friction coefficient. A strong relationship was found between friction and contact stress, whereas the contact stress increased, the friction coefficient decreased. In an attempt to investigate this relationship between contact stress and cartilage friction coefficient, Katta *et al.* (2007) used a finite element model to assess the fluid load support of articular cartilage tissue at different applied loads and hence, contact stresses. The results showed that the magnitude of the load supported by the fluid phase of the cartilage increased with applied load. The results also suggest that the percentage fluid load support was unaffected by applied load throughout the test. This should have suggested that the load carried by the solid phase should have increased with an increase in applied load. Thus, the ratio between the frictional force and the applied load and hence, the friction coefficient should remain constant. However, this was not the case. Instead, friction coefficient of cartilage reduced with an increase in applied stress. This suggested that the frictional force did not increase proportionally with the applied load and thus an “extraneous factor” other than the fluid load support has an effect on the friction of cartilage. It has been suggested that this “extraneous factor” could be flattening of the cartilage surface

asperities or the forces which are present between surface molecules. Another suggestion was that the boundary lubricant molecules are excluded from within the cartilage onto the contact surface under the larger contact stresses.

However, it was demonstrated that there was a limit to this inverse relationship between the contact stress and friction coefficient. Even though increasing the contact stress from 0.2 to 0.5 MPa decreased the coefficient of friction; when subjected to high contact stresses (up to 3.15 MPa), the coefficient of friction increased (Figure 1-22) (Katta *et al.*, 2007; Katta *et al.*, 2008).

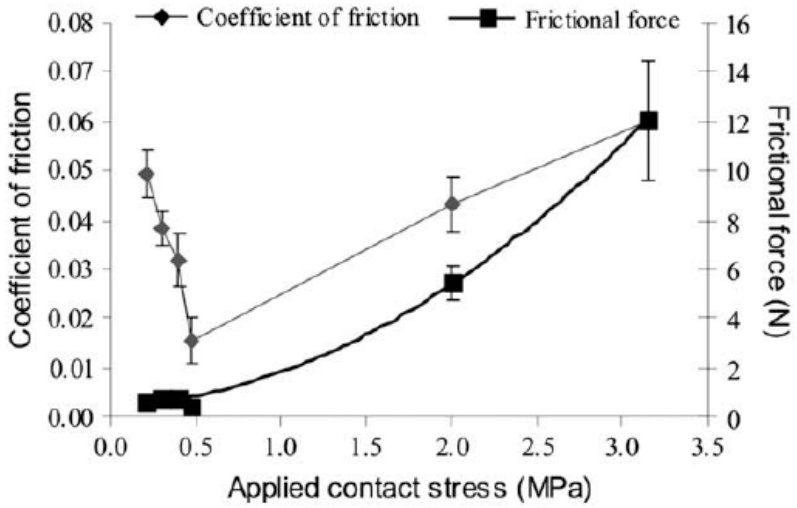

Figure 1-22: The effect of increasing the applied contact stress on the coefficient of friction (Katta *et al.*, 2007; Katta *et al.*, 2008)

The proposed reason for this increase in coefficient of friction was that at higher stress states, the cartilage failed to rehydrate as effectively as it did at the lower stress states; reducing the fluid load support. To test this, Katta *et al.* (2008) applied 3.15 MPa during a pin-on-plate tribological study but used two different stroke lengths; 4 mm and 10 mm. The theory was that even for the larger stress state, the longer stroke length allowed the cartilage to recover and hence lowering the friction coefficient. This proved to be correct, where by using a 10 mm stroke length under 3.15 MPa contact stress, the friction coefficient was similar to using a stroke length of 4 mm under 0.5 MPa contact stress.

All these *in-vitro* studies use simple geometrical models such as pin-on-plate, which have provided useful information regarding the friction and wear of articular cartilage under a variety of contact conditions. However, it is difficult to compare

the loading and unloading of cartilage to that of an entire joint; due to altered motions, forces and cartilage coverage. Hence, this will have an effect on the coefficient of friction. Simple geometrical studies also limit the parameters that can be investigated, such as the effect of radial clearance under physiological loads and motions. These parameters are likely to be important clinically.

1.10.2 Complex Geometry *In-vitro* Models

There are only a few studies that used a natural joint simulation to examine cartilage tribology *in-vitro* (Muller *et al.*, 2004; McCann *et al.*, 2009a; McCann *et al.*, 2009b; Lizhang, 2010). Lizhang (2010) was the only previous study that investigated the effect of femoral head and acetabulum clearance on the wear and friction of cartilage under dynamic loading after the implantation of a hip hemiarthroplasty. This could only be achieved by using an *in-vitro* model with anatomical comparable geometry. It was found that increasing the clearance between the femoral head and acetabulum, and hence increasing the peak contact stress from 5.6 MPa to 10.6 MPa; the friction coefficient after two hours of testing reduced from 0.16 to 0.08. It must be recognised in this study, contact stress was increased by increasing clearance in the joint, which allowed for greater translation of the contact over the cup surface during the cycle. Similar effects of contact stress may not have been found if clearance had been fixed and load varied. By altering the clearance between the femoral head and acetabulum, the relationship between contact stress and coefficient of friction could be examined in a more clinically comparable model. An inversely proportional relationship between contact stress and coefficient of friction was observed. This compares well with the previous simple geometrical model studies (Forster and Fisher, 1996; Katta et al., 2007; Katta et al., 2008)

The only other study that has assessed a natural hip hemiarthroplasty model *in-vitro* was by Müller et al. who compared friction when using a metallic and ceramic femoral head against both a porcine and cadaveric human acetabulum (Muller *et al.*, 2004). It was found that the mean coefficient of friction of the porcine acetabulum was 0.017–0.082 for ceramic and 0.020–0.101 against metal.

The mean coefficient of friction of the cadaveric human acetabulum was 0.017–0.083 for ceramic and 0.019–0.118 for metal.

1.11 Summary of Literature and Research Scope

Earlier studies that used simple geometrical *in-vitro* models have found a complex relationship between contact stress and cartilage tribology. However, to date, studies that have investigated the relationship between contact stress and coefficient of friction with the use of natural joint simulation are limited. All these *in-vitro* studies were no longer than a couple of hours, due to the complexities which govern tissue degradation and contamination. This is a relatively short period of time compared to tribological studies of total joint replacements and is a limitation with regards to drawing conclusions that might affect clinical practice. It was hypothesised that more information could be gained from increasing the duration of testing. Therefore, to address this research gap, a medium term tribological system must be developed and validated.

Hemiarthroplasty of the hip is a common procedure performed on elderly patients who have suffered a femoral neck fracture after trauma. Studies have shown that the prevalence of femoral neck fractures increase with age exponentially (Carroll *et al.*). Due to the aging population, the total number of hip fractures is expected to rise. This could explain an increase of 20,000 reported cases of femoral neck fractures from 2000 to 2010 (The Information Centre for Health and Social Care, 2011). This suggests that the number of hemiarthroplasty procedures will also increase. One of the predominant modes of failure of hip hemiarthroplasty is cartilage erosion arising from mismatching radial clearance (Johnston *et al.*, 1982; Jeffery and Ong, 2000; Sharif and Parker, 2002).

It would be beneficial to extend the period of testing beyond the two hour testing period which Lizhang (2010) achieved (Section 1.10.2). The longer term study that simulates the first several weeks post-surgery will provide better understanding of cartilage tribology after hip hemiarthroplasty has occurred.

1.12 Aims and Objectives

The primary aim of this thesis was to fully develop and validate a medium term hip hemiarthroplasty *in-vitro* system which allows tribological testing for up to a four day period. There were a series of objectives that needed to be addressed to develop and validate the proposed *in-vitro* tribological simulation system (Section 1.12.1 - 1.12.4). After which, the developed simulation system was used to investigate the effect of mismatching hemiarthroplasty clearance on cartilage tribology (Section 1.12.5).

1.12.1 Choice of Animal Model that was Used to Represent Human

The first objective was to compare porcine, ovine and bovine femoral heads to that of human, because the medium term *in-vitro* tribological study would use animal acetabulae to represent human acetabulae. Femoral heads were chosen due to tissue availability. This would allow the most appropriate animal acetabulae to be used. It would also highlight the differences between the chosen animal and human acetabulae which may affect results obtained in the medium term tribological study.

1.12.2 Lubricant and Aseptic Dissection Technique

The second objective was to explore the effect of time dependent degradation and microbial contamination on the tribological properties of cartilage. To fully understand the effects of both time dependent degradation and microbial contamination on the tribological properties of cartilage individually, one must be eliminated. Therefore, developing and refining repeatable dissection technique to obtain the animal's acetabulae in a sterile condition was a predominant part of this objective.

1.12.3 Design of "Vessel" that Housed the *In-vitro* Model

The third objective was to design a friction simulator vessel which encapsulated the hip hemiarthroplasty components. The main requirements of the

fixture were to allow a full range of motion without effecting the friction coefficient measurement, and to maintain sterility during the entire testing procedure.

1.12.4 Contact Mechanics of the *In-vitro* Model

The fourth objective was to determine the contact stress and area for the clearance groups that were used for the medium term *in-vitro* study. The shape of the contact region and the distribution of stress were also investigated.

1.12.5 Effect of Hemiarthroplasty Clearance on Cartilage Tribology

After validating the use of the animal joint (Section 1.12.1), and the chosen lubricant and dissection technique (Section 1.12.2), developing the testing apparatus (Section 1.12.3) and investigating the contact mechanics of the *in-vitro* hemiarthroplasty model (Section 1.12.4); the simulation system would be used to study the effect of mismatching the head and cup geometries on cartilage tribology.

Chapter 2: Materials and Methods

2.1 Introduction

The aim of this chapter is to describe the generic materials, instrumentation and methodologies used throughout this PhD thesis, including the calibration procedures.

2.2 Materials

2.2.1 Phosphate Buffered Saline

Phosphate Buffered Saline (PBS) was used throughout this thesis to store the osteochondral samples and to maintain cartilage hydration. PBS tablets were obtained from MP Biomedicals (OH, United States) and prepared as per the manufactures instructions. One tablet was dissolved per every 100 ml of sterile water. The constituents of the tablets are shown in Table 2-1.

Table 2-1: PBS Constituents provided by MP Biomedicals (OH, United States)

Constituents	**Concentration (mg/litre)**	**Mol. Wt. (DA)**	**Molarity (mM)**
Potassium chloride [KCl]	200.00	74.55	2.68
Potassium phosphate monobasic [KH_2PO_4]	200.00	136.09	1.47
Sodium chloride [NaCl]	8000.00	58.44	136.89
Sodium phosphate dibasic [Na_2HPO_4]	1150.00	141.96	8.10

2.2.2 Bovine Serum

Foetal calf serum (FCS) was bought from Harlan Bioproducts for Science (IN, United States, Catalogue number BT-9501-500). FCS contains a variety of constituents including several types of protein; the major proteins are shown in Table 2-2.

Table 2-2: Protein concentration in FCS from Harlan Bioproducts

Proteins	Concentration (grams/deci-litre)
Total Protein	5.0 - 8.5
Albumin	~4.0
α-Globulin	~0.7
β-Globulin	~0.6
γ-Globulin	~0.7

For all tribological studies throughout this thesis, 25% (v/v) FCS was used, in order to provide a protein concentration (16 – 18 mg/ml) similar to that of natural synovial fluid (approximately 20 mg/ml) (Wang *et al.*, 1998).

2.2.3 PMMA Bone Cement

Non-Sterile Bone Cement

Non-sterile polymethyl methacrylate (PMMA) bone cement was used to secure the porcine acetabulum into the correct position and orientation during the short term tribological tests performed on the friction simulator. Both the solid powder (Cold Cure) and liquid monomer (Rapid Repair Liquid) were obtained from WHW Plastics (Hull, UK) and mixed according to the manufactures instructions. The solid to liquid component ratio was 2:1 and this was carried out in a fume cabinet.

Sterile Bone Cement

High viscosity sterile bone cement kits (typically used in hip and knee replacement surgery) were supplied by DePuy International (Leeds, UK). Each kit contained a 40 g sachet of powder component and an 18.88 g glass vial of the liquid component. Sterile bone cement was used to secure the sterile porcine acetabulae in the latter stages of this project when sterile tribological tests were performed. Two kits (i.e. 80 g) were required for each test.

2.2.4 CoCr Femoral Heads

Cobalt chromium (CoCr) total joint replacement femoral heads were custom made by DePuy International Ltd. (Leeds, UK). These were used during the friction analysis articulating against porcine acetabular cups. A variety of diameters were used to allow control over the clearance (32, 34, 35, 36 and 37 mm). The radial

clearance was taken as the difference between the radius of the acetabulum in the anterior-posterior direction and the radius of the chosen CoCr femoral head.

The arithmetic mean roughness (Ra) of the CoCr femoral heads was determined using the Talysurf 5 model from Taylor Hobson, UK. The machine worked by traversing a diamond tipped stylus (Ø = 5 µm) across the CoCr surface rising and falling over the asperities. These produced an electrical signal which was converted to the profile of the surface. The machine has a vertical resolution of 20 nm, and a traverse speed of 0.5 mm/s and a Gaussian cut-off filter equal to 0.8 mm was used. This was performed twice on each femoral head, perpendicular to each other and averaged. The mean ± standard deviation Ra value for all the femoral heads was 0.006 ± 0.001 µm.

2.3 Specimen Preparation

2.3.1 Natural Femoral Heads

Throughout this thesis, osteochondral samples were taken from the hip joint of humans and a variety of animals. These are summarised in Table 2-3.

Table 2-3: Osteochondral samples that were used throughout this thesis, including the age and the source of the specimen.

Species	Age	Source
Human	Not Known	Leeds General Infirmary, surgery due to femoral neck fractures (NRES Committee approved, 06/MRE03/73).
Porcine	3 - 6 months	Penny's Abattoir, otherwise used for meat in food production.
Bovine	18 – 24 months	Penny's Abattoir, otherwise used for meat in food production.
Ovine	> 4 years	M&C Meats, otherwise used for meat in food production.

There is no age stated for human femoral heads due to ethical restrictions; however, the type of fracture the patients had sustained is most commonly seen in the elderly (Section 1.5.4). The human femoral heads were stored in PBS at 4^{o}C immediately after removal from the patient until transportation to the Tissue Laboratory.

2.3.2 Osteochondral Plugs

Osteochondral plugs were extracted from the femoral head from all species. A circular groove (Ø=9 mm) was created on the cartilage surface, allowing correct positioning of the plug. A stainless steel circular corer (inner Ø = 9 mm) attached to a mechanical drill was then used to drill through the bone to a depth of approximately 10 mm. A low drill speed was used to inhibit temperature increase, which otherwise would cause cartilage damage. PBS was also sprayed on the tissue throughout the coring procedure to lower the temperature from the drilling process and to hydrate the cartilage samples. The plug was extracted by inserting a stainless steel corer with a slightly larger inner diameter around the plug and with a swift, sharp motion the inferior end of the plug was snapped off. The larger inner diameter allowed the plug to be removed from inside the corer with ease. The inferior end of each osteochondral plug was flattened using a file, leaving approximately 5 – 8 mm of bone (Figure 2-1).

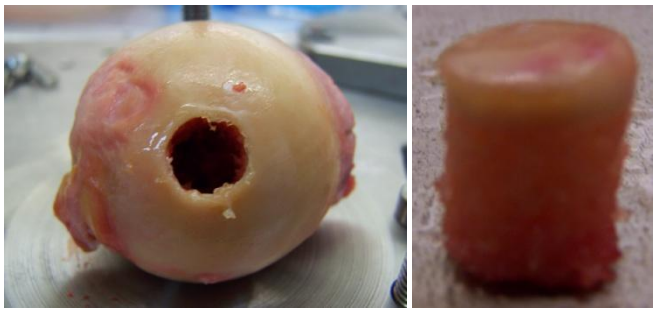

Figure 2-1: Left) Human femoral head with a core extracted from the superior region. Right) The osteochondral plug that was removed from the human femoral head.

All osteochondral plugs were visually inspected for cartilage damage or disease before freezing at -20^{o}C in PBS soaked tissue paper until further use. Previous studies have shown that this freezing process does not affect the frictional properties of articular cartilage (Forster and Fisher, 1996).

2.3.3 Acetabulae (Non-Sterile)

Porcine acetabulae were used to measure friction against cobalt chrome (CoCr) femoral heads in the pendulum friction simulator. These were obtained from porcine hind legs no longer than 24 hours after slaughter. The leg was skinned and the hip was dislocated using a scalpel (Figure 2-2). Care was taken not to

damage the cartilage on the acetabulum side. The entire pelvis was then removed from the leg and all soft tissue (muscle, ligaments and tendons) were dissected from the bone, allowing the distal end of the pelvis to be clamped tightly in the vice.

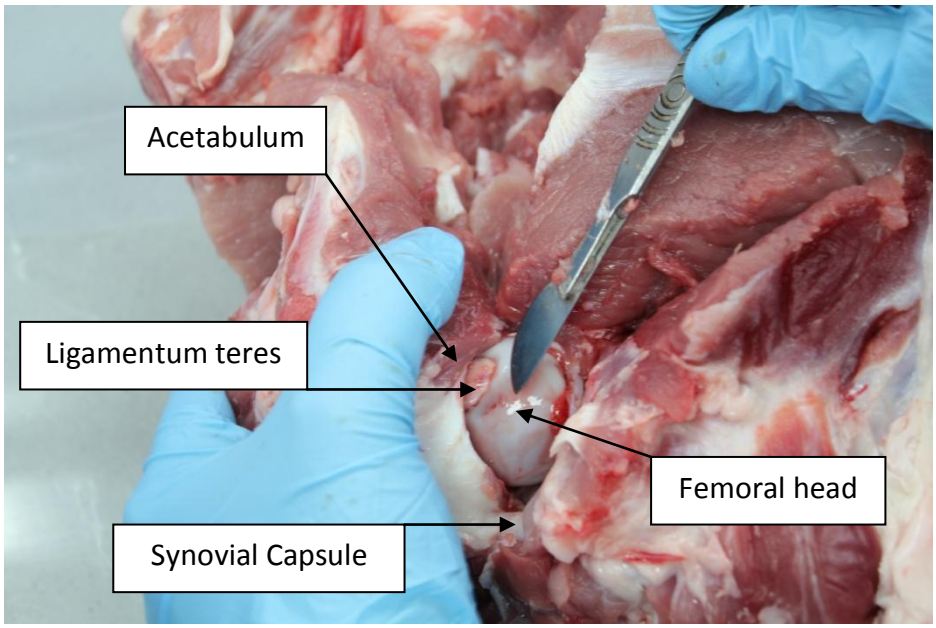

Figure 2-2: The acetabulum was dislocated from the femoral head by cutting around the synovial capsule and severing the ligamentum teres.

After clamping, the excess bone from behind the acetabulum was sawn off using a bone saw, leaving 0.5 – 1.0 mm of bone. Finally, a saw cut was made between the acetabulum and pelvis to remove the acetabulum. A PBS soaked tissue paper was placed in the articulating side of the acetabulum, inserted in a sealable bag and frozen at -20^{o}C until ready to test (Figure 2-3).

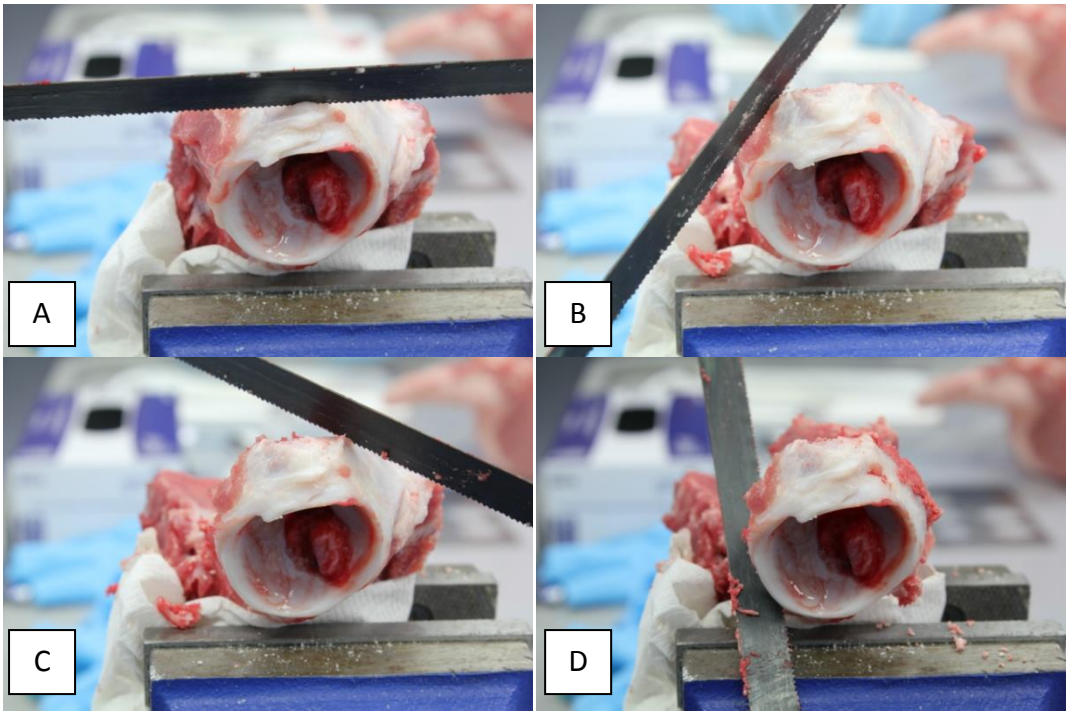

Figure 2-3: Sawing the porcine pelvis to obtain the acetabulum. A) Saw cut was made above the acetabulum, B) left hand side, C) right hand side and then D) final cut was made to remove the acetabulum

2.4 Mechanical Instrumentation and Methods

2.4.1 Indentation Rig - Biomechanical Behaviour of Cartilage

The indentation equipment was used to perform mechanical testing on articular cartilage of osteochondral plugs. The custom made indenter apparatus allowed a constant load that was applied to the articular cartilage surface through a rigid indenter (Figure 2-4). Both, a linear variable differential transducer (LVDT; RDP D5-200H; Electrosence, PA, USA) and a piezo-electric force transformer (Part No. 060-1896-02, Electrosence, PA, USA) were included in the indenter design to measure the indenter displacement and resistant force respectively. The sensitivity of the LVDT was 0.4 µm at 10 mm range and the sensitivity of the load cell was 0.04 N at a 0.1 N range. The plug was attached to the indentation rig beneath the indenter with the use of a collet. A linear bearing was used to reduce friction within the apparatus. The velocity of the descending indenter was controlled by a silicon oil-filled dashpot (to avoid the indenter impacting the articular cartilage surface). The resistive force of the dashpot was measured over a range of 1 to 25 mm/s and

the relationship between resistive force and falling velocity was linear with slope of 0.16 N/mm/s. The maximum reduction in applied force due to viscous damping was calculated to be 6.30×10^{-04} N or 0.08 % of applied force; and hence, assumed to be negligible. Data from the force transducer and LVDT were stored on a computer using LabView 8 software (National Instruments, TX, US).

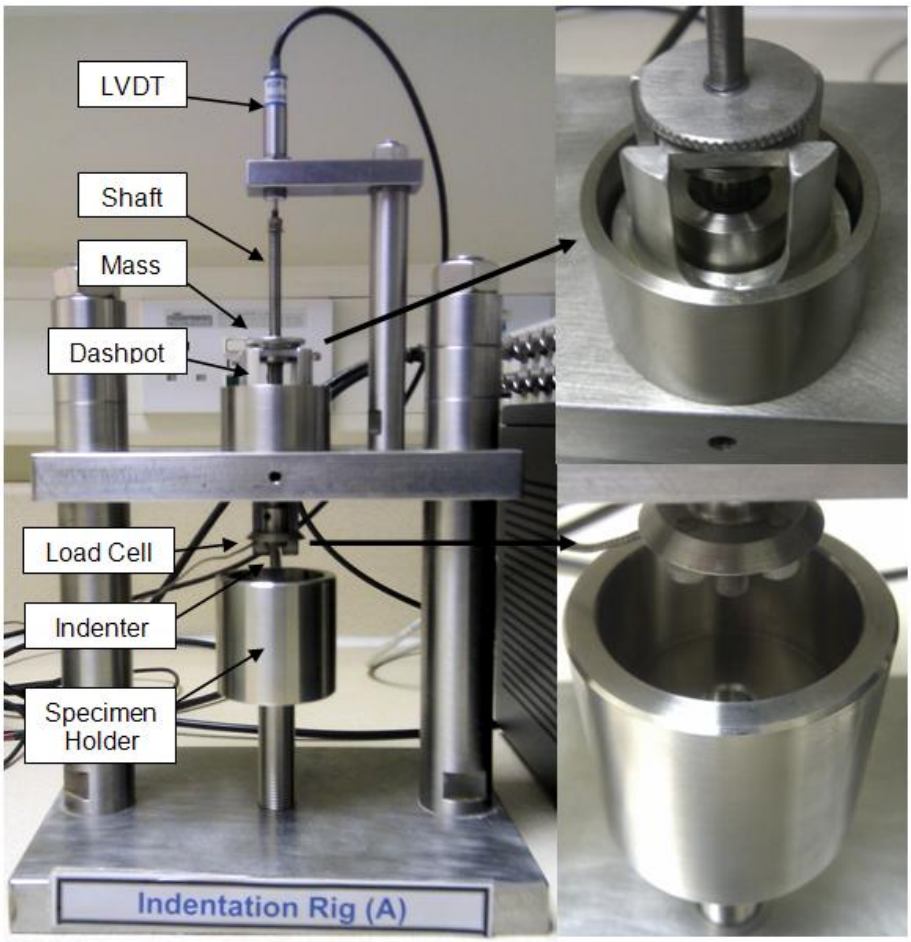

Figure 2-4: Left: Indentation apparatus, Top Right: Dashpot and Bottom Right: Specimen holder which housed the specimen in saline solution during indentation

The plugs were housed in a PBS filled stainless steel bath (Figure 2-4). The height of the bath could be altered so that the surface of the plug could be set approximately 1 mm below the surface of the indenter before testing. After releasing the indenter, the point of indenter/articular cartilage contact was taken when the load rapidly increased.

The tapped hole in the bottom end of the shaft allowed a variety of indenter tips of different shapes (needle, spherical and flat) and sizes (3-6 mm) to be attached. If a particular size and/or shaped indenter were not available, it could be

manufactured per specification. For all indentations in this thesis, a 3 mm diameter hemispherical rigid indenter was used.

Indentation Rig Calibration

The outputs of the LVDT and load cell were in voltage; therefore, calibration was required to convert these outputs into millimetres and Newtons respectively. The LVDT was calibrated using standard steel slip gauges. The output voltages from the LVDT were converted to units of displacement by recording the voltage after sequentially adding slip gauges (step increase of 0.01 mm). Output voltages were plotted against the corresponding cumulative slip gauge height and a linear trendline was plotted (Figure 2-5). The equation of the line was then used as the calibration factor converting voltage to displacement in millimetres.

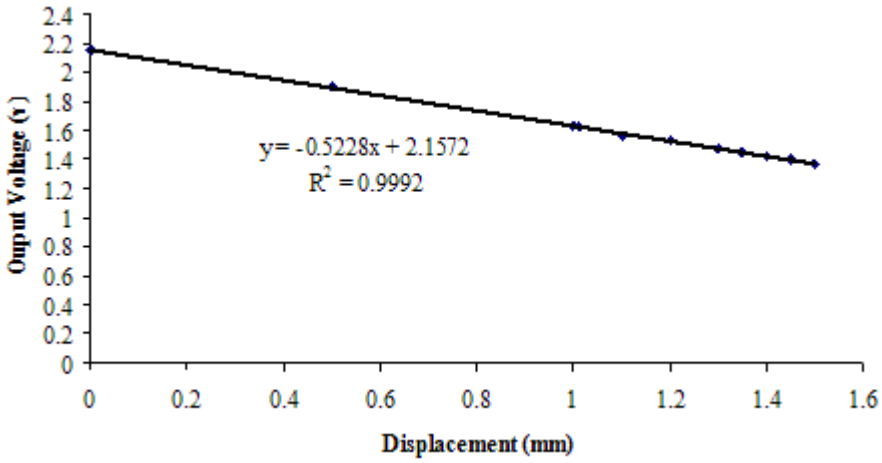

Figure 2-5: Calibration factor for the indentation apparatus to convert output voltage to displacement (mm).

A similar process was also adopted for calibrating the load cell. By incrementally adding known masses, the output voltage could be recorded. The output voltages were plotted against the corresponding masses and a linear trendline was plotted (Figure 2-6). The equation of the line was then used as the calibration factor converting voltage to force in Newtons.

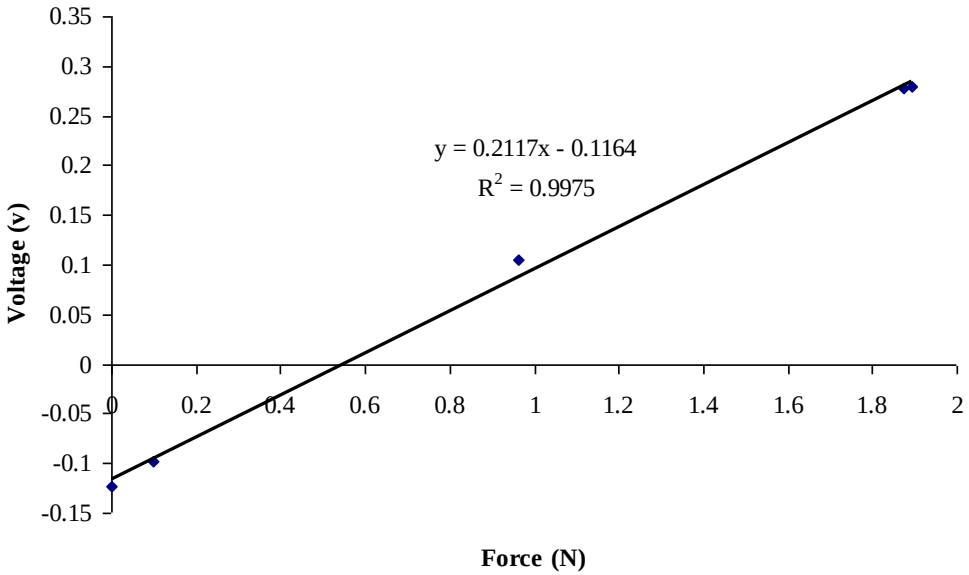

Figure 2-6: Calibration factor for the indentation apparatus to convert output voltage to Force (N).

2.4.2 Determination of Cartilage Thickness

Instron Method

The Instron material testing machine (Instron 3365, Bucks, U.K) was used to determine cartilage thickness of the osteochondral plugs (Figure 2-7). The Instron machine consists of a horizontal arm controlled by a PC via a graphic user interface that moves vertically. A needle (Ø ≈ 0.5 mm) was attached to the Instron arm so that the sharp point was facing down.

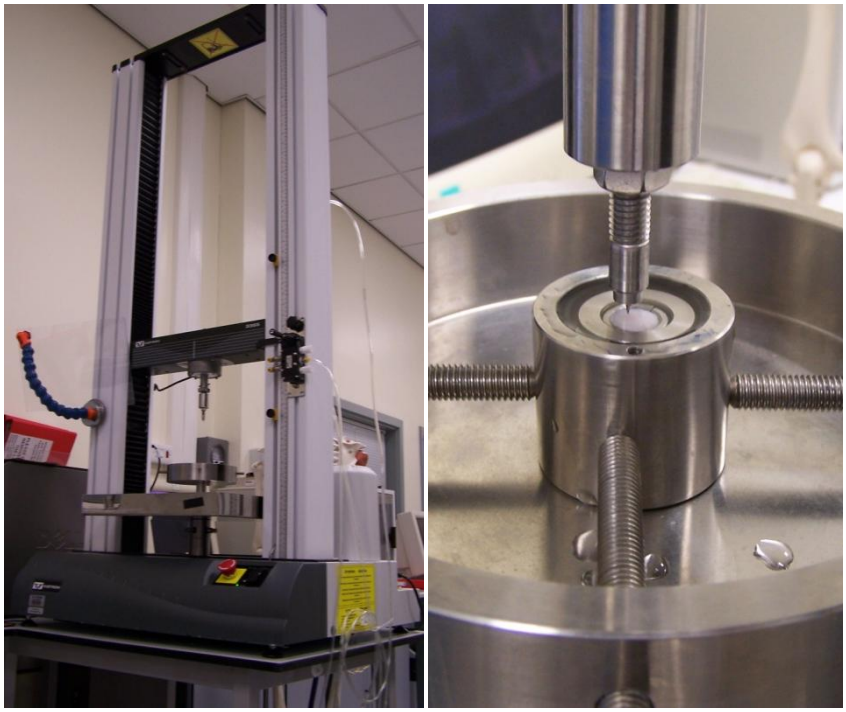

Figure 2-7: Left: Instron material testing machine. Right: Stainless steel bath holding the osteochondral plug.

The osteochondral plug was fixed in a stainless steel bath filled with PBS solution and securely fitted to the Instron base plate situated directly below the needle. The needle was manually lowered so that the tip was less than 1 mm above the articular cartilage surface. The arm was set to move down at 4.5 mm/min driving the needle through the articular cartilage and subchondral bone. The resistance to motion that the needle exhibited was monitored throughout the test via a 500 N load cell.

As the needle travelled above the articular cartilage surface negligible load was recorded (Figure 2-8a). When the needle contacted the articular cartilage surface, the load gradually increased. This point was taken when the load increased above 0.01 N (Figure 2-8b). As the needle travelled through the articular cartilage, the load gradually increased (Figure 2-8c) until it reached the much stiffer bone, where the load rapidly increased (Figure 2-8d-e). This point was calculated by equating the linear equations corresponding to the linear trend lines pre and post needle/bone contact. The needle displacement between points (b) and (d) was taken as articular cartilage thickness.

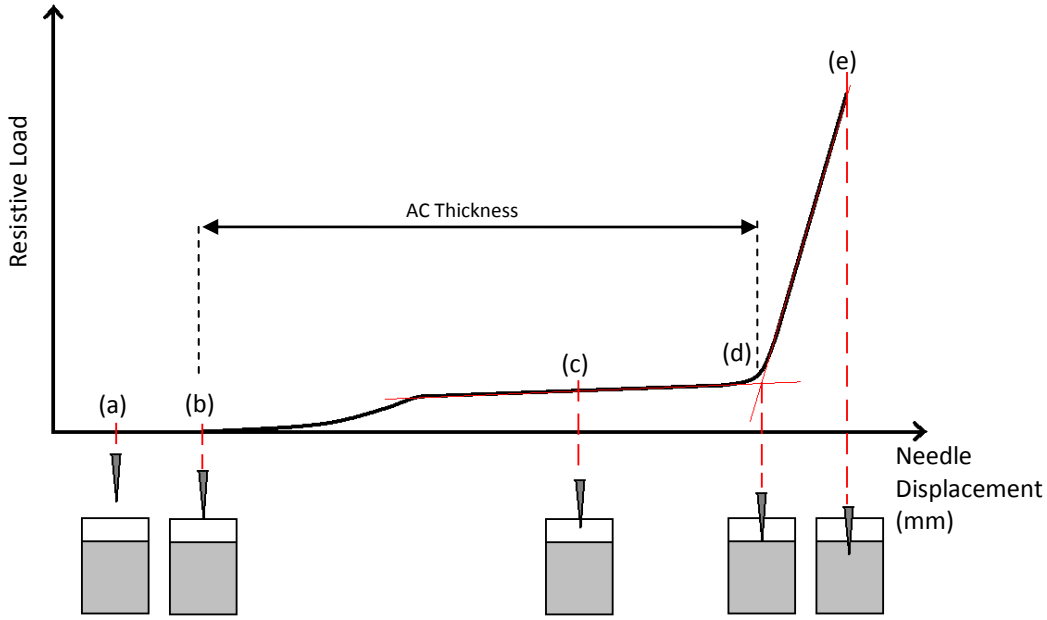

Figure 2-8: Schematic of the results obtained from the needle probing method to measure cartilage thickness

The method of determining cartilage thickness was developed using previously published methods that used a constant load, instead of using a constant feed rate (Shepherd and Seedhom, 1999). Therefore, the results obtained required validation. This method was validated against two other methods currently used to determine cartilage thickness; Nikon profile projector (Pawaskar, 2010) and micro computerised tomography (MicroCT) (Abd Latif, 2011). A bovine leg (18-24 months) was obtained within 24 hours post slaughter. Four plugs were obtained from the patellae/femoral groove. This location on this species of animal was chosen due to being the flattest region of cartilage available. The Instron method of determining cartilage thickness was performed four times on each plug and the values were averaged.

Nikon Profile Projector Method

The Nikon profile projector has been used in previous studies to calculate cartilage thickness (Pawaskar, 2010). The Nikon profile projector emitted a beam of light at the specimen and any diffraction in the light was magnified and projected onto a screen. This was particularly useful when determining the cartilage and bone interface. The specimen is placed onto an x/y translating platform that allows translation in two dimensions. Firstly, the specimen was moved so the surface of

the cartilage was at the centre of the screen (Figure 2-9, Position 1). Crosshairs on the screen allowed this to be done with ease.

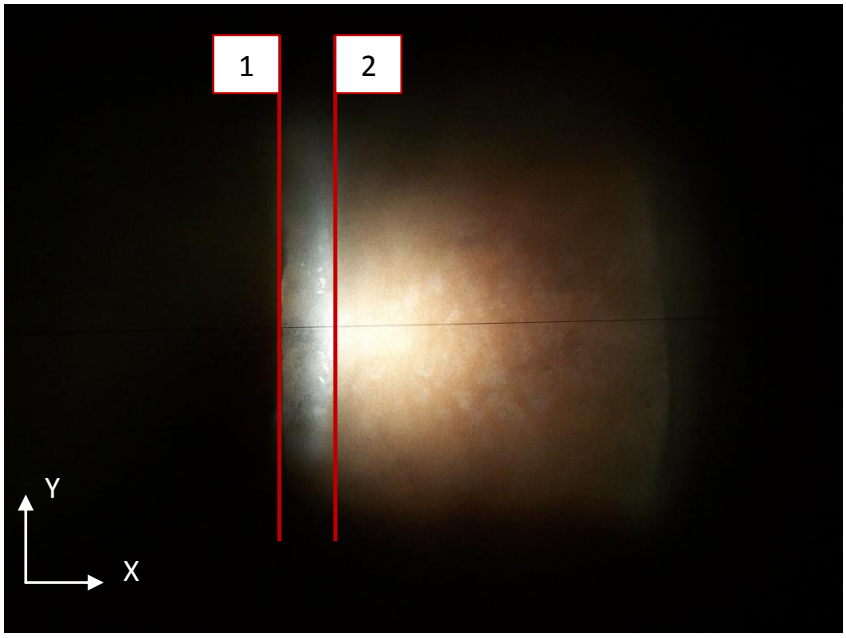

Figure 2-9: Shadowgraph of the osteochondral plug. Line 1 represents the cartilage surface; Line 2 represents the cartilage/bone interface. The distance between Line 1 and 2 is the cartilage thickness.

The x/y translating platform was manually adjusted in the X axis so that the cartilage/bone interface was at the centre of the screen (Figure 2-9, Position 2). The distance moved in the X axis was calculated and taken as the cartilage thickness. The resolution of the Nikon profile projector was 1 µm. This was performed four times around each of the four plugs and averages were taken.

MicroCT

This method was previously used by Abd Latif (2011). The osteochondral plugs were placed in a MicroCT container. Cross-sections of the osteochondral plugs are required for this measurement technique so the orientation of the plugs were important. Since the scans were taken perpendicular to the container walls, the plugs were laid on their side with the help of radio-transparent sponge. The sponge also eliminated any movement of the plugs during scanning which could otherwise cause distortion. A series of two dimensional radiographic scans were performed across the cartilage and bone (parallel to the cartilage surface). Technical assistance in using the MicroCT was provided by Stewart McLure.

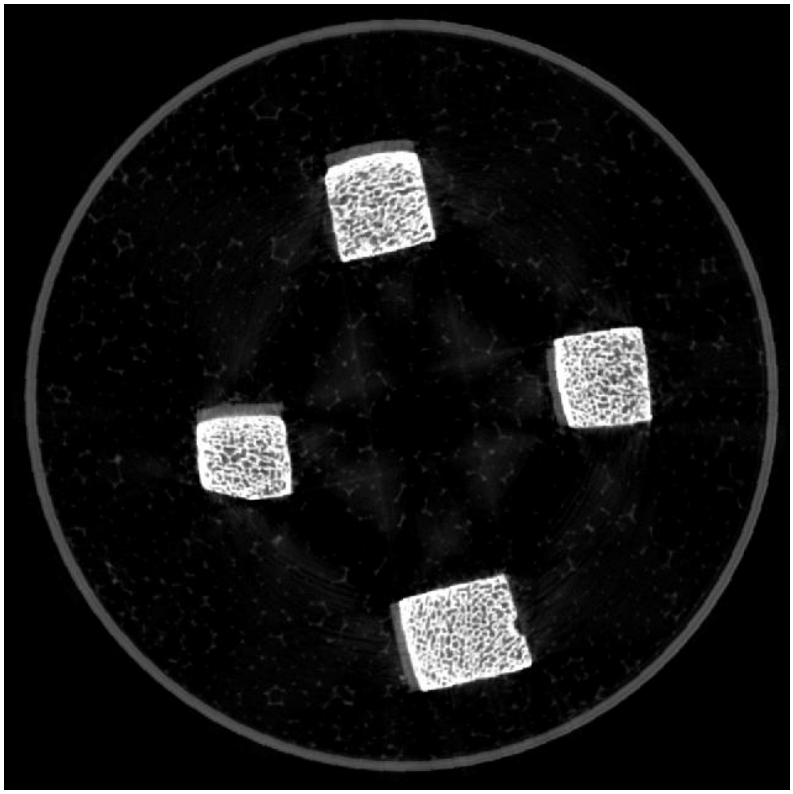

Figure 2-10: MicroCT image of the four osteochondral plugs. These were arranged and orientated so each plug could be indentified in the picture.

The resolution was set to 80 µm. Cartilage is a soft tissue; therefore, the contrast between the open air and cartilage was low. Thus, a Matlab v7.4 code (MathWorks Inc., Boston, MA, USA) described by Abd Latif (2011) was used to increase the contrast of the transposed images. Matlab v7.4 was then used to manually select points on the cartilage surface and the cartilage/bone interface. The Cartesian coordinates of these points were obtained and using Pythagoras theorem, the cartilage thickness was calculated. This was conducted four times on the centre image for each plug.

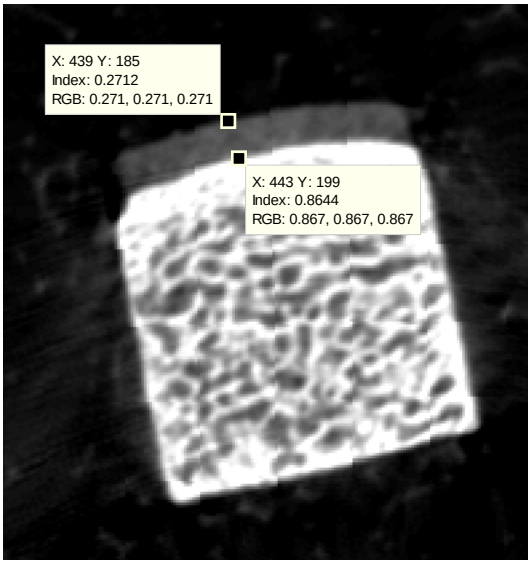

Figure 2-11: The use of datum points with the XY Cartesian coordinates to determine the cartilage thickness.

Validation Results

The thickness for each of the plugs is presented in Figure 2-12. It can be seen that the method proposed in the current study compared well with the MicroCT method. By using an ANOVA with repeated measures (P = 0.05), the Nikon profile projector method showed significantly different results compared to the other two methods ($p<0.05$). This could have been due to measuring the edges of the cartilage plug, which could have become damaged after extraction from the joint. There was also a risk of cartilage dehydration from the beam of light used by the Nikon profile projector. Hence, the Nikon profile projector was not used in this study to measure cartilage thickness.

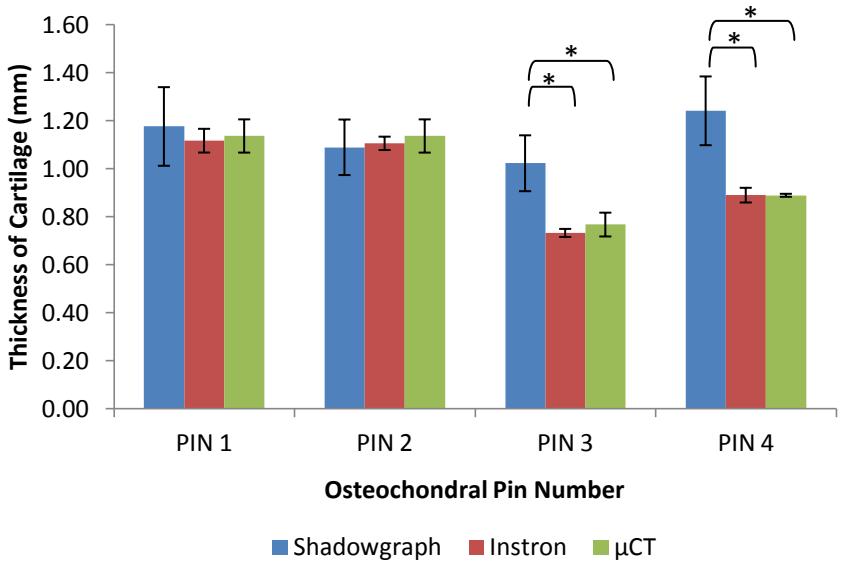

Figure 2-12: Cartilage thickness results of the four plugs using the shadowgraph method, Instron method and the µCT method. Error bars are standard deviations. * $p<0.05$ using ANOVA with repeated measures.

No significant differences were seen between the MicroCT and the Instron method. The MicroCT method allowed the slight undulations of the cartilage surface and cartilage/bone interface to be observed. However, due to the difficulties in imaging soft tissue, the cartilage was not submerged in PBS during the scans. This was to maximise the contrast of the cartilage surface. Therefore, since only an average cartilage thickness was required and the necessity of maintaining cartilage hydration throughout the test, the Instron method was chosen.

2.4.3 Derivation of Mechanical Properties

The results from the creep indentation and thickness tests were both used to derive the intrinsic material properties: equilibrium elastic modulus and permeability. This was completed with the use of an axisymetric biphasic poroelastic finite element (FE) model (Figure 2-13) (ABAQUS, version 6.9-1) created and published by Pawaskar *et al* (Pawaskar, 2010; Pawaskar *et al.*, 2011a).

The articular cartilage was modelled as a poroelastic material (CAX4RP, four node elastic and pore pressure elements) with 80% water content and a void ratio of 4. The Poisson's ratio was assumed to be zero to allow maximum compressibility. For simplicity, the bone was modelled as an elastic solid (CAX4R,

four node elastic elements) with an elastic modulus of 17 GPa and a Poisson's ratio of 0 (Pawaskar, 2010).

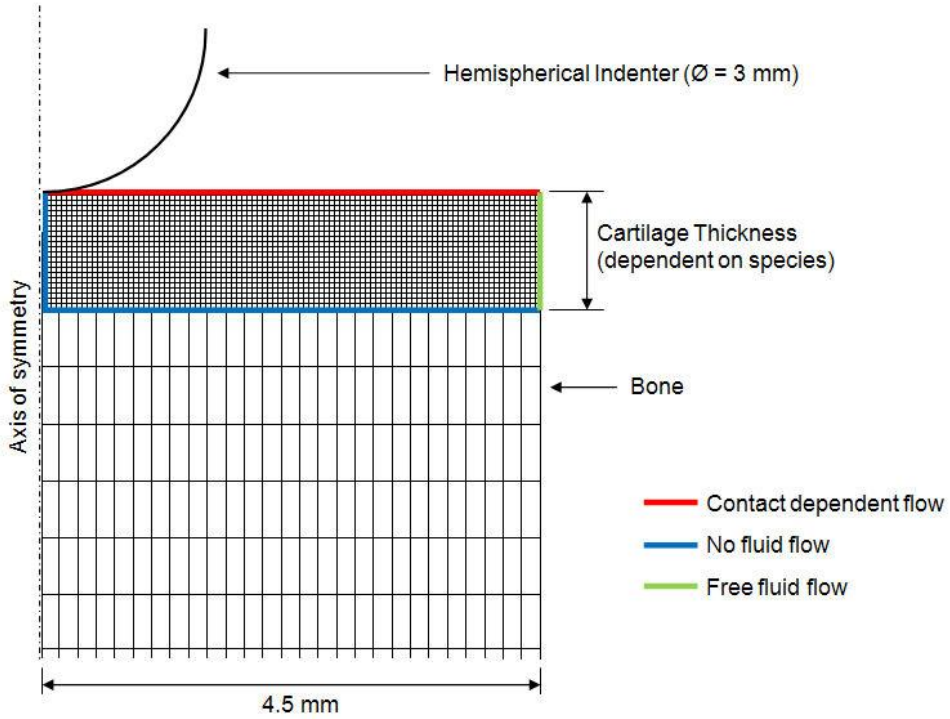

Figure 2-13: Schematic of the axissymmetric FE model of the osteochondral plug, highlighting the axis of symmetry

In the model, load was increased from 0 to 0.8 N and applied through the hemispherical indenter to the cartilage surface over a two second period; and then held constant for further 3600 seconds similar to the *in-vitro* experiments. The predicted curve produced from the FE model after this two second period was automatically adjusted to fit the experimental curve produced during the *in-vitro* indentation of articular cartilage using MATLAB v7.4 (MathWorks Inc, Boston, MA). This was carried out by altering the equilibrium elastic modulus and permeability incrementally. The aim of the curve fitting was to reduce the sum of least square error. To quantify the goodness of fit between the curves, the coefficient of determination between the FE curve and the experimental curve was determined by using Equation 2.1.

$$R^2 = 1 - \frac{SS_{err}}{SS_{tot}} \tag{2.1}$$

Where SS_{err} is the sum of squares of residuals and SS_{tot} is the the total sum of squares. The average ± standard deviation of the coefficient of determination for this thesis was 0.81±0.06. After curve fitting, the resulting equilibrium elastic modulus and permeability were taken as the actual mechanical properties of the articular cartilage. The initial steepness of the curve affected permeability results whereas the final plateau affected the equilibrium elastic modulus. An example of the curve fit is seen in Figure 2-14.

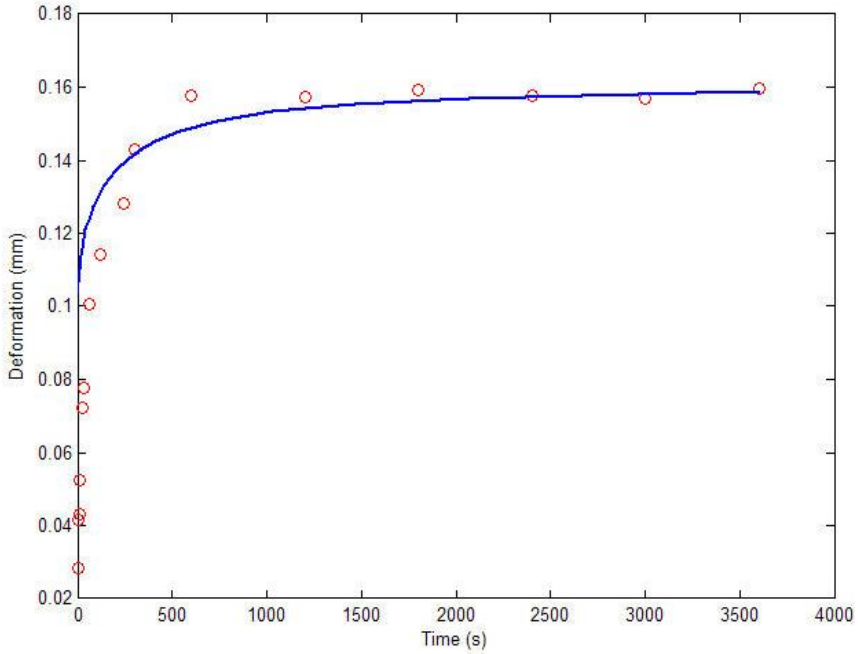

Figure 2-14: An example of a curve fitted graph; circles represent the data from the experimental curve produced during the *in-vitro* indentation and line represents the graph produced by the FE model.

A mesh sensitivity analysis was performed on the finite element model that was used in Chapter 3 to obtain the equilibrium elastic modulus and permeability of cartilage. For this, the bovine model was used and the mesh density was gradually increased from 33.67 elements/mm^2 to 2424.24 elements/mm^2. The effect of altering the mesh density on the equilibrium elastic modulus and permeability results was examined (Figure 2-15).

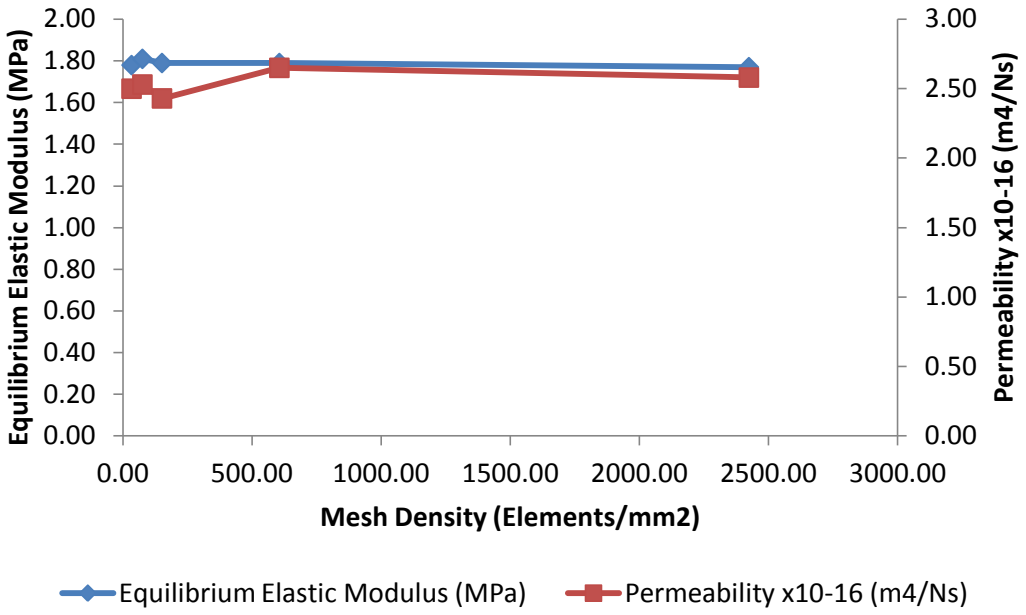

Figure 2-15: The effect of altering the mesh density on the equilibrium elastic modulus and permeability results

By increasing the number of elements from 33.67 elements/mm^2 to 2424.24 elements/mm^2 the equilibrium elastic modulus and permeability varied by 2.10% and 8.30% respectively. Therefore, no relationship between mesh density and the equilibrium elastic modulus and permeability results was found (Figure 2-15). The mechanical property values were unaffected by the mesh density. A mesh density of 151.52 elements/mm^2 was subsequently used.

A sensitivity analysis was performed by Abd Latif (2011) on the same model under similar strain states as the current study to explore the effect of Poisson's ratio and void ratio (hence, water content). It was found that deformation over time curves produced by the FE model remained unaffected when varying the Poisson's ratio from 0.00 to 0.12 or by changing the void ratio from 3.00 to 4.25.

2.4.4 Pendulum Friction Simulator – Friction Coefficient of Cartilage

The ProSim Friction Simulator (Simulation Solutions, Manchester, UK), is a single-station servo-hydraulic machine that can apply a loading cycle and flexion/extension motion simultaneously, similar to that observed in the hip (Brockett *et al.*, 2007). The motions and forces were controlled by a PC via a graphic user interface. The simulator could be split up into two sections. The upper section consisted of a loading frame that applied loads to a motion arm. The

motion arm swings back and forth, replicating the flexion/extension motion seen in the hip. Attached to the motion arm was the CoCr femoral head fixture. Different sized femoral heads could be interchanged between experiments to maintain a relatively consistent clearance between the femoral head and acetabulum.

The lower section of the simulator consisted of a friction measuring carriage which was free to move in the transverse plane. The fixture (containing the acetabulum sample) was screwed on to the friction measuring carriage and by carefully lowering the femoral head (which was attached to the motion arm) into the acetabulum; the friction measuring carriage was allowed to self centre. As the motion arm provided the flexion/extension motion, the friction between the femoral head and acetabulum caused the carriage to exhibit torque. A piezoelectric transducer connected to the front of the friction carriage measured the magnitude of this torque and hence, frictional coefficient between the femoral head and acetabulum. This entailed two assumptions. The first assumption was that friction within the carriage was negligible. This was tackled with the use of two externally pressurised hydrostatic bearings under the carriage that minimised the friction to a negligible amount by orders of magnitude.

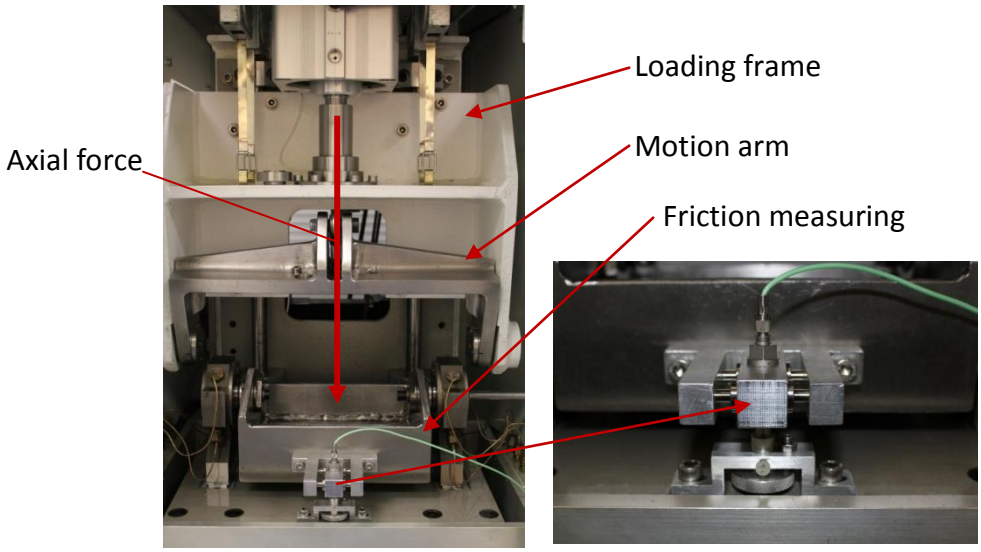

Figure 2-16: Left) The pendulum friction simulator. Right) The piezoelectric transducer.

The second assumption was that centre of rotation (COR) of the acetabulum/femoral head bearing coincided with the COR of the carriage. To ensure that was the case, a custom made rig was used during the PMMA cementing process (Figure 2-17). The rig consisted of a base plate with a vertical

track. A CoCr femoral head was attached to an arm that moved up and down the vertical track. A ring around the vertical track could be set to a pre-defined height which was used to prevent the CoCr femoral head from moving down beyond a certain point. The acetabulum fixture was attached to the base plate so that the centre coincided with the centre of the CoCr femoral head.

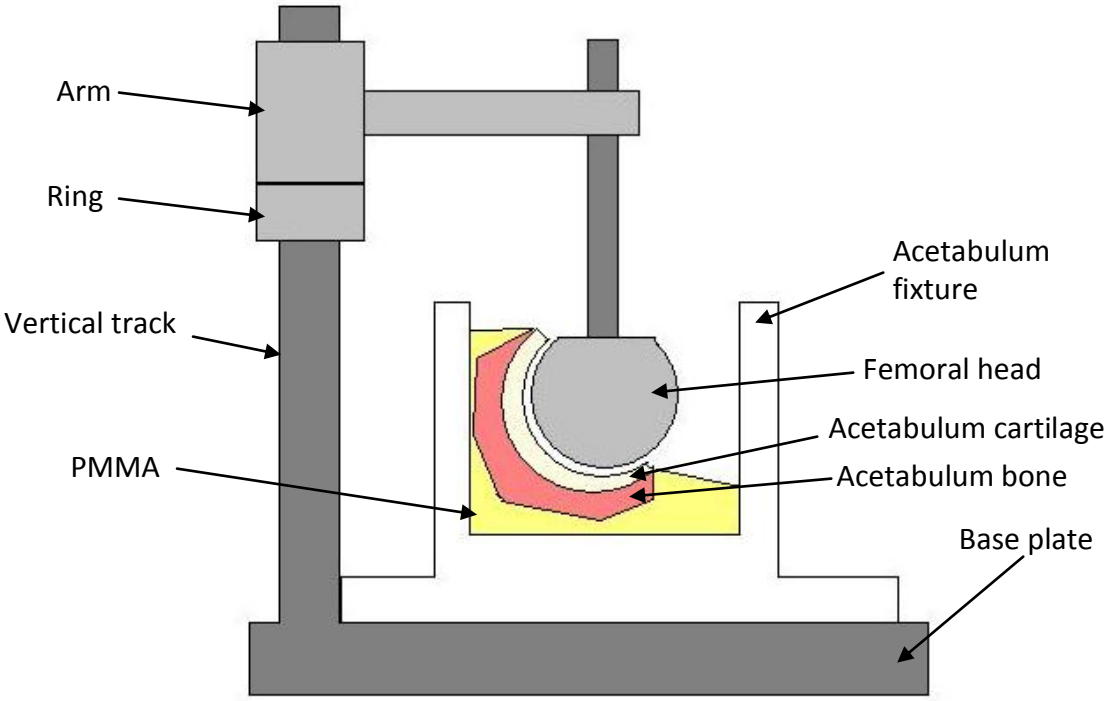

Figure 2-17: Schematic of the cementing fixture to ensure that the COR of the femoral head/acetabulum coincides with that of the COR of the friction simulator

The pendulum friction simulator COR was 63.24 mm from the top of the friction measuring carriage and 72.83 mm from the bottom of the motion arm. Before starting the potting procedure, the ring was set so that the smallest distance between the top of the base plate and the centre of the femoral head was 63.24 mm. The PMMA bone cement was mixed per manufactures instructions (Section 2.2.3) and once putty like, was placed in the acetabulum fixture. The acetabulum was then placed in the centre of the acetabulum fixture and gently pushed down via the femoral head until the arm touched the ring. This ensured the COR was 63.24 mm from the bottom of the friction measuring carriage. The acetabulum was then orientated so that the contact region was located at the centre of the cartilage and four grub screws at the side of the acetabulum fixture were screwed

into the PMMA bone cement to stop axial rotation of the acetabulum during testing.

The femoral head fixture design allowed the femoral head height to be altered. Using slip gauges and a dial test indicator clock (DTI), a height gauge was set to 72.83 mm plus the radius of the femoral head. The femoral head fixture was then placed under the DTI and the height of the femoral head was altered until it was the same height as the slip gauges. This was to ensure that the distance between the COR of the femoral head/acetabulum and the top of the movement arm was 72.83 mm.

To ensure the COR coincides with the centre of rotation of the pendulum friction simulator, after the components were placed in the simulator a “centring rod” was used. This rod was push through the pre-defined hole of the motion arm into the centre of the rotating hydrostatic bearings of the friction simulator. When the centring rod had been inserted, the distance of COR from the bottom of the motion arm was 72.83 mm, and 63.24 mm from the top of the friction measuring carriage. If after placing the hemiarthroplasty model into the friction simulator the centring rod did not push freely through the pre-defined hole of the motion arm and the rotating hydrostatic bearings, the COR of the hemiarthroplasty was not in line with the COR of the simulator. In these instances, the tests were not performed.

Due to the complex geometry of the natural acetabulum, the COR of the joint was not perfectly aligned with the driven centre of rotation of the friction simulator. This offset created an additional torque in the system, thus altered the friction coefficient measurement. This extra torque needed to be established. To measure this extra torque, the setup was run for 121 cycles at 1 Hz with a constant load of 800N (± 15° flexion/extension). The magnitude of the friction coefficient should have been the same during the forward swing (flexion) and reverse swing (extension), but with opposite powers (positive for forward and negative for reverse). Any difference in the magnitudes was due to the extra torque. This difference was measured prior to and after each experiment and averaged and

used to normalise the data from all experiments that involved natural tissue in the friction simulator.

Every month the load cell and frictional torque of the friction simulator were calibrated and the repeatability of the friction measurements were determined.

Load Cell Calibration

The software used to control the friction simulator allowed automatic calibration of the load cell. This involved computing the readings from the friction simulator load cell with measurements attained from a known load cell. A ceramic femoral head and acetabular cup were fitted to the friction simulator and the air pressure valve was opened at five step increments between zero and 150. Opening the air pressure valve caused more pressure to be applied to the friction simulator load cell. A known load cell was used to measure the true force at the different stages of opening the valve and these values were entered into the automatic calibration program. A calibration constant was calculated and used during testing to correct the load applied during the cycle to match the desired load.

Frictional Torque Calibration

The software used to control the friction simulator allowed automatic calibration of the frictional torque. A calibration fixture was also used to calibrate the frictional torque which incorporated a loading arm attached to a PTFE cylinder. Mechanical masses were cumulatively placed on the end of the loading arm and the frictional torque was measured each time. These measurements were inserted into the automatic calibration program and a calibration constant was calculated.

Friction Measurements Repeatability

Frictional coefficient of a ceramic femoral head against a ceramic acetabular cup was measured over a period of 300 cycles. The loading cycle was 25 – 800 N with a flexion/extension of $\pm 15^{o}$ at a frequency of 1 Hz. This cycle was chosen since it was used throughout this thesis for all friction tests. Serum in water (25% (v/v)) was used as the lubricant. Four repeats were performed and the results are shown in Figure 2-18.

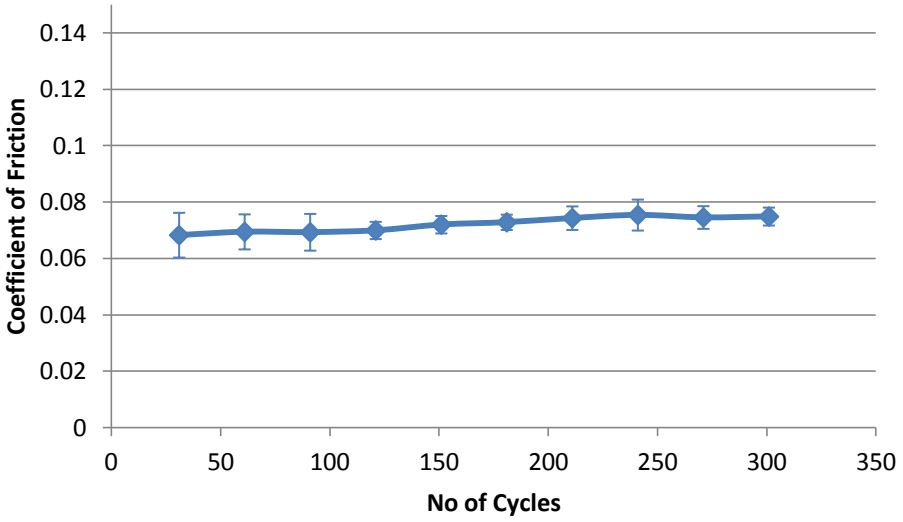

Figure 2-18: Mean average of frictional coefficient of ceramic-on-ceramic total hip replacement over a 300 cycle test (n=4). This highlights the repeatability of the friction simulator (error bars are 95% confidence limits).

2.4.5 Calculating Wear Area

After conducting tribological tests on the pendulum friction simulator, the wear area was calculated. However, due to the concave nature of the acetabulum, simply capturing an image and using the two dimensional image to calculate wear area would not have been accurate. This error would be dependent on the size of the defect in relation to the size of the acetabulum and could be calculated by converting the area of a “dome” of a sphere to its corresponding two dimensional circular area (as if a photo was taken of the “dome”). A plan view of this problem is shown is Figure 2-19.

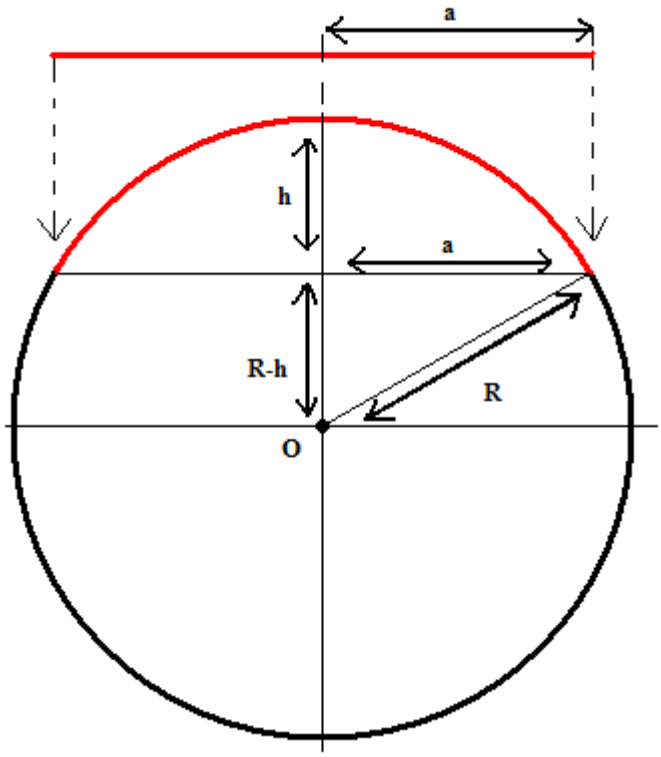

Figure 2-19: Schematic of the circle. The curved red line is the "dome" and the straight red line is the two dimensional circular area.

The curved red line on the circle represents the "dome" and straight red line above the dome represents the two dimensional circular area. The radius of the circle is *a*, *h* is the height of the dome and *R* is the radius of the sphere. The surface area of the dome is:

$$A_{dome} = 2\pi Rh \tag{2.2}$$

Therefore, it was necessary to determine *h* in terms of the known parameters (*a* and *R*). The area of the flat circle is:

$$A_{cirle} = \pi a^2 \tag{2.3}$$

Using Pythagoras theorem, *h* can be calculated in terms of *a* and *R*:

$$a^2 + (R - h)^2 = R^2 \tag{2.4}$$

$$a^2 + (R - h)(R - h) = R^2 \tag{2.5}$$

$$a^2 + R^2 - 2Rh + h^2 = R^2 \tag{2.6}$$

$$a^2 - 2Rh + h^2 = 0 \tag{2.7}$$

$$h^2 - 2Rh + a^2 = 0 \tag{2.8}$$

$$h = \frac{2R \pm \sqrt{4R^2 - 4a^2}}{2} \tag{2.9}$$

$$h = R \pm \sqrt{R^2 - a^2} \tag{2.10}$$

Therefore, this can be inserted into the Equation (2.2) to develop the equation that determines the A_{dome} in terms of the radius of the flat circle (a) and radius of the sphere (R).

$$A_{dome} = 2\pi R(R \pm \sqrt{R^2 - a^2}) \tag{2.11}$$

A graph was generated to show the percentage difference between the area of the dome (true area) and the two dimensional circle (approximated area) in terms of the radius of the flat circle (as a percentage of the Sphere radius) (Figure 2-20).

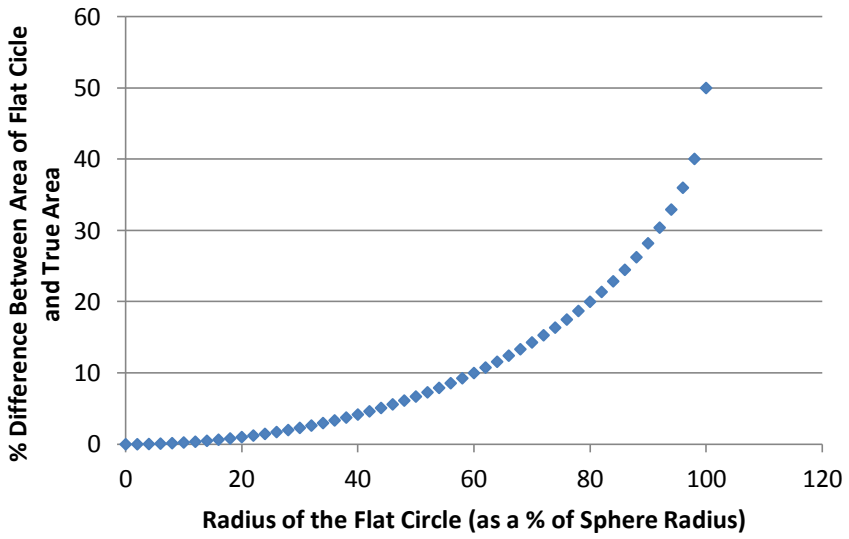

Figure 2-20: Relationship between the radius of the two dimensional circle (as a percentage of the sphere radius) and the percentage difference between the area of the flat circle and the true projected area.

If the distance between the centre and the perimeter of the cartilage wear exceeds 60% of radius of the acetabulum, then the error will be larger than 10% (Figure 2-20). Previous studies have shown the wear area to extend to the peripheral edges of the cup (Lizhang, 2010); therefore, the curvature of the acetabulum must be taken into consideration.

Flexible Film Method

In a previous study, a mould was taken of the acetabulum after wearing (Lizhang, 2010). Clingfilm was then wrapped around the mould and the wear was traced onto the Clingfilm. The Clingfilm was then flattened out and an image was captured. A ruler was included in the image to rescale the images. Using Image ProPlus v3.0 (Media Cybernetics, Inc., MD, USA), the wear area was calculated. This program allowed the image to be rescaled to the true size and the wear area to be traced. The program then automatically calculated the wear area.

In Lizhang (2010) study, this method was performed for four different types of wear depending on the severity. The grading was broadly based upon the International Cartilage Repair Society (ICRS) articular cartilage injury classification grading system (Mats *et al.*, 2000). The four main classifications were: 1) Superficial buffing and discolouring of the cartilage; 2) Scratches that propagate down to less than half the thickness of the cartilage; 3) Scratches that propagate down more than half the thickness of the cartilage up to the subchondral bone; and 4) Cartilage removal, exposing the bone. A grade of zero was given if the cartilage appeared to be undamaged. Wear grade was determined by visual inspection (Figure 2-21).

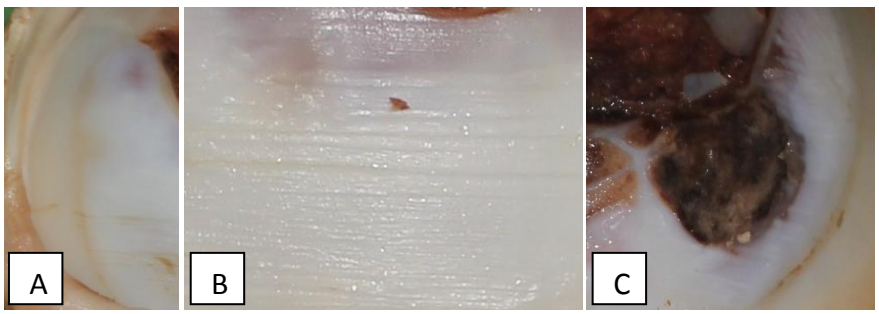

Figure 2-21: Grading system used following the four day *in-vitro* tribological test, showing examples of A) Discolouring and light wear. B) Wear scratches. C) Bone Exposure

However, the accuracy and repeatability of this method has not been determined. Therefore, this was conducted in the current study. To determine the accuracy of this method, an acetabular cup was designed on SolidWorks (Dassault Systèmes, Waltham, MA, USA) which contained three defects with known sizes (281.32, 128.02 and 28.38 mm^2). Each defect had a non-uniform shape and was 1 mm thick. The acetabular cup was then laser sintered using selective laser sintering machine (Vanguard HS HiQ, 3D Systems, SC, USA) with the accuracy of

approximately 100 µm. A mould was taken of this acetabular cup using the same moulding kit used in the previous study known as MicroSet (Warwickshire, UK) (Lizhang, 2010). Once set, Clingfilm was wrapped around the mould and the three defects were traced. Care was taken not to crinkle or stretch the Clingfilm. The film was then straightened out and a photo was taken (Figure 2-22).

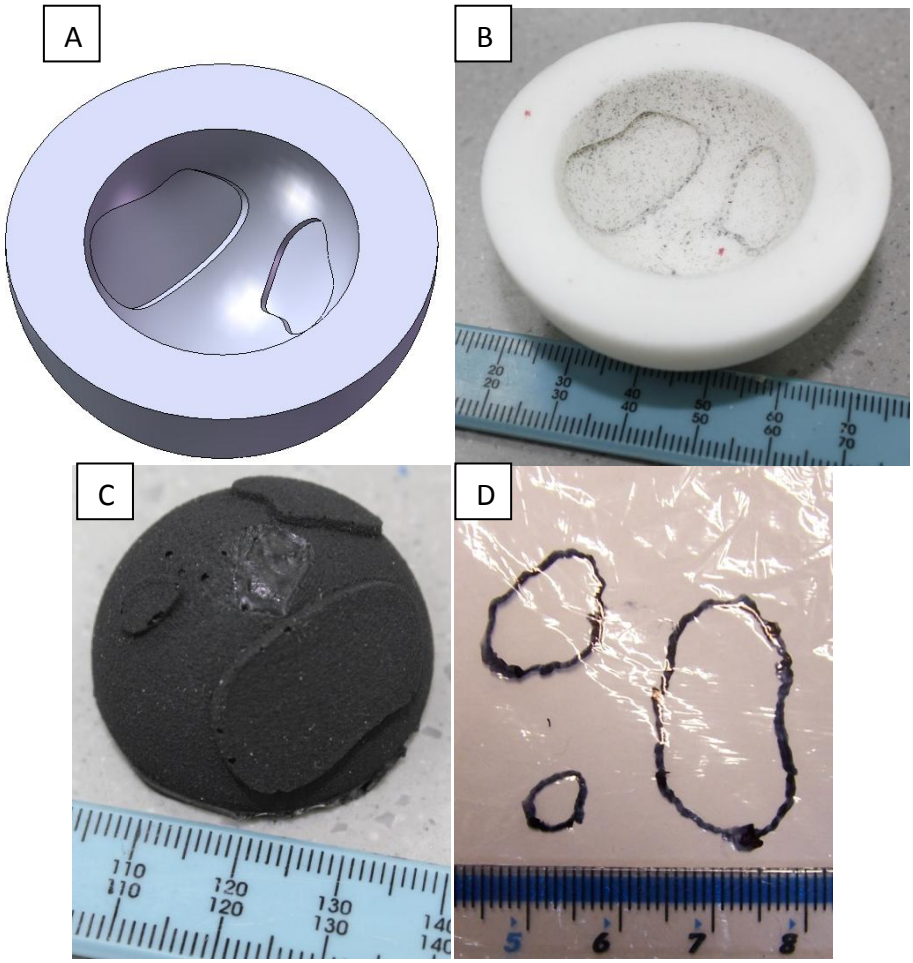

Figure 2-22: A) Solidworks model of the acetabulum including defects, B) Laser sintered acetabulum, C) MicroSet mould taken from the laser sintered acetabulum, D) Trace of the defects after wrapping the Clingfilm around the mould.

Using Image ProPlus software, the edges of the defects were traced and the area was recorded. To determine the accuracy of this method, the values obtained from Image ProPlus were compared to the true area. This was conducted five times to establish the repeatability. It must be noted that the difference between the model of the cup and the laser sintered cup was unknown. However, this was thought to be small in comparison to the human error during tracing.

Table 2-4: Average area calculated using the flexible film method compared to the true area.

Average area ± standard deviation, n=5 (mm^2)	True Area (mm^2)	Percent Difference
263.32 ± 10.39	281.32	6.40%
107.34 ± 8.39	128.02	16.15%
18.513 ± 1.93	28.38	34.76%

For large defects, the percentage error was relatively small (Table **2**-**4**). The standard deviations were also small for all the defect sizes, therefore making this method repeatable. However, for the medium and small sized defects, the error was relatively large. Thus, it was decided that this method was not adequate for measuring small defects, and another method must be developed and validated. The new method is described below.

Three Dimensional Mapping Method

This method involved directly projecting wear, traced on a two dimensional photo, onto a three dimensional computer model. This involved producing a mould using MicroSet (Warwickshire, UK). However, due to the acetabulum being set at an angle, a wall of plasticine was created around the cup so the moulding fluid filled the entire cup. Another piece of plasticine was also placed at the bottom of the cup and two indentations were made. These indentations were used as reference points (Figure 2-23).

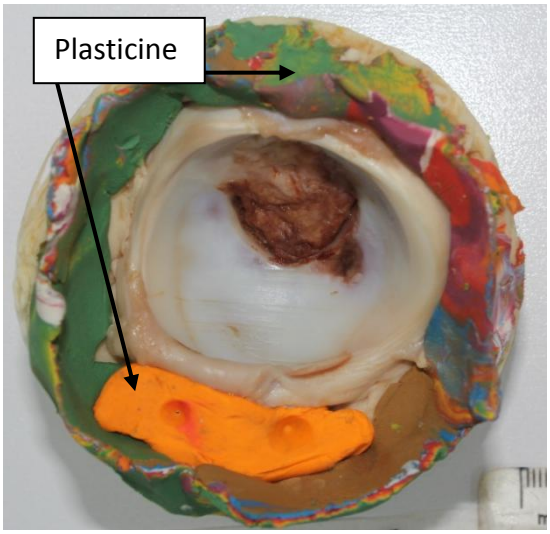

Figure 2-23: Photograph taken of the acetabulum taken vertically downwards.

A photo was taken vertically downwards of the acetabulum with the use of a "bullseye" spirit level. A mould was created of the entire cup using the MicroSet

moulding kit. To obtain a three dimensional model of the mould, a three dimensional scanner was used (NextEngine, Inc., CA, USA). Due to using laser light, the black mould was first spray painted white using white hairspray as instructed in the user manual. A flat piece of white card was pinned and included in the scan to the back to allow the model to be oriented later. To obtain a model of the entire mould, three scans were performed on each mould (30^{o} increments) and automatically fused together using anatomical landmarks. The accuracy of the three dimensional scanner was approximately 100 µm. This was converted to a standard tessellation language (stl) mesh file.

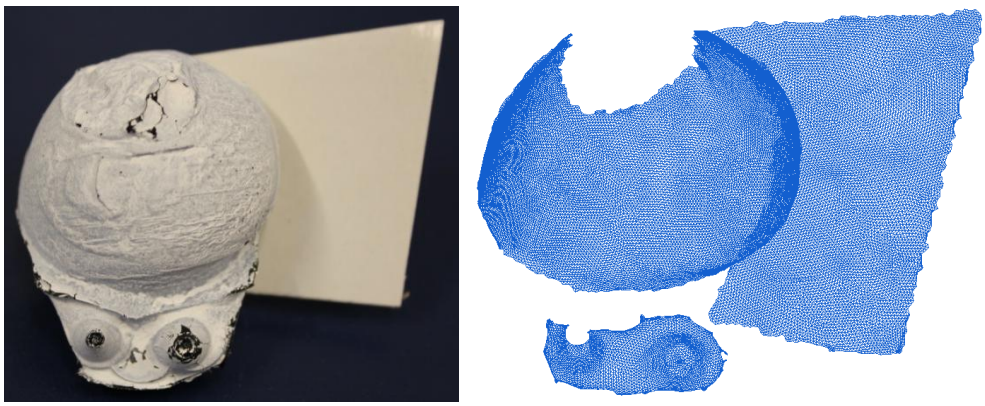

Figure 2-24: Left) Photograph of the mould after being sprayed with white hairspray with a card pinned to the back. Right) Corresponding surface mesh of the mould and card.

The mesh was then opened using Solidworks (Dassault Systèmes, Waltham, MA, USA) and was converted to a surface using the wizard supplied in the program. The orientation of the surface was corrected using the scanned white card. After the surface was created, the corresponding photo was opened, superimposed over the model and orientated parallel to the scanned white card. By using the indentations on the mould and the image of the same indentation, the photo could be resized and orientated over the mould. The wear scars were then traced onto the photo and by using the "extrude" feature, the traces were projected onto the three dimensional model. The areas of these extrusions on the model was calculated using the "measure" tool and taken as the wear area.

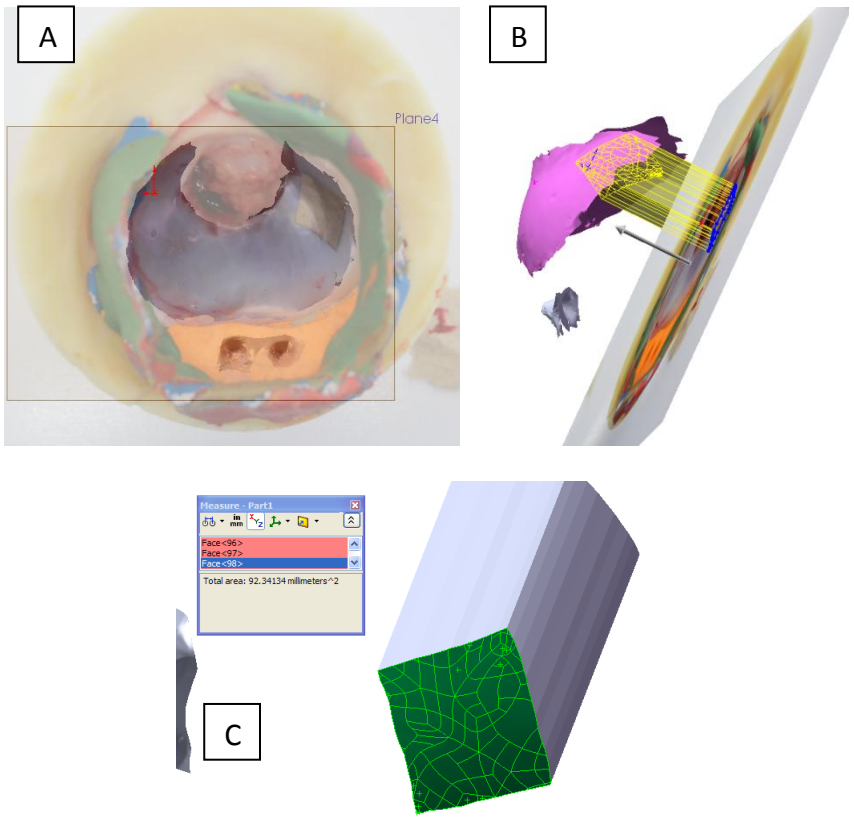

Figure 2-25: A) Overlaying the image onto the 3D model. B) Projecting the traced square onto the 3D model. C) Calculating the area of the square after projecting onto the 3D model

To determine the accuracy of this method a square was cut out of a piece of tissue paper (Figure 2-26). A photo of this square was taken and the "true" area was measured using Image ProPlus. This was 92.37 mm^2. This square was placed at the peripheral edge of a porcine acetabular cup. The moistness of the cartilage allowed the paper square to adhere to the surface. This represented the wear. The procedure described previously was then performed. This was repeated on three different acetabulae using the same paper square to determine the repeatability.

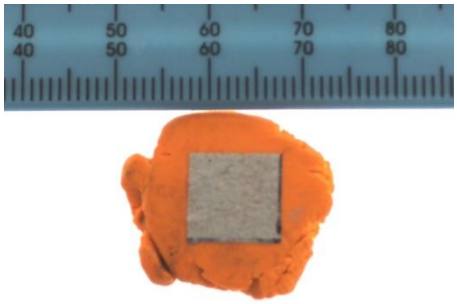

Figure 2-26: Photograph of the tissue paper square used to validate the three dimensional mapping method.

The average percentage difference between the calculated area and the true area was 1.41±1.94% (mean ± standard deviation), which was much less than the error obtained in the flexible film method. The standard deviation was also much smaller than the flexible film method making it more repeatable. Therefore, this method was used to calculate the wear area on the acetabular surface.

2.5 Biological Instrumentation and Methods

2.5.1 Swabbing

Swabbing is a commonly used technique to test for microbial production on an abiotic or biotic surface. The porcine acetabulum cartilage was swabbed to test for microbial contamination on the cartilage surface in Chapters 4, 5 and 7. A cotton wool swab was wiped over the entire articulating surface, placed in vial of nutrient broth (so that the cotton wool was submerged), and the wooden handle was snapped off over the rim of the vial. The vial was finally closed and place in the incubator at 37^0C for 48 hours. This process was performed in a sterile environment to eliminate cross contamination.

2.5.2 Agar Plating

Agar plating is a common method to test for microbial production in lubricants such as culture media. The lubricant was tested for microbial contamination in Chapters 4 and 7. A 2 ml lubricant sample was taken using a 1 ml filter tip attached to a 1000 pipette and placed in a 5 ml sterile bijou using aseptic technique. Two hundred microlitres of lubricant were removed from the pot and

pipetted on the Agar surface. A new filter tip was used for each agar plate to prevent cross-contamination. Three agar plates were used: nutrient agar, heated blood agar and Sabauroud dextrose agar. Nutrient agar is a basic medium which promotes the growth of non-fastidious bacteria. Heated blood agar is an enriched medium which facilitates the growth of most pathogenic bacteria (Quinn, 2002). Sabauroud dextrose is commonly used for the cultivation of pathogenic and non-pathogenic fungi (Atlas and Snyder, 1995). The nutrient agar and heated blood agar were incubated for 48 hours at 37°C and Sabauroud dextrose agar plates were incubated for 48 hours at 27°C.

2.5.3 Histology

Background details in regards to histology are discussed in Sections 1.8.1 and 1.9.4. In the current study, histology was used to assess the condition of the micro-architecture of the cartilage after the tribological studies. These were compared to cartilage taken from fresh samples.

Tissue Fixation

A section of acetabulum cartilage was removed from the desired location of the tissue and placed in plastic histology embedding cassettes (Histosette®). These were submerged in 10% (v/v) neutral buffered formalin (NBF) for 48 hours. NBF was used to fix the tissue and maintain tissue morphology through the histological procedure. An automated tissue processor (Leica TP1020, Milton Keynes, UK) (Figure 2-27) was then used to sequentially immerse the cassettes in:

- 70% (v/v) ethanol for 1 hour,
- 90% (v/v) ethanol for 1 hour,
- Absolute ethanol for 2 hours and 20 minutes,
- Absolute ethanol for 3 hours and 20 minutes,
- Absolute ethanol for 4 hours and 20 minutes,
- Xylene (Genta Medical, York, UK) for 1 hour,
- Xylene for 1 hour and 30 minutes,
- Xylene for 2 hours,
- Molten paraffin wax for 1 hour 30 minutes

- Molten paraffin wax for 2 hours.

Figure 2-27: The automated tissue processor (Leica TP1020, Milton Keynes, UK)

Paraffin Wax Embedding

After the automated tissue processing was complete, the tissue was removed from the cassettes and placed in metallic moulds using heated tweezers. Molten wax was then poured into the mould and one half of the cassette was placed on top of the mould to allow the paraffin wax block to be mounted on the microtome. The moulds were then left to solidify on ice packs until the wax block could be removed from the metallic mould.

Sectioning

The paraffin wax block was mounted on a microtome (Leica, Milton Keynes, UK) and 5 µm sections were created. The sections were placed in a 40°C heated water bath before being collected on Superfrost Plus microscope slides. The slides were placed on a hot plate for twenty minutes at 55°C, which melted the paraffin wax onto the slide, securing the sections throughout the staining process.

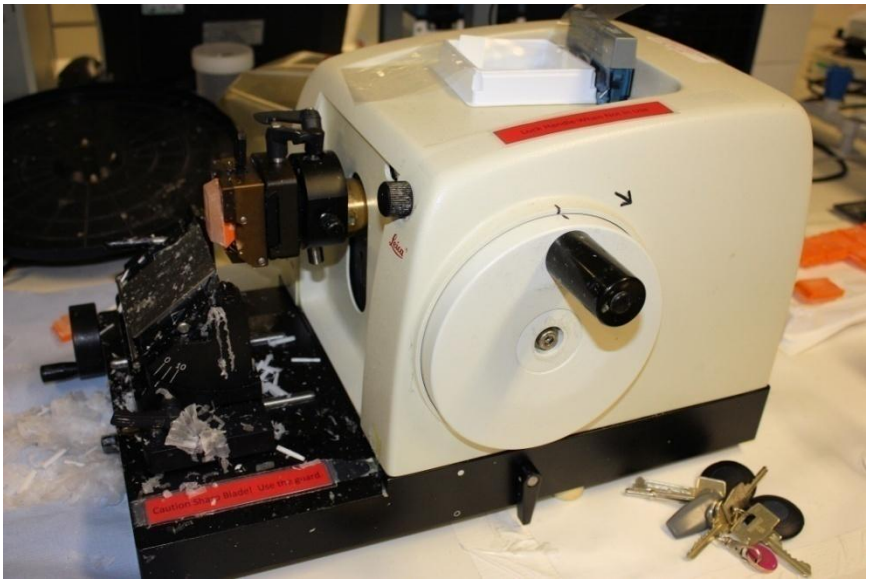

Figure 2-28: The microtome used to cut 5 µm sections (Leica, Milton Keynes, UK).

Dewaxing and Rehydrating of Sections

Prior to staining, the remaining paraffin wax required removal and the tissue needed to be rehydrated. The slides were placed in a slide holder and sequentially immersed in:

- Two lots of Xylene for 10 minutes each,
- Three lots of graded (100%) ethanol for three, two and two minutes respectively,
- 70% ethanol for two minutes,
- Running tap water for three minutes.

Haematoxylin and Eosin Staining

Haematoxlin and eosin was used to visually examine the general micro-architecture of the cartilage. After dewaxing and rehydrating, the slides were sequentially immersed in:

- Haematoxylin (Thermo Fisher Scientific Ltd., Leicestershire, UK) for one minute ,
- Running tap water until the water ran clear,
- Eosin (VWR International Ltd., Pennsylvania, USA) for three minutes.

Alcian Blue Staining

Alcian blue staining was used to visually examine the GAG distribution within the cartilage. After dewaxing and rehydrating, the slides were sequentially immersed in:

- 1% Alcian Blue for 15 minutes,
- Running tap water for one minute and rinse in distilled water,
- Periodic acid (Sigma-Aldrich Co., Dorset, UK) for five minutes and then rinse with distilled water three times,
- Schiffs Reagent (Sigma-Aldrich Co., Dorset, UK) for 15 minutes,
- Running tap water for five minutes,
- Haematoxlin (Thermo Fisher Scientific Ltd., Leicestershire, UK) for 90 seconds and rinse in running tap water until it ran clear.

Dehydrating and Mounting of Sections

After staining, the sections were dehydrated by sequentially immersed in:

- 70% ethanol for five seconds,
- Three lots of ethanol (100%) for one, two and three minutes respectively,
- Two lots of Xylene for 10 minutes each,

After dehydrating the sections, a drop of DPX mountant (Thermo Fisher Scientific Ltd., Leicestershire, UK) was placed on top of each section and a coverslip was placed on top. This was left to set for a minimum of four hours. Care was taken to not entrap air bubbles between the slide and cover slip as this could affect the visualization of the tissue in the microscope. The DPX mountant resists disturbance of the stained sections and also allow the sections to be clearly observed in the microscope.

The stained sections were observed using the Olympus BX51 light/fluorescent microscope (Olympus UK Ltd., Hamburg, Germany) using 40x to 400x magnifications. The images were digitally captured using Cell B software (Olympus, Hamburg, Germany).

2.5.4 Quantification of Glycosaminoglycan Content in Cartilage

The following describes the process for quantification of GAGs in the cartilage sample, first developed by Dr. Stacy-Paul Wilshaw and later modified by Miss. Hazel Fermor (Internal SOP: "Quantification of Glycosaminoglycan Content in Tissue Samples", No. 041). This was used to compare GAG concentration in worn and unworn cartilage. The process involved solubilising the cartilage to release the GAGs, supplying a dye that exhibits a colour of a specific wavelength which attaches to the GAGs, quantifying the amount of colour with that specific wavelength and converting that to GAG concentration. The reagents and their compositions are described in Table 2-5.

Table 2-5: Reagents and their compositions used in the quantifying of GAGs procedure.

Reagent	**Composition**
Digestion buffer	To one litre of PBS with 0.788 g L-Cysteine Hydrochloride and 1.8612 g disodium ethylenediaminetetraacetic acid were added. The pH was adjusted to 6.0 ± 0.1 and the solution stored at room temperature for up to six months.
Papain digestion solution	1250 Units of papain (Sigma-Aldrich Co., Dorset, UK) was dissolved in 25 ml of digestion buffer.
Assay buffer	137 ml of 0.1 M sodium di-hydrogen orthophosphate and 63 ml 0.1 M di-sodium hydrogen orthophosphate was mixed. The pH was adjusted to 6.8 and stored at room temperature for up to three months.
DMB Dye solution	16 mg of 1,9 dimethylene blue was dissolved into 5 ml of ethanol and 2 ml of formic acid. 2 g of sodium formate (VWR International Ltd., Pennsylvania, USA) was added to the mixture and the volume was increased to 1000 ml using distilled water. The pH was adjusted to 3.0. This was then store at room temperature until use for up to three months.

<u>Digestion of Cartilage</u>

Prior to using the GAG assay, the cartilage was digested using protease to release the GAG molecules. To do this, approximately 10-30 mg of tissue was removed from the desired location(s) and then macerated using a scalpel and forceps. The exact mass of the tissue was measured using a balance three times and a mean average was taken (±0.0001 g). The macerated tissue was placed in sterile universal tubes and lyophilized in a freeze dryer for 48 hours (-40 to -50 °C at 1 mbar). The mass was measured again to allow the dry weight and hence water

content to be calculated. Papain digestion solution (5 ml) was added to each universal tube containing the cartilage sample and incubated (60 °C) in a water bath for 36 hours.

GAG Assay of Digested Cartilage

Before adding the dye to the cartilage and measuring the intensity of colour with a specific wavelength (known as optical densities or absorbance); a method of converting optical densities to GAG concentration needed to be established. This was performed by plotting known concentrations of GAGs (standard calibration solutions) with optical densities. The standard concentrations were made up using chondroitin sulphate B (Sigma-Aldrich Co., Dorset, UK) and assay buffer at 0, 3.125, 6.25, 12.5, 25, 50, 100, 150, 200 $\mu g.ml^{-1}$. These were pipetted into a clear flat-bottomed 96 well plate (40 µl) and DMB dye solution (250 µl) was added to each well. After shaking for two minutes on a plate shaker, a spectrophotometer was used at 525 nm to measure the optical densities. The optical densities of the standard concentrations were normalised against the "blank" unused wells. The results were plotted against the chondroitin sulphate B concentration (Figure 2-29). The linear equation from this standard graph allowed the conversion between optical density and concentration of GAGs.

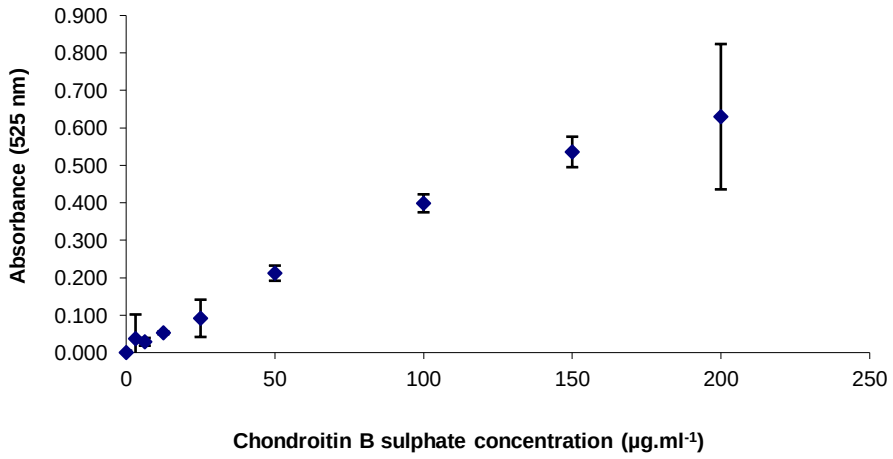

Figure 2-29: Standard graph of chondroitin sulphate B concentration against absorbance (525 nm) used to convert optical density to GAG concentration.

To measure the GAG concentration of the cartilage samples, the digested samples were further diluted to 1 in 50 in assay buffer. This allowed the absorbance to be within the linear range of the standard graph (Figure 2-29). The

samples were pipetted into a clear flat-bottomed 96 well plate (40 µl of each) and DMB dye solution was added to each well (250 µl). These were then shaken on a plate shaker for two minutes.

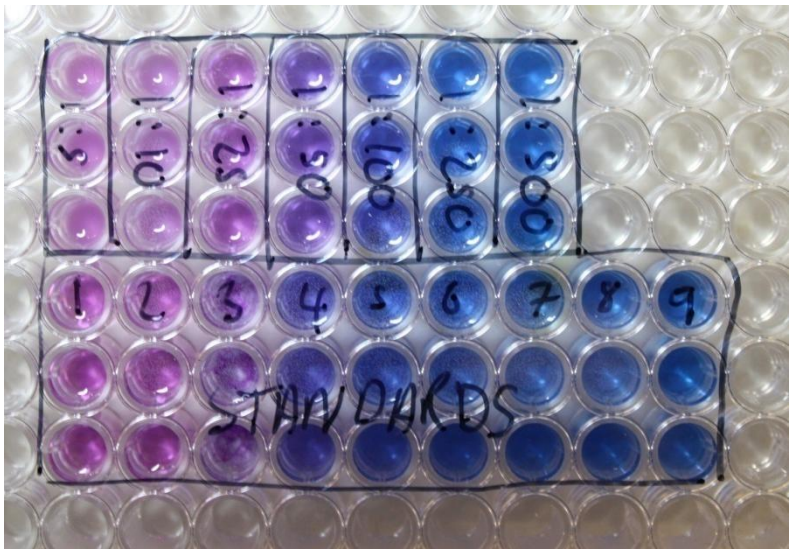

Figure 2-30: An example of a 96 well plate containing the diluted pre-digested samples after the DMB dye solution was added.

A spectrophotometer was used at 525 nm to measure the optical densities which were normalised against the "blank" wells. The values from the digested cartilage could then be interpolated using a linear regression of the standard curve to determine the GAG concentration.

2.5.5 Sterilisation of Equipment

Sterilisation of equipment was needed for the studies conducted in Chapter 4, 5 and 7. This was performed by either hot air sterilisation using an oven (SANYO OMT225, SANYO Biomedical Europe BV) or by moist heat sterilization using an autoclave (Astell, Kent, UK). The hot air sterilisation involved heating at 190°C for four hours, where the moist heat sterilisation involved heating at 121°C for 15 minutes.

2.6 Statistical Analysis

Data is presented as the mean ± 95% confidence limits unless otherwise stated. One-way ANOVA was used to test for significant differences ($p \leq 0.05$) between different species with geometry or thickness as the parameter.

For the results that used percentages, such as the percent deformation, the values were first transformed using arcsine and significant differences were determined using one-way ANOVA ($p \leq 0.05$). Confidence limits of ± 95% were calculated and the values were back transformed before creating the graphs. This transformation is commonly used to normalise percentage data, where the maximum and minimum are bounded to 0% and 100% respectively (Wheater and Cook, 2000; Dytham, 2002; Quinn and Keough, 2002; Townend, 2002). Additionally, it is used to correct the inherent skewness due to most the values were below 30% (Wheater and Cook, 2000).

The cartilage deformation (Chapter 3) and friction (Chapter 4 and 7) over time curves obtained in this thesis were in a form of a "Growth curve" as described by Matthews *et al.* (1990). Therefore, the final value (at the two hour points) could be used for statistical analysis. This was carried out using one-way ANOVA followed by determination of significant differences between the group means using a Scheffé post-hoc test as this has been described as the most conservative post-hoc test (Vincent, 2005) ($p \leq 0.05$).

Chapter 3: Comparison of Human and Animal Femoral Head Chondral Properties

3.1 Introduction

In this thesis, the tribology of hip hemiarthroplasty will be assessed *in-vitro*. However, due to availability and ethical restrictions, human acetabulae were not used. Instead, a hip joint from a quadruped will be used to represent human.

The tribological function of articular cartilage is directly associated with the intrinsic mechanical properties; in particular stiffness and fluid content. These intrinsic mechanical properties are governed by the micro-architecture of the extracellular matrix (ECM). The ECM of articular cartilage consists primarily of proteoglycan, collagen II, interstitial water and dissolved ions. The proteoglycan content and degree of collagen II cross linking contribute to the stiffness of articular cartilage in compression; whereas the degree of anisotropy of collagen II has been related to the tensile stiffness. Fluid retention is associated with both the interaction between the interstitial fluid and solid matrix and the electronegative charge of GAGs (Mow and Hayes, 1997).

The loads and motions applied to the articular cartilage in the body affect the production and micro-architecture of the ECM (Mow and Hayes, 1997). Most cartilage samples used for the investigation of articular cartilage are taken from quadrupeds; however, the loads and motions experienced in the joint are different compared to bipeds (humans). Physiological makeup of the cartilage may also vary and be species dependent.

Despite several studies over several decades using porcine, bovine and ovine cartilage samples to investigate function and the effect of biomaterials (Muller *et al.*, 2004; Ozturk *et al.*, 2004; Naka *et al.*, 2005; Northwood *et al.*, 2007; McCann *et al.*, 2009a); the authors are not aware of any studies that have examined the biomechanical differences in articular cartilage between these animal and human tissues. The aim of this study was to investigate the mechanical differences between human and easily accessible animal (porcine, bovine and ovine) articular

cartilage of the femoral head. Hence, to establish the optimum animal joint that represents the human hip. The following parameters were compared; femoral head geometry, cartilage thickness, equilibrium elastic modulus and permeability.

3.2 Materials

3.2.1 Specimens

Femoral heads were acquired from the hind legs of six pigs, sheep and cows no longer than 24 hours after slaughter (Section 2.3). All were slaughtered for inclusion in human consumption and the age of the animals was determined by availability in the food chain. Six human femoral heads were obtained at surgery carried out due to femoral neck fractures (NRES Committee approved, 06/MRE03/73) (Section 2.3). Visual inspection of all the articular cartilage samples showed no signs of degradation or swelling. Samples were wrapped in tissue soaked in saline solution and frozen at -20^{o}C until testing (up to a maximum of 30 days).

3.2.2 Specimen Preparation

Prior to testing, the specimens were thawed in a warm water bath and the diameters of the femoral heads were measured in the posterior/anterior and superior/inferior directions using a Vernier calliper (±0.01 mm). Osteochondral plugs (Ø = 9 mm) were extracted using the method described in Section 2.3.2. The location of the cores was halfway between the acetabular fossa/articular cartilage junction and the articular cartilage/femoral neck junction on the superior section of the femoral head (Figure 3-1). The aim of this study was to examine the use of animal cartilage to represent human in functional testing where the loads and motions mimic that of a human joint. Therefore, this location was chosen because it is the primary weight bearing region of the human femoral heads and this would be translated to the animal samples in the mechanical testing. This standardised method of locating the point of interest was similar to that used in previous studies (Shepherd and Seedhom, 1999).

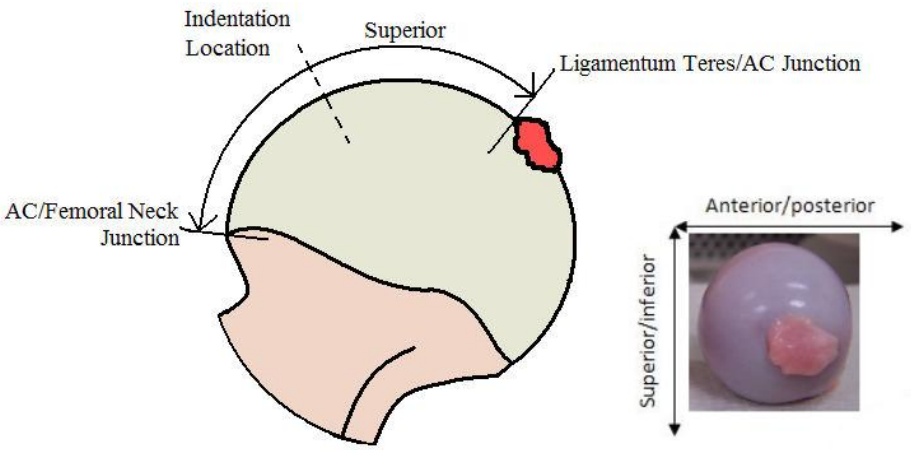

Figure 3-1: Osteochondral plugs were taken halfway between the cartilage/femoral neck and acetabular fossa/cartilage junction (indentation location).

3.3 Methods

3.3.1 Mechanical Behaviour of Articular Cartilage

In order to investigate the time dependent response of the articular cartilage and hence, calculate the mechanical properties; creep indentation was performed on each osteochondral plug. The custom made indenter apparatus discussed in Section 2.4.1 was used to measure deformation of cartilage under a constant load of 0.8 N through a rigid hemispherical indenter (Ø = 3 mm). The full load was applied within 0.2 seconds of the indenter contacting with the cartilage surface. The creep deformation response due to fluid flow was monitored over one hour, which was in the range of previous studies (0.25 – 3 hours) (Kempson *et al.*, 1971; Mow *et al.*, 1984; Jurvelin *et al.*, 1990; Jurvelin *et al.*, 1997). LabView 8 software collected data at 5 Hertz throughout the test. To allow the data to be more manageable and to reduce the effect of noise, 10 data points were averaged at 4.8, 6, 12, 24, 30, 60, 120, 240, 300, 600, 1200, 1800, 2400, 3000 and 3600 seconds; these were plotted.

3.3.2 Thickness Measurements

After indentation, the osteochondral samples were allowed to recover fully by immersing in saline solution for 30 minutes. The plugs were then housed in a stainless steel bath filled with saline solution and placed in a mechanical testing

machine (Instron 3365, Bucks, U.K.). Using the methods described in Section 2.4.2, the cartilage thickness of each plug was measured in four locations in a square pattern (approximately 2 mm between each location) and averaged.

3.3.3 Mechanical Properties

The mean deformation curve produced in Section 3.3.1 and the thickness measurements in Section 3.3.2 for each species was used in conjunction with the FE model created and published by Pawaskar *et al.* (2010 and 2011) to derive the equilibrium elastic modulus and permeability for each species. This axisymetric biphasic poroelastic model was described in Section 2.4.3.

3.3.4 Statistical Analysis

Graphs are presented and statistical differences were determined using the methods described in Section 2.6.

3.4 Results

3.4.1 Femoral Head Geometry Measurements

Significant differences in average femoral head diameter were observed between all animals (Figure 3-2). Bovine femoral heads were the largest with an average diameter of 64.4±4.0 mm, which was significantly larger than human (46.8±5.7 mm). Human femoral heads were significantly larger than porcine (35.6±0.7 mm) and ovine (23.2±1.4 mm).

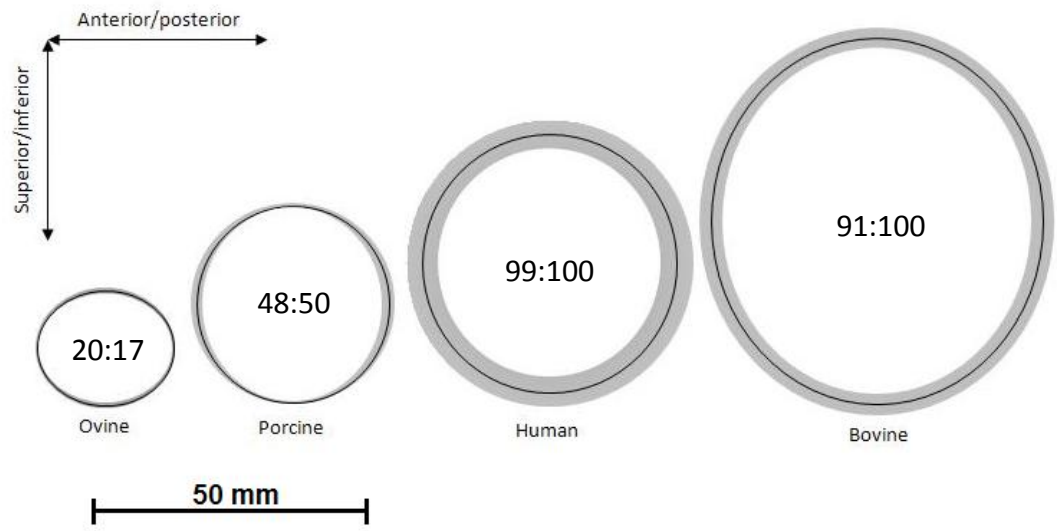

Figure 3-2: Scaled schematic representing the shape of femoral head of different species (to scale). The black line represents the mean and the gray areas represents 95% confidence limits (n=6). The ratios of the diameters measured between the anterior/posterior and superior/inferior directions are displayed.

Measurements of the anterior/posterior and superior/inferior diameters of the femoral heads were also compared and presented as the mean ± standard deviation. The diameters measured in different directions of the human femoral heads were the most similar with an average difference of 1.0±1.2%. The difference between the diameters measured in different directions of the ovine femoral heads was the largest with an average difference of 15.3±3.3%. Bovine femoral head diameters also had a large difference between the diameters compared to human (average difference of 9.5±1.7%). The diameters of the bovine femoral heads were much larger in the superior/inferior direction compared to the anterior/posterior direction; as opposed to ovine in which the opposite was observed. The diameters of the porcine femoral head had a difference of 3.53±1.78% where diameter the superior/inferior direction was larger.

3.4.2 Articular Cartilage Thickness

Human cartilage was 1.82±0.18 mm thick, which was significantly thicker than cartilage from all the animal joints (Figure 3-3). Bovine cartilage thickness (1.32±0.13 mm) was not found to be significantly different to porcine cartilage (1.22±0.05 mm). Ovine cartilage was 0.52±0.10 mm thick, which was significantly thinner than all the other species.

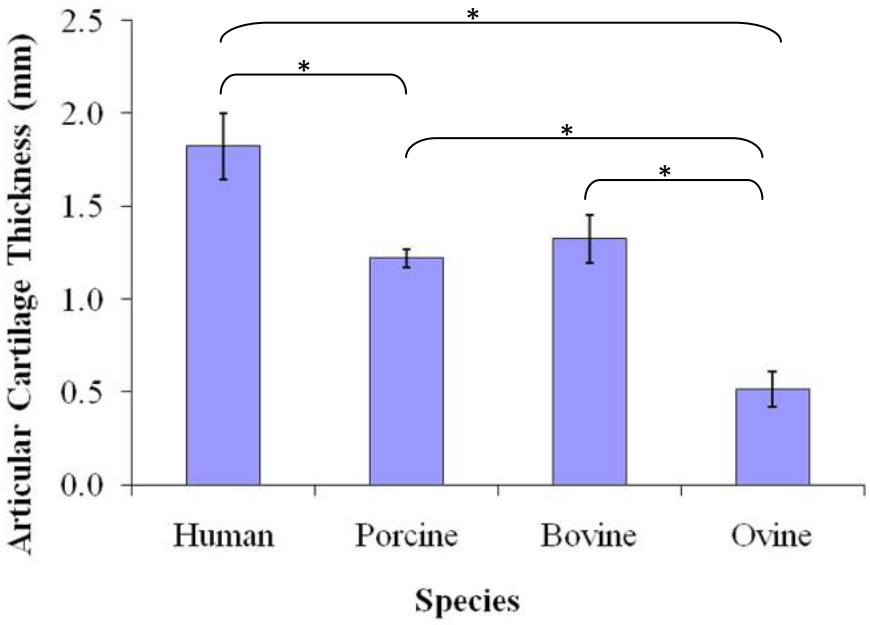

Figure 3-3: Articular cartilage thickness for all species (Mean ± 95% confidence limits) (n=6)
*significant difference ($p<0.05$)

3.4.3 Mechanical Behaviour of Articular Cartilage

Osteochondral samples from all species initially deformed rapidly then, the deformation plateaued (Figure 3-4). Total deformation as a percent of total thickness after one hour was significantly less for human cartilage (6.87±2%) compared to the quadrupeds (mean ± standard deviation). Ovine cartilage deformed the most (33.2±13%) compared to all the species, this was significantly more than bovine (22.47±2%). However, no significant difference was observed between porcine (28.82±3%) and ovine.

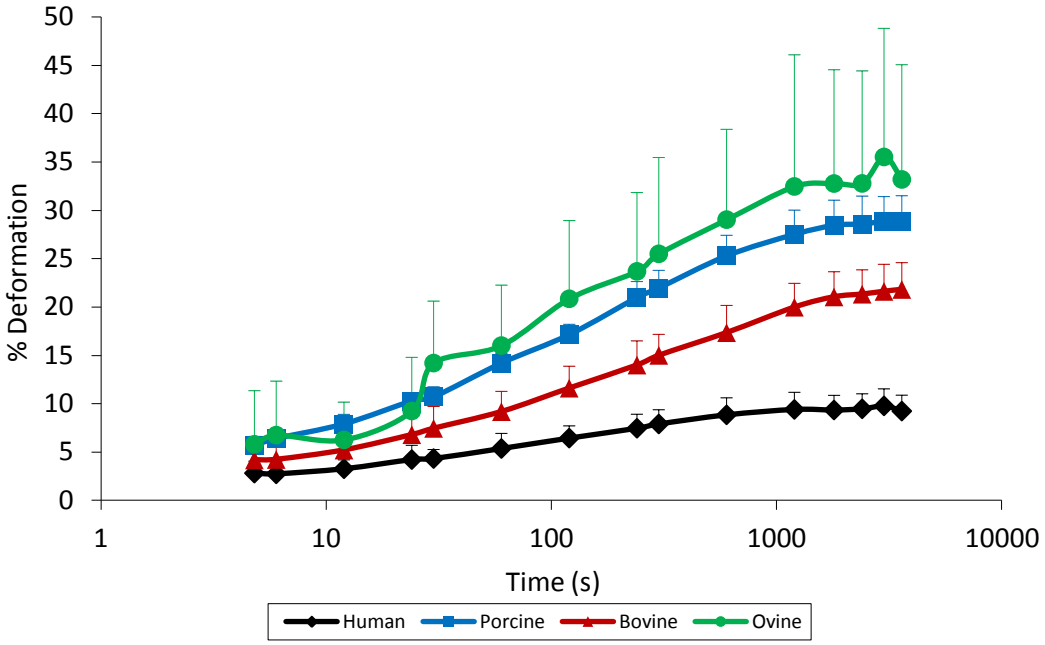

Figure 3-4: Deformation as a percent of total undeformed cartilage thickness over a period of 3600 seconds (Mean + 95% confidence limits) (n=6).

3.4.4 Mechanical Properties of Articular Cartilage

Human articular cartilage had a higher equilibrium elastic modulus (4.89 MPa) compared to porcine (1.15 MPa) and bovine cartilage (1.84 MPa) and ovine cartilage (2.58 MPa) (Figure 3-5).

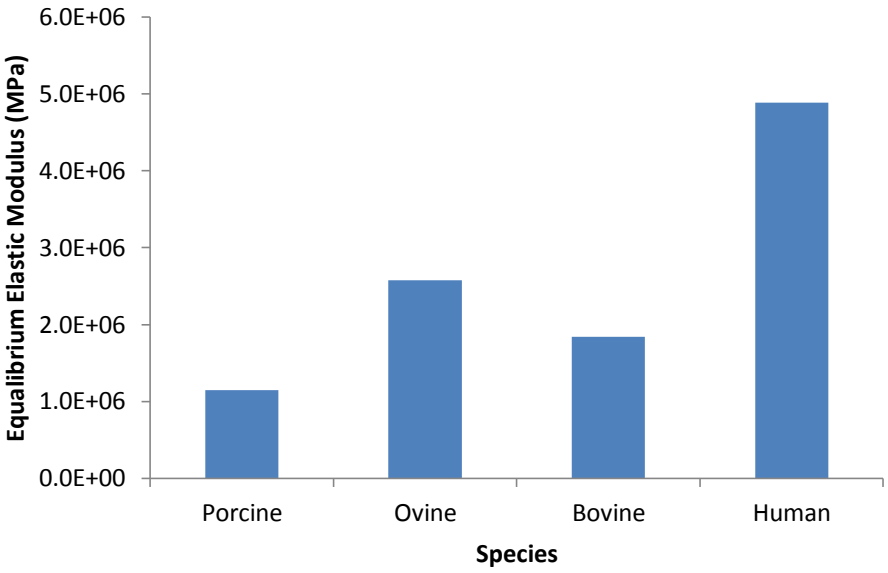

Figure 3-5: Equilibrium elastic modulus of articular cartilage for all species

Porcine was the most permeable with a permeability of $5.53x10^{-16}$ M^4/Ns, whereas ovine was the least permeable ($7.50x10^{-17}$ M^4/Ns). Bovine and human had a permeability of 3.03 $x10^{-16}$ M^4/Ns and 1.40 $x10^{-16}$ M^4/Ns respectively (Figure 3-6).

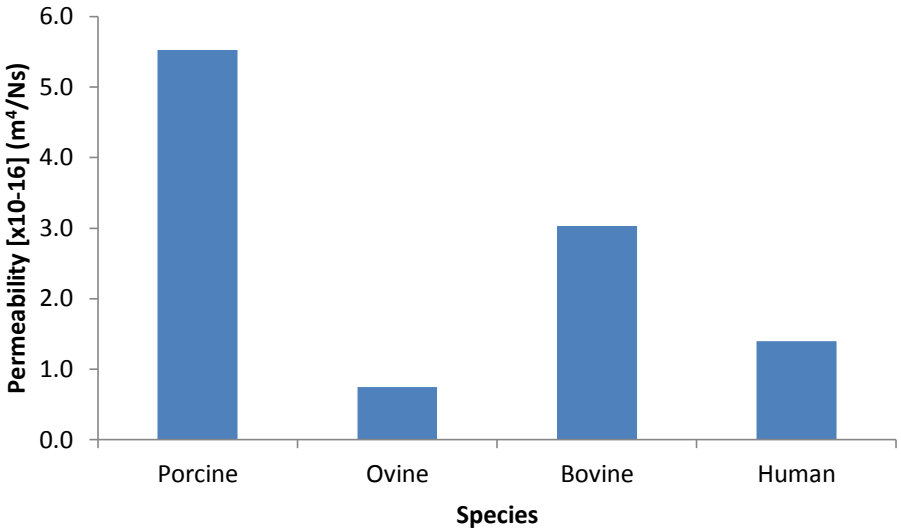

Figure 3-6: Permeability of articular cartilage for all species

3.5 Discussion

In the current study, variations between different species of quadrupeds commonly used in *in-vitro* assessments were successfully examined in terms of geometry of the femoral heads, cartilage thickness and intrinsic mechanical properties of articular cartilage. These results were compared to human femoral heads.

3.5.1 Femoral Head Geometry

A positive correlation between femoral head size was observed when comparing between the sizes of species of quadrupeds (Warrington (2001)). Bovine had a significantly larger femoral head compared to all species and ovine had the smallest. This comparison was not made in previous studies due to limited quadrupeds tested. Porcine femoral heads were found to be the most similar to human heads in terms of geometry, which could be due to the similar body weights between the two species.

3.5.2 Articular Cartilage Thickness

A positive correlation between femoral head diameter and cartilage thickness was established when comparing animal species (excluding humans). However, this correlation was not observed in a previous study (Athanasiou *et al.*, 1995), where baboon had thicker cartilage compared to canine even though canine had a larger femoral head diameter. This suggests that femoral head diameter is possibly positively correlated with cartilage thickness between species of quadrupeds only.

Athanasiou *et al.* (1995) compared the thickness of articular cartilage from the hip of a variety of species including human, also using a needle probing method. It was stated that human cartilage (1.39 ± 0.16 mm) was significantly thicker than canine (0.47 ± 0.14 mm), baboon (0.68 ± 0.14 mm) and bovine (1.26 ± 0.17 mm) cartilage (Athanasiou *et al.*, 1995). The current study also found that human femoral heads exhibited significantly thicker articular cartilage compared to quadrupeds. Another study by Athanasiou *et al.* (1991) compared cartilage thickness taken from human, bovine, canine, cynomolgus monkey and leporine knee joints (Athanasiou *et al.*, 1991). It was also concluded that human exhibited the thickest cartilage compared to the other species.

In a previous study by Simon (1971), it was suggested that within the same species, thickness was positively correlated with magnitude of deformation (Simon, 1971). However, the strength of these correlations were not presented. In the current study, a weak correlation between thickness and magnitude of deformation was observed in the bovine samples (r^2 = 0.60); however, no correlation was observed for human, porcine and ovine tissue.

3.5.3 Articular Cartilage Biomechanical Properties

The biomechanical properties of articular cartilage taken from human and quadrupedal hips were determined. Human cartilage was found to have higher equilibrium elastic modulus compared to all the other species. This agrees with a previous study that compared the aggregate modulus of bovine, human, canine and baboon in terms of the biomechanical properties of articular cartilage (Athanasiou *et al.*, 1995). A study by Simon also concluded that human cartilage

was the stiffest when compared to bovine and canine for both the patella and ankle joint (Simon, 1971). However, an earlier study by Athanasiou et al. examined differences in the aggregate modulus of knee cartilage between bovine, canine, human, monkey, and rabbit (Athanasiou *et al.*, 1991). It was found that human cartilage was not significantly different to that of other species in terms of stiffness and that human cartilage was not the stiffest. Athanasiou et al. also concluded that the size of the animal (body weight) does not correlate with stiffness of hip cartilage when comparing between species (Athanasiou *et al.*, 1995). The current study also did not find a correlation between animal body weight and stiffness.

The present study considered tissues from various species which were not age matched, since the animal tissues were collected from species at a time when they were most commonly slaughtered for commercial food production. This provides useful information where young animals are used in fundamental studies of cartilage tribology. However, further work is needed to map progression of cartilage change with age in individual species. This was considered beyond the scope of this study that focused on readily available samples. This would be important in ensuring animal cartilage properties are appropriately matched to human.

The equilibrium elastic modulus of human cartilage was greater in the current study compared to the aggregate modulus obtained in previous studies (1.44 ± 0.08 MPa) (Athanasiou *et al.*, 1995). However, these results cannot be directly compared, due to the aggregate modulus takes into account the entire biphasic material and the equilibrium elastic modulus only takes into account of the solid component after fluid has exuded and equilibrium is reached (Section 1.4.1). This high stiffness of human cartilage could be due to the source of the human samples. In a previous study, the hip joints were taken from relatively young cadavers aged between 24-50 yrs with a mean of 36 years (Athanasiou *et al.*, 1994; Athanasiou *et al.*, 1995). It has been reported that cartilage becomes stiffer with advancing age, due to a process known as Maillard reaction producing high levels of advance glycation end products (AGE) (Verzijl *et al.*, 2000; Verzijl *et al.*, 2002). This reaction causes an accumulation of crosslinks between collagen fibres, turning the cartilage from a white colour to a yellow brown (Bank *et al.*, 1998). The theory of AGEing has

also been supported by other groups (Saudek and Kay, 2003). In the current study, femoral heads were taken from patients who have suffered femoral neck fractures. These patients were typically older than the samples used in previous studies. Therefore, the human cartilage in the current study could be stiffer due to the accumulation of AGE products. The human cartilage used in this study was a yellow brown colour, which supports this observation (Figure 3-7).

Figure 3-7: Yellow brown colour of human femoral head

The strain exhibited during deformation in this study was large (up to 30%). The equilibrium elastic modulus is strain dependant; therefore, this could explain the larger equilibrium elastic modulus values than expected. The relationship between strain state and equilibrium elastic modulus also highlights another limitation to the study. Due to using a consistent load of 0.8 N, pins with differing thicknesses will also exhibit different strain states; and hence could affect the calculated equilibrium elastic modulus.

In the current study porcine cartilage exhibited larger permeability compared to all the other species. Human cartilage exhibited less permeability compared to porcine and bovine cartilage samples; however, ovine cartilage was the least permeable. Athanasiou et al. (1995) examined the permeability of cartilage for all the species and concluded that human cartilage was the least permeable. The permeability values obtained in this study are within the reported range from previous studies (Lai and Mow, 1980), except for ovine where permeability was

found to be lower. However, the permeability of ovine femoral head cartilage has not been examined in previous studies.

The difficulties in fitting the initial region of the deformation over time curve must also be taken into consideration. It has been well documented that in this region, the experimental and theoretical creep deformation differ (Mow *et al.*, 1989; Setton *et al.*, 1994; Keenan *et al.*, 2009). This difference is due to a number of factors. Such as in the model used in the current study, friction between the indenter tip and cartilage surface was assumed to be zero. However, initially during indentation of cartilage, friction does occur as a function of time, which is difficult to model (Mow *et al.*, 1989; Setton *et al.*, 1994). Also, initial loading conditions between the experimental and theoretical creep tests are difficult to match exactly (Roemhildt *et al.*, 2006). Another limitation of the model is that it is exhibits linear isotropic homogeneous mechanical properties. Therefore, it does not take into account the well documented depth-varying properties of cartilage (Mow *et al.*, 1989).

3.6 Conclusion

The rationale for this experiment was to establish the “optimum” animal tissue to use in the medium term hip hemiarthroplasty model in terms of its mechanical and geometrical properties. However, the results have concluded that there is no “optimal” joint. The size and roundness of porcine hips are the most similar to human hips, whereas ovine hips are the least comparable. However, ovine hip cartilage exhibited mechanical properties similar to that of human cartilage. Porcine hips are the most different in terms of equilibrium elastic modulus and permeability; both are integral to the tribology of cartilage. Bovine cartilage of the femoral head has the most similar thickness to human cartilage.

The joint which will be chosen to represent human is porcine. The reasons for this are that porcine femoral heads are the most round compared to the other species and hence, are most comparable to humans. Therefore, the contact region between the round CoCr femoral head and the porcine acetabular cups should be the most similar to human acetabular cups. However, the differences in thickness

and mechanical properties between porcine and human cartilage must be taken into consideration when analysing the medium term tribology.

Chapter 4: Validation of the Medium Term *In-vitro* Tribological Model

4.1 Introduction

Due to the aging population, research into alternatives to the gold standard total joint replacement has recently increased; specifically procedures that aim to preserve the natural joint. Therefore, the tribology of cartilage has become a subject of interest. Many previous studies that have investigated friction and wear of cartilage using a variety of materials and contact stresses have produced invaluable results and conclusions. However, all the previous *in-vitro* studies investigating the tribology of cartilage were only conducted over the short term (hours) (Malcom, 1976; Pickard *et al.*, 1998; Ateshian *et al.*, 2003; Katta *et al.*, 2007). This is a relatively short period of time compared to tribological studies of total joint replacements and is a severe limitation with regards to drawing conclusions that might affect clinical practice. It was hypothesised that more information could be gained from increasing the duration of testing.

When testing cartilage over an extended period of time, difficulties such as maintaining the mechanical integrity of cartilage and eliminating contamination must be considered. This could be approached by using certain additives to the already established lubricant used in *in-vitro* biotribological studies (serum diluted in water). Therefore, to conduct a medium term tribological test: the lubricant must, A) exhibit similar tribological properties to synovial fluid, B) maintain the tribological properties of articular cartilage, and C) to eliminate contamination and microbial growth in the lubricant and on the cartilage surface. These will be discussed in detail below:

A. <u>Exhibit Similar Tribological Properties to Synovial Fluid</u>

Many studies that have investigated cartilage tribology have used foetal bovine serum (FBS) diluted in water as a substitute for synovial fluid (Muller *et al.*, 2004; Cui and Xiong, 2009; Qian and Ge, 2009). The concentration of FBS varies between studies, however, the common aim was to match the protein concentration (albumin) with that of synovial fluid (12-30 g/l in the normal human

joint) (Koopman and Moreland, 2005). However, these lubricants are hypotonic due to the use of water as the dilutant. This could increase the flow of water into the cartilage due to an increase in osmotic pressure created by the large difference in salt concentration. As discussed in Section 1.7, fluid content of the matrix is a major factor in the tribology of cartilage. By altering the osmotic pressure and increasing the fluid content of cartilage, the tribology could be affected.

B. Maintain the Tribological Properties of Articular Cartilage

Previous studies have attempted to maintain cartilage viability over an extended period of time (Kantomaa and Hall, 1988; Parkkinen *et al.*, 1992; Dumont *et al.*, 1999; Strehl *et al.*, 2005; Bian *et al.*, 2008; Wimmer *et al.*, 2008). These studies primarily concentrated on the viability of chondrocytes with the aim of maintaining the ECM. Therefore, culture medium (e.g. Dulbecco's modified Eagle's Medium) has been used to provide a supply of nutrients to the cells. Other common constituents which have been used to maintain chondrocyte viability are growth factors and ascorbate (Dumont *et al.*, 1999; Strehl *et al.*, 2005; Bian *et al.*, 2008). However, these studies primarily concentrated on small volumes of cartilage due to the difficulties of nutrient diffusion in large tissue samples. For the majority of these studies, the bone was also removed due to concerns regarding osteocytes (bone cells) becoming necrotic and releasing mediators of inflammation that would degrade the cartilage matrix.

The majority of these studies aimed to maintain chondrocyte viability to extend the shelf life of allografts prior to use in surgery. These studies therefore focussed upon maintenance of cartilage viability for a long period of time (14 to 56 days). In the current study, only the mechanical function of cartilage under tribological conditions was assessed over a period of four days. Therefore, the viability of chondrocytes was not the main concern, and the research focussed on the constituents of the cartilage that govern the tribological properties such as the extracellular matrix and fluid content. A previous study had introduced proteinase inhibitors to storage solutions to eliminate enzymatic digestion of cartilage (Katta, 2007). However, the effect of dramatically reducing chondrocyte viability on the

tribological properties is yet to be determined and thus will be considered in this Chapter.

C. Eliminate Contamination and Microbial Growth

The superficial layer of cartilage is extremely important for tribological properties; this was discussed in detail in Section 1.7.1. This is due to the interactions between the molecules on the surface of the cartilage and the lubricant. Microbial growth in the lubricant and on the surface might affect this interaction and hence, alter the tribology of cartilage (especially over an extended period of time). Thus eliminating contamination of the acetabulum is essential to perform a medium term tribological test. Previous studies used a variety of antibiotics and antifungals to eliminate contamination arising from the dissection and tissue processing (Kantomaa and Hall, 1988; Parkkinen *et al.*, 1992; Dumont *et al.*, 1999; Strehl *et al.*, 2005).

Both the time dependent degradation of cartilage and the contamination within the system can affect the frictional response of the natural acetabular cup. Therefore, in order to distinguish between the effects of each factor individually, it was necessary to eliminate one at a time. First, efforts were made to eliminate microbial growth within the lubricant and on the cartilage surface. Therefore, the extent of cartilage degradation in terms of the effect on the tribological properties of cartilage could be determined; and hence, the effect of contamination on cartilage tribology also. This was addressed by improving the dissection technique. Due to the novelty of aseptically dissecting the acetabular cup, this was done incrementally and the repeatability of the technique was assessed.

The aim of this section was to validate the proposed medium term tribological *in-vitro* model. This was carried out by assessing the proposed lubricant. The effect of contamination on the tribology of cartilage, and thus the need to maintain sterility was also determined. The overall degradation of the tissue and its effect on cartilage tribology was then established. The structure of this chapter is depicted in the flow chart below (Figure 4-1).

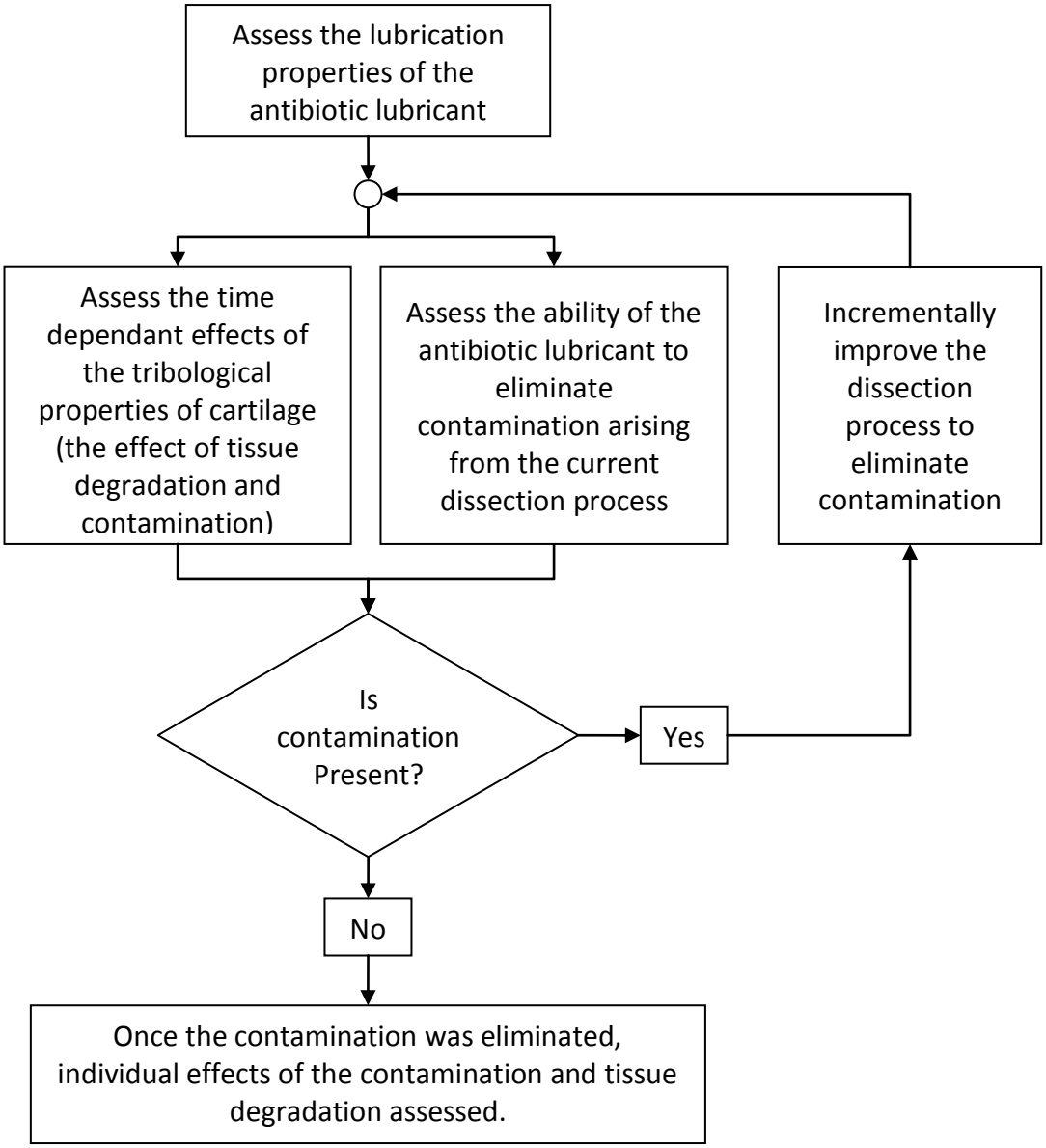

Figure 4-1: Flow Chart of the Validation of the Medium Term *In-vitro* Tribological Model

4.2 Materials and Methods

A lubricant was prepared based on the three criteria discussed in Section 4.1 (antibiotic lubricant). To minimise bacterial contamination that originated from the dissection process, antibiotics penicillin and streptomycin (Penstrep) were used. These had been commonly used in previous studies that aimed to maintain osteochondral explants (Kantomaa and Hall, 1988; Parkkinen *et al.*, 1992). To minimise fungal contamination, Amphotericin B was used. Aprotinin which is a proteinase inhibitor was used to minimise the degradation of the ECM (Katta,

2007). To obtain a lubricant with a similar concentration of proteins to that of synovial fluid and hence have similar tribological properties, 25% (v/v) new born calf serum was included in the lubricant (Wang *et al.*, 1998; Northwood *et al.*, 2007). PBS was used as the diluent to maintain osmotic homeostasis and hence, eliminate the swelling effect that could occur when using a hypotonic diluent such as water. The working concentrations of each constituent used in the antibiotic lubricant are shown in Table 4-1.

Table 4-1: Antibiotic Lubricant Constituents

Constituents	**Working Concentration**
Aprotinin	10 KlU ml^{-1}
Amphoteracin B	25 µgml
Penstrep	100 μml^{-1}
New born calf serum	25 % (v/v)
PBS	Balance

The antibiotic lubricant (200 ml) was prepared and sealed in a 480 ml sterile polypropylene container (Cole-Parmer, Illinois, USA). These were stored for no longer than 48 hrs at 5 ^{o}C until ready for use.

This Chapter aimed to compare the antibiotic lubricant to 25% (v/v) FBS in water (hypotonic) lubricant and 25% (v/v) FBS in PBS (isotonic) lubricant. Comparisons between the lubricants were made based on three criteria. 1) Tribological properties in the short term, 2) time dependent effects of the lubricant on cartilage tribology over a four day period, and 3) ability of each lubricant to minimise contamination arising from the proposed sterile dissection process. The methodologies used to conduct this assessment are described below.

4.2.1 Lubrication Properties of the Antibiotic Lubricant

Eighteen porcine hind legs (six months old) were obtained within 24 hours of slaughter (Section 2.3). The acetabulae were dissected using the methods described in Section 2.3.3, and the diameters were measured using a Vernier calliper (± 0.01 mm) in the anterior/posterior direction. A CoCr femoral head (Section 2.2.4) was selected to allow a clearance of 0.6-1.2 mm; which was the standard clearance used in Lizhang (2010) study. The acetabulae were then

prepared and mounted in the pendulum friction simulator as described in Section 2.4.4.

The friction simulator applied a flexion/extension angle ±15° with a 25 to 800 N cyclic load for a two hour period (Figure 4-2). This loading regime was used by Lizhang (2010) and was comparable with hip load experienced in quadrupedal gait (Bergmann *et al.*, 1984; Bergmann *et al.*, 1999). The friction was recorded at every 30th cycle for the first 100 cycles, every 150th cycle up to the 1000th cycle, and every 300th cycle up to the end of the test. Prior to and after each test, a constant load friction test was conducted to calculate the frictional offset as described in Section 2.4.4.

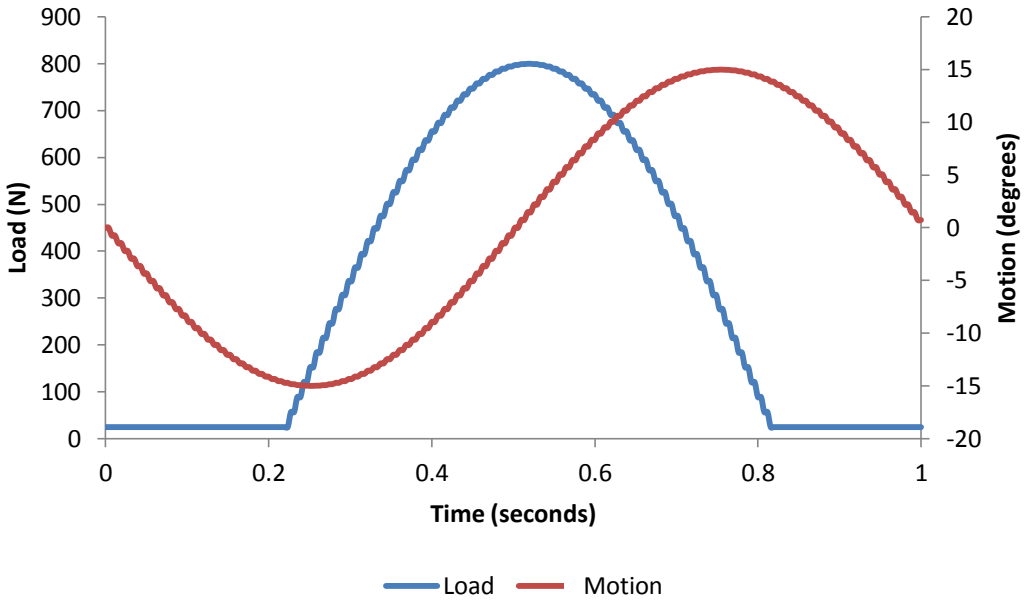

Figure 4-2: Loading and motion cycle applied by the pendulum friction simulator

This method was performed on each acetabulum using either the antibiotic lubricant (n=6), the hypotonic lubricant (n=6), or the isotonic lubricant (n=6).

4.2.2 Time Dependent Effect of the Tribological Properties of Cartilage

Twelve six month old porcine hind legs were obtained within 24 hours after slaughter (Section 2.3). In order to minimise contamination, the dissection technique described in Section 2.3.3 was modified.

The initial part of the dissection was conducted on the dissection bench. The entire hip joint was removed from the porcine leg using a sterile scalpel holder and

sterile blade (Section 2.5.5). Care was taken not to rupture the capsule as this would contaminate the acetabular cup cartilage. The medial section of the pelvis was clamped to the dissection bench and using a sterile hacksaw, excess bone was removed from the acetabulum (leaving approximately 5-10 mm of subchondral bone). The remaining soft tissue was removed from the hip joint, still keeping the capsule intact.

The hip was sprayed with 70% (v/v) ethanol in order to kill surface contaminants on the exposed tissue. Ethanol destroys microbial cells by causing membrane damage and rapid denaturation of proteins, leading to interference with metabolism and cell lysis. This mode of action is enhanced by the presence of water (McDonnell and Russell, 1999). After being sprayed with 70% v/v ethanol, the tissue was immediately placed in the Class II cabinet. The femoral head and acetabulum were separated using sterile dissection equipment and the acetabulum was placed in a container containing the sterile lubricant.

The pots containing the acetabulum and sterile lubricant were agitated at 1 Hz on an orbital shaker at room temperature for four days. The acetabulum was then taken out of the pot and the diameter was measured using the technique described in Section 4.2.1. A CoCr femoral head (Section 2.2.4) was chosen to create a clearance of 0.6 – 1.2 mm. The acetabulum and selected CoCr femoral head were then mounted on the pendulum friction simulator as described in Section 2.4.4. The lubricant from each pot was used as the lubricant for the experiment.

A flexion/extension angle of ±15^{o} with a 25 to 800 N cyclic load was applied to the acetabulae for a two hour period. The friction was recorded at every 30th cycle for the first 100 cycles, every 150th cycle up to the 1000th cycle, and every 300th cycle up to the end of the test. The tests were performed using either the antibiotic lubricant (n=4), the hypotonic lubricant (n=4), or the isotonic lubricant (n=4). To investigate the time dependant effects of each lubricant, the friction was compared to the friction obtained from the previous experiment (Section 4.2.1).

4.2.3 Ability to Minimise Contamination

Each time the test detailed in Section 4.2.2 was performed on an acetabulum; a 2 ml sample of the lubricant was taken prior to immersing the acetabulum in the lubricant (to ensure the lubricant was prepared aseptically), and this was repeated after the four day test period. This was conducted in a class II cabinet using a 1000 µl pipette and filter tips. The samples were plated out under sterile conditions onto nutrient agar plates, heated blood agar plates and Sabauroud agar plates using the methods described in Section 2.5.2. To test for microbial formation on the cartilage surface, a swab of the cartilage was taken using a cotton wool swab (Section 2.5.1). The swabs were placed in a vial of nutrient broth and incubated for 48 hrs at 37°C. This was performed prior to and after agitating each acetabulum in the lubricant.

4.2.4 Statistical Analysis

Graphs are presented and statistical differences were determined using the methods described in Section 2.6.

4.3 Results

4.3.1 Lubrication Properties

The lubrication properties of the different lubricants were determined by measuring the friction over time in a two hour tribological test using a hemiarthroplasty simulation (Section 4.2.1). For all three lubricants, friction increased with time. The rate of increase in friction was large initially and gradually reduced towards the end of the two hour period (Figure 4-3).

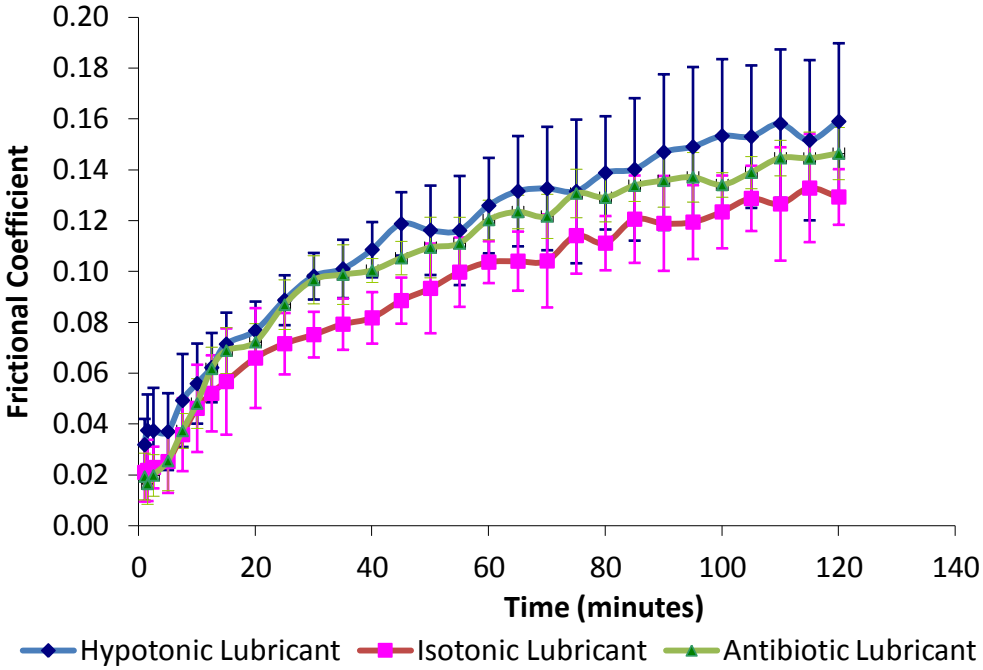

Figure 4-3: Friction over two hours using fresh acetabular cups (n=6) in a pendulum friction test versus a CoCr head using three different lubricants: hypotonic, isotonic and antibiotic lubricants. Data was presented as the mean (n=6) ±95% confidence limits.

After two hours of tribological testing, the friction measured in the sample tested with the isotonic lubricant was significantly lower (0.13±0.01) compared to the friction measured with the hypotonic lubricant (0.16±0.03) ($P<0.05$). There was no significant difference between the friction determined in the samples tested with antibiotic lubricant and the hypotonic lubricant as well as the antibiotic lubricant and the isotonic lubricant after two hours (Figure 4-4).

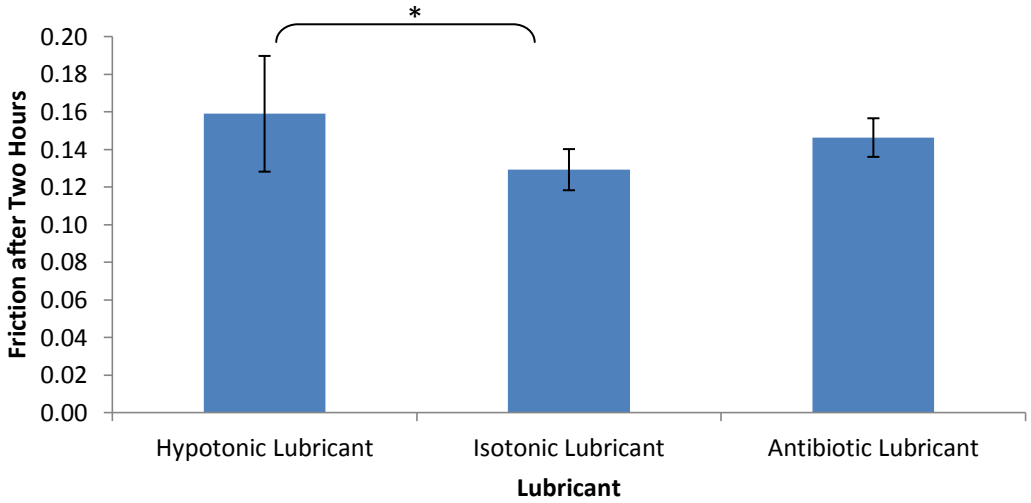

Figure 4-4: Mean friction after two hours of fresh acetabular cups (n=6) using the three lubricants: hypotonic, isotonic and antibiotic lubricant. Data was presented as the mean (n=6) ±95% confidence limits.

4.3.2 Time Dependant Effects on Tribology

The time dependant degradation of the acetabular cartilage was determined by agitating the acetabulum samples in each of the lubricants for four days and then tribologically testing for two hours as described in Section 4.2.2. The friction results from these tests were compared to the two hour friction results using fresh acetabulae (Section 4.3.1).

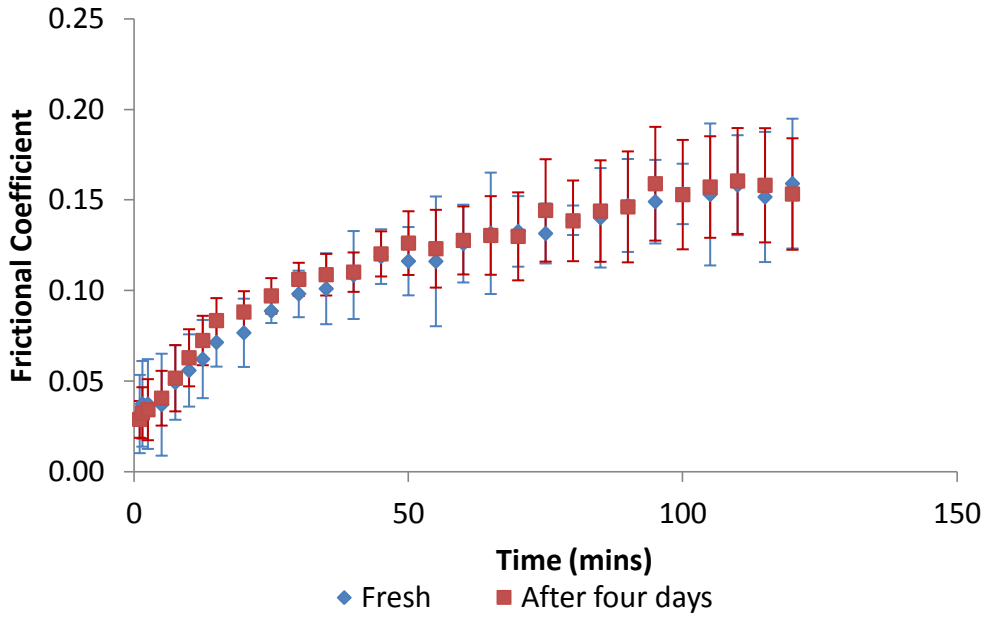

Figure 4-5: Mean friction over time of acetabular cups agitated in the hypotonic lubricant (n=4) compared to fresh acetabular cups (n=6). Data was presented as the mean ±95% confidence limits.

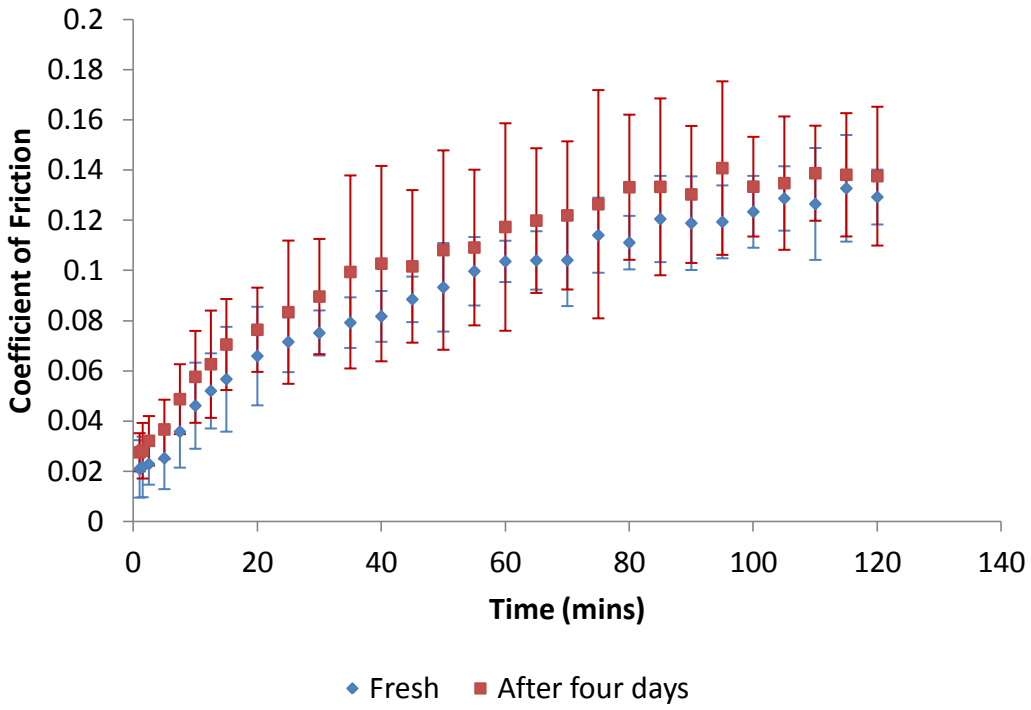

Figure 4-6: Mean friction over time of acetabular cups agitated in the isotonic lubricant (n=4) compared to fresh acetabular cups (n=6). Data was presented as the mean ±95% confidence limits.

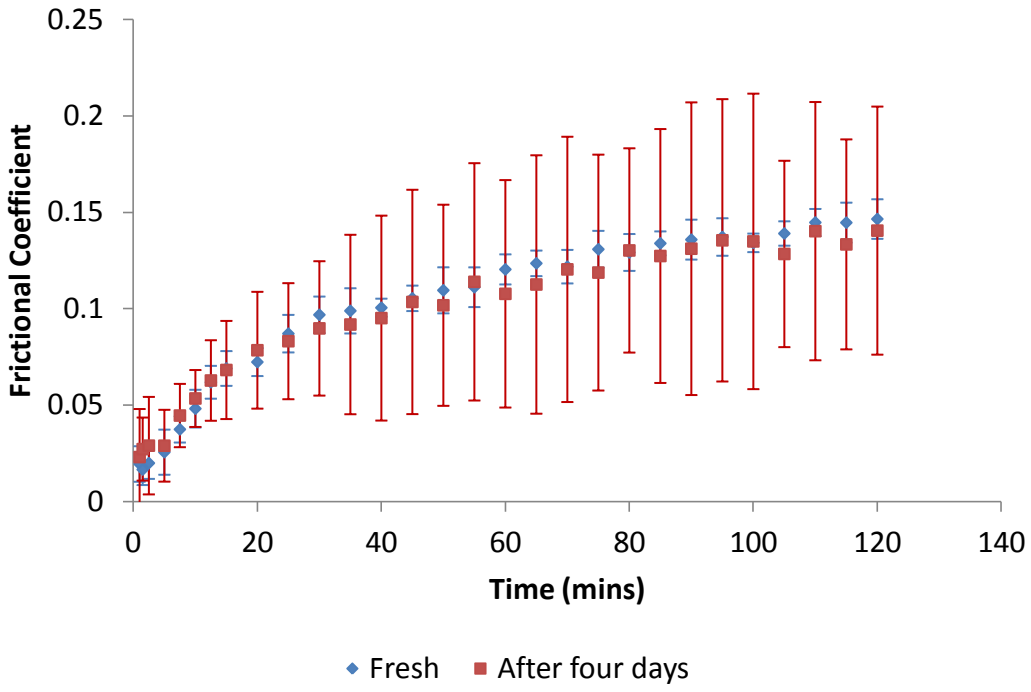

Figure 4-7: Mean friction over time of acetabular cups agitated in the antibiotic lubricant (n=4) compared to fresh acetabular cups (n=6). Data was presented as the mean ±95% confidence limits.

The results shown in Figure 4-5 to Figure 4-7 showed that agitating the acetabulae in each of the lubricants had no significant effect on the short term frictional response of the cartilage ($p > 0.05$).

4.3.3 Ability to Minimise Contamination

Typical examples of the nutrient agar, heated blood agar, Sabauroud agar and the nutrient broth swabs are shown in Figure 4-9 and Figure 4-9. All samples were contaminated after four days of agitation, regardless of the lubricant constituents. The nutrient agar and heated blood agar showed that there were bacteria present which are highly likely to be pathogenic. The Sabauroud agar showed that there was also fungi contamination of the lubricant.

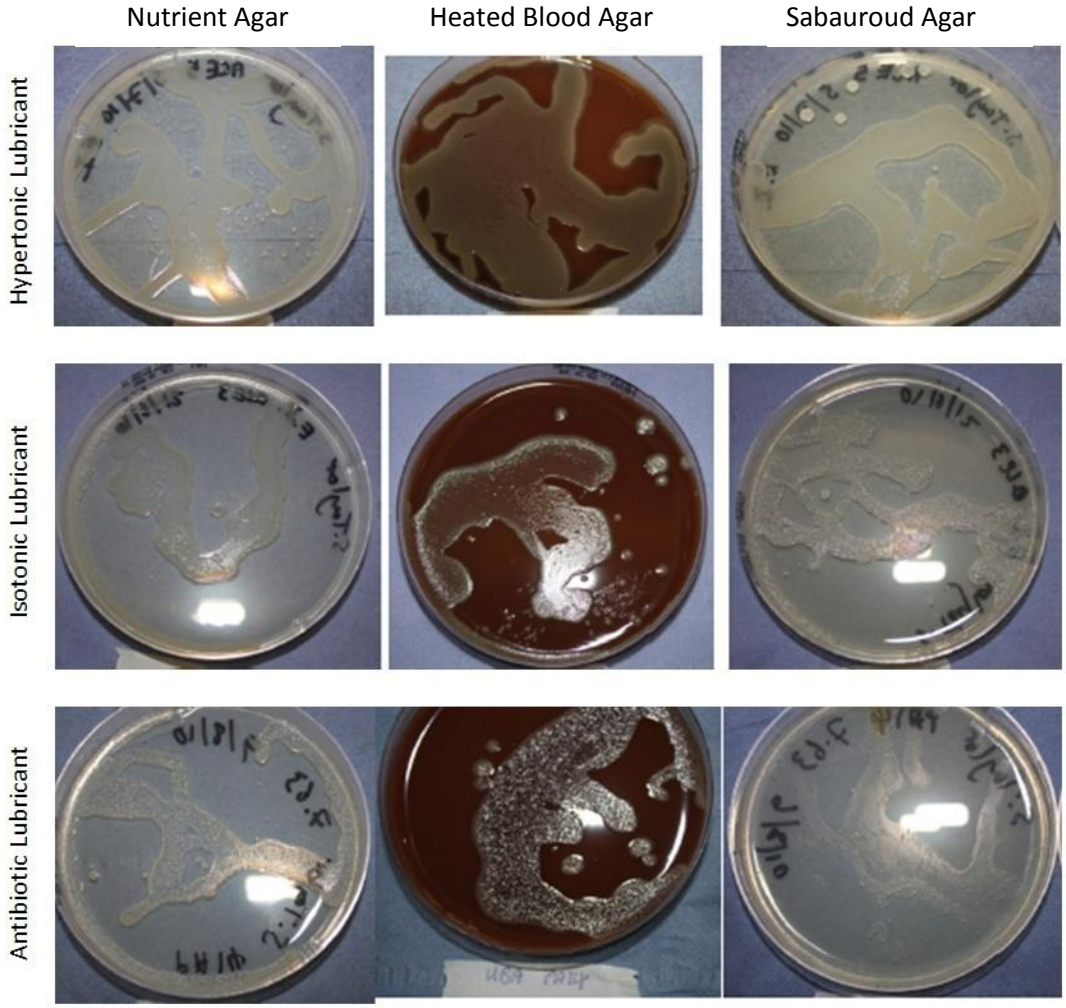

Figure 4-8: Typical agar plates of each lubricant after four days in agitation including nutrient agar, heated blood agar and Sabauroud agar. The results suggest that bacteria and fungi were present.

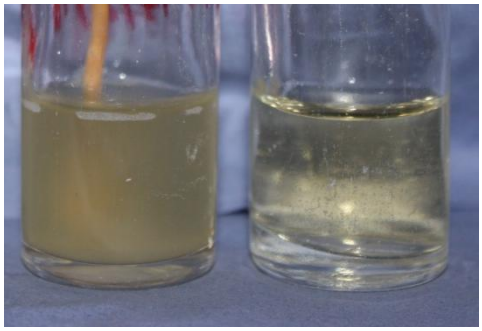

Figure 4-9: Typical nutrient broth after swabbing the cartilage (left) compared to the non-contaminated negative control nutrient broth (right).

Since the lubricants were sterile prior to inserting the acetabulae, the results suggested that the antibiotic lubricant was ineffective in eliminating microbial contamination arising from the current dissection technique. The high levels of contamination also suggested that the results obtained in Section 4.3.2 could be a result of a combination of both cartilage degradation and contamination (specifically microbial growth on the cartilage surface). Hence, in order to determine the time dependant degradation of cartilage alone, it was essential to eliminate contamination. This would also allow the effect of microbial contamination on the friction of cartilage to be determined. The aseptic dissection technique discussed in Section 4.2.2 was further developed, in order to eliminate the sources of contamination.

4.4 Improvement of Aseptic Dissection Process

Incremental improvements were made to the previous method used to remove the acetabulum (Section 4.2.2). Each time the acetabulum was dissected, a swab of the cartilage surface was taken (described in Section 2.5.1), placed in nutrient broth and incubated at 37°C for 48 hours. The acetabulae were then placed in 480 ml sterile polypropylene containers containing the antibiotic lubricant (200 ml), and agitated at 1 Hz for 4 days. After agitation, a 2 ml sample of the lubricant was taken to be later agar plated (as described in Section 2.5.2) and another swab was taken of the cartilage surface. The following Section describes the various improvements made to the dissection process.

4.4.1 Method Development – Phase One

Sawing in Cabinet

Using the original technique, swabs taken from the cartilage surface prior to placing in the antibiotic lubricant showed no contamination. This suggested that the source of contamination was not within the capsule; but more likely to be on the subchondral bone. This could have originated from sawing behind the acetabulum on the workbench. To minimise the risk of contamination during sawing, this was performed in a sterile environment. A clamp was designed and manufactured to allow the acetabulum to be sawn off inside the Class II cabinet (Appendix 4). The clamp was made out of stainless steel to allow for sterilisation by autoclaving (Section 2.5.5). Therefore, the entire hip joint was removed from the porcine leg on the dissection workbench, using a sterile scalpel to detach the pelvis and a sterile hacksaw to cut through the femur. This was then placed in the class II cabinet. The femoral head was fully dislocated using a second set of sterilised dissection equipment and the pelvis was clamped in the custom made clamp. A sterilised hack saw was used to cut around the back of the acetabulum prior to placing it into the antibiotic lubricant. Sterile gloves were used for dissection and sawing within the class II cabinet.

Excess Soft Tissue

Previously, excess soft tissue was removed from the joint. It was thought that transporting less tissue into the sterile environment (class II cabinet) would reduce the risk of transferring microbes that could be residing on the soft tissue. However, this left the pelvic bone exposed to contaminants. These contaminants could transfer to the sterile saw blade (whilst sawing in the class II cabinet) and thus infect the deeper bone. Therefore, to further minimise the risk of contamination from the sawing process; excess soft tissue surrounding the pelvis was left untouched prior to placing the hip joint into the class II cabinet. This protected the surface of the bone from contaminants. The tissue was then removed in the class II cabinet prior to sawing using a sterile scalpel.

Effect on Contamination

The dissection technique with these improvements was conducted on four porcine legs obtained within 24 hours after slaughter. These were swabbed before and after inserting into the antibiotic lubricant and a sample of the lubricant were agar plated after four days of agitation. Only one out of the four repeats was sterile after agitation. Therefore, these improvements had the potential to eliminate contamination. However, repeatability was not yet achieved. Further improvements were therefore made to ensure the acetabulae were dissected aseptically.

4.4.2 Method Development – Phase Two

Using Fresh Tissue

Previously, the porcine legs were obtained from the abattoir within 24 hours after slaughter (Section 4.2.2). Contamination of the tissue could occur between the slaughter and receiving the tissue. Thus, reducing this time could reduce the risk of the tissue becoming contaminated prior to starting the dissection process. A method of sourcing the legs was established in which the time between slaughter and start of dissection was only two hours.

Aseptic Technique on the Workbench

A major source of contamination could have been a result of dissecting the hip joint on the workbench, since here there was no protection from the environment. A common method used in aseptic techniques is to use a Bunsen burner. By placing the flame close to the fresh porcine leg, the contaminated air around the leg heats up, causing it to rise, away from the tissue via convection; hence, reducing the risk of contamination.

To further reduce the risk of contamination from dissection on the workbench; a metallic tray wrapped in tinfoil was dry heat sterilised at 180 °C for four hours (Section 2.5.5). After the hip was detached from the leg and the Bunsen burner was turned off, the hip was immediately coated in 70% v/v ethanol and placed on the tray under the tinfoil for 10 minutes. This acted as a sterile

environment, allowing the alcohol to destroy the remaining contaminants on the surface of the soft tissue before transferring it to the class II cabinet.

The Effect on Contamination

Four fresh porcine legs were obtained within two hours of slaughter. The acetabular cups were dissected using both incremental improvements described in Section 4.4.1 and 4.4.2. Swabs were taken before and after inserting the acetabulae into the antibiotic lubricant and a sample of the lubricant was taken after four days of agitation and agar plated. All of the four acetabulae and lubricants showed no signs of contamination on the cartilage surface and within the lubricant respectively. Therefore, by including all the improvements discussed in this Chapter, contamination was eliminated.

4.4.3 Further Improvements

Minor improvements were made to the dissection process to further reduce the risk of contamination.

- Previously, the clamp was assembled in the class II cabinet. However, this could increase the risk of contamination. Therefore, the clamp was assembled prior to sterilisation.
- A blade was attached to the scalpel holder prior to sterilisation for the same reason.

4.5 Final Sterile Dissection Protocol

The porcine leg was obtained within two hours of slaughter and placed on a work bench. The Bunsen burner was set to a hot blue flame and placed near the pelvis. A dissection kit was opened close to the flame and a sterile scalpel blade was inserted into the scalpel holder and swiped through the flame. There was a protruding bone from the pelvis which originated from the removal of the leg in the abattoir. Starting from 10 – 15 mm anterior to the pelvic bone, a scalpel cut was made parallel to the femur until the knee was reached (Figure 4-10A). The scalpel blade was swiped through the Bunsen flame regularly to minimise

contamination of the blade. Care was taken not to sever the synovial capsule of the hip. The muscles and other soft tissue anterior to the femur were removed (this may include the patella of the knee). A cut through the muscle 30 – 40 mm inferior to the hip joint, perpendicular to the direction of the femur was made and all muscle and soft tissue medial to the femur was removed (Figure 4-10B).

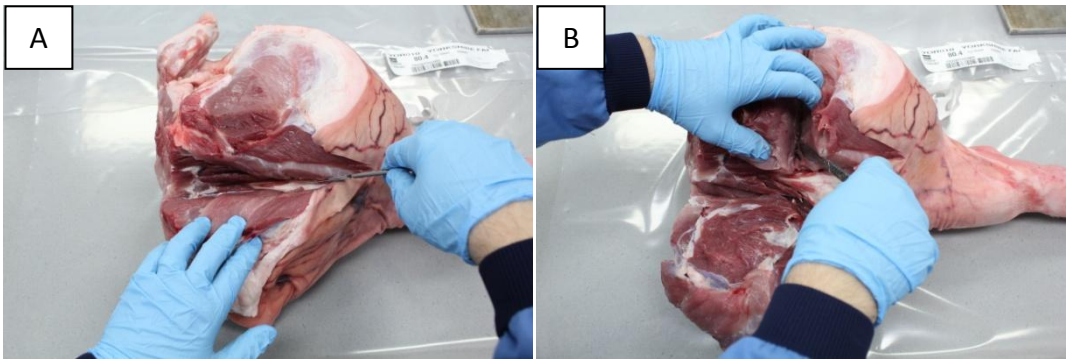

Figure 4-10: The initial cuts during the final sterile dissection protocol. A) Cut anterior and parallel to the femur. B) Cut 30 – 40 mm inferior to the hip joint.

The small hack saw was removed from the tin foil and the blade was swiped through the flame. The femur was sawn 30 – 40 mm inferior of the junction in order to remove the femoral head from the rest of the bone. A scalpel was used to remove muscles from the lateral and posterior side of the pelvis and finally, the hip was removed by cutting the muscle and soft tissue inferior to the hip. The Bunsen burner was then turned off.

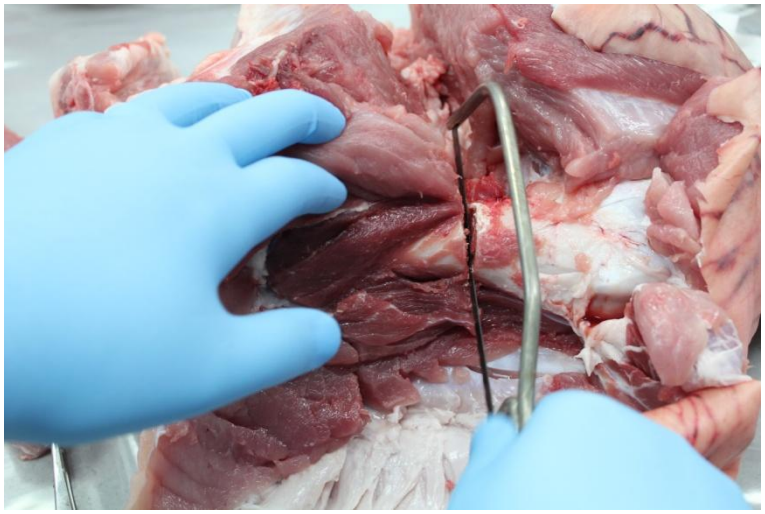

Figure 4-11: Saw cut across the femur during the final sterile dissection protocol

The edges of the top layer of the tin foil on the metal tray were loosened. The hip was sprayed with 70% v/v ethanol and placed under the loosened foil layer. This was left for 10 minutes before placing the following in the Class II cabinet:

a. Sterile dissection kit
b. Clamp
c. Large saw
d. One of the lubricant pots
e. Sterile surgical gloves
f. Nutrient broth
g. Swabs
h. Tray along with the hip joint

Using non-sterile gloves, all the foil were unwrapped and the dissection kit was opened. Care was taken not to place the saw directly on the work surface (by leaving a layer of foil between the saw and the work surface). Care was also taken not to touch any of the equipment with the non-sterile gloves. The sterile gloves were worn after this point. By using only the forceps to hold the hip in place, the femoral head was removed (Figure 4-12A) and the pelvis was placed in the clamp so that the acetabulum was facing upwards (Figure 4-12B).

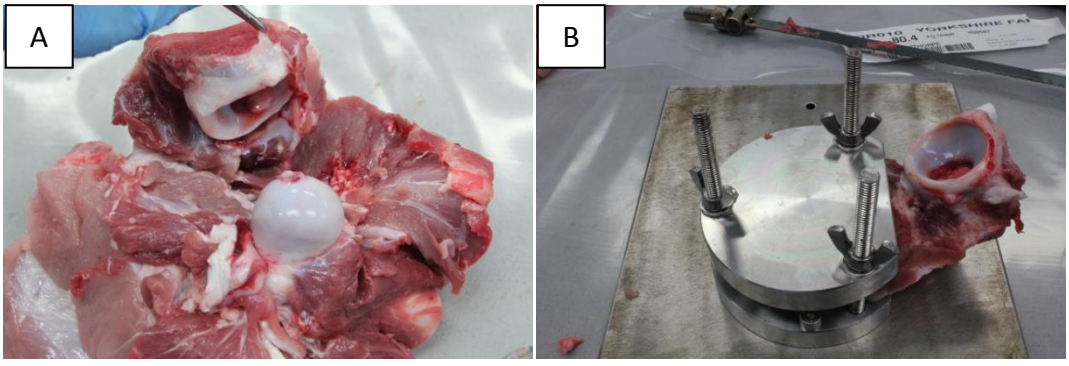

Figure 4-12: A) The femoral head was removed from the acetabulum. B) The pelvis was tightened into the clamp.

After tightening the clamp, the lateral part of the pelvis (the part furthest away from the clamp) was cut 5 mm away and tangential to the articular cartilage surface using the sterile saw (Figure 4-13A). This was repeated for the anterior and posterior parts of the pelvis (Figure 4-13 B and Figure 4-13C). Excess subchondral bone was removed (Figure 4-13D) and finally, the medial section of the pelvis was cut off; leaving only the acetabulum (Figure 4-13E and Figure 4-13F).

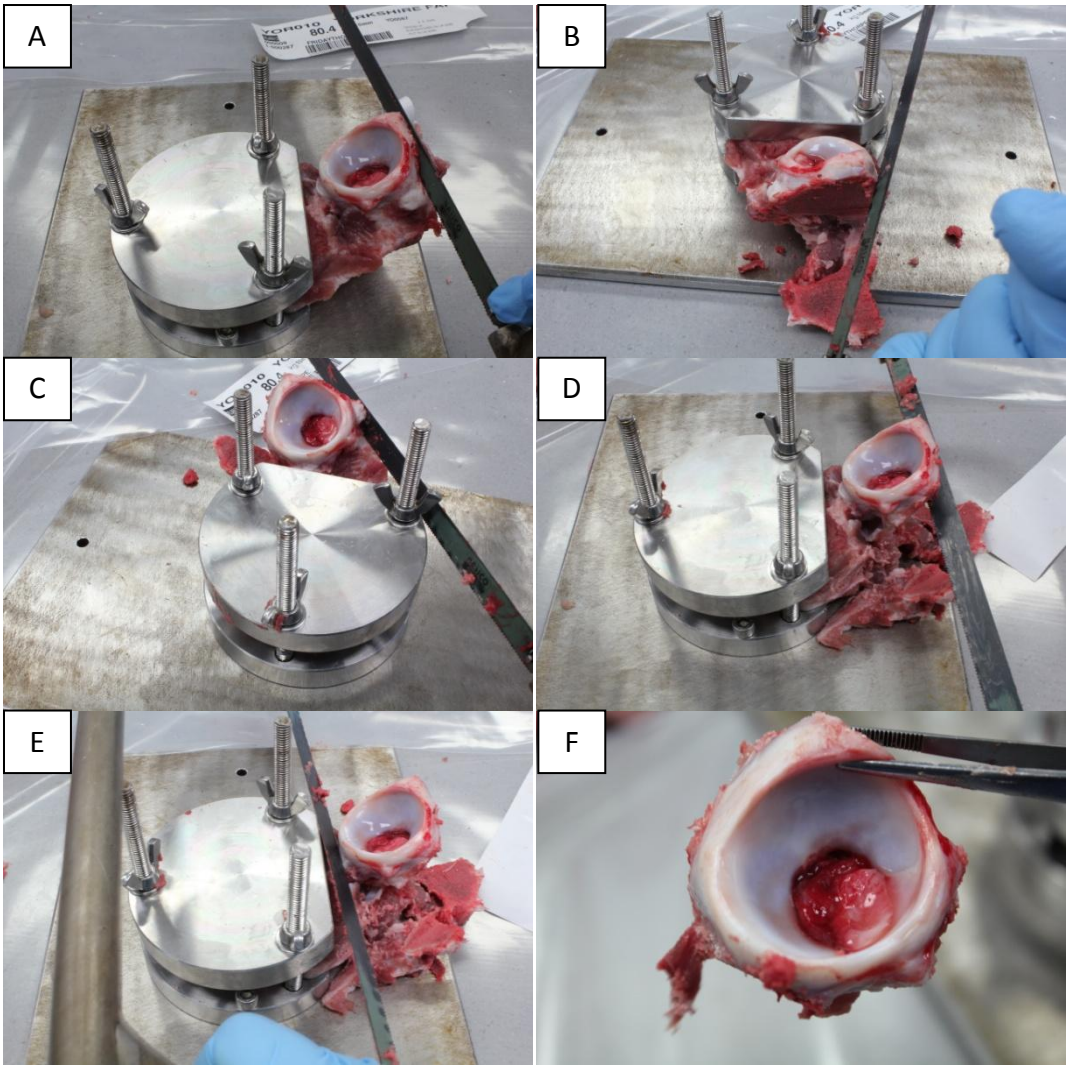

Figure 4-13: The sawing process within the class II cabinet. Saw cut on the A) superior section of the pelvis, B) posterior section of the pelvis and C) anterior section of the pelvic. D) Excess subchondral bone was removed and E) the acetabulum was finally removed from the pelvic. F) A dissected acetabulum.

The cartilage surface was swabbed and the swabs were placed in the nutrient broth. This was then incubated at 37°C for 48 hours. Using only the forceps, the acetabulum was placed in the lubricant pot and the lid was tightened.

4.6 Individual Effect of Contamination and Tissue Degradation on Cartilage Tribology

4.6.1 Introduction

A repeatable method of dissecting a porcine acetabulum aseptically was established (Section 4.4). Therefore, the effect of contamination and degradation of cartilage on the biotribology was individually determined.

4.6.2 Method

Four porcine legs were obtained within two hours of slaughter. These were dissected using the technique described in Section 4.5. Each acetabulum was tested using the methodologies described in Sections 4.2.2 and 4.2.3. Only the antibiotic lubricant was used in this study.

4.6.3 Results

Typical examples of the nutrient agar, heated blood agar, Sabaurouds agar and the nutrient broth swabs obtained following testing are shown in Figure 4-14. Contamination was not present in any of the four repeats.

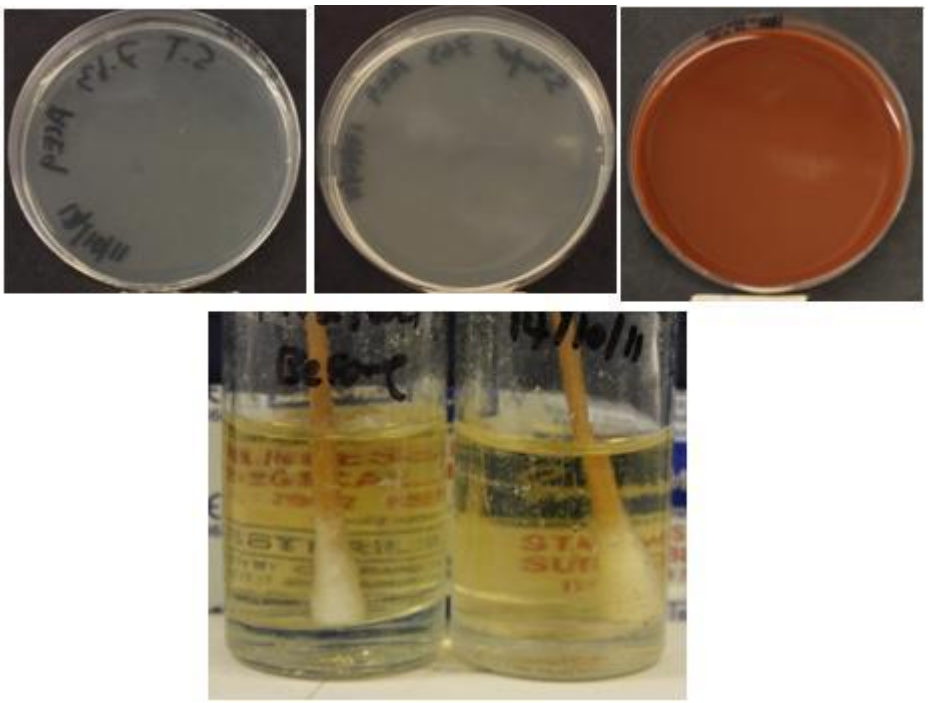

Figure 4-14: Top: Typical agar plates after four days in agitation after using the aseptic dissection technique. Bottom: Typical nutrient broth after swabbing the cartilage (left) compared to the non-contaminated negative control nutrient broth (right).

In the absence of contamination, the time dependent degradation of cartilage was assessed (Figure 4-15). The results showed that in the absence of contamination and microbial growth on the cartilage surface, the friction coefficient after two hours (0.21±0.06) was significantly higher than both the fresh (0.15±0.01) and agitated but contaminated (0.14±0.06) samples ($p < 0.05$).

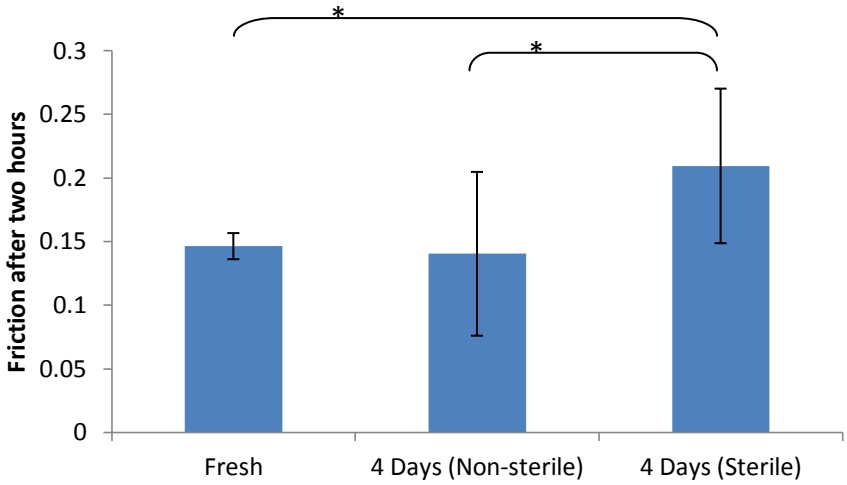

Figure 4-15: Friction of acetabulae at two hours after agitating in the antibiotic lubricant in a sterile and non-sterile condition compared to fresh acetabulae. Data is presented as the mean (n=4) ±95% confidence limits. *significant difference ($p<0.05$)

4.7 Discussion

4.7.1 Friction over Time

The aim of this Chapter was to assess the antibiotic lubricant that was intended to use in the medium term tribological test; however, it is important to discuss the standard friction curve. Friction increased throughout the test (Figure 4-3). The rate of increase was large initially and gradually reduced towards the end of the test. This has typically been seen in previous studies that have examined cartilage friction (Forster and Fisher, 1996; Forster and Fisher, 1999; Katta *et al.*, 2007). The reason for this increase has been attributed to the gradual loss of fluid within the cartilage. Therefore, over time, less of the load is supported by the fluid phase and more is supported by the solid phase, thus increasing the friction between the articulating surfaces.

The equipment, loading and motion profiles, and the method of selecting the CoCr femoral head used in this Chapter was the same as Lizhang (2010). Therefore, the results can be directly compared. Lizhang used 25% (v/v) serum in water as the lubricant and reported a friction of 0.15±0.02 after two hours of testing. This was in the same range as reported in the current study (0.16±0.03). Therefore, this

method of determining cartilage friction was repeatable with low inter-observer variability.

It is important to note that friction did not plateau throughout the test. Therefore, the maximum friction of cartilage in this configuration was unknown and thus, emphasising the need for longer term tests.

4.7.2 Lubrication Properties

The results suggested that using PBS instead of water significantly lowered friction ($p< 0.05$). This was observed when comparing results from the isotonic and hypotonic lubricants. The reason for this apparent relationship between PBS concentration and friction could be due to the delicate balance between the ions in the PBS and within the cartilage. Therefore, when the isotonic lubricant was used, this balance was maintained; and excess fluid flow into the cartilage due to osmotic pressure was prevented. This balance of water is essential for the complex lubrication regimes discussed in Section 1.7; specifically boosted and weeping lubrication which is directly related to the flow of fluid in and out of the cartilage (Fein, 1967; Walker *et al.*, 1968a). For the hypotonic lubricant, this balance may not have been reached and hence, in order to dilute the higher concentration of ions in the cartilage, water flowed into the cartilage causing it to swell. This disrupted the lubrication regimes and increased friction.

Therefore, it is important to include PBS instead of water in the antibiotic lubricant. There was no significant difference between the antibiotic lubricant and the standard hypotonic lubricant in terms of friction.

4.7.3 Effect of Contamination on Friction

To compare the effect of contamination on friction of the acetabular cartilage, the contaminated samples that had been agitated for four days in the antibiotic lubricant were compared with the sterile samples that were also agitated for four days in the antibiotic lubricant. Friction significantly increased once contamination and microbial formation on the cartilage surface was eliminated. This suggested that either the contamination of the lubricant or the cartilage surface aids the lubrication.

A possible explanation for the increase in friction in the absence of contamination is that microbial biofilm formation may aid cartilage lubrication. The definition of a biofilm is a subject of great debate (Karatan and Watnick, 2009). However, it is commonly accepted that a biofilm is an extremely thin layer (or several layers) of microbial growth that is adhered to either abiotic or biotic surfaces. The creation of this binding is complex and beyond the scope of this thesis. Multilayered biofilm matrices are comprised of a variety of molecules which provide structural integrity and allow small molecules into and out of the biofilm. It is believed that up to 97% of the matrix is water (Sutherland, 2001). However, other constituents include polysaccharides, proteins, lipids and glycolipids. A study by Souza *et al.* (2010) studied the effect that biofilm production on titanium and aluminium oxide (Al_2O_3) samples had on the coefficient of friction. Using a pin-on-plate apparatus and artificial saliva as the lubricant, the friction in the absence of a biofilm was 0.5. Once the biofilm had formed on the titanium articulating surface, the friction reduced to 0.05. This tenfold decrease in friction was partially attributed to the matrix constituents (glycoproteins and lipids in particular). Glycoproteins are proteins found in synovial fluid and have been found to have a major role in aiding joint lubrication (Swann *et al.*, 1981a). Lipids consist of a hydrophilic polar head group and a hydrophobic tail, found on the articular surface of cartilage and are also thought to aid joint lubrication.

Souza *et al.* (2010) also performed scanning electron microscopy of the titanium samples and discovered that the polysaccharide chains ruptured and formed into “rolls” during shear; followed by a “snowball” effect. These were described as acting as “miniature roller bearings” and thus could also be a reason for the reduction in friction.

In the current study, it was not known whether the microbial contamination on the cartilage was in the form of a biofilm. However, the results reflect that of the Souza *et al.* (2010) study. Therefore, these results suggested that in order to examine the medium term tribology of cartilage, sterility is essential.

In the study that compared the lubrication properties of the different lubricants (Section 4.3.1), it was noticed that when adding other constituents such

as antibiotics to the antibiotic lubricant, the friction increased significantly compared to the isotonic lubricant. This was possibly due to the antibiotics reducing the microbial formation. Therefore, the added lubrication properties of the microbes would also be reduced, thus increasing friction. This could also be the reason for the significant reduction in friction when using the isotonic lubricant compared the hypotonic lubricant, due to bacteria thriving in physiological medium.

4.7.4 Time Dependent Degradation

To assess the time dependent degradation of cartilage over four days; the fresh samples were compared with the sterile samples that had been agitated for four days in the antibiotic lubricant. There was a significant increase in friction after four days of agitation. This suggested a degree of cartilage degradation which had significantly affected its tribological response. Even though this was undesirable, the effect of this degradation was now known and could be incorporated into the analysis of the friction results from the four day tribological tests.

4.8 Conclusion

The aim of this study was to validate the medium term *in-vitro* tribological model. This was carried out by A) assessing the lubrication properties of the proposed antibiotic lubricant, B) determining the time dependant effects on the cartilage tribology, and C) determining the effect of contamination on cartilage tribology.

- An isotonic lubricant (with the inclusion of PBS) produced a lower coefficient of friction compared to a hypotonic lubricant. This could have been due to the isotonic lubricant maintaining cartilage hydration.
- The antibiotic lubricant alone could not eliminate contamination arising from the original dissection technique. Therefore, the dissection technique was improved to assess the individual effects of time dependant degradation and contamination on cartilage friction.

- In the absence of contamination, friction of cartilage increased. This supported the theory that the contamination on the cartilage surface was a biofilm.
- It was also noted that there was a time dependent effect on the friction, where after four days of agitation in the antibiotic lubricant, the short term friction increased. This supported the theory that the cartilage matrix degraded over the four days.
- This must be taken into consideration when analysing the data after the medium term tribological test, as this may have an effect on the performance of the hemiarthroplasty.

Chapter 5: Development of the Friction Simulator Vessel

5.1 Introduction

Studies that investigated the tribological properties of cartilage in the past concentrated on the short term and thus, minimising contamination was not paramount. However, results obtained in this thesis have shown the importance of maintaining sterility when conducting medium term tribological tests on cartilage (Chapter 4). Therefore, the standard fixtures used in previous studies (including the experiments conducted in Chapter 4) cannot be used in the medium term *in-vitro* model, as this leaves the system open to contamination.

Hence, the aim of this Chapter was to design, develop and validate a new friction simulator vessel that maintained sterility. This vessel was tested for its ability to maintain sterility. Also, due to altering the designs of the standard fixtures, the measured friction coefficient by the friction simulator could have been affected. Thus, this was also examined.

5.2 Design Specification

To design the friction simulator vessel, a design specification was produced through an incremental process. The aim of a design specification is to highlight the compulsory requirements known as the demand (D) and the non-compulsory requirements known as wishes (W) of the vessel. The final design specification is shown in Table 5-1.

Table 5-1: Final design requirements for the friction simulator vessel, highlighting the demands (D) and wishes (W).

D W	Requirements
	1. Geometry
D	• To encase an acetabular and a unipolar hemiarthroplasty femoral head. The acetabular size is below:

Diameter (approx.)	65 mm
Depth (approx.)	35 mm

D	• Must be able to be attached to the single station friction simulator.
D	• The centre of rotation must remain consistent with previous fixtures used in the single station friction simulator (63.24 mm from the bottom and 72.83 mm from the top).
	2. Kinematics and Kinetics
D	• To allow kinematics of the friction simulator (±15^{o}).
D	• To withstand the dynamic forces applied by the simulator (75~800N). The waveforms are below:

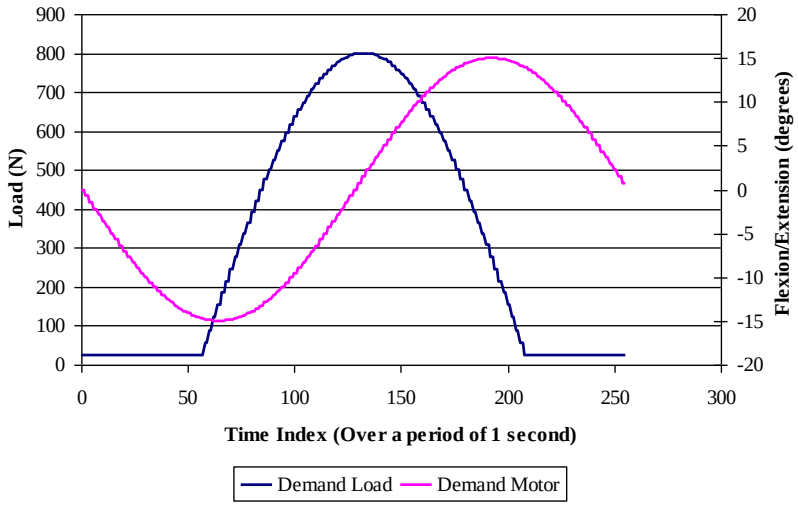

	3. Sterility
D	• Inside to remain sterile throughout assembly and testing.
D	• Must be able to encompass the existing silicon gaiters.

D W W D	**4. Usability** • To allow the acetabular and femoral components to be replaced between each tests. • To allow easy assembly and disassembly in a class 1 or 2 cabinet. • To allow friction to be measured throughout testing. **5. Materials** • All equipment must be sterilisable by autoclave.

5.3 Use of Silicon Gaiters

One of the main criteria of the simulator vessel was to eliminate microbial infection from the environment. A suggested method for this was to incorporate silicon gaiters that will allow the entire hemiarthroplasty model to be encapsulated, preventing contaminants from entering. Silicon gaiters are regularly used in total joint replacement studies and are designed to attach to the two fixtures, encapsulating the entire joint. For total joint replacement studies, this would then be filled with the lubricant. The use of a silicon gaiter is ideal for the current study because of three reasons: 1) It is non-permeable and hence protects the joint from contaminants, 2) It is flexible and thus minimises restriction of the joint during testing and 3) Silicon is autoclavable and hence, can be sterilised prior to use.

It was important to determine if the gaiters became more brittle after autoclaving to prevent cracking during testing which could result in contamination, thus affect friction. The effect of autoclaving the silicon gaiters on its mechanical properties were determined. Two gaiters were obtained and thirty 5 mm wide strips were cut longitudinally across one gaiter and twenty four 5 mm wide strips were cut circumferentially across the other. A die cutter was used for repeatability. The longitudinal strips were split into four groups of six and each of the groups of materials was autoclaved 1, 2, 4, 6 times (Section 2.5.5). The circumferential strips were split into three groups of six and autoclaved 1, 2, 4 times respectively. An additional two groups of control samples were cut longitudinally and circumferentially and were not autoclaved (n=6). The strips were placed in the

Instron 3365 material testing machine (Section 2.4.2) and held in place using pneumatic clamps. The Instron was set to apply a pre-tension of 0.2 N, and then pull the strips at a constant feed rate of 100 mm/min, whilst measuring the resistive force. Stress and strain was also calculated in real time by inputting the dimensions of the strips respectively prior to starting the test. After the rapid fracture of the strips, the Instron automatically stopped the test and the ultimate tensile stress and strain were obtained by recording the values immediately prior to fracture. The mechanical properties of the silicon gaiters after autoclaving were compared using student t-test (p=0.05).

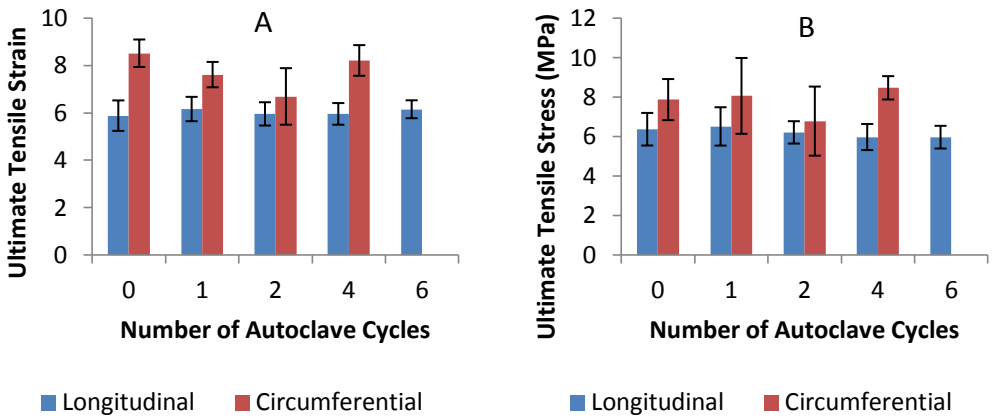

Figure 5-1: The ultimate tensile strain (A) and stress (B) of the silicon strips after autoclaving

Autoclaving had no significant effect on the ultimate tensile stress or strain of the silicon material (Figure 5-1) and, hence the gaiters could be sterilised via autoclave multiple times without the risk of cracking ($p > 0.05$). Therefore, the silicon gaiters were selected as a viable option to ensure the hemiarthroplasty components are kept free from contaminants.

5.4 Design Solution

A model of the design solution was created on Solidworks (Dassault Systèmes, Waltham, MA, USA). To maintain simplicity, the overall design of the vessel was based upon the current fixation holders made for the friction simulator. Fundamentally, the previous design consisted of two parts; a femoral head and

acetabular cup fixture. The femoral head fixture remained largely the same whereas most of the modifications were concentrated on the acetabular fixture.

The previous acetabular fixture (Lizhang, 2010) resembled a cup that encompassed the porcine acetabulum and PMMA bone cement (Figure 5-2). At the lower section of the cup was a wider section that allowed the fixture to be secured to the friction simulator via bolts. Around the sides of the cup were four holes that allowed grub screws to be screwed into the bone cement before setting. This prevented the PMMA and the acetabulum from rotating during testing. At the base of the cup holder was a tapped hole which included a grub screw. This allowed the acetabulum sample to be removed.

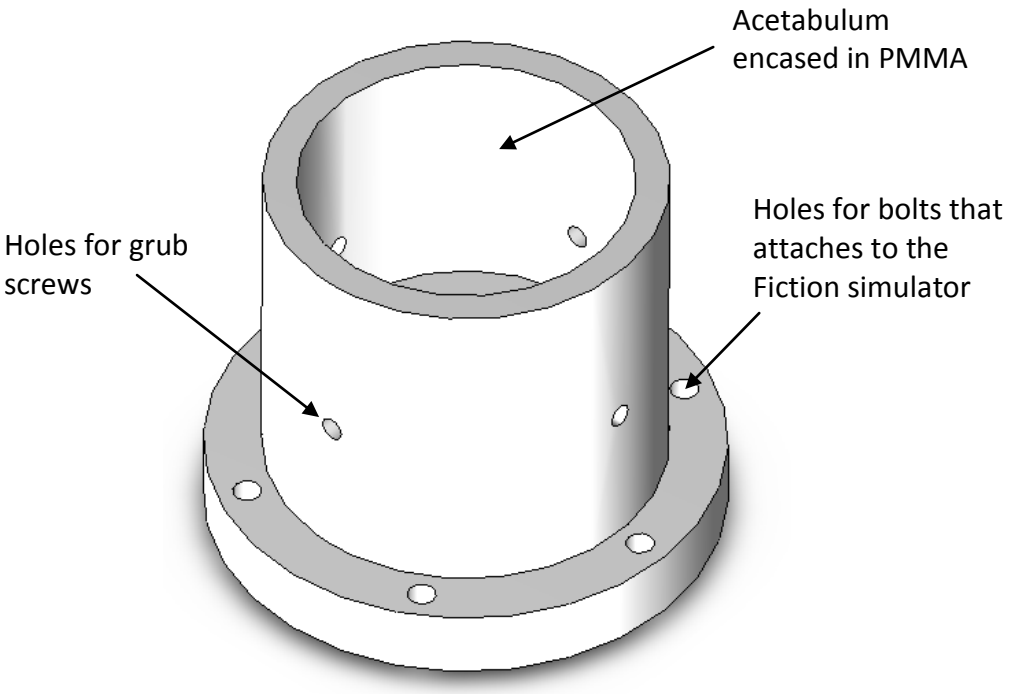

Figure 5-2: Original acetabulum fixture used by Lizhang et al. (2010).

The first modification was to include a method of attaching the silicon gaiter to the acetabular and femoral head fixture. For this, grooves were included in the design of both the femoral head and acetabular fixture. This allowed the ridge on both ends of the silicon gaiters to be slotted in (Figure 5-3).

Figure 5-3: Left) Groove that allowed the ridge on both ends of the silicon gaiters to be slotted in. Right) Stainless steel jubilee clip was then wrapped around the gaiters over the ridges.

A stainless steel jubilee clip was then wrapped around the gaiters over the ridges and tightened to create an air tight seal (Figure 5-3). The location of the grooves determined how stretched the gaiters were during the test. Hence, to minimise this affect, the location of the groove was lowered (Figure 5-4).

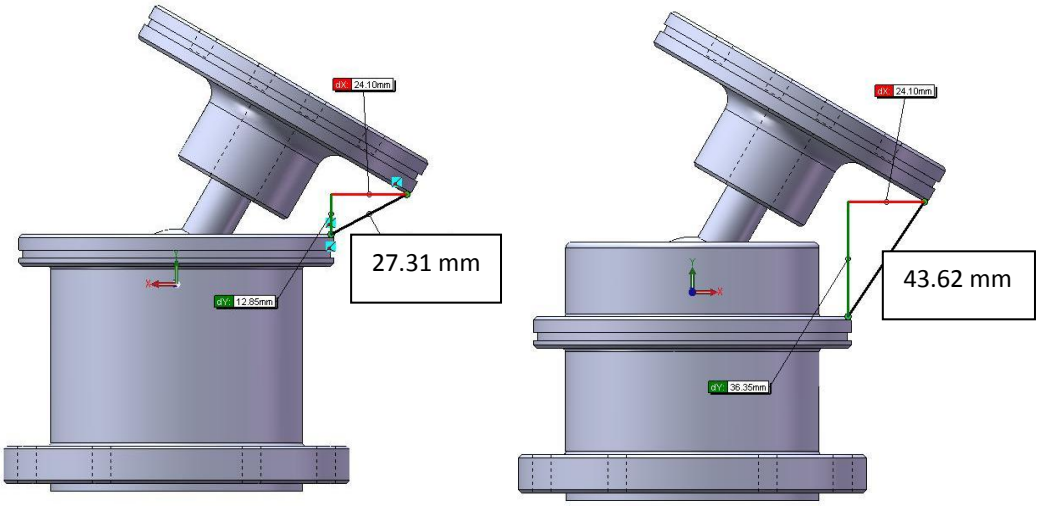

Figure 5-4: The effect to moving the location of the grooves for the silicon gaiters. The dimensions are calculated using Solidworks (Dassault Systèmes, Waltham, MA, USA).

It can also be seen in Figure 5-4 that holes for the grub screws were not included. This was because the holes could have been a source of contamination. Instead, “dimples” were drilled into the bottom of the cup. PMMA cement would fill these dimples prior to setting; thus, the axial force during testing would stop the PMMA from rotating out of the dimples. However, a hole at the bottom of the cup needed to be included to allow the cement to be removed after testing so that the fixture could be reused. However, instead of using a grub screw, the hole was

counterbored and a bolt was used. A silicon washer was included to create an air tight seal.

Rendered pictures of the acetabular and femoral head fixture can be seen in Figure 5-5 and Figure 5-6 respectively. These were manufactured in house from stainless steel 316 to provide corrosion resistance, which is important when autoclaving.

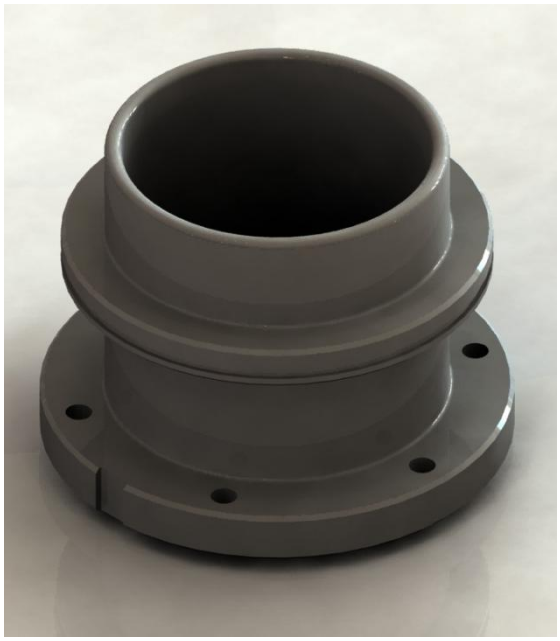

Figure 5-5: Rendered picture of the acetabular fixture created using Solidworks (Dassault Systèmes, Waltham, MA, USA).

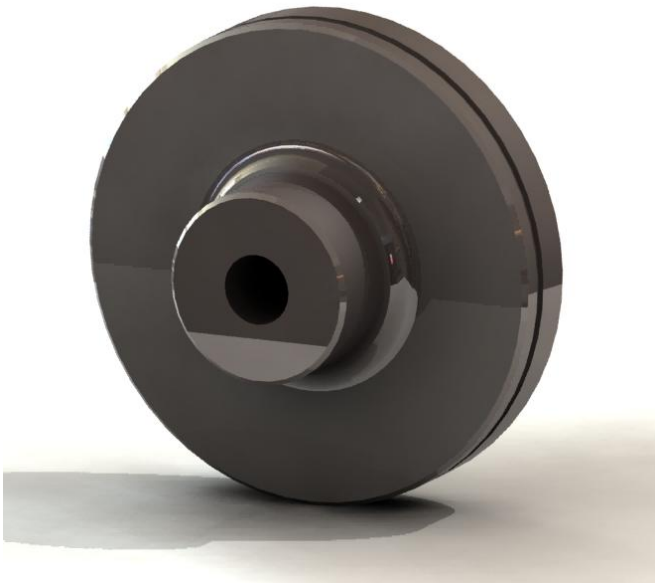

Figure 5-6: Rendered picture of the femoral head fixture created using Solidworks (Dassault Systèmes, Waltham, MA, USA).

5.5 Setting up the Friction Simulator Vessel

The friction simulator vessel must be set up in an aseptic environment; therefore, a new methodology was developed. Prior to starting, a cobalt chrome (CoCr) femoral head was attached to the femoral head fixture and the height of the femoral head was set to 72.83 mm using the methodology described in Section 2.4.4. The femoral head fixture was then attached to the vertical track of the device discussed in Section 2.4.4 (Figure 5-7). Using the actual femoral head fixture (for the tribological studies), as opposed to a separate femoral head fixture, allowed the femoral head fixture to be suspended in the correct orientation so that the silicon gaiter could be attached without resulting in twisting. The height of the ring that limits the lowest height the femoral head fixture could travel on the vertical tract was set so the centre of rotation (COR) of the femoral head was 63.24 mm from the top of the base plate (as described in Section 2.4.4). The acetabular fixture was then attached to the base plate so that the centre of the fixture is aligned with the COR of the femoral head with the use of a stainless steel washer.

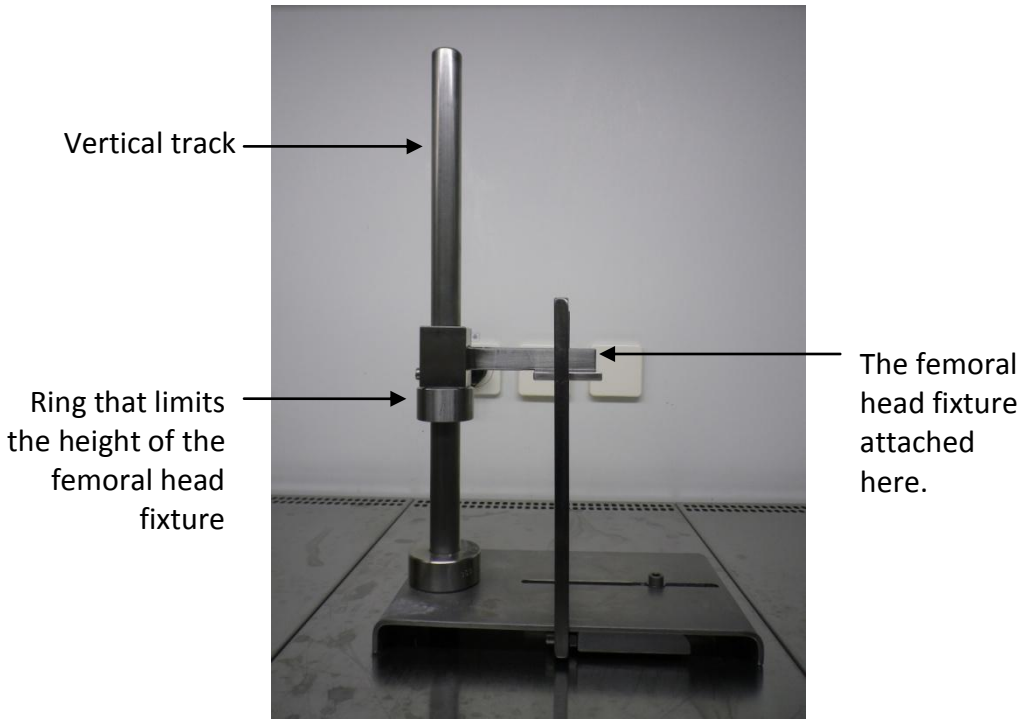

Figure 5-7: The cementing device.

The cementing device with the femoral head and acetabular fixture attached was then sealed in autoclavable bags and sterilised via autoclave (Section 2.5.5).

The silicon gaiter, stainless steel jubilee clips, spatula and two pairs of forceps were also placed in separate autoclavable bags and sterilised using an autoclave (Section 2.5.5). This was left overnight to cool down for two reasons. Firstly, the femoral head was used to push down on the acetabulum; thus, it could have damaged the cartilage if it was not left to cool down. Secondly, the speed of which the bone cement cures is temperature dependent. If used immediately after autoclaving, the heat within the acetabular fixture would speed up the curing process; not providing enough time to mount the acetabulum in the correct position. The bags containing the apparatus were then sprayed with 70% v/v ethanol, placed in a class II cabinet and opened.

Two 40 g sachets of sterile bone cement powder component and two vials of the liquid counterpart (Section 2.2.3) were emptied into the acetabular fixture and stirred using the spatula (Section 2.2.3). Once putty-like, the acetabulum was placed on top of the bone cement in the centre of the acetabular fixture using the forceps. The femoral head fixture was lowered, pushing the acetabulum down until the COR was 63.24 mm from the top of the base plate. Using forceps, the acetabulum was then orientated so that the contact region was in the centre of the cartilage; between the labrum and acetabular fossa. Once the sterile bone cement cured and cooled, 50 ml of the lubricant was added using a sterile syringe. The gaiter was then attached to the femoral head and acetabular fixture and secured using the stainless steel brackets (Figure 5-8). The femoral head fixture was detached from the cementing device and the entire vessel was placed into the friction simulator.

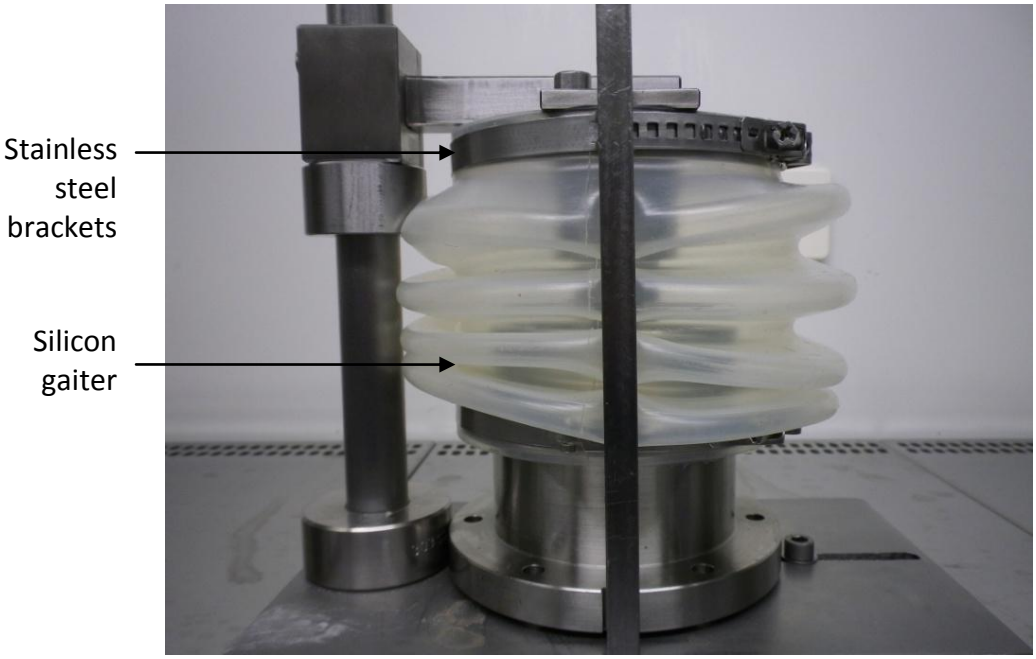

Figure 5-8: The friction simulator vessel attached to the cementing device

5.6 Effect of Silicon Gaiters on Friction Measurements

The pendulum friction simulator calculated the friction coefficient using the measured torque. By including a silicon gaiter in the design of the vessel, the silicon stretched and compressed during flexion and extension. This could have affected the torque and hence, the calculated friction coefficient. Thus any change to the friction coefficient was determined in order to fully validate the use of the friction simulator vessel.

5.6.1 Method

An alumina femoral head and acetabular cup (Ø = 28 mm) was obtained from DePuy International Ltd. (Leeds, UK). Alumina bearings were chosen due to exhibiting repeatable friction coefficient (Brockett *et al.*, 2007) and thus, the effect of the gaiter could be more readily detected compared to using natural cartilage. The femoral head was attached to the femoral head fixture and the height was corrected as described in Section 2.4.4 and 5.5. The alumina acetabular cup was setup using the methodology described in Section 5.5. A centring rod was used to ensure that the COR of the femoral head and acetabular cup was in line with the COR of the pendulum friction simulator (Section 2.4.4).

The friction of the alumina bearings was determined using the pendulum friction simulator with 25% v/v FBS in sterile water as the lubricant. A 25-800 N dynamic load was applied with a flexion/extension of ±15°.

To measure extra torque within the system, the peak load of 800 N was firstly applied during mid flexion for 300 cycles (forward), then again during mid extension for 300 cycles (reverse). The friction coefficient was measured every 5th cycle for 30 cycles. The magnitudes of all the friction coefficients obtained during both the forward and reverse cycles were averaged and taken as the friction coefficient of the bearing. This methodology was different than the methodology described in Section 2.4.4, where a separate 121 cycle test was performed prior to and after the tribological test. The reason for this was because, wear of the alumina bearings are relatively low (near negligible) compared to natural cartilage and hence, it was safely assumed that friction would be unaffected by sequential testing. Therefore, the friction coefficient magnitude obtained in the first 30 cycles of the forward test should be the same as the last 30 cycles of the reverse test. This could not be performed for the tribological tests that involved cartilage due to excessive wear and reduction in fluid load support during the initial cycles. This method was conducted with (n=4) and without (n=4) the gaiter attached. These were compared and significant differences were tested using one-way ANOVA with repeated measures ($P = 0.05$).

5.6.2 Results

No significant difference in friction coefficient was observed in friction testing that used a gaiter and without a gaiter ($p > 0.05$) by using a one-way ANOVA with repeated measures (Figure 5-9). However, it can be seen on that the friction coefficient varied more with inclusion of a gaiter compared to without a gaiter.

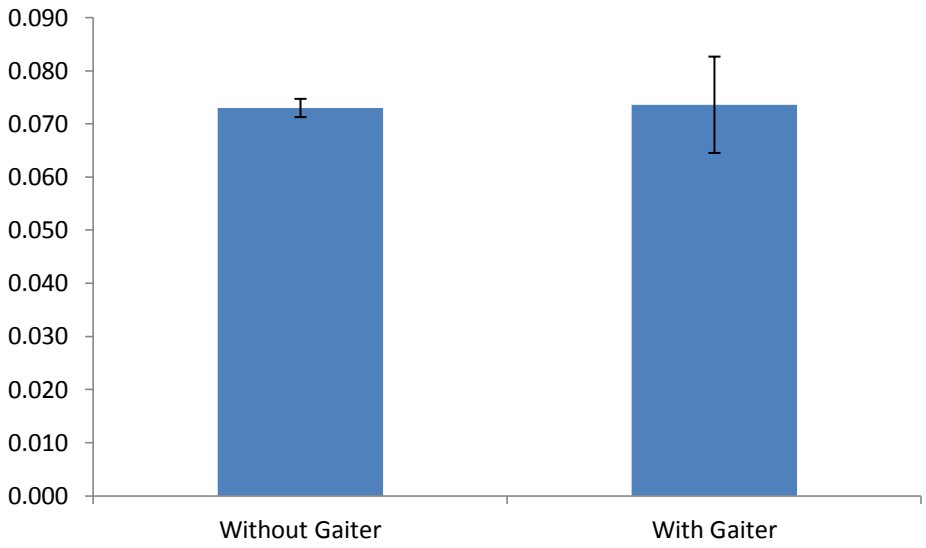

Figure 5-9: The average friction coefficient of the alumina bearings in a pendulum friction simulator with (n=4) and without (n=4) the gaiter attached. Error bars are standard deviations.

5.7 Sterility of the Friction Simulator Vessel

A major requirement for the friction simulator vessel was to eliminate contamination. Therefore, the ability of the vessel to maintain sterility was also assessed.

5.7.1 Methods

Prior to starting, 25% v/v FBS in water (200 ml) was mixed aseptically and a 2 ml sample was taken. This sample was agar plated on nutrient agar, heated blood agar and Sabourauds agar using the methodology described in Section 2.5.2. After 48 hours of incubation at 37°C, 37°C and 27°C respectively, the plates were visually inspected for contamination.

A CoCr femoral head and alumina acetabular cup (Ø = 28 mm) was obtained from DePuy International Ltd. (Leeds, UK). It must be noted that this is not a bearing combination recommended for clinical practice. The femoral head was attached to the femoral head fixture and the cementing fixture was assembled as described in Section 5.5. All the equipment was sterilised via autoclave along with the alumina acetabular cup (Section 2.5.5). The acetabular cup was then mounted

in cement in the class II cabinet and the gaiter was attached as described in Section 5.5.

The friction simulator vessel was placed in the friction simulator. The friction coefficient was not measured because this was not the aim of this study; therefore, the load was kept at a constant 25 N with a flexion/extension of ±15°. After two eight hour periods, the friction simulator vessel was sprayed with 70% v/v ethanol and placed into the class II cabinet where the femoral head fixture was removed. A 2 ml sample was taken of the lubricant and was agar plated on nutrient agar, heated blood agar and Sabourauds agar using the methodology described in Section 2.5.2. After 48 hours of incubation in 37°C, 37°C and 27°C respectively, the plates were visually inspected for contamination.

5.7.2 Results

Contamination was not observed on the agar plates prior to and after the two eight hour periods as demonstrated by the absence of microbial growth on the agar plates (Figure 5-10).

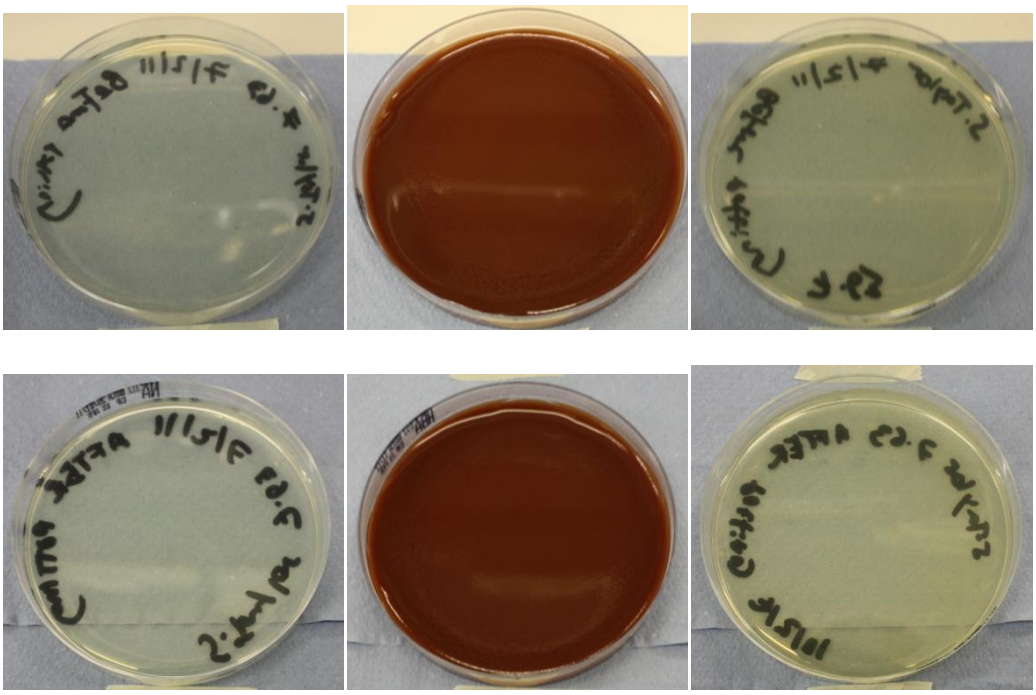

Figure 5-10: Agar plates of the samples of the lubricants taken prior to (top) and after (bottom) the two eight hour period. From left to right: nutrient agar, heated blood agar and Sabourauds agar.

5.8 Discussion of the Friction Simulator Vessel

The aim of this section was to design, develop and validate a friction simulator vessel that will be used for the medium term tribological tests without affecting the frictional torque measurements and maintaining sterility. The specification of the vessel was to be reusable, allowing the friction of hip hemiarthroplasty to be accurately measured without the risk of contamination.

By first developing a design specification, the design solution successfully addressed all the criteria needed to test hip hemiarthroplasty in the medium term. The design solution could be used with ease inside a class II cabinet and was able to withstand the kinematics and kinetics of the friction simulator. With the use of Solidworks, the risk of impingement during the ranges of motion detailed in the project specification was assessed prior to manufacturing. However, there were two main criteria which had to be examined after the friction simulator vessel was manufactured; ability to allow friction coefficient to be measured, and ability to prevent contamination.

5.8.1 Ability to Allow Friction Coefficient to be Measured

Due to the reasons described in Section 5.3, a silicon gaiter was chosen to encapsulate the hemiarthroplasty joint with the aim to prevent contaminants entering the vessel. However, due to adding an extra constraint to the vessel, this could affect measured torque and hence, the friction coefficient. If this was the case, the results obtained during the medium term tribological analysis would be inaccurate. Therefore, the friction of an alumina total hip replacement was measured with and without a gaiter.

The results demonstrated that the average coefficient of friction was unaffected with inclusion of the gaiter. However, the spread of the data was larger with the inclusion of the gaiter. This should to be taken into consideration when discussing the results obtained from the friction simulator vessel.

By using the friction simulator vessel with a ceramic total hip replacement, which has tighter tolerances compared to the hemiarthroplasty model, the method of cementing the acetabular cup was accurate in regards to aligning the COR.

5.8.2 Ability to Prevent Contamination

The primary reason for using a silicon gaiter was to eliminate microbes entering the vessel and causing contamination. This needed to be verified. To do this a medium term test was simulated using a sterilised alumina acetabular cup which represented the natural porcine acetabulum. By taking a sample of the lubricant prior to and after the simulation, the ability of the silicon gaiter to prevent contamination could be assessed along with the sterility of the cementing technique.

The results from visually inspecting the agar plates showed no signs of contamination entering the vessel, either during the cementing procedure or during the medium term tribological test. Therefore, this validates the use of the silicon gaiter to prevent contamination and the methodology of cementing; which will be used during the medium term tribological tests.

5.9 Conclusion

The aim of this Chapter was to design, develop and validate the friction simulator vessel that will be used for the medium term tribological study of hip hemiarthroplasty. The friction simulator vessel allowed the porcine hip hemiarthroplasty model to be tribologically tested. After manufacturing, the vessel was tested for validation purposes. The following were observed:

- The inclusion of a silicon gaiter made no significant difference to the friction coefficient results; thus, did not produce extra torque within the vessel. Therefore, the friction coefficient can be measured in real time throughout the medium term tribological test.
- However, even though the average friction of the ceramic bearing does not change when using the silicon gaiter, there was more variation in the results. Therefore, this will need to be discussed when considering the medium term friction data.
- The friction simulator vessel also inhibited microbial infection, which is important for the tribological study.

- The aseptic cementing and setting up methodology allowed the hemiarthroplasty model to be prepared aseptically and the COR to coincide with the COR of the friction simulator.

Chapter 6: Effect of Clearance on Contact Stress and Area

6.1 Introduction

The condition of contact (contact area and stress) greatly affects the tribological properties of cartilage (Forster and Fisher, 1996; Katta et al., 2007; Katta et al., 2008). This has been discussed in Section 1.10. Therefore, it is vital to understand the contact area and stress of the proposed medium term tribological system.

The aim of this Chapter was to determine the contact stresses that will be exhibited in the medium term hemiarthroplasty model. Contact area and stress were determined for the hemiarthroplasty model with matched and mismatched geometries. These clearance groups will be used in the medium term tribological test. The distribution of contact, and hence the shape of the contact region were also assessed. However, before conducting the study, the methodology to determine contact area and stress was developed and validated.

6.2 Development and Validation of the Spectrodensitometer Method

Pressure sensitive films have been commonly used in previous studies to analyse contact stress and contact area (Lizhang, 2010). For this study, Fuji pressure sensitive film (Sensor Products, LLC, USA) was used to obtain the contact area and contact stress. The FujiFilm was available as a “mono-sheet” or a “two-sheet” depending on the sensitivity. The “mono-sheet” is layered with first a colour developing material, and then a micro-encapsulated colour forming material. When pressure is applied to the sheet, the microcapsules burst releasing the colour forming material. This then reacts with the colour developing material forming a red patch. The intensity of the red with a specific wavelength corresponds to the magnitude of pressure applied to the film. The “two-sheet” FujiFilm works in a similar way; however, the colour developing material is coated onto one sheet and the micro-encapsulated colour forming material is coated onto the other. The

“two-sheet” configuration only works when the sheets are placed together so that the coatings are in contact.

To measure contact stress, a spectrodensitometer (500 Series, Sensor Products Inc., Madison, NJ, USA) was used which measured the intensity of red with the specific wavelength. A value was then given which represented the intensity of red that was later used to calculate contact stress at the point the reading was taken with the use of the PointScan (Version 2.15, Sensor Products Inc.) software.

The thickness of the “mono-sheet” film is 110±5 µm and each sheet of the “two-sheet” film is 90±5 µm. The error of these films is ±10% or less at 23°C when measured with a densitometer (FUJIFILM Recording Media GmbH., 2007).

Even though FujiFilm has been used in previous studies, one of the main problems with FujiFilm is that it involves wrapping a flat surface onto a spherical ball. To achieve a perfect fit is not possible and hence, in previous studies, FujiFilm has been cut out in a variety of shapes to obtain the best possible fit. Three shapes which have been used are: “petal” (Bay *et al.*, 1997; Michaeli *et al.*, 1997; Pawaskar, 2010), “rosette” (Anderson *et al.*, 2008) and the “horseshoe” (Lizhang, 2010) which are displayed in Figure 6-1.

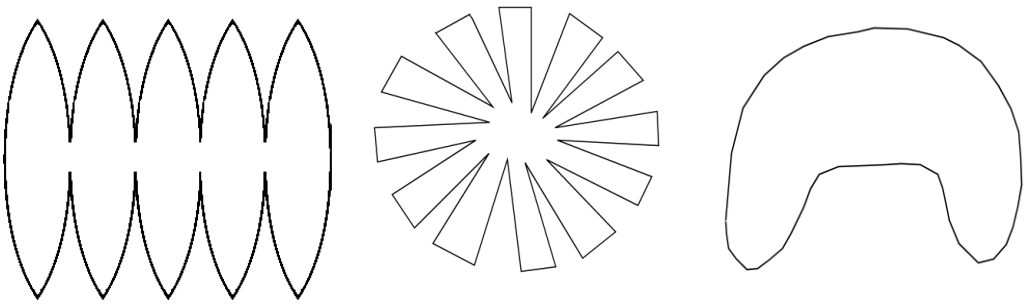

Figure 6-1: From left to right: The petal shape, rosette shape and horseshoe shape used in previous studies to measure contact area and stress with pressure sensitive film.

FujiFilm is also grouped by sensitivities and there are several sensitivity groups tailored to measuring extremely low stresses to high stresses. Therefore, the aim of this part of the study was to compare the three shapes used in previous literature and establish which shape and sensitivity group should be selected to measure contact area and contact stress.

As cartilage has time dependent deformation under load, the contact area and stress measured must be determined with respect to a particular time reference point. For this study the contact area and stress will be calculated at the end of the tests. Hence, this was the reference point for the current study.

6.2.1 Materials

Three acetabulae were obtained from porcine right hind legs (Section 2.3.2). These were frozen at -18 °C with a PBS soaked tissue paper until required for testing, where the acetabulae (in the specimen bags) were placed in a hot water bath for one hour to thaw.

Previous studies have shown that for contact area, superlow Fujifilm is the most effective due to being the most sensitive (Lizhang, 2010; Pawaskar, 2010). Therefore, this would display more of the contact than a less sensitive film. For the current study, superlow Fujifilm was used to measure contact area. Previous studies have also shown that either low or medium Fujifilms were appropriate for the contact stress in an *in-vitro* hemiarthroplasty model (Lizhang, 2010; Pawaskar, 2010). Therefore, the superlow (obtained from the contact area study), low and medium Fujifilms were used for the contact stress analysis.

6.2.2 Methods

To keep the orientation of the acetabular cup consistent with the friction studies, the three acetabulae were cemented into the acetabular cup fixture using the methods described in Section 2.4.4. The diameters were measured using a Vernier calliper (±0.01) in the anterior/posterior direction and a CoCr femoral head (Section 2.2.4) was selected to allow a radial clearance of 0.6-1.2 mm; which was the standard clearance used in Lizhang et al. (2010) study. The femoral head was attached to the friction simulator femoral head fixture (Section 2.4.4).

The Fujifilm was cut into the either the “petal”, “rosette” or the “horseshoe” shape (Figure 6-1). With an attempt to standardise the shapes, a template was drawn on thick card and cut out. This was used to trace the shape on the Fujifilm using a mechanical pencil. The Fujifilm was placed on the femoral head and Clingfilm was wrapped around, securing the Fujifilm around the femoral head

(Figure 6-2). Clingfilm was used to protect the Fujifilm from water damage arising from the interstitial fluid within the cartilage. Care was taken not to crease the Clingfilm or to apply pressure to the Fujifilm as this could affect the results. The Clingfilm was secured around the femoral head fixture stem using adhesive tape.

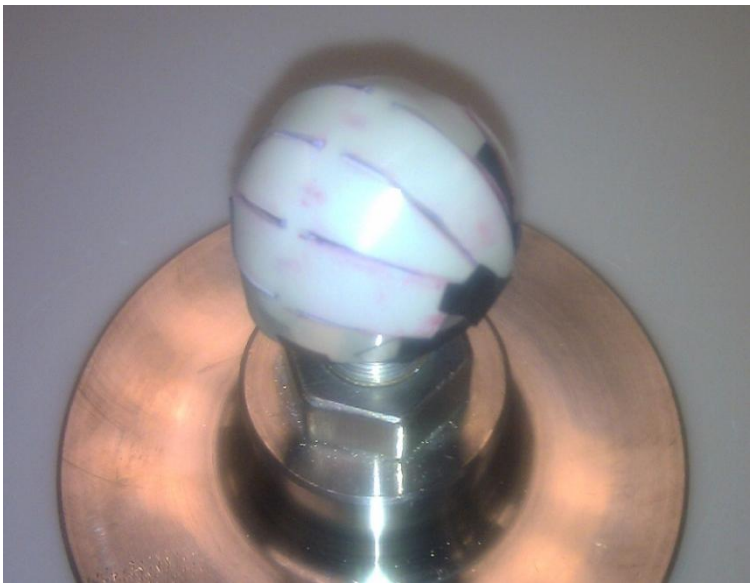

Figure 6-2: The petal shape Fujifilm attached to the CoCr femoral head.

The acetabulum cemented in the acetabular cup fixture was placed on the Instron 3365 material testing machine (Section 2.4.2). The cup fixture was constrained in all three planes with the use of a base plate. The femoral head fixture was placed upside down so that the femoral head was resting inside the cup. A horizontal platform attached to the loading arm of the Instron was lowered so that the femoral head fixture could not rotate and fall out of the cup (Figure 6-3). By not attaching the femoral head fixture to the Instron directly, the femoral head was allowed to self centre in the acetabular cup.

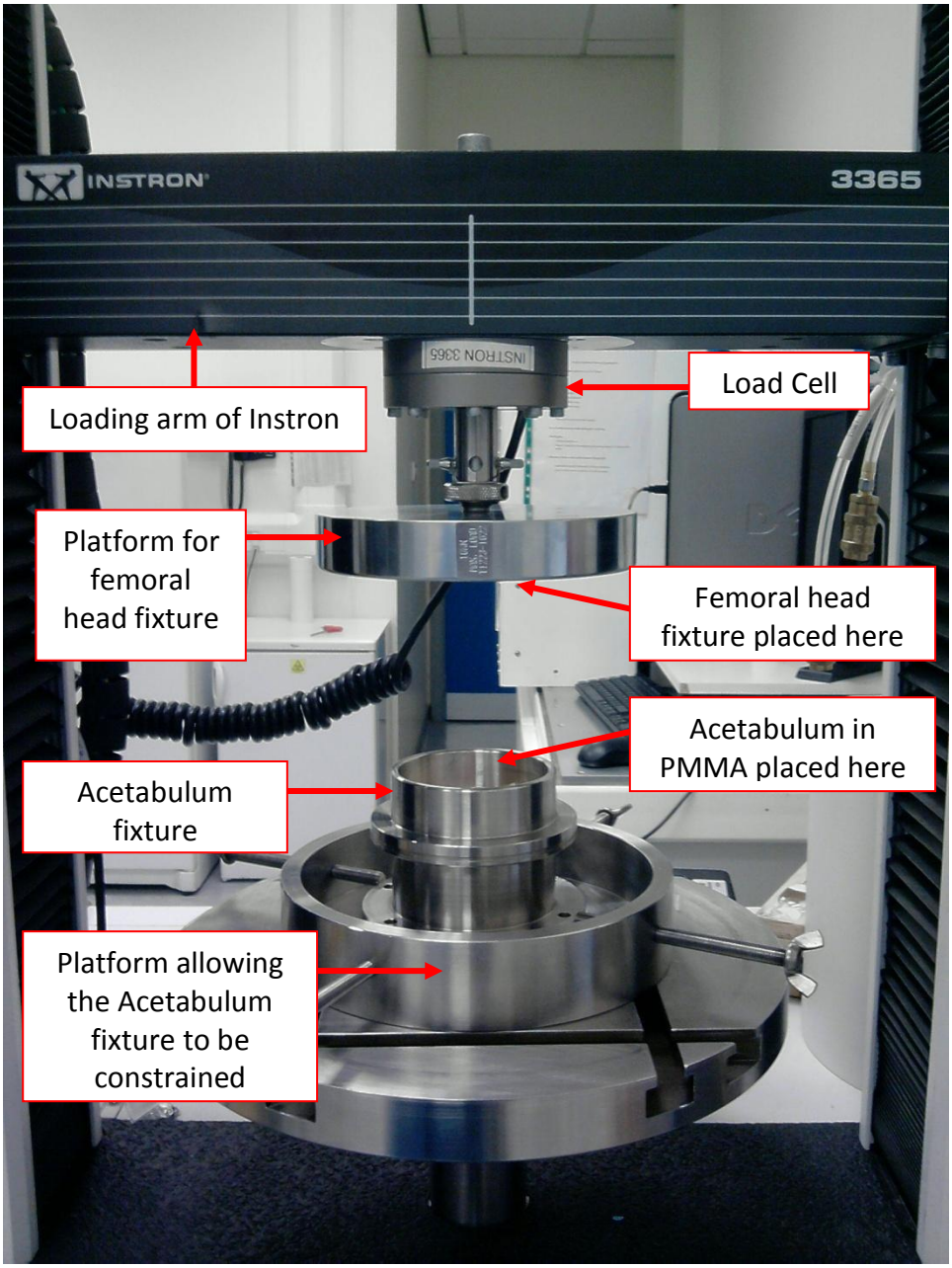

Figure 6-3: Instron material testing machine used to calculate contact area and stress.

The Instron was set to apply a pre load of 0.1 N. The load was then increased up from 0.1 N to 800 N over 20 seconds and held for a further 30 seconds (Figure 6-4). A maximum load of 800 N was chosen due to being the peak load applied during the tribological experiments (Chapters 4 and 7). The displacement of the femoral head fixture over time was captured.

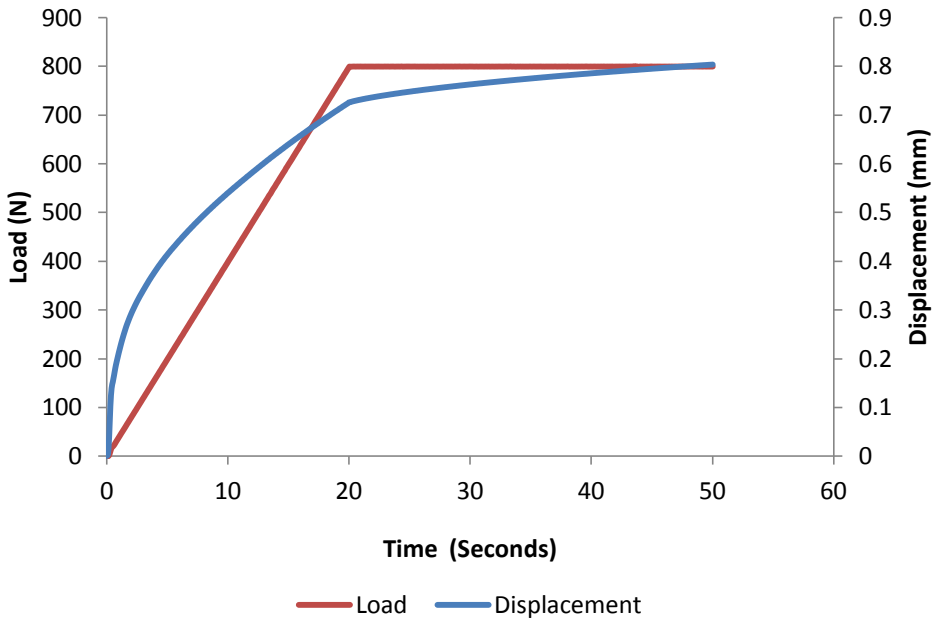

Figure 6-4: Applied load and resulting femoral head displacement during the contact area and stress test.

The femoral head was then removed from the acetabulum and the Fujifilm was recovered. The Fujifilm was observed for evidence of folds or crinkles that could affect the contact area or stress results.

The method described up to this point was common for both contact area and contact stress measurements. However, the analysis that was conducted on the Fujifilm was different depending on if the contact area or contact stress was being measured.

Contact Area

As discussed previously (Section 6.2.1), the superlow Fujifilm (highest sensitivity) was used to measure the contact area due to having the best possible chance of capturing the entire contact area. Photographs were taken of the Fujifilm with a scale marker and the area of the coloured region was measured using Image ProPlus (Media Cybernetics, Inc., MD, USA). This was done both manually and using the automatic method. The manual method involved tracing around the peripheral edges of the coloured region. The automatic method which was included in the Image ProPlus software used a detection algorithm controlled by inputting a threshold value. The coloured region was selected roughly in the centre and the area which exhibited that colour was measured.

The main parameter that affected the results obtained from the automatic method was the threshold value. To investigate the effect of the threshold value on the results obtained via the automatic method, the threshold value was incrementally increased from 25 to 150. It was hypothesised that as the threshold value increased, the area selected and measured would also gradually increase until the entire red region was selected. After this point, the selected area would rapidly increase with increasing threshold value. The point at which the area rapidly increased was taken as the "most appropriate" threshold value for that specific Fujifilm. The range of values obtained as a percentage of the mean was calculated.

Contact Stress

Contact stress was measured using the superlow Fujifilm used to measure the contact area, as well as the low and medium Fujifilms. A spectrodensitometer (FUJIFILM Recording Media GmbH., 2007) was pre-calibrated using a white datum obtained from the supplier. The spectrodensitometer reading was taken five times across the coloured region. These values were inputted into the PointScan (Version 2.15, Sensor Products Inc.) software to obtain the corresponding stress value. Both the peak contact stress (highest stress value recorded) and the average contact stress were obtained.

Statistical Analysis

To assess the intra-observer variability for each of the Fujifilm shapes, the entire process was repeated three times on each acetabulum using each Fujifilm shape to obtain three results of contact area (using the manual and automatic method) and contact stress. The range was worked out as a percentage of the mean, which was used to determine the intra-observer variability of each Fujifilm shape.

Data is presented as the mean ± 95% confidence limits unless otherwise stated. One-way ANOVA was used to test for significant differences ($p \leq 0.05$) between the Fujifilm shapes and the automatic verses the manual method of working out contact area.

6.2.3 Results

Initial Observation

It was immediately seen that there were large crinkles in the "horseshoe" shaped Fujifilm (Figure 6-5). This could have affected the stress and area results. Therefore, the "horseshoe" shape was excluded from the rest of the analysis.

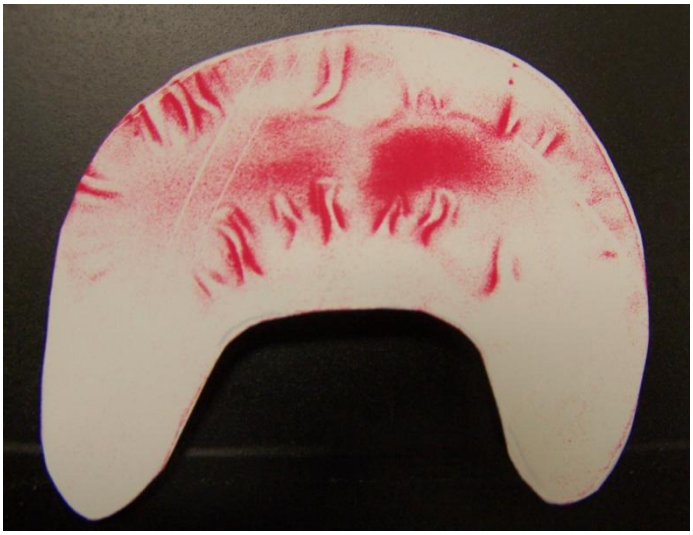

Figure 6-5: An example of the horseshoe shape Fujifilm after the applying the force. The crinkles are seen on the edges of the Fujifilm.

Contact Area

The measured mean contact area and standard deviation of each of the three acetabulae are shown in Table 6-1. The rosette shaped Fujifilm exhibited a larger contact area compared to petal shaped Fujifilm for two of the three acetabulae. However, the petal shaped Fujifilm showed a larger contact area than the rosette for the third acetabulum.

Table 6-1: Contact area for acetabulae samples (n=3) measured using both the rosette and petal shaped Fujifilm

	Rosette (mm^2)		Petal (mm^2)	
	Mean	**Standard Deviation**	**Mean**	**Standard Deviation**
Ace1	155.39	4.05	150.72	7.11
Ace2	193.45	26.21	145.85	1.34
Ace3	145.53	6.13	160.56	5.65

To measure the intra-observer variability, the range of area values obtained for each acetabulum were calculated as a percentage of the mean. The range

percentage for each acetabulum was averaged to give an average percentage range for the rosette and petal shape (Table 6-2).

Table 6-2: The percentage range of contact area values obtained when using manual method

	Rosette (%)	Petal (%)
Ace1	5.21	9.44
Ace2	27.10	1.83
Ace3	8.42	7.03
Average	13.58	6.10

The results indicate that the value of area measured varied more when the rosette shape was used compared to the petal.

The use of the automatic method of obtaining contact area as opposed to the manual tracing method was analysed. An example of the relationship between threshold value and area value is shown in Figure 6-6. As the threshold value increased, the area value increased gradually up to a certain point, after which, the area value increased rapidly. The threshold value prior to the rapid increase in contact area value was taken as the "optimum" threshold value. The red line represents the value obtained in the manual method.

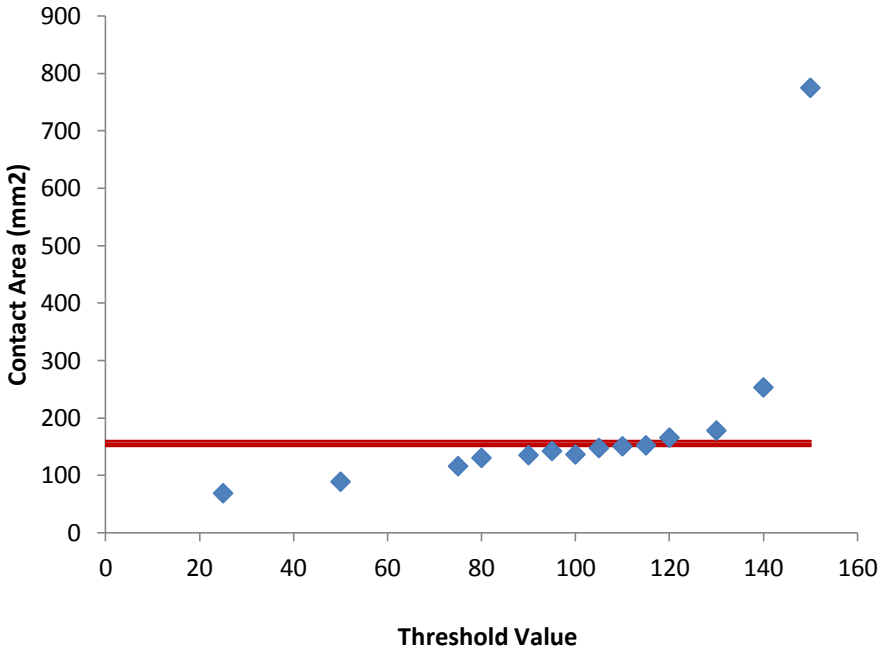

Figure 6-6: An example of the effect of altering the threshold value on the automatic method results for contact area. The red line represents the manual method result.

The "optimum" threshold values were recorded for each acetabulum and are displayed in Table 6-3.

Table 6-3: The "optimum" threshold value for each acetabulum

	Rosette	Petal
Ace1	110	100
Ace2	115	90
Ace3	75	90

The contact area obtained using the automatic method with the threshold values stated in Table 6-3 are shown in Table 6-4. Similar to the manual method, neither the Rosette nor the Petal shape exhibited a larger contact area; where, two of the three acetabulae showed a larger contact area when a rossette shape was used.

Table 6-4: Contact area for the acetabulae (n=3) for both the petal and rosette shape Fujifilm

	Rosette (mm^2)		Petal (mm^2)	
	Mean	**Standard Deviation**	**Mean**	**Standard Deviation**
Ace1	166.44	20.77	131.26	5.04
Ace2	155.38	5.41	131.26	4.30
Ace3	131.10	4.71	143.81	0.95

The average percentage range was also calculated for the automatic method for obtaining contact area (Table 6-5). Again, the area value varied more when the rosette shape was used compared to the petal.

Table 6-5: The percentage range of contact area values obtained when using the automatic method

	Rosette (%)	Petal (%)
Ace1	30.20	10.40
Ace2	8.46	7.16
Ace3	8.88	1.61
Average	15.85	6.389

Contact Stress

The super low, low and medium Fujifilms were used to calculate contact stress. The superlow Fujifilm was too sensitive under the applied stress and the values were out of the range of the PointScan software. The medium Fujifilm was also out of range and it was not sensitive enough. Therefore, the low Fujifilm was used to calculate contact stress. No significant difference between the petal and rosette shape was observed (Figure 6-7) ($P = 0.05$).

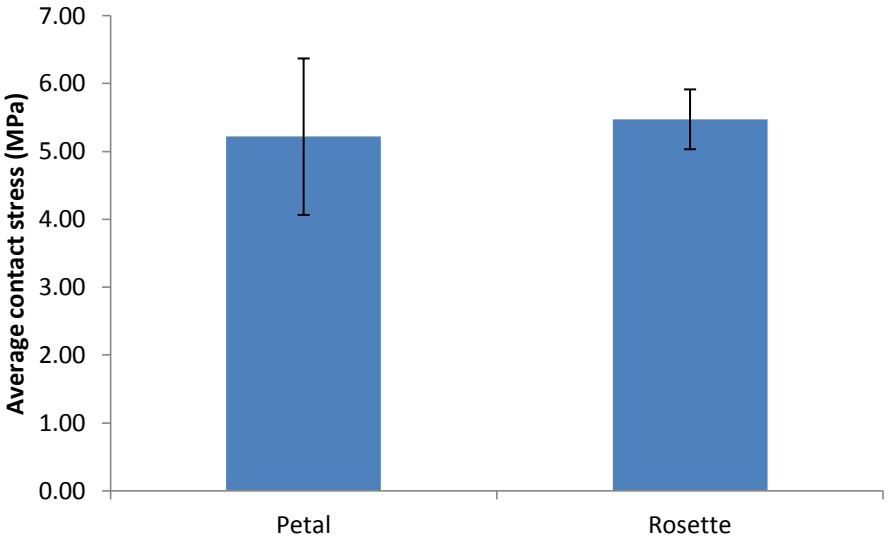

Figure 6-7: Mean contact stress (n=3) measured using the petal and rosette shaped Fujifilm. Error bars are 95% confidence limits (P=0.05).

The average percentage range was also calculated for the contact stress for both the rosette and petal shaped Fujifilm. The petal shaped Fujifilm showed larger intra-observer variability when compared to petal (Table 6-6).

Table 6-6: The percentage range of contact stress values for both the Rosette and Petal shape

	Rosette (%)	Petal (%)
Ace1	7.47	26.9
Ace2	26.4	43.0
Ace3	21.5	19.5
Average	18.5	29.8

6.2.4 Discussion

The aim of this part of the study was to develop and validate the methodology used to measure contact area and stress in the hemiarthroplasty model. To do this, three different shapes of Fujifilm appropriate for measuring a spherical surface were selected from previous literature (Bay et al., 1997; Michaeli et al., 1997; Anderson et al., 2008; Pawaskar 2010; Lizhang 2010) and the repeatability were compared. For the contact area, the use of an automatic method built into the Image ProPlus software was also examined.

Firstly, the horseshoe shape was eliminated after observing crinkles in the film. This was due to not conforming within the femoral head and acetabulum. These marks were also observed by Lizhang (2010), who called them “Extra” contact areas possibly originating from the ball sliding into the cup. However, due

to the set up described in Section 6.2.2, the femoral head was already self-centred before the load was applied and hence, this sliding effect was eliminated. Therefore, it is believed this was due to the Fujifilm not conforming to the spherical surface and hence, crimpled during compression.

No significant difference was observed in the measured contact areas using either the rosette or petal shaped Fujifilm (P = 0.05). However, in calculating the average percentage range using the manual method, the results indicate the petal shaped Fujifilm produced more repeatable results (Table 6-2). This was also the case when using the automatic method (Table 6-5).

No difference in repeatability was observed between using the manual or automatic method to calculate contact area. However, the threshold value greatly affects the contact area value, and the “most appropriate” threshold value is acetabulum dependent (Figure 6-6 and Table 6-3).

The cartilage was still deforming under constant load due to creep, and did not reach equilibrium as observed in Figure 6-4. Therefore, the maximum contact area was not reached. However, the deformation due to creep is much smaller than the total deformation, so the effect on contact area has been assumed to be negligible.

The optimum Fujifilm sensitivity to obtain contact stress measurements was the low Fujifilm. However, for larger contact stresses, medium Fujifilm may have to be used. No significant difference in average contact stress values were observed between the petal and rosette shape (P = 0.05). However, the results suggest that the variability in contact stress values were larger for the petal compared to the rosette. The contact stress value is highly dependent on the location of interest and hence, this could have contributed to the variability.

6.2.5 Conclusion

The petal shape Fujifilm provided the most repeatable contact area result. The manual method will be used on the Image ProPlus software as the automatic method is highly dependent on the threshold.

6.3 Defining the Clearance Groups

In the experiments previously conducted in this thesis, the clearance was chosen based on the previous study by Lizhang et al. (2010). This involved measuring the diameter of the acetabulum using a vernier calliper and selecting a CoCr femoral head size to allow for a 0.6-1.2 mm radial clearance. However, this method is not used in clinical practice. There are two common methods of sizing the correct hemiartroplasty femoral head in surgery. The first is to use Vernier callipers to measure the size of the natural femoral head and select the metallic femoral head with the most similar size. The second is similar to the first, but circular templates are used to determine the diameter of the natural femoral head. Circular templates will be used to determine appropriate head size for the rest of this thesis.

Two different clearance groups will be considered; matched and mismatched. For the matched clearance group, the natural femoral head was slotted through circular templates with diameters 32 mm, 34 mm, 35 mm, 36 mm and 37 mm (Figure 6-8). The smallest diameter hole the natural femoral head could fit through comfortably (without forcing it) was chosen as the corresponding diameter of the CoCr femoral head. This method was also used for the mismatched geometries. However, due to clinical practice commonly using 2 mm increments for the diameters of hemiarthroplasty femoral head, a CoCr femoral head was chosen 2 mm smaller than the diameter of the selected template hole. This was to simulate selecting a metallic femoral head an increment smaller than optimum.

Figure 6-8: The circular template used to measure the size of the natural femoral head and select the CoCr femoral head.

6.4 Materials

Eight porcine right hind legs were obtained within 24 hours of slaughter (Section 2.3). The porcine acetabulae were dissected using the methods described in Section 2.3.3. Four porcine legs were used to calculate contact area and stress with matched geometries and the other four for mismatched geometries (Section 6.3). The porcine acetabulae were cemented using the method described in Section 2.4.4 and then frozen wrapped in PBS soaked tissue paper at -18°C until day of use.

For this study, all the contact area measurements were taken using superlow Fujifilm. For all the matched geometries, the contact stress was measured using low Fujifilm (2.5 – 10 MPa). However, for three of the four mismatched geometries, the medium Fujifilm (10 – 49 MPa) was required due to the stress exhibited being too high to be measured by the low Fujifilm. All the Fujifilms were cut into a “petal” using the card template (Figure 6-1).

6.5 Method

The porcine acetabulae and the equivalent femoral heads were set up using the methodology described in Section 6.2.2. As described previously, a pre-load of 0.1 N was applied by the Instron material testing machine, and then the load was ramped up to 800 N over 20 seconds. The load was kept constant for a further 30 seconds (Figure 6-4). A maximum load of 800 N was chosen due to being the peak load during the tribological experiments.

After removal of the femoral head fixture, the contact area was measured using the manual method described in Section 6.2.2. The contact stress was measured using a spectrodensitometer (FUJIFILM Recording Media GmbH., 2007) as described in Section 6.2.2. Five readings were taken over the coloured region and the mean was taken of the corresponding stress values to calculate average contact stress. The peak contact stress was taken as the largest value of the five readings. Contact stress was measured first for both the matched and mismatched geometries, then contact area was measured. Between measuring contact stress and contact area, the acetabulum was submerged in PBS for a minimum of one hour to ensure maximum recovery of cartilage deformation. Prior to starting, the PBS was drained off, reducing the risk of water damage to the Fujifilm.

A previous study showed that the value of stress from the PointScan software was sensitive to the humidity and temperature of the experiment location (Pawaskar, 2010). Therefore, the temperature and humidity was recorded every hour during the test using pre-calibrated temperature and humidity meter (Tenmars TM-183, Taipei, Taiwan). This has an accuracy of ±2.5% for 30% ~ 80% and ±0.8°C for -20°C ~ 60°C. The average temperature and humidity was inputted into the PointScan software (Table 6-7).

Table 6-7: Parameters provided as inputs into the PointScan software

Parameter	Value
Length of Exposure (seconds)	50
Relative Humidity (%)	50.41
Temperature (°C)	21.1

6.6 Theoretical Contact Stress

A mathematical model was used to also predict the maximum contact stress of the hemiarthroplasty with matched and mismatched geometries. A model proposed by Dowson *et al.* (1991) was adopted which used a ball on a semi-infinite solid. This was derived from Hertzian contact theory. The maximum contact stress was calculated using Equation (6.1).

$$p_o = \frac{3F}{2\pi a^2} \tag{6.1}$$

Where p_o is maximum contact stress, F is the maximum normal load and a is the half-width or radius of contact zone. This can be be calculated using Equation (6.2).

$$a = \left(\frac{3FR_x}{2E'}\right)^{\frac{1}{3}} \tag{6.2}$$

Where R_x is the equivalent radii (as if the acetabular cup was flattened), and E' is equivalent elastic modulus which is worked out using Equation (6.3).

$$\frac{1}{E'} = \frac{1}{2}\left(\frac{1-{v_1}^2}{E_1} + \frac{1-{v_2}^2}{E_2}\right) \tag{6.3}$$

Where v_1 and v_2 are the Poisson's ratio of the CoCr femoral head and cartilage on the acetabulum respectively; and E_1 and E_2 are the elastic modulus of both the CoCr femoral head and acetabular respectively. Equations (6.2) and (6.3) were used to calculate radius of the contact area theoretically. Due to measuring the contact area directly using Fujifilm, the maximum contact stress was calculated by adapting Equation (6.1) to Equation (6.4). Therefore, Equations (6.2) and (6.3) were no longer needed.

$$p_o = \frac{3F}{2A} \tag{6.4}$$

Where A is the contact area between the femoral head and acetabulum worked out using Fujifilm. The average theoretical contact stresses were calculated using the average contact areas from both the matched and mismatched

geometries. These results were then compared to the results obtained from the spectrodensitometer and PointScan software (Section 6.5).

6.7 Statistical Analysis

Data is presented as the mean ± 95% confidence limits unless otherwise stated. One-way ANOVA was used to test for significant differences ($p \leq 0.05$) between the matched and mismatched geometry groups.

6.8 Results

6.8.1 Distribution of Contact Area on Acetabulae Samples

For both the matched and mismatched geometry groups, the contact area was not a uniform shape. The contact was split into two distinct areas with less contact in the centre (Figure 6-9). A larger horseshoe shape was seen in the matched geometry group compared to a more concise region for the mismatched geometry group (Figure 6-9).

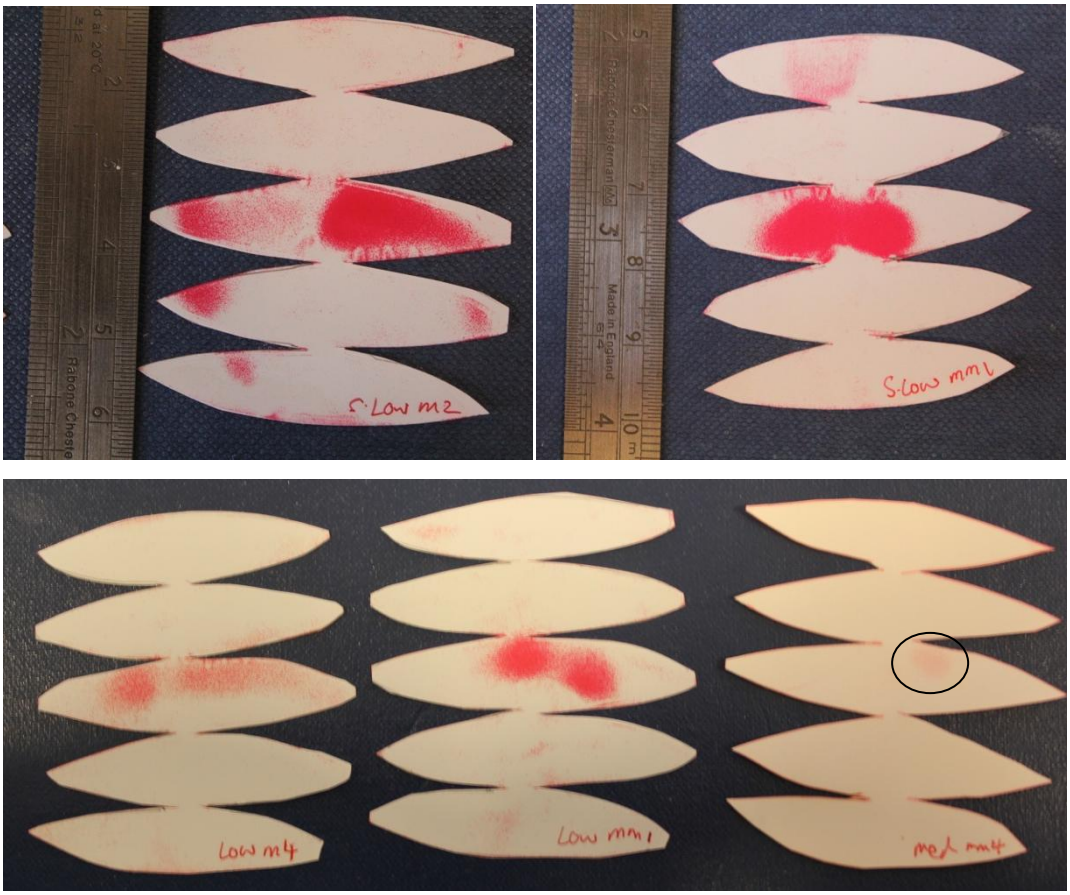

Figure 6-9: Examples of the Fujifilm after testing. Top left: Superlow Fujifilm with matched geometries. Top right: Superlow Fujifilm with mismatched geometries. Lower Left: Low Fujifilm with matched geometries. Lower Middle: Low Fujifilm with mismatched geometries. Lower Right: Medium Fujifilm with mismatched geometries (circle indicates location of contact).

6.8.2 Contact Area

The contact area of the hemiarthroplasty model was significantly larger in the matched geometries group (290±60 mm^2) compared to the mismatched geometries (178±77 mm^2) group (p=0.05) (Figure 6-10).

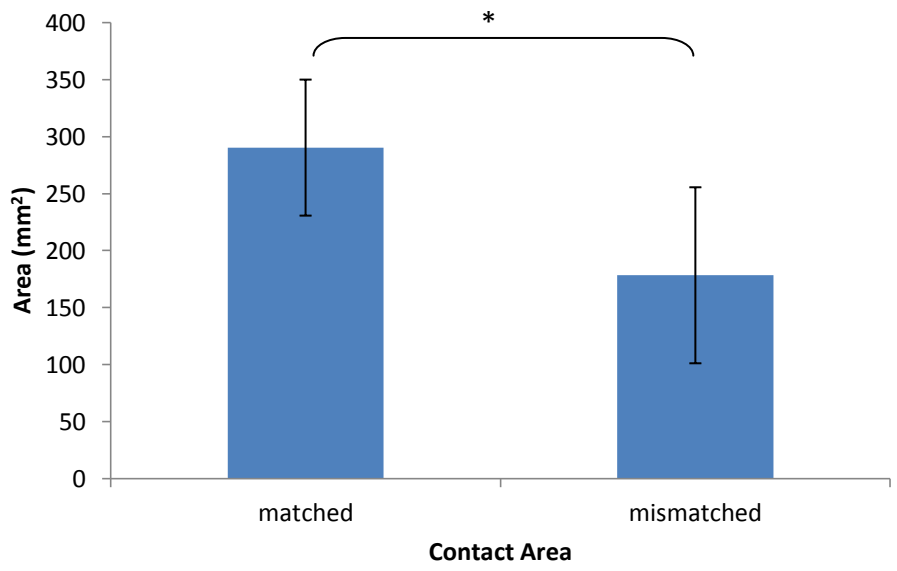

Figure 6-10: Contact area calculated for the matched and mismatched geometry groups (n=4). Error bars are 95% confidence limits (P=0.05). *significant deference (p<0.05)

6.8.3 Contact Stress Using PointScan

The results also show that there was a significant difference in average contact stress between the matched (4.66±1.65 MPa) and mismatched (8.05±3.37 MPa) geometry groups (p=0.05). However, there was not a significant difference between the matched (6.88±4.39 MPa) and mismatched (12.69±6.61 MPa) geometry groups with regards to peak contact stress (P>0.05) (Figure 6-11).

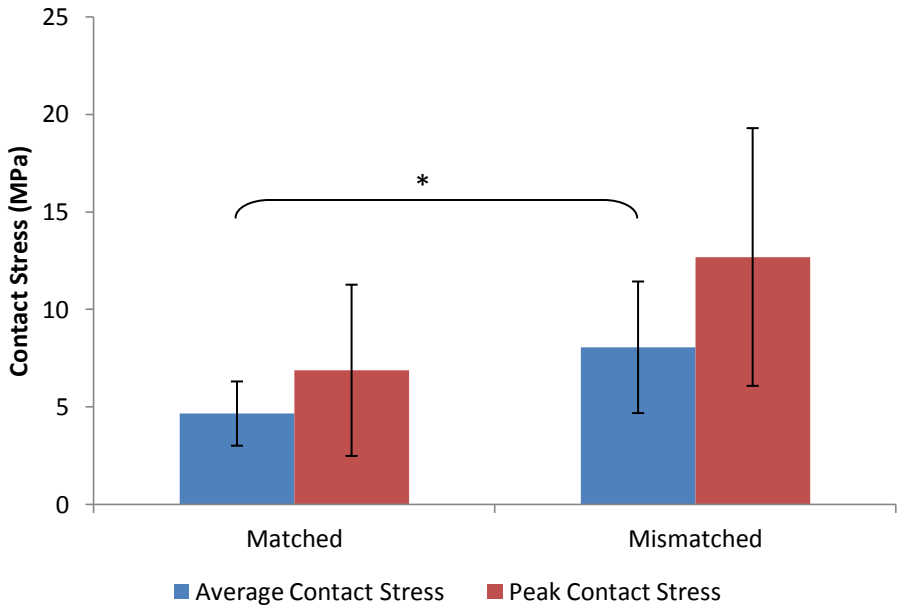

Figure 6-11: The average and peak contact stress calculated for the matched and mismatched geometries using the spectrodensitometer method (n=4). Error bars are 95% confidence limits (p=0.05). *significant deference (p<0.05)

6.8.4 Contact Stress Using Hertzian Theory

The contact stress calculated using Hertzian contact analysis was much lower than the measured value from the PointScan technique. This was apparent in both the matched and mismatched geometries (Figure 6-12). The peak contact stress for the matched geometry group was calculated to be 3.79 MPa and for the mismatched geometry group 7.71 MPa; as opposed to 6.88±4.39 MPa and 12.69±6.61 for the PointScan results respectively.

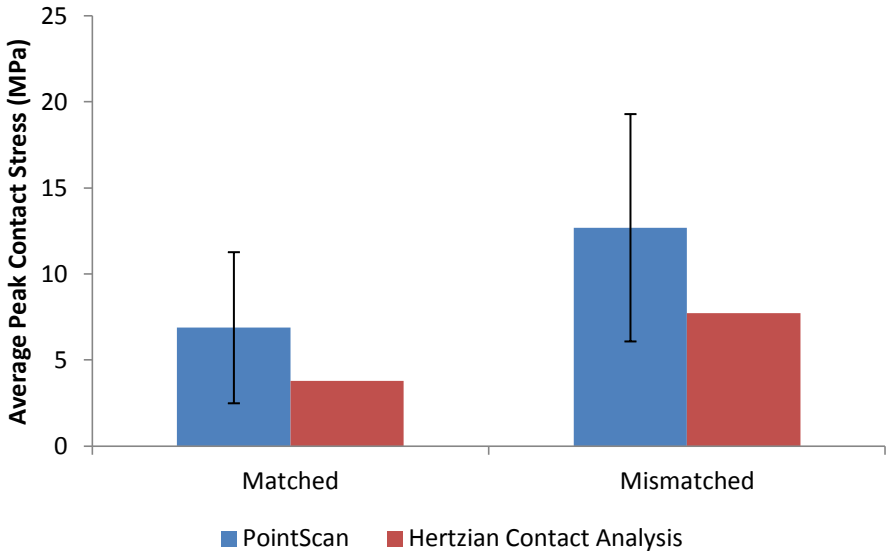

Figure 6-12: The average peak contact stress using the spectrodensitometer method compared to the Hertzian contact analysis (n=4). Error bars are 95% confidence limits (P=0.05).

6.9 Discussion

6.9.1 Distribution of Contact on Acetabulum

The contact region for the matched geometries was in a horseshoe shape, following the shape of the acetabular cartilage. This is similar to the shape seen in previous studies that also examined contact stress/area within the natural hip joint. A study by Konrath et al. used pressure sensitive film in the rosette shape to measure contact area and stress in cadaver hip joints using a constant force and similar methodology used in the current study (Figure 6-13) (Konrath *et al.*, 1999).

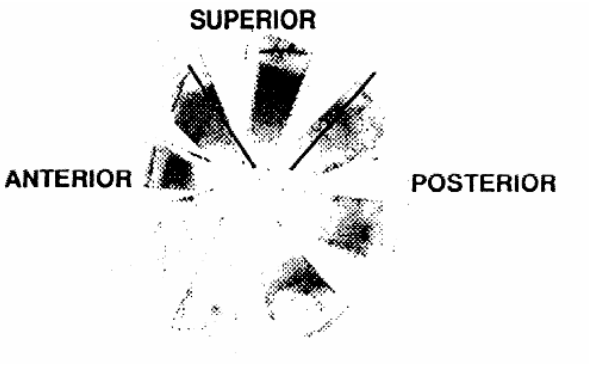

Figure 6-13: Pressure sensitive film used to calculate contact pressure in the cadaveric hip (Konrath et al., 1999)

It was found that the contact region of the intact hip was observed peripherally, over the entire cartilage surface. However, for the current study, the majority of the contact was on the anterior and posterior sides of the acetabulum. The central part of the contact region exhibited some degree of contact, although much less than the anterior and posterior sides. This can be seen more clearly in the low Fujifilm (Figure 6-9). The reason for this central region of less support was due to the skeletal maturity of the pig. Due to being only three to six months of age (Table 2-3), the bone has not fully developed and hence, a growth plate was present in the centre of the acetabulum running from the peripheral edge of the acetabular cup (near to the labrum) to the acetabular fossa (Figure 6-14).

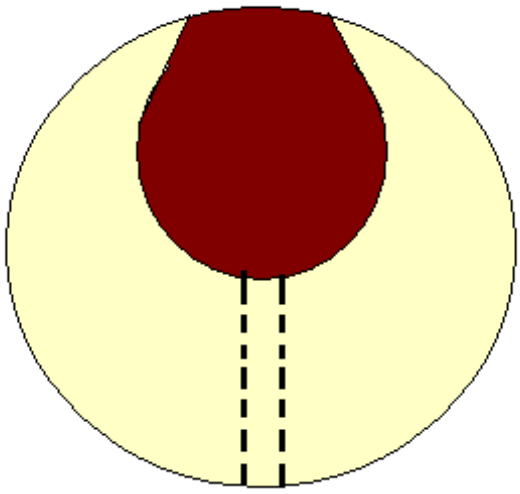

Figure 6-14: Schematic of the acetabulum cartilage (yellow) and the acetabular fossa (red). The region between the two dotted lines is the location of the growth plate.

Therefore, the 800N load was mainly supported by the regions either side of the growth plate. The same effect of the growth plate was also seen in a study by

Lizhang (2010) who also examined contact stress and area of a porcine acetabulum against a metallic femoral head.

This is an extremely important observation as this highlights a limitation of using an animal joint to represent human, independent of the limitations discussed in Chapter 3. Instead of spreading the contact stress over the entire contact region, the contact stress was concentrated on either side of the growth plate and hence, this could have a major effect on the frictional shear stress during the tribological study. Thus, the wear mechanism and the magnitude of damage could also be affected.

This “dual” contact region on either side of the growth plate was also seen for the mismatched geometry group. However, instead of a horseshoe shape, the contact region was more concentrated in the centre. Therefore, not all the acetabular cartilage was in contact with the CoCr femoral head.

6.9.2 Contact Area and Stress

It is important to consider the difference in contact area during the tribological test of articular cartilage as this directly affects the surface area of cartilage in contact with the lubricant and hence, its opportunity to recover. In previous studies, it has been concluded that the fluid load support is a major factor in the friction coefficient and frictional shear stress and thus the opportunity for fluid inhibition is also important. As expected, contact area was significantly smaller for the mismatched geometry group compared to the matched geometry group. This is in an agreement with a similar study conducted by Lizhang (2010) who also found an inverse relationship between radial clearance of hip hemiarthroplasty and contact area.

As discussed in Section 1.9.1 and 6.1, contact stress is an important factor in the tribology of cartilage. It has been shown to directly affect the coefficient of friction and more importantly, the frictional shear stress; as this governs the wear of cartilage. Therefore, contact stress of the proposed medium term *in-vitro* model must be investigated in order to fully understand the frictional result obtained. Contact stress was measured using Fujifilm and a spectrodensitometer. Due to the

inverse relationship between contact area and contact stress, for the mismatch geometry group the contact stress was larger compared to the matched geometry group. This was only significant for the average contact stress. This confers with the study by Lizhang (2010) who also found the contact stress significantly increased with an increase in radial clearance. The values of contact stress were found to be within the range of other hip hemiarthroplasty models. Rushfeldt et al. used instrumented endoprostheses to investigate the stress distribution in the acetabular cartilage (Rushfeldt *et al.*, 1981). A hip joint simulator was used to apply loads of up to 2250 N with prostheses with differing sizes. A peak pressure of 6.78 MPa was observed for a closely fitted prosthesis with a 2.5 times body weight (1350 N); whereas for the 2 mm undersized prostheses exhibited a peak contact stress of 14.3 MPa.

6.9.3 Hertzian Contact Theory

As well as using the Fujifilm and spectrodensitometer to measure contact stress, a simple theoretical model based on Hertzian contact theory was also used. For both the matched and mismatched geometry groups, the peak contact stress calculated using Hertzian theory was at least 1.6 times smaller when compared to the spectrodensitometer method. The reason for this could be due to the assumptions made in the Hertzian theoretical model. Firstly, Hertzian contact theory assumes that the materials are homogeneous and linearly elastic. However, as discussed in Section 1.4, cartilage is inhomogeneous and viscoelastic in nature.

The Hertzian contact theory also assumes the object is perfectly spherical with a uniform contact region. In reality, the acetabulae were not perfectly spherical and most of the contact was supported either side of the growth plate (Section 6.8.1); therefore, the contact region was not uniform. This could cause stress concentrations on either side of the growth plate which could also account for the larger stress values obtained using the spectrodensitometer.

The distribution of stress on the porcine acetabulae would be different to that of a fully skeletally mature human due to the existence of the growth plate. Therefore, this will need to be taken into consideration when discussing the results of the medium term tribological study.

6.10 Conclusion

This chapter aimed to obtain a better understanding of the contact stresses that will be present in the proposed medium term tribological study. It was found that:

- The contact shape of both the radial clearance groups was affected by the growth plate that ran across the cartilage. This affected the contact stress distribution on the acetabular cartilage, where most of the load support was on either side of the growth plate. However, by applying the loads that will be used in the medium term tribological study, the contact stress was within the same range of previous reported data that used hemiarthroplasty in a human hip model. This shows that even though there is a non-uniform contact due to the growth plate, the stresses can be representative to that *in-vivo*.
- The average contact stresses were also shown to be larger in the mismatched geometry group compared to the matched geometry group. This is due to the load being concentrated on a smaller contact area.
- The effect of the growth plate must be taken into consideration when analysing the magnitude and distribution of wear on the acetabular cartilage.

Chapter 7: The Effect of Mismatching Hip Hemiarthroplasty Geometry on Friction and Wear in the Medium Term

7.1 Introduction

Hemiarthroplasty of the hip is a common procedure performed on elderly patients who have suffered a femoral neck fracture after trauma. However, cartilage erosion arising from mismatching radial clearance has been previously described as one of the predominant modes of failure (Johnston et al., 1982; Jeffery and Ong, 2000; Sharif and Parker, 2002). Studies have shown that the prevalence of femoral neck fractures increase with age exponentially (Carroll et al., 2011). Due to the aging population, the total number of hip fractures is expected to rise. This could explain an increase of 20,000 reported cases of femoral neck fractures from 2000 to 2010 (The Information Centre for Health and Social Care, 2011).

Therefore, the aim of this study was to investigate the relationship between radial clearance and cartilage wear and friction over four periods of eight hours (a total of 115,200 cycles). The studies that have been described in this thesis helped develop and validate the choice of animal joint (Chapter 3), the lubricant (Chapter 4), the sterile dissection process (Chapter 4), the vessel in which the hemiarthroplasty model would be tested (Chapter 5), and the contact mechanics of the proposed *in-vitro* model (Chapter 6). The effect of matching and mismatching the geometries of the natural acetabular cup and metallic femoral head will be compared in terms of friction coefficient, frictional shear stress, wear area/grade. Additionally cartilage thickness will be assessed and histological and biochemical analysis completed.

7.2 Materials and Methods

7.2.1 Specimen Preparation

Eight porcine right hind legs were obtained within two hours of slaughter (3-6 months old). Four acetabulae were tribologically tested using a CoCr femoral head

with matched geometries and the other four with mismatched geometries as described in Section 6.3. These were dissected aseptically to obtain the acetabulum using the methodology described in Section 4.5. For each porcine acetabulum, two pots of antibiotic lubricant were mixed aseptically using the methods described in Section 4.2. After sterile dissection, the acetabulum was placed in one of the pots containing the antibiotic lubricant. The other pot was used as a negative control to test for contamination.

7.2.2 Tribological Testing

The acetabulum was taken out of the pot containing the sterile antibiotic lubricant within 16 hours after dissection and cemented in the acetabular fixture and the friction simulator vessel was assembled using the method described in Section 5.5. This was fitted into the friction simulator and the centring rod was used to test if the centre of rotation (COR) of the bearing was in the correct location (Section 2.4.4).

A dynamic load of 25 N to 800 N was applied to the cartilage with a flexion/extension of ±15° for a period of eight hours (28,800 cycles). This was repeated three more times on consecutive days with 16 hours of unloading between each testing increment. To factor in the offset value as discussed in Section 2.4.4, a two minute tribological test with a constant 800 N load and a ± 15° flexion/extension was conducted before and after each 8 hour test. An offset value was calculated (Section 2.4.4) for each 8 hour testing period and was used to normalise the data.

During tribological testing, the negative control pot of lubricant was agitated at 1 Hz for the entire four days. After four days, the cartilage was swabbed and the swab was placed in a vial of nutrient broth (Section 2.5.1). A sample of the lubricant from both the negative control pot and the friction simulator vessel (2 ml) were plated on nutrient, heated blood and Sabourauds agar (Section 2.5.2). The nutrient broth was incubated for 48 hours at 37°C. The nutrient agar, heated blood agar and Sabourauds agar plates were incubated for 48 hours at 37°C, 37°C and 27°C respectively. The agar plates and nutrient broth were then inspected for the presence of contamination.

7.2.3 Friction Coefficient

Throughout the tribological test, friction coefficient was measured at intervals using a logarithmic scale. Every 30th cycle for the first 100 cycles, 150th cycle up to the 1000th cycle, 300th cycle up to the 10,000th, and every 1800th cycle thereafter friction coefficient was recorded. The friction was recorded during peak demand load a mid-swing. This was conducted for both the matched (n=4) and mismatched (n=4) geometry groups.

7.2.4 Frictional Shear Stress

Frictional shear stress was "predicted" using the average contact stress calculated for the matched and mismatched geometry groups in Chapter 6. For the average frictional shear stress ($\bar{\tau}$), the following equation was used:

$$\bar{\tau} = \mu\bar{p} \tag{7.1}$$

Where μ is the friction coefficient during mid swing at peak load and $\bar{p}$ is the average contact pressure which was 4.66 MPa and 8.06 MPa for matched and mismatched geometry groups respectively. To calculate maximum frictional shear stress (τ_o), the following equation was used.

$$\tau_o = \mu p_o \tag{7.2}$$

Where μ is friction coefficient and p_o is the maximum contact pressure which was 6.88 MPa and 12.69 MPa for matched and mismatched geometry groups respectively.

7.2.5 Wear Area/Grade

After tribological testing for four days, the cartilage surface was visually inspected for wear. Wear was categorised into four types based on those described by Lizhang (2010): no wear, light damage or discolouring, wear scratches (not full thickness), and bone exposure as described in Section 2.4.5. These are in order of severity. Macroscopic observations were used to establish the type of wear. If the cartilage looked undamaged then it was categorised as "no wear". If the cartilage exhibited a different colour compared to fresh cartilage in the absence of scratches or morphological changes then this was categorised as "light wear". If scratches

were present but with no exposure of bone then this was classified as “wear scratches”. If bone was exposed, this was classified as “bone exposure”. An example of these wear types are shown in Figure 2-21.

In order to quantify the wear on the cartilage surface, the areas of each type of wear were calculated in terms of the percent coverage of the total cartilage area. This was carried out using the three dimensional mapping method described in Section 2.4.5 as this was shown to be the most repeatable method. Firstly, the entire articular cartilage area was calculated. Then, areas of the “light wear”, “wear scratches” and “bone exposure” were calculated. The total cartilage surface area minus the sum of the wear areas was taken as the area of “no wear”. The percentage coverage of each type of wear was calculated for each acetabulum and averaged over the matched and mismatched geometry groups.

7.2.6 Cartilage Thickness

After analysing the wear area on the cartilage surface, an osteochondral plug was taken from each acetabulum in the scratched region on the anterior side. This was then set up on the Instron material testing machine and the thickness of the cartilage was measured four times on each plug and an average was taken (Section 2.4.2).

Untested control samples were also measured, where four fresh legs were obtained within 2 hours of slaughter and the acetabulae were dissected using the method described in Section 2.3.3. A plug was taken out of each of the four acetabulae in the same region as the acetabulae used in the tribological study. The thickness of each of these plugs was measured using the Instron material testing machine (Section 2.4.2). The thickness was measured four times for each plug and the mean was calculated.

7.2.7 Histological Analysis

The micro-architecture and micro-morphology of the cartilage was also analysed after the four day tribological test with the use of histology. The cartilage was removed from the osteochondral plugs after measuring cartilage thickness in

Section 7.2.6 by slicing through the “tidemark” with a scalpel. These plugs include the fresh controls. Plugs were also taken in the “light damage” region of the cartilage and the cartilage was removed. The cartilage discs were then sliced in half with a scalpel perpendicular to the wear scars.

The cartilage samples were then fixed in 10% v/v formalin, processed and embedded in paraffin wax as described in Section 2.5.3. The wax blocks were then sliced into 5 μm thick sections and placed on glass slides ready for staining.

To observe the general micro-architecture and micro-morphology of the cartilage, haematoxylin and eosin (H&E) stain was used. The distribution of GAGs was observed using the Alcian blue stain, both of which are discussed in detail in Section 2.5.3. The slides were then observed using an Olympus BX51 light/fluorescent microscope (Olympus UK Ltd.) at 40x to 400x magnification. The images were then digitally captured using Cell B software (Olympus, Hamburg, Germany).

7.2.8 GAG Quantification Analysis

The concentration of GAGs in the cartilage was quantified and compared with fresh cartilage. Between 10 mg (w/w) to 30 mg (w/w) of cartilage was removed from the rest of the scratched region of the tribologically tested and fresh acetabulae. Care was taken not to use the central region of the acetabulum because the cartilage within the growth plate could affect the results. The samples were weighed, freeze dried, weighed again and digested in Papain digestion solution as described in Section 2.5.4. The GAG concentration was determined in the digests using the DMB assay as described in Section 2.5.4 and the absorbance was measured using a spectrophotometer (Multiscan Spectrum. Thermor Labsystems). The concentration of GAGs was measured in micrograms per milligrams of cartilage (d/w).

To ensure the amount of absorbance was within the linear range of the spectrophotometer and to convert the absorbance to concentration of GAGs; controls of chondroitin sulphate B (Sigma-Aldrich Co., Dorset, UK) and assay buffer

were used with differing concentrations. This was described in detail in Section 2.5.4.

7.2.9 Statistical Analysis

Statistical differences were determined using the methods described in Section 2.6. Data was presented as the mean ± 95% confidence limits unless otherwise stated. One-way ANOVA was used to test for significant differences ($p \leq 0.05$). For the results that used percentages, such as the wear area, the values were first transformed using arcsine and significant differences were determined using one-way ANOVA ($p \leq 0.05$). Confidence limits of ± 95% were calculated and the values were back transformed to percentages before creating the graphs. Correlations between parameters were calculated using coefficient of determination (r^2).

7.3 Results

7.3.1 Sterility

The agar plates of the lubricant samples taken from the friction simulator vessel and the negative control pots after the four day tests showed no signs of microbial growth. The swabs taken from the cartilage surface after the four day tribological tests also showed no signs of contamination.

7.3.2 Friction Coefficient

The friction coefficient was measured over an 8-hour duration on four consecutive days, with recovery of the cartilage for 16-hours between test measurements. The results are shown in Figure 7-1, in which the 16-hours between increments (days) are indicated by dashed lines.

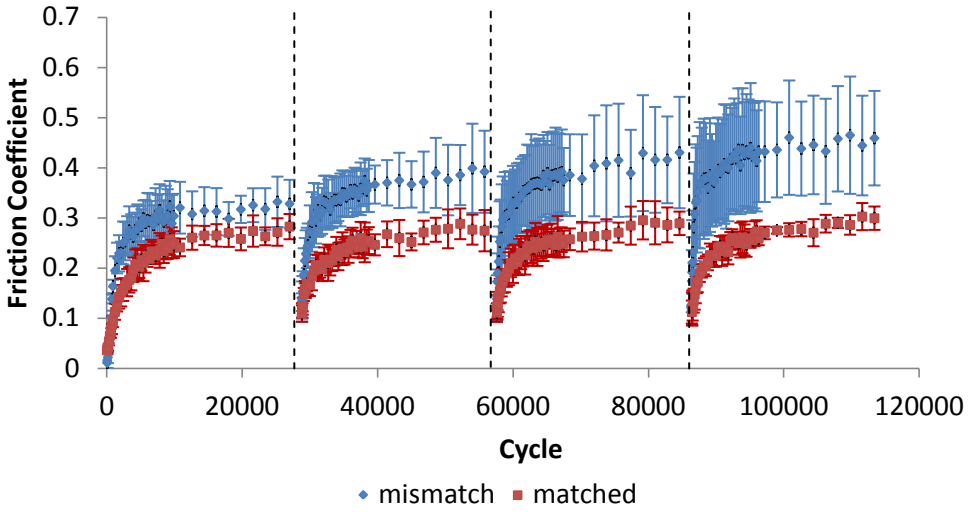

Figure 7-1: Mean friction coefficient over time for the matched (red) and mismatched (blue) geometry groups (n=4). Dashed lines represent 16 hours of unloading. Error bars are standard deviation.

For the matched geometry group, the friction coefficient gradually increased during each day to 0.29 ± 0.02 at the 28800th cycle (Figure 7-2). However, the initial friction coefficient after 30 cycles was significantly lower on the first day compared to the other days ($p<0.05$). For the mismatched geometry group, the friction coefficient after 30 cycles was also significantly lower on the first day compared to the consecutive days ($p<0.05$). However the average friction coefficient after 28800 cycles also increased each day from 0.31 on the first day to 0.42 on the fourth day. This increase was not significant ($p=0.05$).

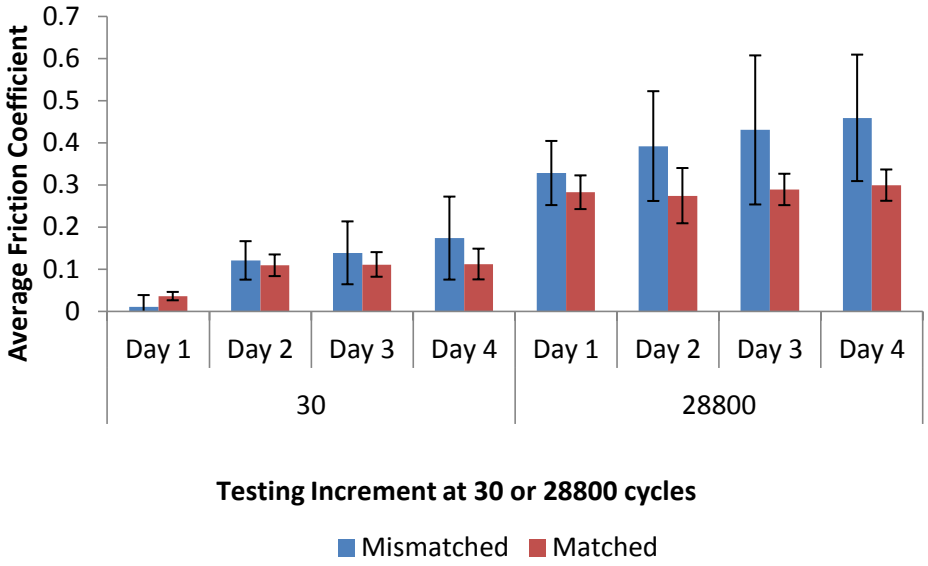

Figure 7-2: Mean friction coefficient after 30 and 28800 cycles for each of the four days (n=4) when using matched and mismatched geometries. Error bars represent 95% confidence limits.

In all cases except for the first 30 cycles on the first day, the friction coefficient was higher for the mismatched geometry group compared to the matched geometry group. However, this was significantly different only on the fourth day after 28800 cycles ($p<0.05$).

7.3.3 Frictional Shear Stress

The frictional shear stress was predicted by using the contact stress obtained in Chapter 6 and the friction coefficient in this Chapter. Due to the direct relationship between the friction coefficient and frictional shear stress governed by Equation (7.1) and (7.2), the frictional shear stress varied with testing days in a similar manner to the friction coefficient (Figure 7-3).

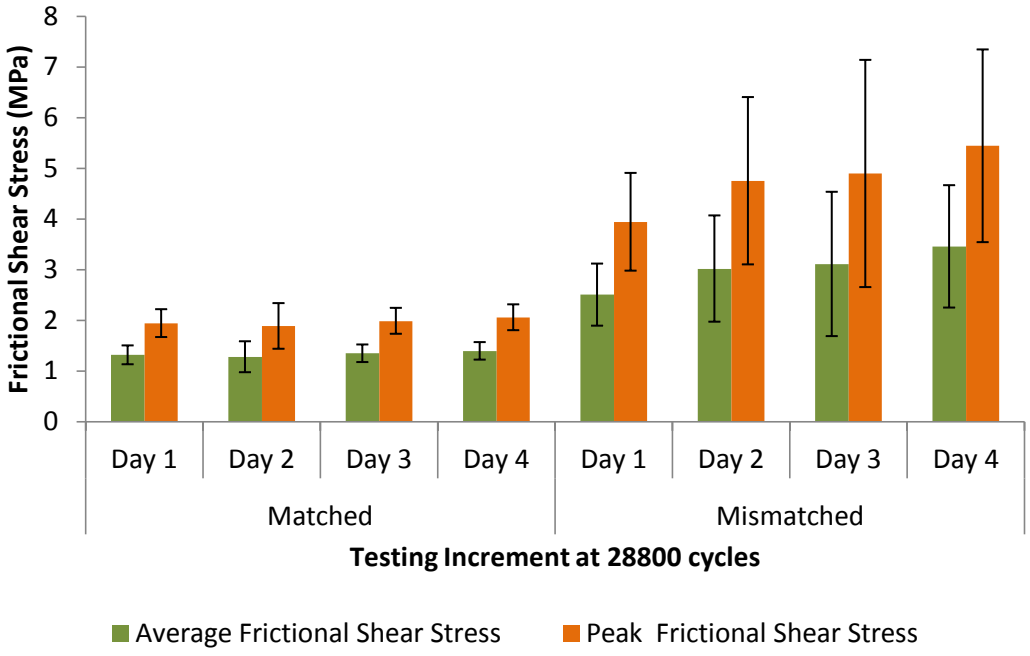

Figure 7-3: Mean and peak frictional shear stress after 28800 cycles for each of the four days (n=4). Error bars represent 95% confidence limits.

No significant differences were observed with respect to testing days; therefore, the friction shear stress were averaged over the entire four days. Differences in mean frictional shear stress between the matched and mismatched groups were observed (Figure 7-4). It was found that the peak and average frictional shear stress was significantly higher in the mismatched geometry group compared to the matched geometry group ($p<0.05$).

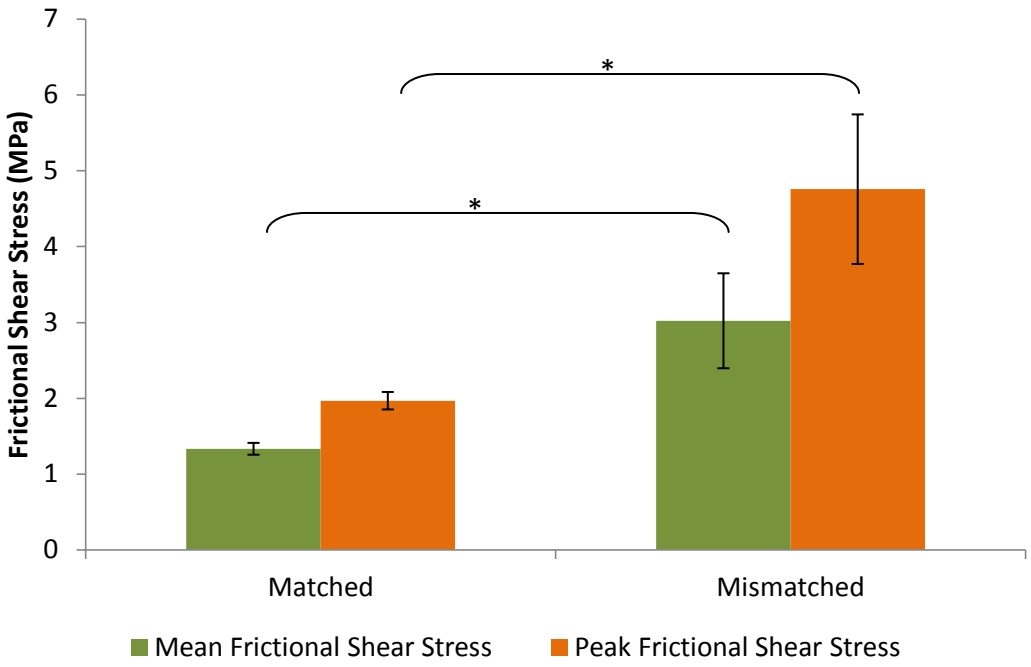

Figure 7-4: Mean and peak friction shear stress taken over four days between matched and mismatched geometry groups. Error bars represent 95% confidence limits. *significant difference ($p<0.05$)

7.3.4 Wear Area/Grade

Macroscopic observations of the acetabulae showed the position of different grades of wear from both the matched and mismatched geometry groups (Figure 7-5). For matched geometry group, the majority of the wear was observed proximal to the acetabular fossa. In all four acetabulae, bone exposure was more apparent on the anterior side. Some bone exposure was observed on the posterior side however, no bone exposure was observed in the centre of the acetabulum samples.

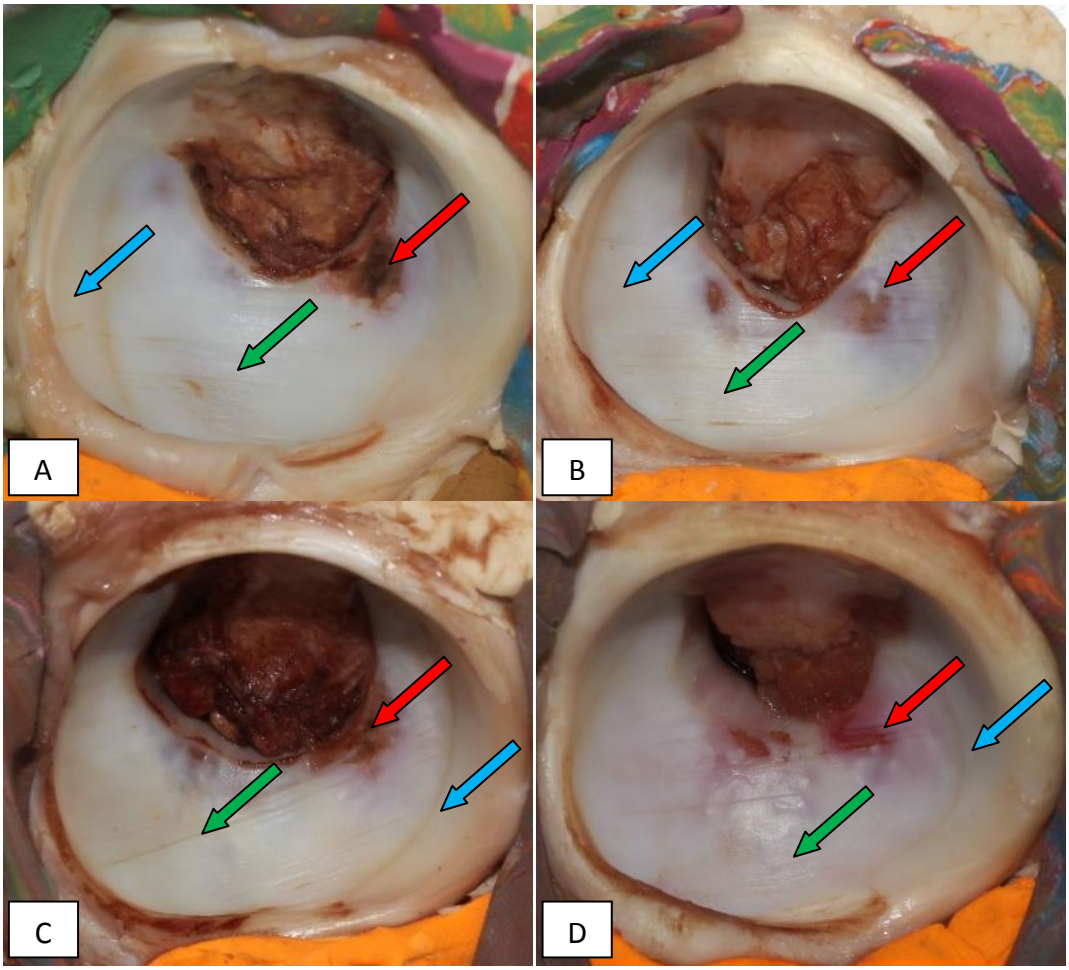

Figure 7-5: Photographs of the four acetabulae of the matched geometry groups depicting the wear on the cartilage surface. Red arrows indicate bone exposure, green arrows indicate wear scratches and blue arrows indicate discolouring.

Scratches were mainly present in the centre of the cup running in the direction of the flexion/extension motion during the tribological test. Light wear and discolouration was observed on the peripheral edges of the scratches. Undamaged cartilage was seen on the peripheral edges of the acetabulae, in the far anterior/superior and posterior/superior regions.

Large regions of bone exposure were found in two acetabulae in the mismatched geometry group which were also proximal to the acetabular fossa (Figure 7-6 A and B). For one of the acetabular, bone exposure was in a form of a fissure (Figure 7-6D). The shape of this cartilage fissure was such that a flap was formed which, when peeled back revealed that more bone was exposed.

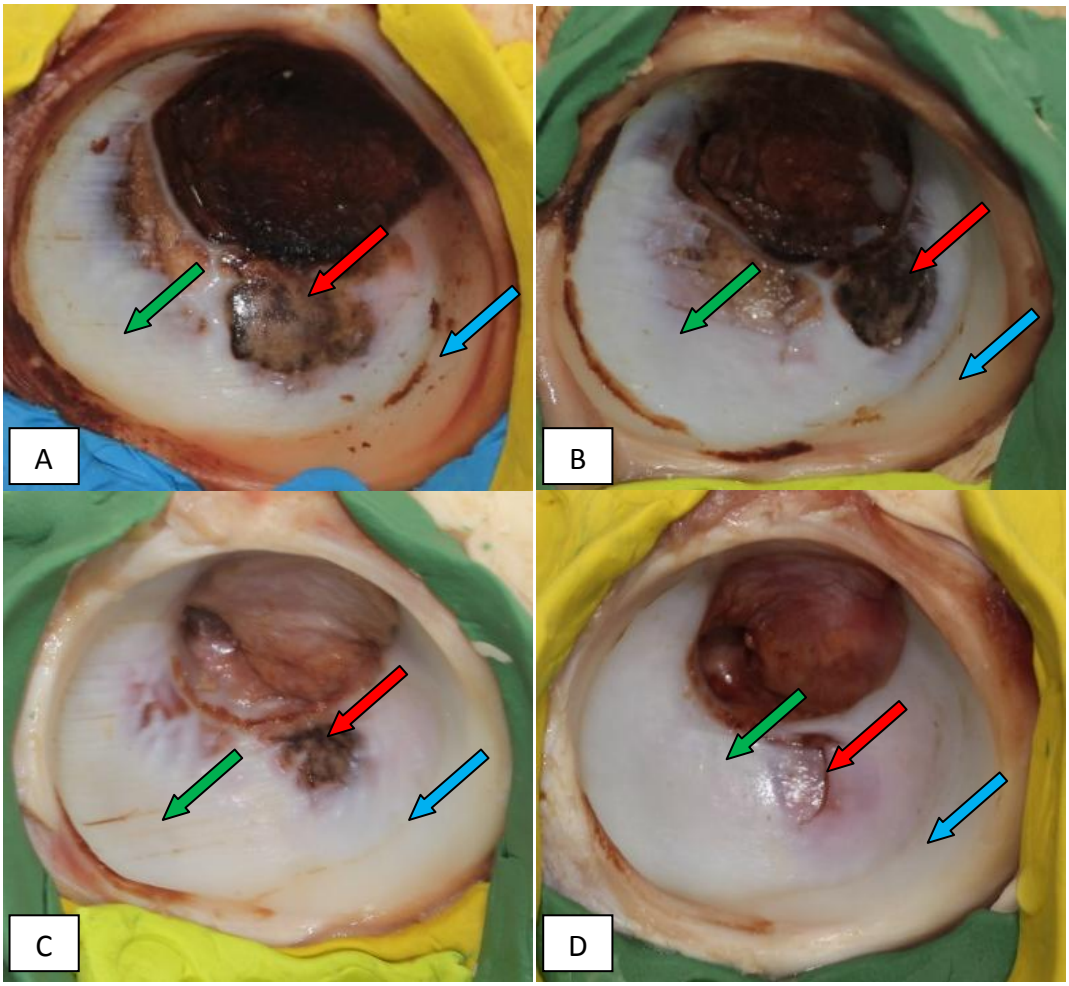

Figure 7-6: Photographs of the four acetabulae of the mismatched geometry groups depicting the wear on the cartilage surface. More bone exposure could be generally seen in the mismatched geometry groups compared to the matched geometry group. Red arrows indicate bone exposure, green arrows indicate wear scratches and blue arrows indicate discolouring.

The colour of the ligamentum teres was darker than observed in fresh tissue for the two acetabulae which exhibited larger bone exposure (Figure 7-6 A and B). This was not seen for the matched geometry group. There was also discolouration of the subchondral bone in three of the four acetabulae, where a black/gray colour was observed.

The areas of the regions with different grades of wear were calculated in terms of percentage coverage. For both the matched and mismatched geometry groups, the majority of the cartilage did not exhibit any wear (Figure 7-7). Surface scratches were the most predominant type of wear; however, significantly lower in terms of percentage coverage than unworn areas for both matched and mismatched geometry groups ($p<0.05$). There was no significant difference

between bone exposure and light damage for both the matched and mismatched geometry groups.

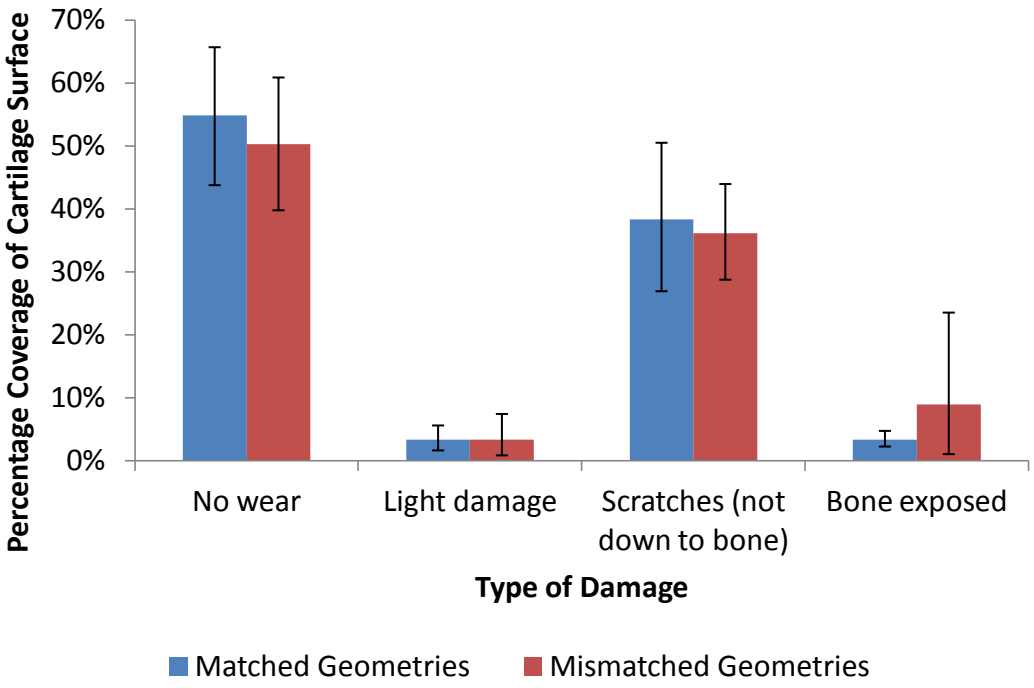

Figure 7-7: Mean percentage coverage of the different categories of wear between the matched and mismatched geometry groups (including the fourth sample with a mismatched geometry). Error bars represent 95% confidence limits (n=4).

Due to the one of the acetabulae from the mismatched geometry group exhibiting a cartilage fissure, the results were skewed for percentage coverage of bone exposure. After discounting the acetabulum with the fissure (Figure 7-8) there was a significantly larger bone exposure in the mismatched geometry group compared to the matched geometry group ($p<0.05$). Also, bone exposure was significantly more predominant than light damage in the mismatched geometry group ($p<0.05$). There was no significant difference in the percent coverage of unworn, slightly damaged and scratched cartilage between the matched and mismatched geometry groups ($P=0.05$).

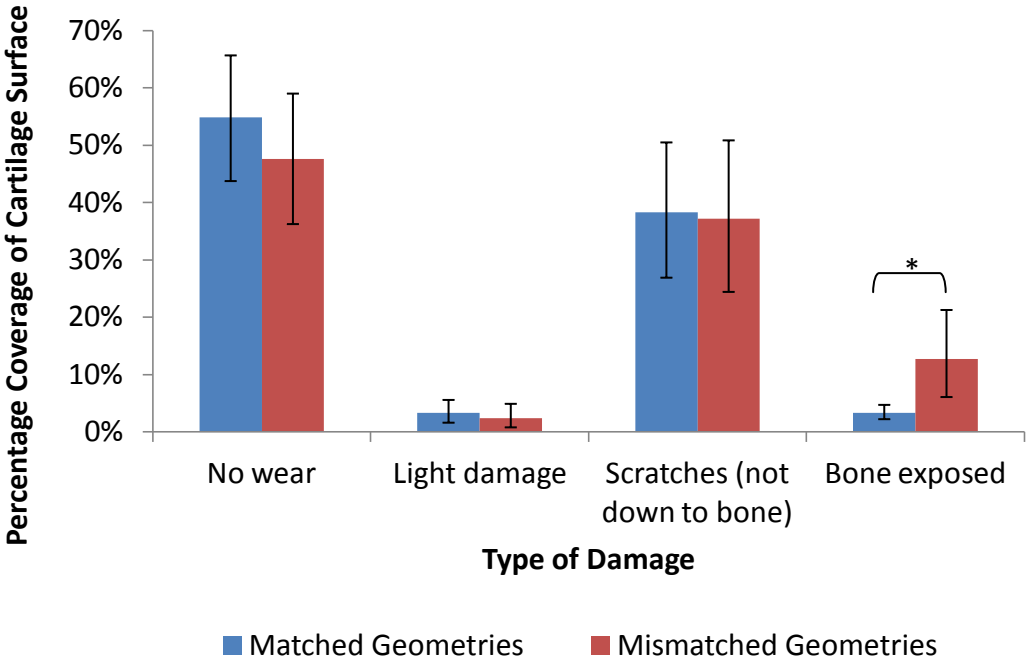

Figure 7-8: Percentage coverage of the different categories of wear between the matched and mismatched geometry groups (not including the fourth sample with a mismatched geometry). Error bars represent 95% confidence limits (n=4 for matched geometries, n=3 for mismatched geometries). *significant difference ($p<0.05$)

7.3.5 Cartilage Thickness

The thickness of the cartilage in the scratched areas of the acetabulae was measured and compared with the osteochondral samples taken from fresh controls (n=4) in a similar location of the acetabulum. The average cartilage thickness was lowest in the mismatched geometry groups and both the matched and mismatched geometry groups exhibited thinner cartilage compared to the fresh controls (Figure 7-9). However, these differences were not significant (P=0.05).

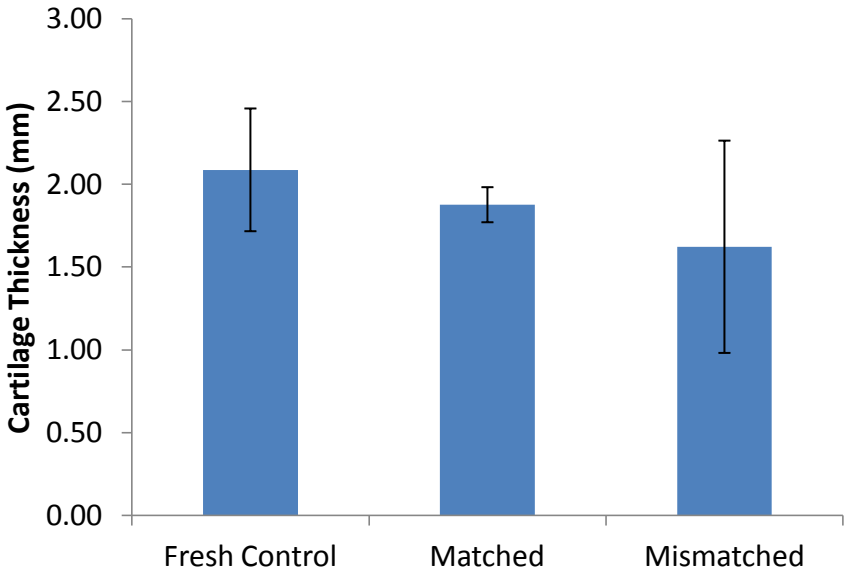

Figure 7-9: Cartilage thickness of the fresh control, matched and mismatched geometry groups. Error bars represent 95% confidence limits (n=4).

7.3.6 Histological Analysis

Histological analysis was performed on cartilage sections that were taken perpendicularly across the wear scars and compared with cartilage taken from the same location on fresh acetabulae. This was to compare the micro-morphology of the cartilage as well as the micro-architecture. Both H&E and Alcian blue stains were used.

Hematoxylin and Eosin

H&E stain was used to observe the general microstructure of the cartilage. Examples of the fresh control sections are shown in Figure 7-10. The surface was smooth with negligible asperities. There was a dense pink layer on the surface of the cartilage which could corresponded to the densely woven collagen fibres which are located in the superficial zone of the cartilage (Mow and Ateshian, 1997).

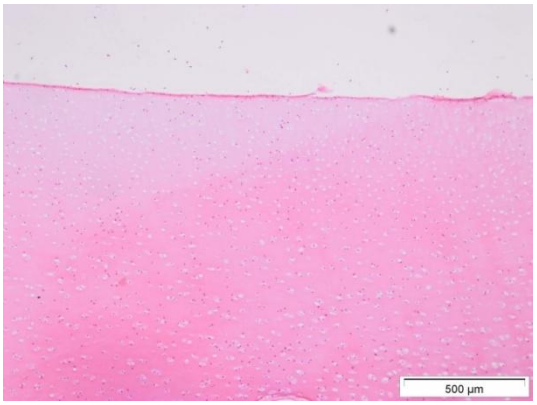

Figure 7-10: Example of the fresh control sections stained with H&E (40x magnification). A deep pink colour can be seen in the superficial zone which represents the intact collagen fibres.

Sections of worn cartilage from the matched geometry group are shown in Figure 7-11. Asperities could clearly be seen and were much larger near the area of bone exposure (Figure 7-11 A-B) compared to the lightly damaged region (Figure 7-11 E-F). Nearer the bone exposure region, the undulations were approximately 100 to 300 µm in size, which was estimated using image ProPlus v3.0 (Media Cybernetics, Inc., MD, USA). In the light damage region, undulations were also commonly seen microscopically (30-80 µm in size), which could not be observed macroscopically.

The thickness of the pink layer on the surface of the cartilage was also thinner than the fresh controls. This can be seen clearly on Figure 7-11 D where, in some cases, this layer was removed.

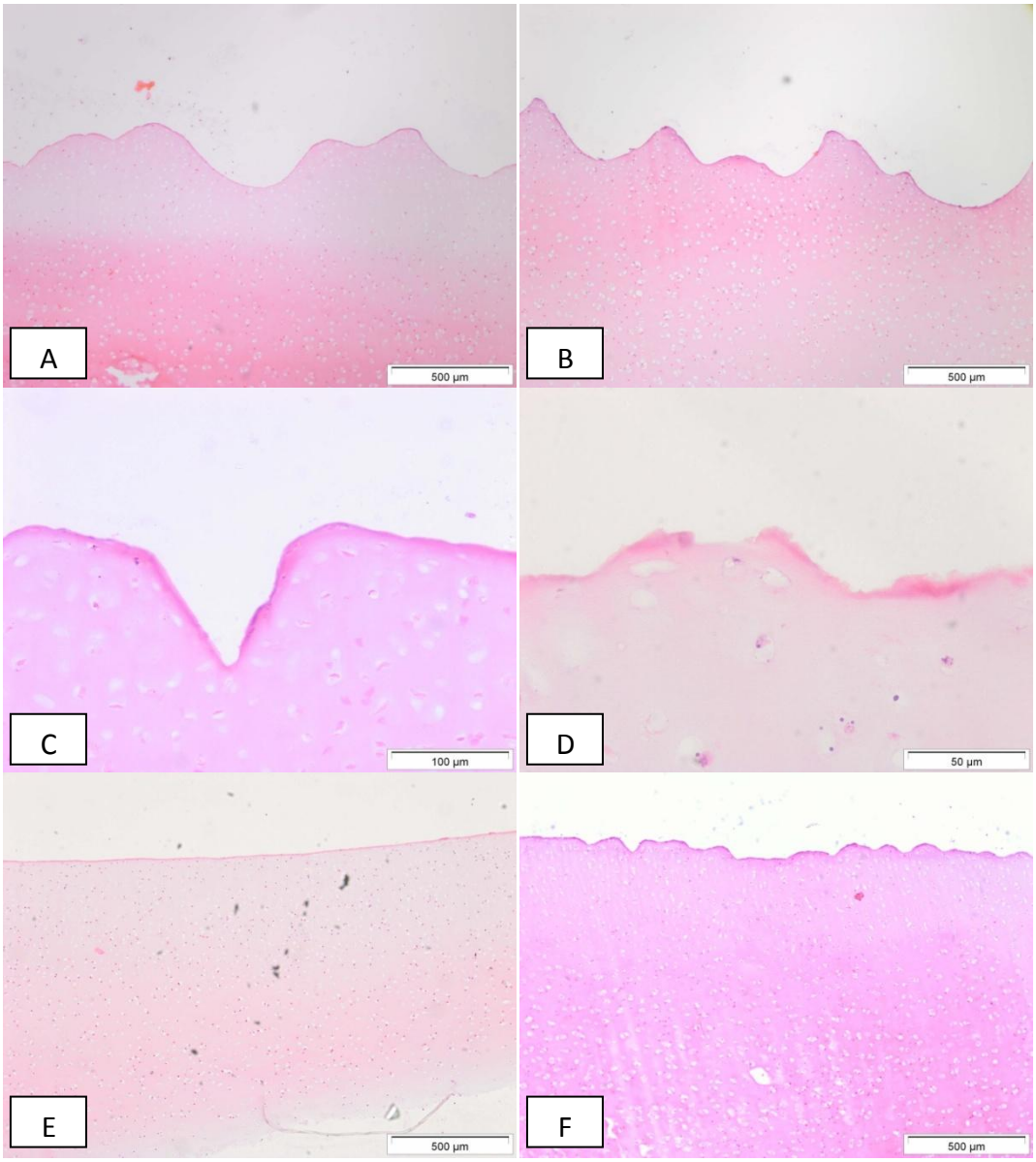

Figure 7-11: Examples of the matched geometry group sections stained with H&E. A-D) "Scratched" region. E-F) "light wear" region. (A, B, E, and F are 40x magnification. C is 200x magnification. D is 400x magnification). Undulations and breaks in the superficial zone can be clearly seen.

Large undulations were also observed in the mismatched geometry group. However, there were more "fractures" on the cartilage surface (Figure 7-12 A & C). The thickness of the pink layer on the cartilage surface which represents the collagen fibres was also variable and in some cases, absent.

The "flap" that was created in the form of a cartilage fissure was observed microscopically in Figure 7-12 D. The cartilage was only approximately 300 µm thick in this region.

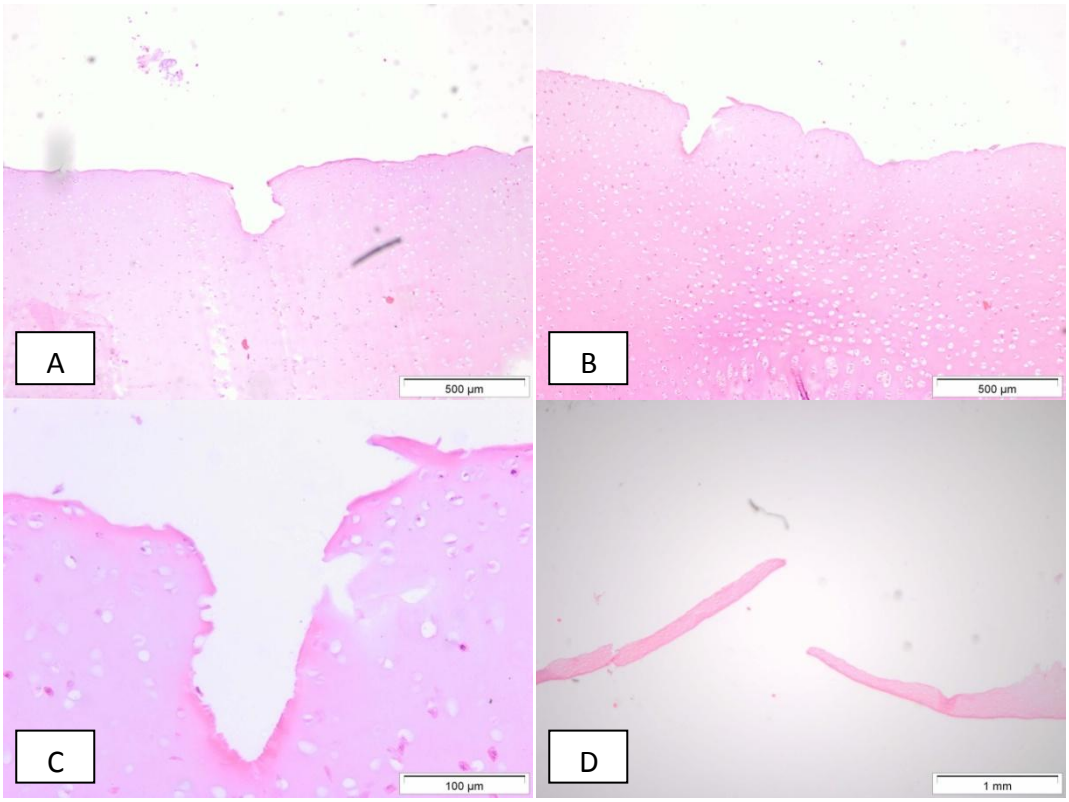

Figure 7-12: Examples of the mismatched geometry group sections stained with H&E (in the "scratched" regions). A and B are 40x magnification. C is 200x magnification. D is 4x magnification.

Alcian Blue

Staining with Alcian blue was used to observe the GAGs within the cartilage from the fresh control, matched geometry and mismatched geometry groups. A uniform distribution of blue in the fresh control cartilage is shown in Figure 7-13.

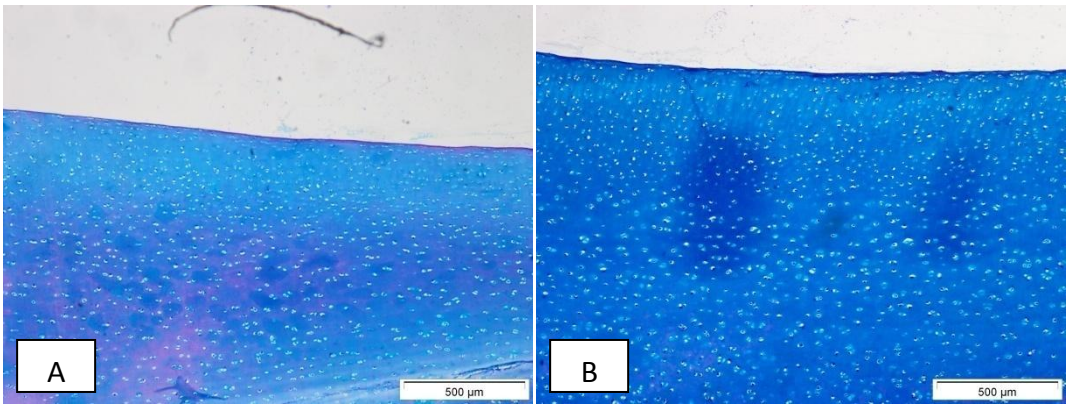

Figure 7-13: Examples of the fresh control sections stained with Alcian blue (40x magnification).

Large undulations are seen on the cartilage surface in the matched geometry group with fractures (Figure 7-14) similar to the H&E stained sections (Figure 7-11).

However, there were no differences in the colour intensity and distribution of blue between the matched geometry and fresh control groups.

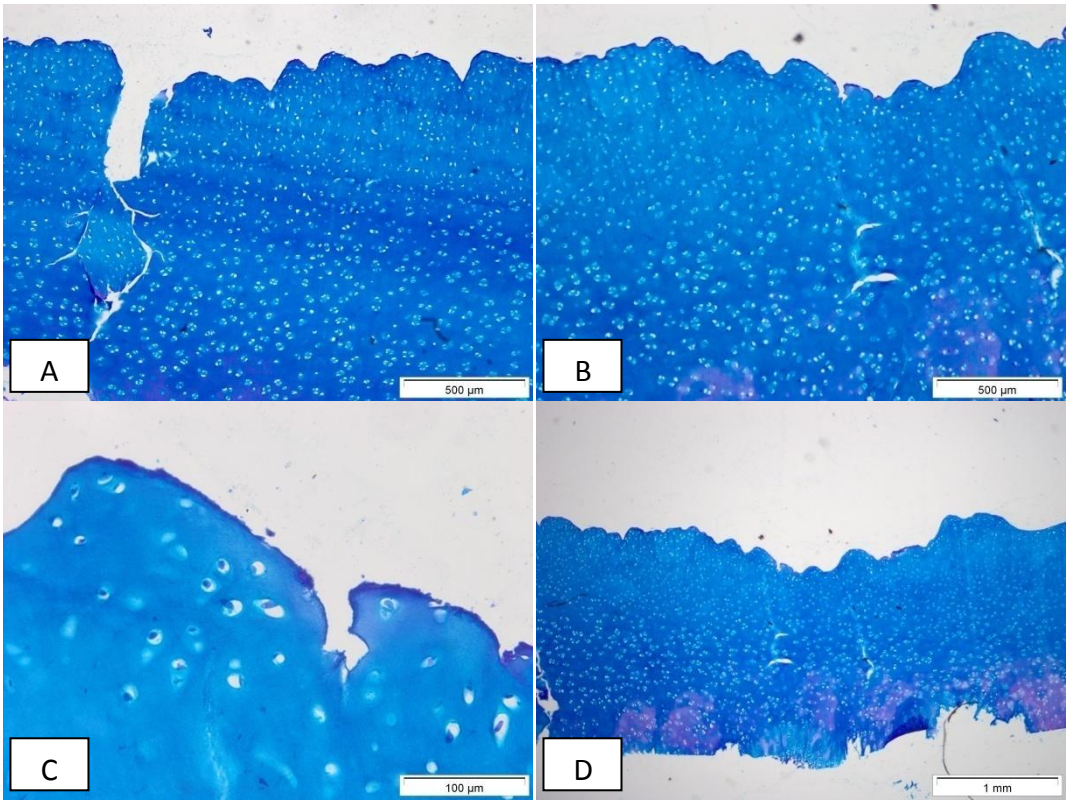

Figure 7-14: Examples of the matched geometry group sections stained with Alcian blue ("Scratched" region). A and B are 40x magnification. C is 200x magnification. D is 4x magnification.

Large surface cracks and undulations were also seen in the mismatched geometry group, similar to the matched geometry group. However, most of the sections exhibited a pinker colour in the middle to deeper zones as opposed to blue (Figure 7-15). This suggested that there was GAG loss in this group.

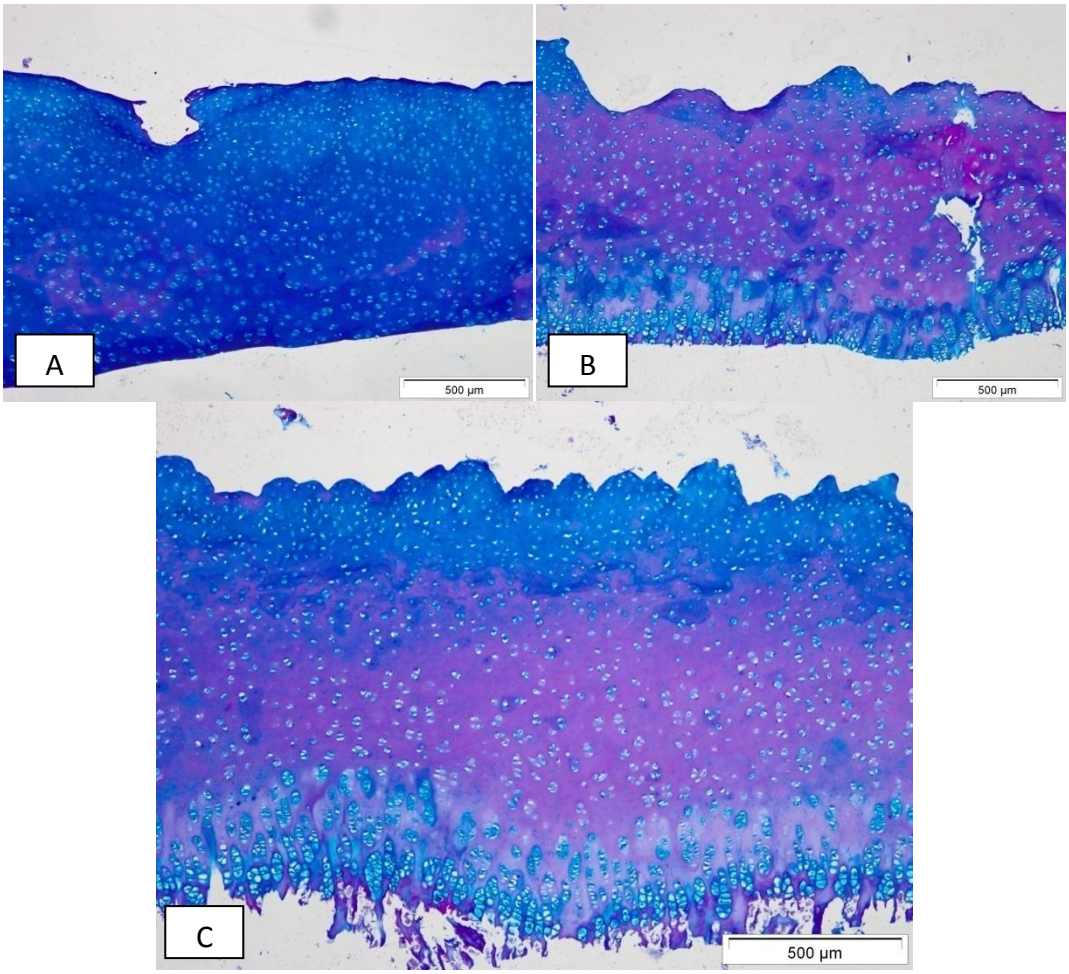

Figure 7-15: Examples of the mismatched geometry group sections stained with Alcian blue ("Scratched" region). A, B and C are 40x magnification.

7.3.7 GAG Quantification Analysis

The GAG content of the remaining cartilage was also quantified for the matched and mismatched geometry groups and compared to fresh cartilage (Figure 7-16). The cartilage from the mismatched groups exhibited significantly lower concentrations of GAGs per dry weight of cartilage compared to the fresh control ($p<0.05$). Cartilage from the matched geometry group also exhibited lower mean concentration of GAGs compared to the fresh control; however, this was not significant ($P=0.05$). Cartilage from the mismatched geometry group exhibited lower mean concentration of GAGs compared to the matched geometry group, however, this was also not statistically significant ($P=0.05$).

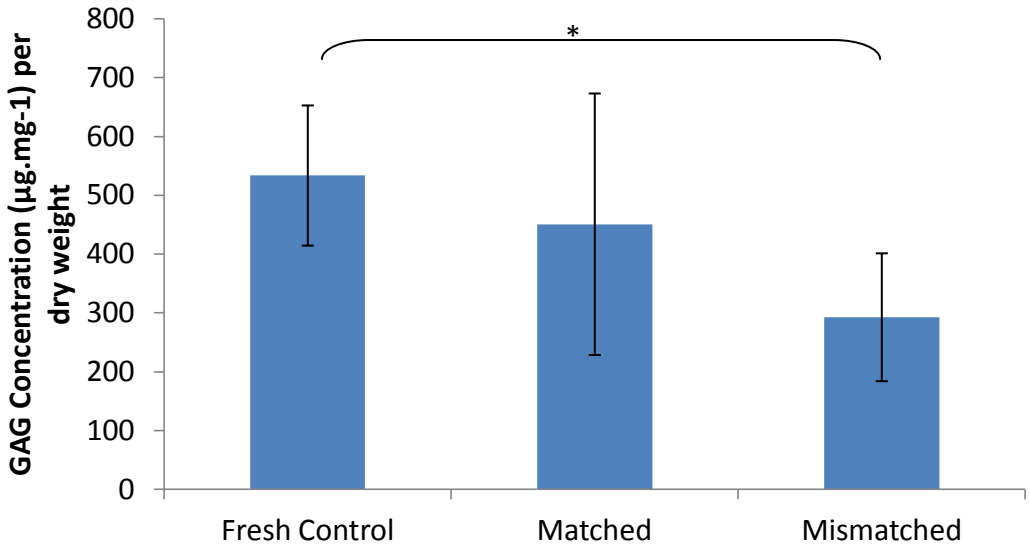

Figure 7-16: Mean GAG concentration per dry weight of cartilage for fresh control, matched and mismatched geometry groups. Error bars represent 95% confidence limits (n=4). Significant difference was observed between fresh control and mismatched geometry groups. *significant difference ($p<0.05$)

7.4 Discussion

In this section, the relationship between radial clearance and hip hemiarthroplasty tribology in the medium term will be discussed. The effect that limitations of the model, which were demonstrated in the previous Chapters (Chapter 3 – 6), could have on the results in this Chapter will be discussed further in Chapter 8.

7.4.1 Friction Coefficient

Friction coefficient was measured during tribological testing for four periods of eight hours with approximately 16 hours of intermediate unloaded periods. Over the eight hour testing period, the relationship between friction coefficient and time was similar to that of the short term test conducted in Chapter 4. Whereby, the friction initially rapidly increased. The rate of increase gradually reduced to an equilibrium period. This relationship between duration of test and friction coefficient of cartilage was discussed by Forster and Fisher (1999) and later by Krishnan *et al.* (2004). During continuous sliding, fluid is expelled from the cartilage and hence, decreasing fluid load support and increasing the proportion of the load

supported by the solid phase. This increases the friction between the surfaces. Over time, the rate of fluid expulsion reduces as the majority of the load is supported by the solid phase, causing the friction coefficient to plateau. Therefore, the friction of cartilage is governed by the biphasic nature of the cartilage tying together the theories of biphasic mechanical properties (such as stress relaxation and creep) presented in Section 1.4.4 and biphasic lubrication presented in Section 1.7.3. The friction coefficient plateaued more so in the eight hour tests compared to the two hour tests conducted in Chapter 4 and in previous studies which used short testing periods (Forster and Fisher, 1996; Katta *et al.*, 2007; Lizhang, 2010). This shows that fluid load support was still maintained during the time periods considered by these studies. This was possibly due to the testing length being too short to allow solid load support to reach equilibrium, and thus some degree of fluid load support was maintained. This also suggests why the friction coefficient reached a maximum of 0.29 and 0.42 for matched and mismatched geometry groups respectively as opposed to 0.16 which was found in both Chapter 4 and the study by Lizhang (2010).

In both the matched and mismatched geometry groups, the friction coefficient rapidly reduced during the unloaded periods. This was possibly due to the fluid that was expelled from the cartilage during testing periods, being re-absorbed into the cartilage during the unloaded periods. This re-absorption could be attributed to the electro-negativity of the GAGs and Donnan osmotic pressure created by the difference in ion concentration within the cartilage matrix compared to the antibiotic lubricant (Section 1.3.2). This highlights cartilages' extraordinary ability to recover, even after the application of harsh tribological conditions.

There was, however, a difference seen in this recovery period between the matched and mismatched geometry groups. For the matched geometry group, the friction coefficient after 30 cycles was lower during the first testing period, compared to the other testing periods. Therefore, some cartilage damage must have occurred during the first testing period. It is assumed the damage may also affected the cartilage's ability to fully recover, such as damage to the superficial zone which is impermeable to the charged ions residing in the interstitial fluid. This would have had an effect on the Donnan osmotic pressure, altering the fluid load

support of the cartilage. The friction coefficient at 30 cycles also did not change between the second and fourth testing period. This suggests that the majority of damage the cartilage exhibited during the four days occurred during the first testing period.

For the mismatched geometry group, the average friction coefficient after 30 cycles increased during each testing period; suggesting that the damage to the cartilage was continuous throughout the four days, which was dissimilar to the matched geometry group. This was more apparent in the acetabulae with a larger proportion of severe wear.

In previous studies, it was suggested that there was a negative correlation between friction coefficient and applied stress at low stress states (Katta *et al.*, 2007; Katta *et al.*, 2008). This inverse relationship was also seen in the Lizhang (2010) study that used similar stresses to those in the current study. However, the opposite was seen in the current study, where the friction coefficient after the four days of testing was significantly higher for the higher stress mismatched geometry group compared to the matched geometry group. Therefore, there must also be an extraneous factor other than magnitude of stress that governs the relationship between contact stress and friction coefficient. The length of the test was much longer in the current study compared to other studies that have demonstrated this inverse relationship. After eight hours of testing, the majority of the interstitial fluid was expelled from the cartilage, thus solid to solid contact could be assumed to be the primary lubrication regime. This could reverse the relationship between contact stress and friction coefficient of cartilage to that commonly seen in total hip replacements where artificial materials interact (Brockett *et al.*, 2007).

There was more variation in friction coefficient for the mismatched groups compared to the matched groups. This was possibly due to the variability in the severity of wear observed on the acetabular surface after the four days in the mismatched geometry group. The relationship between the proportion of bone exposure and the friction coefficient after four days of testing is shown in Figure 7-17. There is a strong positive correlation between friction coefficient and proportion of bone exposure (r^2 = 0.87). This could also explain why there was a

positive correlation between contact stress and friction coefficient; whereby there was significantly more bone exposed in the higher stress mismatched geometry group compared to the matched geometry group ($p<0.05$).

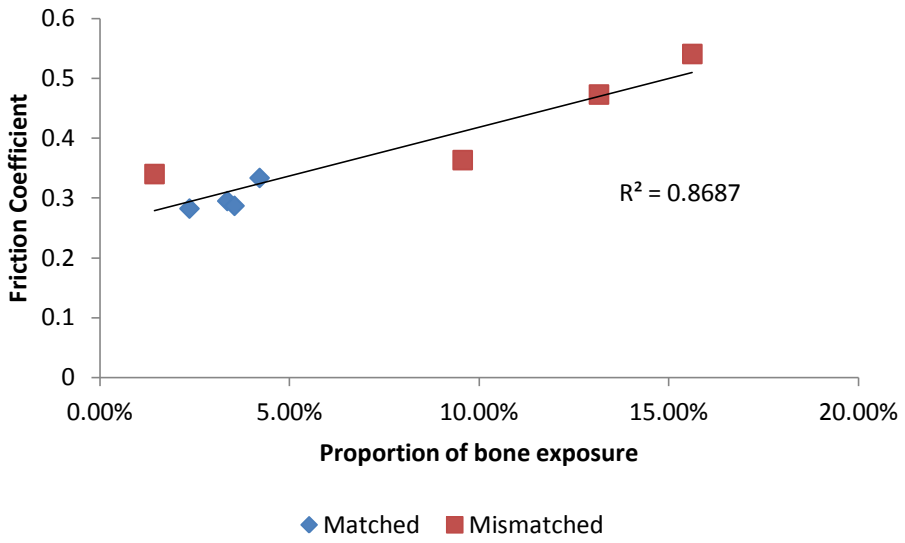

Figure 7-17: Correlation between friction coefficient and proportion of bone exposure for both the matched and mismatched geometry groups.

7.4.2 Frictional Shear Stress

The microstructure of cartilage allows it to withstand high hydrostatic pressures and compressive loads; however, the resistance to shear stress is low due to its biphasic nature. Therefore, it has been suggested that frictional shear stress is a major factor in the mechanical degradation and fibrillation of cartilage (Harris *et al.*, 1975; Yamagata *et al.*, 1987; Kosashvili *et al.*, 2008; Pawaskar *et al.*, 2011b). In the current study, frictional shear stress could only be predicted since actual contact area of each replicate of the test was not known. Instead, the average contact stress calculated in Chapter 6 using the spectrodensitometer method was used to predict the frictional shear stress.

A positive correlation was found between frictional shear stress and the proportion of bone exposure following cartilage wear during the test with an r^2 value of 0.752 and 0.761 for average and peak frictional shear stress respectively (Figure 7-18 A). However, it can be clearly seen that the fourth mismatched acetabulum which was shown in Figure 7-6 D, did not conform to the other values (Figure 7-18 A - circled in red). Once removed the r^2 increased to 0.995 and 0.996

for average and peak frictional shear stress respectively (Figure 7-18 B) Therefore, this suggests that the "fissure" which was created in the fourth mismatched acetabulum should not be grouped with the "bone exposure" category of wear.

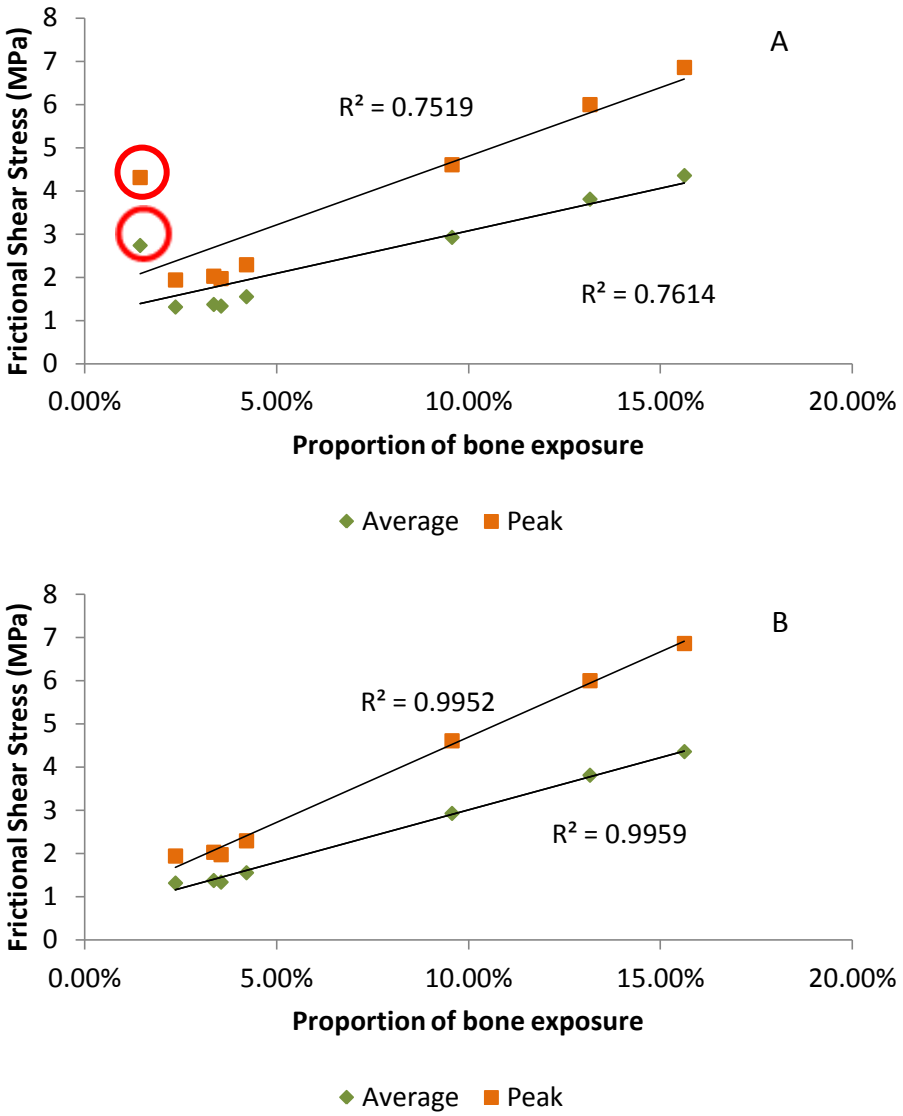

Figure 7-18: Correlation between friction coefficient and proportion of bone exposure for both the matched and mismatched geometry groups. A) Includes the fourth mismatched acetabulum (circled in red). B) Does not include the fourth mismatched acetabulum.

This strong positive correlation between frictional shear stress and the proportion of bone exposure supports the findings of past studies that also suggested frictional shear stress is a major contributor to the mechanical wear of cartilage (Harris *et al.*, 1975; Yamagata *et al.*, 1987; Kosashvili *et al.*, 2008; Pawaskar *et al.*, 2011b). This highlights the importance of frictional shear stress in tribological studies that involve articular cartilage.

The matched geometry group exhibited a significantly lower average and peak frictional shear stress compared to the mismatched geometry group ($p<0.05$). This could be attributed to the difference in the magnitude and severity of wear observed on the cartilage surface between the matched and mismatched geometry groups.

The frictional shear stress calculated in the current thesis was larger compared to Lizhang (2010) who also used a porcine acetabular model to tribologically assess hip hemiarthroplasty. However, the contact stresses calculated for the matched and mismatched geometry groups in Chapter 6 were similar to the contact stress calculated in Lizhang (2010) study for the medium (0.6-1.2 mm) and extra large clearances (greater than 1.8 mm) respectively. Therefore the increase in frictional shear stress must be attributed to the larger frictional coefficients observed in the current study compared to Lizhang (2010).

7.4.3 Wear Area/Grade

There are many methods that have been used in the past to visually analyse macroscopic wear on the cartilage surface such as the French Society of Arthroscopy (Dougados *et al.*, 1994) Arthroscopy Osteoarthritis Scale (Klashman *et al.*, 1995) and the ICRS scoring method (Brittberg and Winalski, 2003). This makes comparison with previous studies difficult. In the current study, the wear was categorised into four groups: no wear, light damage/discolouring, wear scratches (not to the bone), and bone exposure. There was a consistent pattern of wear macroscopically for the matched geometry group, in which most of the severe wear was located on the anterior region of the acetabulum proximal to the acetabular fossa. The reason for this is unknown but it could be due to regional differences in the thickness of cartilage. There was no bone exposure observed in the centre of the acetabulum due to the presence of a growth plate. Severe wear was also observed mainly in the anterior region of the acetabulum proximal to the acetabular fossa for the mismatched geometry group. The location of the severe wear was not affected by the clearance.

Cartilage is aneural and hence, the pain generated from cartilage erosion after hip hemiarthroplasty is caused by the metallic femoral head articulating

against the subchondral bone. Therefore, bone exposure is an important category of wear and must be used to compare between the matched and mismatched geometry groups. It was suggested in Section 7.4.2 that the “fissure” observed on the fourth mismatched acetabulum cartilage surface should not be grouped with the “bone exposure” wear category. This was due to skewing the linear relationship between bone exposure and frictional shear stress. Therefore, if the fourth mismatched acetabulum was removed from the group, there was significantly more bone exposure for the mismatched geometry group compared to the matched geometry group. Bone exposure was not seen in previous studies, this was possibly due to the testing duration which was significantly longer in the current study compared to previous studies (Lizhang, 2010).

7.4.4 Cartilage Thickness

Cartilage thickness was also measured on the scratched region of the acetabular cartilage. Even though the average thickness was thinner after four days of tribological testing with matched geometries compared to fresh cartilage, and even thinner with mismatched geometries; no significant differences were seen. The reason for this could be found by examining the micro-morphology of the scratched region. The micro-morphology will be discussed in more detail in Section 7.4.5; however, the undulations observed on the cartilage surface made the thickness highly location dependent (Figure 7-11 and Figure 7-12). The distance between the peaks and troughs of these undulations were up to 300 µm and hence could mask the true difference between the fresh, matched geometry and mismatched geometry groups.

7.4.5 Histological Analysis

In order to fully understand the mechanical effects of the tribological study, the microscopic effects of the cartilage were investigated. As discussed in Section 7.4.4, large undulations on the cartilage surface with a distance of 300 µm between the peaks and troughs were observed using the H&E and Alcian Blue stains. The undulations corresponded to the cross-section of the wear scars. After staining with H&E, the most superficial layer was not always ruptured and hence, these

undulations could be the result of permanent morphological damage (Figure 7-11 and Figure 7-12). However, there were certain areas with ruptures in the superficial zone. This was more apparent in the mismatched geometry group compared to the matched geometry group.

In previous studies that histologically studied articular cartilage after *in-vivo* articulation with a metal head, fibrillation and rupture of the superficial zone was observed. A study by Cook *et al.* (1989) implanted 49 unipolar hemiarthroplasties into canine hips and histologically assessed the cartilage after two weeks to 18 months post implantation. After two months, deep fibrillations were present on the surface of the acetabulum (Figure 7-19).

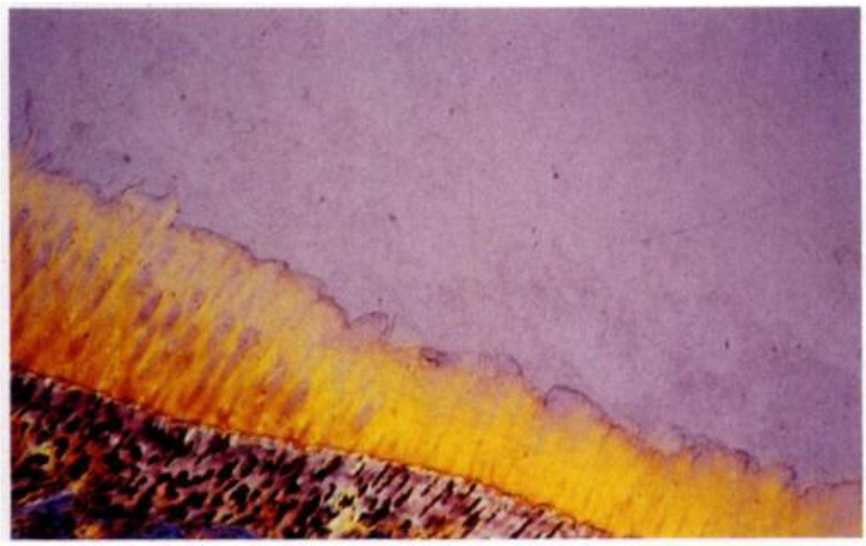

Figure 7-19: Histological sections stained with basic fuchsin and toluidine blue and observed under polarised light, x 50. This shows severe fibrillation after implantation of a unipolar hemiarthroplasty (Cook et al., 1989).

These fibrillations were not commonly seen in the current study. Instead larger undulations were seen. This could be due to only flexion/extension was applied in the current study compared to the complex motions observed *in-vivo*. Also, the loading cycle in the current study was a simplified version of the loading cycle observed *in-vivo*. However, the large fibrillations seen in the mismatched geometry group (Figure 7-15) were also observed in previous studies (Figure 7-20) (Laberge *et al.*, 1992; Kerin *et al.*, 2003). The microscopic wear observed in the current study has been commonly seen in *in-vivo* studies that examined cartilage

post implantation of hip hemiathroplasties. Thus, the results obtained in this study may allow conclusions that might affect clinical practice.

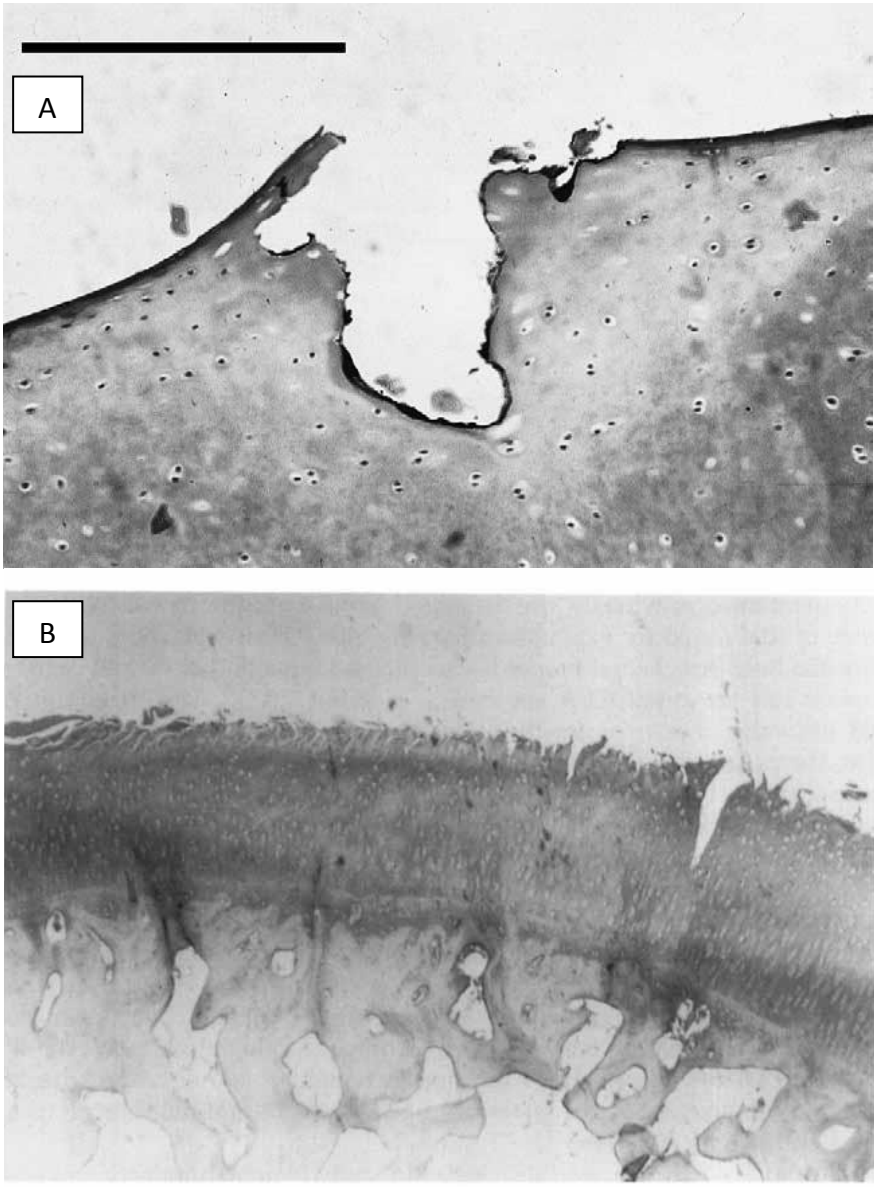

Figure 7-20: A) Histological section stained with Masson's blue trichrome (bar length = 200 µm) showing a large fissure after *in-vitro* tribological testing (Kerin et al., 2003). B) Histological section stained with Safranin-0 (magnification x100) showing large and small fissures after implantation (LaBerge et al., 1992).

Undulations on the cartilage surface were still present but became less severe further from the bone exposure in the "lightly damaged" region. Therefore, this shows that in some cases, mechanical damage to the tissue could not be detected using only macroscopic observation, microscopic analysis was needed.

Alcian Blue stain was used to analyse the distribution of GAGs within the tissue. This was depicted as the blue colour in Figure 7-13 to Figure 7-15. There was no noticeable difference in the intensity and distribution of blue between the fresh control and matched geometry groups in the scratched regions. This suggested that the GAGs remained unaffected in the matched geometry group during the four day tribological study. However, the intensity of blue was reduced in the majority of the sections taken from the mismatched geometry groups. The distribution of blue was also less uniform compared to both the fresh and matched geometry groups. This suggested damage to the micro-architecture of the cartilage, specifically the GAGs.

GAGs are multiple polysaccharides chains which covalently bound to a core protein to forming a large molecule known as a proteoglycan (Mow and Ateshian, 1997). This is discussed in detail in Section 1.3.2. All GAGs contain sulphate and carboxyl groups which are negatively charged. This high negative charge serves three purposes: 1) to resist compression loads in the joint due to the repulsion between the negatively charges, 2) to attract counterions which enable cartilage hydration through Donnan osmotic pressure, and 3) to resist interstitial fluid flow, lowering the permeability of the cartilage. These three functions of GAGs give cartilage its phenomenal tribological properties. If the GAG chains become disrupted, mobilised or removed from the matrix entirely, this would have a significant effect on the tribological properties of the cartilage, escalating the degradation. This was shown in a previous study by Katta et al. (2008) who treated cartilage samples with chondroitinase ABC to induce loss of GAGs. It was found that there was a loss of compressive stiffness and the friction coefficient was increased by over 50%; owing to the loss of biphasic lubrication (Katta *et al.*, 2008).

7.4.6 GAG Quantification Analysis

The results from the biochemical analysis of GAG content supported the histological assessment, where there was a significant reduction in GAG concentration in the mismatched geometry group compared to the fresh control. The consequences of GAG depletion in terms of the tribological properties of

cartilage were discussed in Section 7.4.5. There was no significant reduction in GAG concentration in the matched geometry group compared to the fresh controls.

As discussed in Section 7.4.5, a previous study found an inverse relationship between GAG concentration and the coefficient of friction of cartilage (Katta *et al.*, 2008). In the current study, the average friction coefficient after four days of testing was significantly higher for the mismatched geometry group compared to the matched geometry group. Whereas, the average GAG concentration was lower for the mismatched geometry group compared to the matched geometry group; though, this was not significant (p=0.05). However, when correlating the friction coefficient after four days and the GAG concentration for each of the eight acetabulae (Figure 7-21), a negative correlation was observed; however, the correlation factor was low (r^2 = 0.28).

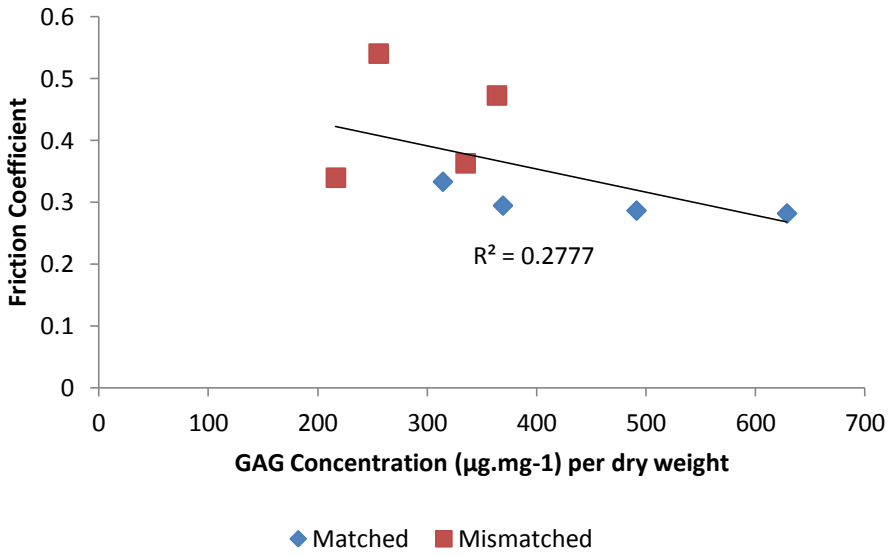

Figure 7-21: Correlation between friction coefficient and GAG concentration per dry weight of cartilage for both the matched and mismatched geometry groups.

7.5 Conclusion

The aim of this study was to investigate the relationship between radial clearance and cartilage wear and friction for a period of four days (115,200 cycles). Two groups were used: matched and mismatched geometry groups. The matched geometry group used a CoCr femoral head with a diameter most similar to the diameter of the natural femoral head. The mismatched geometry group used a

CoCr femoral head with a diameter 2 mm smaller than the matched CoCr femoral head diameter. The following were found:

- The friction coefficient increased over the 28,800 cycles. The rate of increase was high initially, then gradually reached equilibrium.
- During the unloading periods, the cartilage recovered. This reduced the friction coefficient dramatically.
- For the matched geometry group, the initial friction coefficient on the first testing period was lower than the initial friction coefficient on the subsequent testing periods. Demonstrating that the majority of the damage has occurred during the first testing period.
- For the mismatched geometry group, the initial and final friction coefficient of each test period gradually increased over the four testing periods suggesting damage occurred throughout the four days of testing.
- The frictional shear stress was larger in the mismatched geometry group compared with the matched geometry group.
- The frictional shear stress was found to correlate with the proportion of severe wear.
- There was no significant difference between the matched and mismatched geometry groups in terms of cartilage thickness in the scratched region. This was due to the undulations caused by the articulating CoCr femoral head observed microscopically.
- There was a significantly lower concentration of GAGs residing in the cartilage after four days of testing compared to fresh cartilage in the mismatched geometry group. No significant difference was found between fresh and matched geometry group.
- The result from the biochemical analysis confirmed well with the histological analysis that also showed that the distribution of GAGs after four days of testing with mismatched geometries was less uniform than the matched geometry group.

7.6 Clinical Significance

Results show mismatching the femoral head by up to 2 mm in terms of diametrical clearance can have significant consequences on the wear and friction of the natural acetabulum. Eventually, this would lead to a more rapid cartilage erosion and hence, failure of the hip hemiarthroplasty. This is important to consider since the diameter increments for hip hemiarthroplasty used clinically are commonly 2 mm; so this mismatch is likely to occur clinically resulting in sub optimal clinical outcomes.

Chapter 8: Overall Discussion and Conclusion

The primary aim of this thesis was to design, develop and validate a medium term *in-vitro* tribological model in order to study the relationship between radial clearance and cartilage wear and friction in hip hemiarthroplasty for an extended period. The studies that were conducted in this thesis helped validate the choice of animal joint (Chapter 3), lubricant (Chapter 4), aseptic dissection process (Chapter 4), the vessel in which the hemiarthroplasty simulation system was tested (Chapter 5), and contact mechanics (Chapter 6). Investigating these aspects of the *in-vitro* tribological model allowed the limitations to be highlighted which could have an effect on the results obtained in the main study in Chapter 7. These limitations which were discovered in the previous Chapters (Chapter 3 – 6), will be discussed further in this Chapter.

8.1 Choice of Animal Joint

Femoral heads taken from animal joints were used due to the limited availability associated with ethical issues and variability of human acetabulae. After a series of experiments that compared porcine, bovine and ovine femoral heads to human; porcine was chosen to represent human in the medium term tribological tests (Chapter 3). The choice was based on hip geometry; where by the "roundness" and the average diameter of the porcine femoral head was most comparable to that of humans. Therefore, it was hypothesised that the contact region between the round CoCr femoral head and the porcine acetabulae should be the most similar to that of human. Porcine acetabulae were also used in a previous study which examined friction coefficient of hip hemiarthroplasty in the short term (Lizhang, 2010). Using porcine cups allows comparisons to be made with this study.

However, as discussed in Section 3.6, there was no optimum joint that could be used, where each animal joint had limitations. The main limitation of the porcine cartilage was that the mechanical properties were least similar to human compared to ovine or bovine. The equilibrium elastic modulus was lower whilst the permeability was higher. The tribological properties of cartilage are governed by

the intrinsic mechanical properties, specifically the flow of interstitial fluid in and out of the cartilage matrix (Mow and Ateshian, 1997). With a higher permeability, fluid retention is compromised and hence, the flow of fluid out of the cartilage would be more rapid, diminishing the fluid load support. Friction of cartilage is governed by fluid load support, where by the friction between the fluid phase and the counter face is negligible compared to the friction between the solid phase and the counter face (Forster and Fisher, 1996; Forster and Fisher, 1999). Hence, as fluid is excluded from the cartilage due to applied load, the solid load support increases, thus increasing the friction coefficient (Katta *et al.*, 2007). The rapid loss of fluid out of the porcine cartilage would in turn increase solid load support at an accelerated rate compared to human cartilage. Therefore, the initial rate of increase of friction coefficient could be lower if a human acetabulum was used compared to the results in the current study where porcine acetabulae were used.

The lower equilibrium elastic modulus of porcine cartilage compared to human could also have had an effect on the morphology of the worn cartilage. Large undulations were seen in Figure 7-11 and Figure 7-12, with some damage to the most superficial layer. These undulations could be permanent deformation caused by the soft porcine cartilage. Human cartilage was found to be much stiffer (Section 3.4.4). Therefore, human acetabular cartilage could be less prone to deformation and hence, more cracks to the cartilage surface may occur due to fatigue instead. In a previous study, fatigue fracture of cartilage was attributed to the stiffening of the extra cellular matrix (Verzijl *et al.*, 2002).

8.2 Effect of Contamination and Time Dependent Degradation

The proposed lubricant was validated and a sterile dissection process was developed in Chapter 4. By eliminating the contamination, the effect of contamination and cartilage degradation on the friction coefficient of cartilage could be individually determined.

Microbial contaminants within the lubricant and on the cartilage surface were found to lower short term friction coefficients significantly ($p<0.05$). Due to the contaminated samples exhibiting microbial growth in the lubricant and on the

cartilage surface simultaneously, determining the effects on friction coefficient individually could not be performed. However, an earlier study conducted by Souza et al. (2010) found that biofilm production between two articulating surfaces lowered the friction coefficient by tenfold. This supports the theory that the microbial growth on the cartilage surface was a biofilm. Due to the findings that contamination of the *in-vitro* system lowers friction coefficient, efforts were made to eliminate contamination during the medium term tribological study.

However, after comparing fresh cartilage and sterile cartilage after four days of agitation in the lubricant, there was a degree of time dependent degradation which was observed as a significant increase in the short term friction coefficient. Therefore, this might have an effect on the results obtained in Chapter 7. The average increase in friction coefficient was 0.06 which is approximately 25% of the lowest friction coefficient value obtained after four days of tribologically testing (Chapter 7). Although this is a significant large percentage, the effect of degradation would occur to all the replicates in both the matched and mismatched geometry groups. Hence, it would be unlikely that the conclusions drawn from comparing the matched and mismatched geometry groups would be affected. The degree of degradation could be lowered by either increasing the concentration of Aprotinin or attempting to maintain chondrocyte viability and functionality. However, this was beyond the scope of this project.

8.3 Tribological Vessel

In Chapter 4, it was found that contamination significantly reduced the friction coefficient and hence must be eliminated during the medium term tribological test. Therefore, a vessel was designed to be used in conjunction with the friction simulator to test the hemiarthroplasty model in an aseptic environment. Silicon gaiters were chosen to encapsulate the hemiarthroplasty, due to being autoclavable and flexible. However, this added an extra constraint between the femoral head and acetabular cup fixtures.

Even though the average friction did not change between using and not using the silicon gaiters, it was found that it varied the friction more. This could have

affected the friction coefficient. However, the friction coefficient ranged by 0.022 as opposed to 0.005 when the gaiter was not used. This range is less than 10% of lowest friction coefficient value obtained after 28,800 cycles. And the range of the values obtained within the matched and mismatched geometry groups were 0.051 and 0.200. Therefore, this will have a small effect on the overall friction coefficient value.

8.4 Contact Mechanics

The difference between the matched and mismatched geometry groups was determined in terms of contact stress and area in Chapter 6. It was found that the contact stress was significantly larger in the mismatched geometry group compared to the matched geometry group, which was probably due to the significantly smaller contact area.

It was also found that the contact region was more predominant in both the anterior and posterior regions of the acetabulum. Contact stress was relatively lower in the central region suggesting that most of the load was supported by the anterior and posterior regions of the acetabulum. This was most likely to be due to the presence of a growth plate located in the centre of the acetabulum, highlighting another limitation of using porcine acetabulae to represent human. This limitation was due to the skeletally maturity of the animal model and was an addition to the limitations discussed in Section 8.1.

In Section 7.4.2, a strong positive correlation was found between frictional shear stress and severe cartilage wear. This supports previous papers that have also linked frictional shear stress with prevalence of cartilage degeneration (Harris *et al.*, 1975; Yamagata *et al.*, 1987; Kosashvili *et al.*, 2008; Pawaskar *et al.*, 2011b). In Chapter 7, location of severe wear was predominantly on the anterior and posterior sides of the acetabulum. These locations coincide with the locations of high contact stress and due to the positive correlation between contact stress and frictional shear stress (with a given frictional coefficient), the areas either side of the growth plate also exhibited the highest frictional shear stress. This could be the reason for the locations of the severe wear such as bone exposure.

Hemiarthroplasties are commonly implanted into adults, where the bone has already skeletally matured. Therefore, this effect of the growth plate on the contact stress distribution would not occur, thus the wear would be more central compared to what was observed in Chapter 7.

8.5 Clinical Importance

It has been well documented that one of the primary complications after the implantation of hip hemiarthroplasty is acetabular erosion. This may be attributed to excessive contact stress caused by inappropriate fit between the metallic prosthesis and the natural acetabular cup, known as mismatched head size (Harris *et al.*, 1975; Yamagata *et al.*, 1987; van der Meulen *et al.*, 2002; Krishnan *et al.*, 2004). Even though *in-vitro* studies that aimed to investigate cartilage tribology with varying contact stresses have been conducted, there has only been one *in-vitro* study that have investigated the effect of varying radial clearance in hip hemiarthroplasty on the tribology of cartilage (Lizhang, 2010). However, the length of test was two hours. This was a relatively short period of time compared to tribological studies of total joint replacements and is a severe limitation with regards to drawing conclusions that might affect clinical practice. Also, due to the aim of Lizhang (2010) study, which was to correlate radial clearance with friction coefficient, the CoCr femoral head was selected by measuring the diameter of the natural acetabulum using a vernier calliper. This methodology of selecting the femoral head is not practiced clinically. Instead, the natural femoral head is measured either with circular templates, hemispherical templates or vernier callipers and the prosthesis is chosen with the closest matched geometry.

Studies that have investigated these methodologies have primarily concentrated on the accuracy (Jeffery and Ong, 2000; Kosashvili *et al.*, 2008; Samoto *et al.*, 2008). Kosashvili et al. (2008) measured the accuracy of using a vernier calliper by comparing the results with the results obtained from a coordinate measuring machine. It was found that the average diameter clearance between the natural femoral head and acetabulum was 0.73 ± 0.37 mm (mean ± standard deviation) with a maximum of 1.46 mm when using a vernier calliper. This

was significantly larger than the clearance measured using the coordinate measuring machine which was found to be 0.36 ± 0.29 mm. The clearance obtained from the calliper method was further increased to 1.01 ± 0.44 mm with a maximum of 1.96 mm when rounded down to the nearest millimetre. Jeffery and Ong (1999) found that the difference between using the full circle templates and vernier callipers is 0.72 mm.

The results obtained in Chapter 7 showed that by increasing the radial clearance by 1 mm, cartilage wear, friction coefficient and frictional shear stress dramatically increased whilst lowering GAG concentration. Due to the variation in the methodologies described above and the fact that hemiarthroplasties are commonly supplied in 2 mm diameter increments, the significant affect on acetabular cartilage longevity must be considered. Therefore, in order to increase the longevity of the implant, tighter controls have to be put into place when selecting the appropriate femoral head size.

It was also observed in Chapter 7 that for both the matched and mismatched geometry groups, cartilage recovery significantly lowers friction coefficient. This highlights the importance of cartilage recovery in terms of patient rehabilitation after tissue preserving procedures such as hemiarthroplasty.

8.6 Further Work

In this thesis, the aim was to develop an *in-vitro* tribological testing model that assessed the tribology of hip hemiarthroplasty in the medium term. In the future, methods such as the aseptic dissection technique and the vessel developed in this thesis could be used to extend the length of testing to longer term (such as several weeks). The results in Chapter 4 showed that there were signs of degradation which affected the friction coefficient of the cartilage. Therefore, to extend the length of testing, the chondrocyte viability and functionality must be maintained to ensure the degradation is purely resulting from the tribological study. This could be achieved with the use of culture media and growth factors, which are commonly used in tissue engineering studies.

It was shown in Chapter 7 that cartilage recovery is important for its tribological properties. With continuous testing, the friction coefficient, and hence frictional shear stress increased to a level high enough to cause major cartilage degeneration over the eight hours. By including recovery periods in future *in-vitro* testing, it allows the experiment to be more reflective of reality; as recovery periods often occur throughout the day (via sitting, reclining or shifting body weight from one foot to the other during long periods of standing). However, this would increase the length of the test, losing a major advantage of *in-vitro* tribological simulation testing. Therefore, further experiments could be performed to investigate if the tests can be accelerated by removing recovery periods. For this, the effect of altering the recovery periods' length and frequency must be examined on the tribological properties of cartilage.

It was discussed in Section 8.5, the effect of recovery on cartilage tribology is also important to consider in regards to patient rehabilitation. Therefore, a future study into the balance between patient exercise and cartilage recovery could also be performed in terms of lengths and frequency of the recovery periods. The mobilisation strategies after a surgical procedure following a femoral neck fracture (including hemiarthroplasty) proposed by the National Institute for Health and Clinical Excellence (CG124 Hip fracture: The Management of Hip Fracture in Adults) states that the patient should be mobilised on the day after surgery (unless medically or surgically contraindicated) and patient's mobilisation should be conducted at least once a day along with regular physiotherapy reviews. There are currently no guidelines on the method, duration and frequency of physiotherapy. By conducting further studies, the benefits of cartilage recovery can be better understood and hence, allow for a more effective mobilisation strategy.

As well as extending the length of testing, the entire motions of the hip including abduction/adduction and internal/external rotation could also be factored in. This will produce more clinical relevant results compared to the results in Chapter 7 that only applied flexion/extension due to the limitation of the friction simulator.

There are other tissue preserving procedures currently used clinically besides from hip hemiarthroplasty. Other procedures such as allograph implantation and mosaicplasty are used to treat localised degraded cartilage. Osteotomy of the femoral head or pelvic is a common procedure to correct misalignment or orientation of the hip joint. These procedures aim to preserve as much natural tissue as possible, including the articular cartilage. Therefore, the general concepts used in this thesis could be adopted to explore the cartilage tribology after these procedures in the medium term. The concepts in this thesis could also be used to examine tissue engineered cartilage in the medium term. This model could also act as a batch style bioreactor that provides the necessary mechanical stimuli during culture to produce a tissue with mechanical properties more comparable to that of native cartilage. However, there will be a compromise between mechanical stimuli and cartilage wear, which must be investigated.

8.7 Overall Conclusions

- In Chapter 3, it was found that porcine acetabulum was the most appropriate match to human and hence was used for the medium term model. However, there were significant differences in equilibrium elastic modulus and permeability between porcine and human cartilage.
- In Chapter 4, it was found that contamination significantly lowered friction coefficient. Therefore, this indicated that efforts were needed to be made to eliminate contaminants entering the *in-vitro* system during the medium term test. However, it was also found that even with the presence of proteinase inhibitors, the cartilage did suffer from time dependent degradation and hence, increased the friction coefficient.
- In Chapter 5, a friction simulator vessel was designed, manufactured and validated. The vessel was found to eliminate contaminates from entering the system during testing and the friction was unaffected.
- In Chapter 6, it was found that the mismatched geometry group showed a significantly larger contact stress compared to the matched geometry group. This was possibly due to the smaller contact area in the mismatched geometry

group, originating from the larger clearance. However, due to the presence of a growth plate in the centre of the porcine acetabulum, the shape of the contact region was not spherical. Instead, there were two distinct regions of contact, either side of the growth plate.

- In Chapter 7, it was found that after four days of tribological testing, the friction coefficient, frictional shear stress and bone exposure was significantly larger in the mismatched geometry group compared to the matched geometry group. It was also found the GAG concentration significantly decreased after four days of testing in the mismatched geometry group, but this was not significant for the matched geometry group. This result was also seen in the Alcian blue stained cartilage.
- Friction coefficient and frictional shear stress dramatically reduced after the unloaded periods. A correlation between frictional shear stress and bone exposure was found and hence, allowing the cartilage to recover could significantly reduce cartilage wear. This finding is important clinically in regards to patient rehabilitation. A future study into the balance between patient exercise and cartilage recovery could also be performed in terms of lengths and frequency of the recovery periods.
- Future *in-vitro* experiments that aim to investigate cartilage tribology over an extended period of time could discount the recovery periods with the aim to accelerate the test. However, further tests must be performed to study the effect of the length and frequency of the recovery periods and if the wear of cartilage after an accelerated test is similar to wear of cartilage after a longer test which include recovery periods.

Appendix 1: Publication List

Journal Papers

- S. D. Taylor, E. Tsiridis, E. Ingham, Z. Jin, J. Fisher and S. Williams. Comparison of human and animal femoral head chondral properties and geometries. Proceedings of the Institution of Mechanical Engineers, Part H: Journal of Engineering in Medicine. 2012, 226:55-62

- H. L. Fermor, S. W. D. McLure, S. D. Taylor, S. L. Russell, S. Williams, J. Fisher, E. Ingham. Biological, biochemical and biomechanical characterisation of articular cartilage from the porcine, bovine and ovine hip and knee. Journal of Biomedical Materials Research part B: Applied Biomaterials. SUBMITTED.

Conference Abstracts

- S. Taylor, J. Ingram, E. Ingham, J. Fisher and S. Williams. Frictional response of cartilage after prolonged walking and recovery – an *in-vitro* study. International Cartilage Repair Society, Montreal Canada. May 2012. Poster 71

- S. Taylor, E. Tsiridis, E. Ingham, Z. Jin, J. Fisher and S. Williams. Assessment of femoral heads from different species for use in an *in-vitro* simulation. British Orthopaedic Research Society, Cambridge. June 2011. Poster.

- S. Taylor, E. Tsiridis, E. Ingham, Z. Jin, J. Fisher and S. Williams. Comparison of Human and Animal Femoral Head Chondral Properties and Geometry. Orthopeadic Research Society. Long Beach CA, USA. May 2011. Poster.

- S. Taylor, E. Tsiridis, E. Ingham, Z. Jin, J. Fisher and S. Williams. Comparison of human and animal chondral properties. International Cartilage Repair Society, Sitges. September 2010. Poster.

Appendix 2: Engineering Drawings

Coring Fixture

This clamp was used to secure the human femoral head whilst removing an osteochondral plug. It was also used to secure the porcine pelvis whilst sawing off the acetabulae during aseptic dissection.

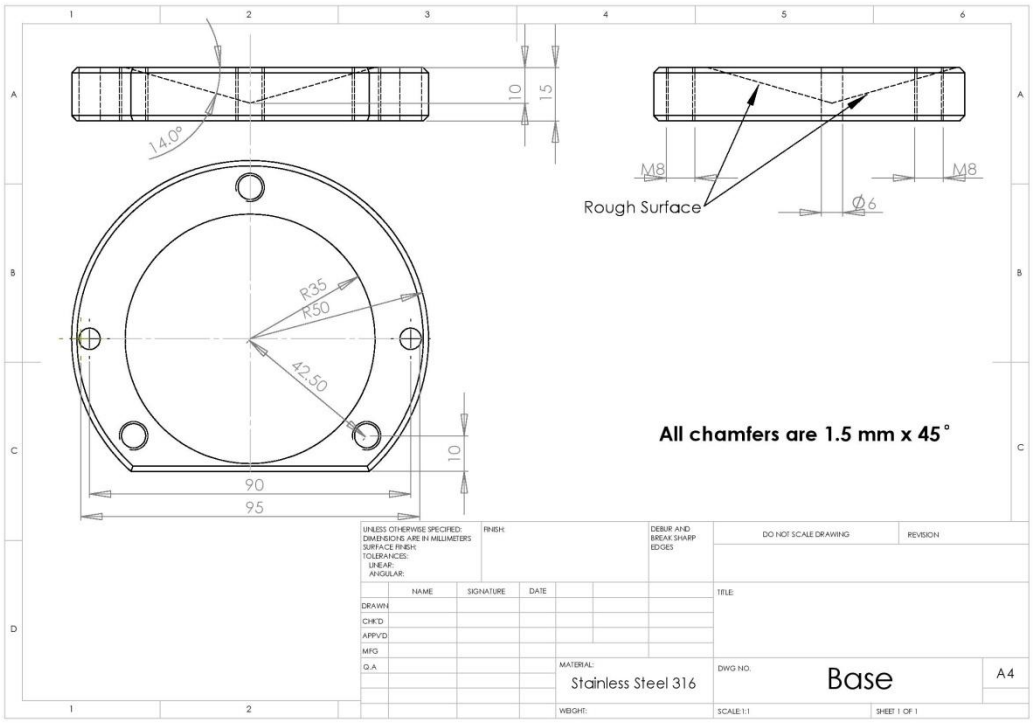

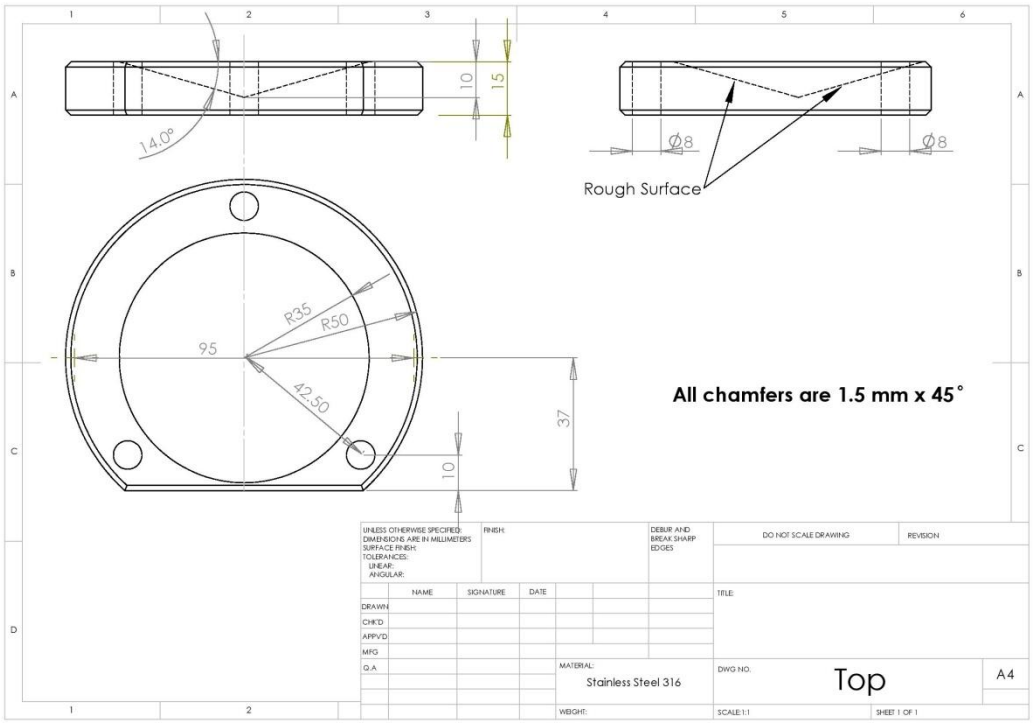

Cabinet Clamp

For health and safety reasons, human tissue had to be dissected in a class II cabinet. This clamp was used to secure the coring fixture (see previous) in the class II cabinet during coring. It was also used to secure porcine acetabulae in the class II cabinet during aseptic dissection.

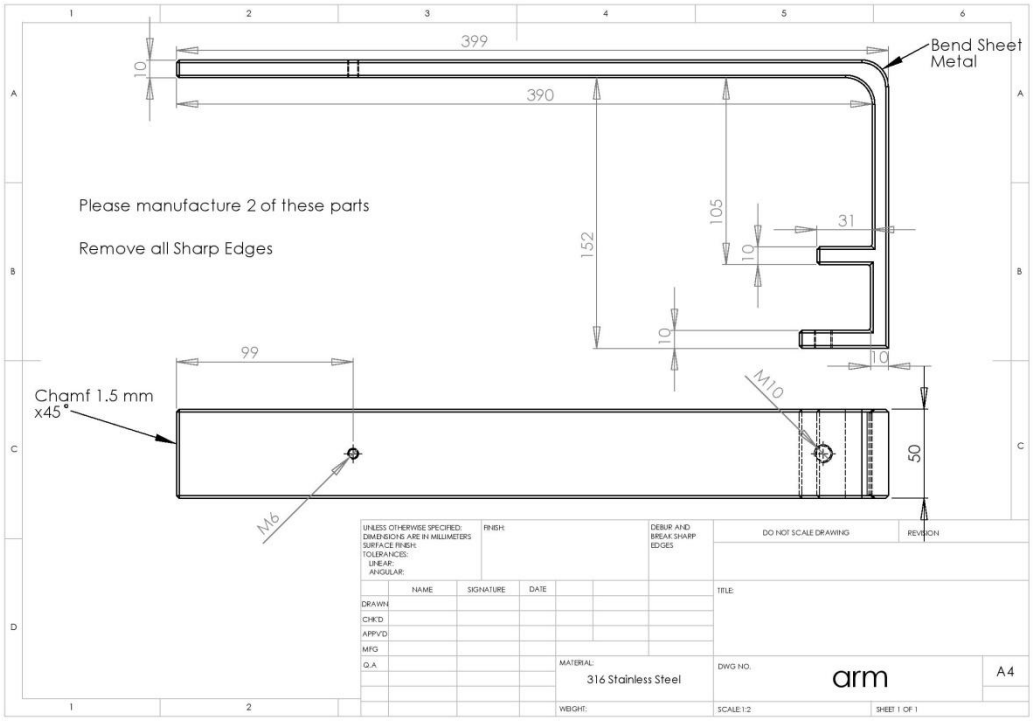

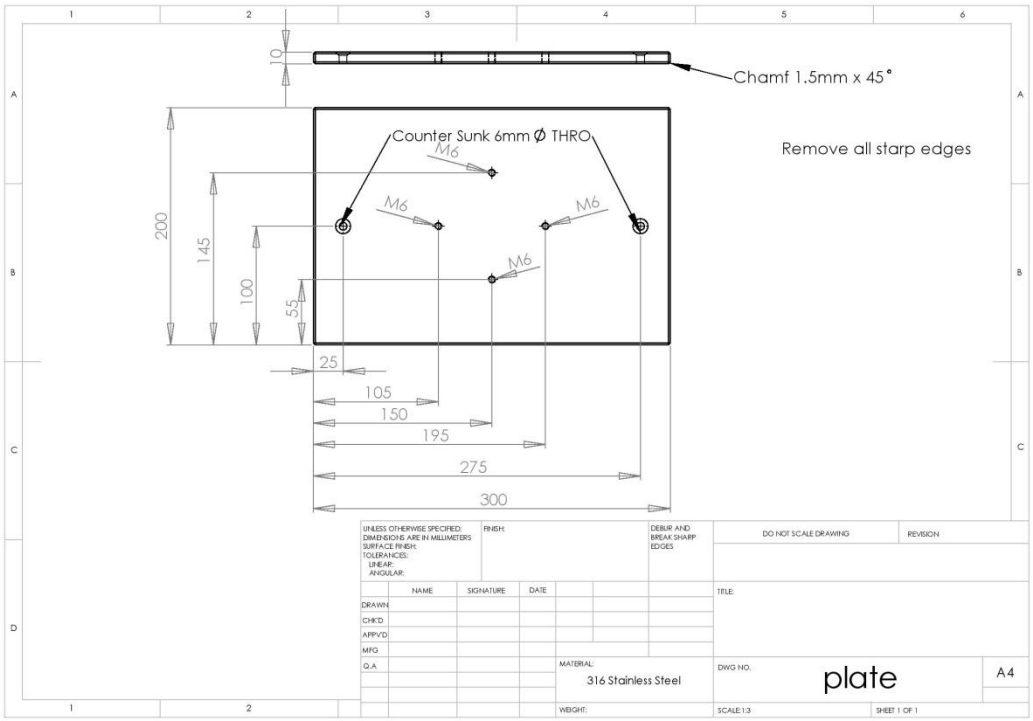

Friction Simulator Vessel

Developed in Chapter 5, this was used to tribologically test hip hemiarthroplasty in the medium term under sterile conditions.

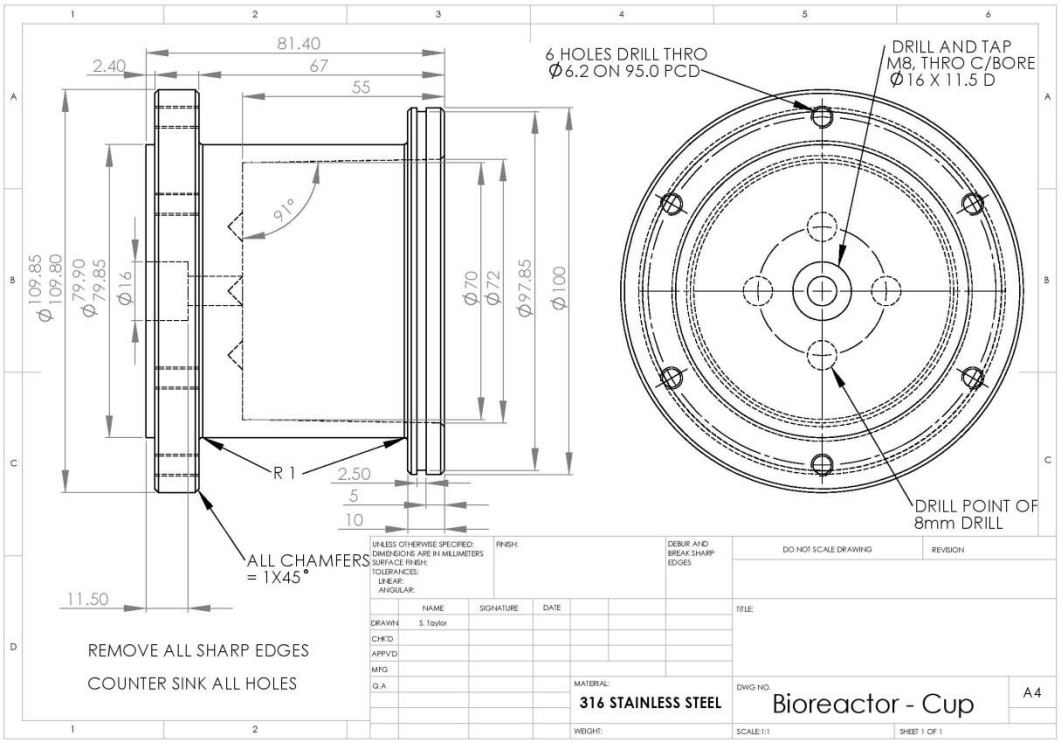

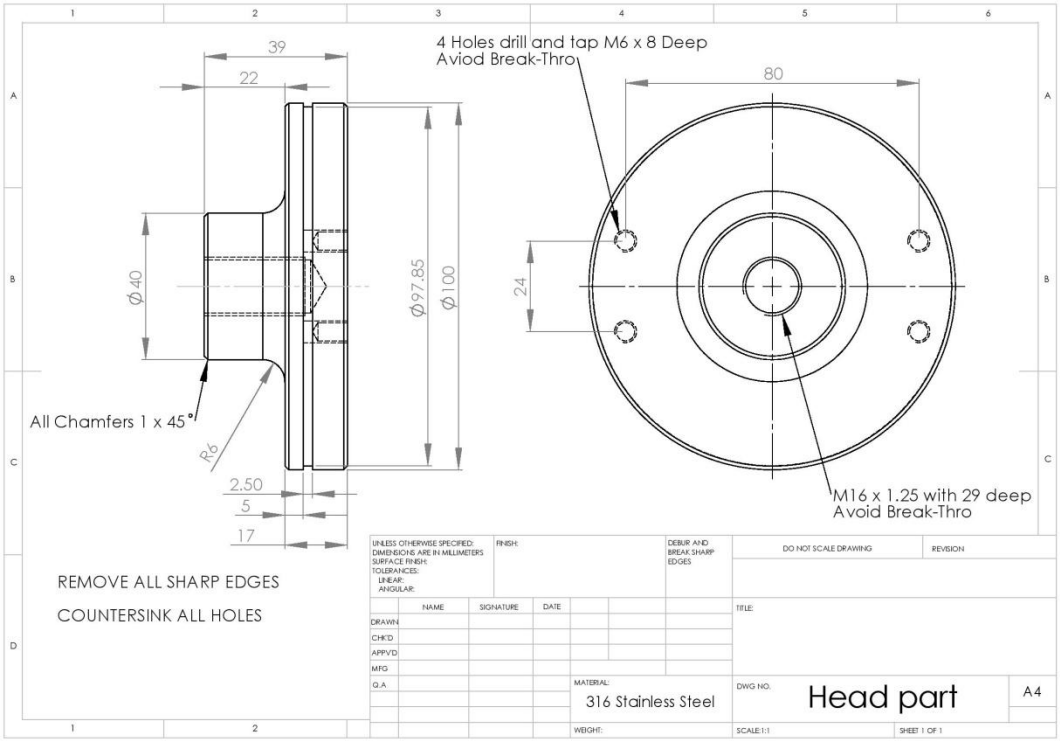

References

2011 07/06/11 Cited in: [http://www.hesonline.nhs.uk/Ease/servlet/ContentServer?siteID=1937&categoryID=214]

ARTHRITIS RESEARCH CAMPAIGN, 2005 (April 2005) September 2008 Cited in: [http://www.arc.org.uk/arthinfo/patpubs/6025/6025.asp]

NHS Institute for Innovation and Improvement 07/06/11 Cited in: [http://www.institute.nhs.uk/quality_and_value/high_volume_care/fractured_neck_of_femur_facts.html]

ABD LATIF, M. J. (2011) Characterisation and Modelling of Spinal Facet Joints. *School of Mechanical Engineering.* Leeds, University of Leeds.

ABRAHAMSEN, B., VAN STAA, T., ARIELY, R., OLSON, M. & COOPER, C. (2009) Excess mortality following hip fracture: a systematic epidemiological review. *Osteoporosis International,* 20**,** 1633-1650.

ADAMS, D. & SWANSON, S. A. (1985) Direct measurement of local pressures in the cadaveric human hip joint during simulated level walking. *Ann Rheum Dis,* 44**,** 658-66.

AKIZUKI, S., MOW, V. C., MULLER, F., PITA, J. C., HOWELL, D. S. & MANICOURT, D. H. (1986) Tensile properties of human knee joint cartilage: I. Influence of ionic conditions, weight bearing, and fibrillation on the tensile modulus. *J Orthop Res,* 4**,** 379-92.

AL-TUBAIKH, J. A. (2010) *Internal Medicine: An Illustrated Radiological Guide,* Heidelberg, Germany, Springer.

AN, Y. H. & MARTIN, K. L. (2003) *Handbook of histology methods for bone and cartilage,* Totowa, NJ, Humana Press.

ANDERSON, A. E., ELLIS, B. J., MAAS, S. A., PETERS, C. L. & WEISS, J. A. (2008) Validation of finite element predictions of cartilage contact pressure in the human hip joint. *J Biomech Eng,* 130**,** 051008.

ATESHIAN, G. A., SOLTZ, M. A., MAUCK, R. L., BASALO, I. M., HUNG, C. T. & LAI, W. M. (2003) The role of osmotic pressure and tension-compression nonlinearity in the frictional response of articular cartilage. *Transport in Porous Media,* 50**,** 5-33.

ATHANASIOU, K. A., AGARWAL, A. & DZIDA, F. J. (1994) Comparative-Study of the Intrinsic Mechanical-Properties of the Human Acetabular and Femoral-Head Cartilage. *J Orthop Res,* 12**,** 340-349.

ATHANASIOU, K. A., AGARWAL, A., MUFFOLETTO, A., DZIDA, F. J., CONSTANTINIDES, G. & CLEM, M. (1995) Biomechanical properties of hip cartilage in experimental animal models. *Clin Orthop Relat Res,* 316**,** 254-66.

ATHANASIOU, K. A., ROSENWASSER, M. P., BUCKWALTER, J. A., MALININ, T. I. & MOW, V. C. (1991) Interspecies Comparisons of Insitu Intrinsic Mechanical-Properties of Distal Femoral Cartilage. *J Orthop Res,* 9**,** 330-340.

ATLAS, R. M. & SNYDER, J. W. (1995) *Handbook of media for clinical microbiology,* Boca Raton ; London, CRC Press.

BANK, R. A., BAYLISS, M. T., LAFEBER, F. P., MAROUDAS, A. & TEKOPPELE, J. M. (1998) Ageing and zonal variation in post-translational modification of collagen in normal human articular cartilage. The age-related increase in non-enzymatic glycation affects biomechanical properties of cartilage. *Biochem J,* 330 (Pt 1)**,** 345-51.

BAY, B. K., HAMEL, A. J., OLSON, S. A. & SHARKEY, N. A. (1997) Statically equivalent load and support conditions produce different hip joint contact pressures and periacetabular strains. *J Biomech,* 30**,** 193-6.

BEDI, A., CHEN, N., ROBERTSON, W. & KELLY, B. T. (2008) The management of labral tears and femoroacetabular impingement of the hip in the young, active patient. *Arthroscopy,* 24**,** 1135-45.

BELL, C. J., INGHAM, E. & FISHER, J. (2006) Influence of hyaluronic acid on the time-dependent friction response of articular cartilage under different conditions. *Proc Inst Mech Eng [H],* 220**,** 23-31.

BENNETT, G. A. (1942) *Changes in the knee joint at various ages : with particular reference to the nature and development of degenerative joint disease,* New York, Commonwealth Fund.

BENTLEY, G., BIANT, L. C., CARRINGTON, R. W., AKMAL, M., GOLDBERG, A., WILLIAMS, A. M., SKINNER, J. A. & PRINGLE, J. (2003) A prospective, randomised comparison of autologous chondrocyte implantation versus mosaicplasty for osteochondral defects in the knee. *J Bone Joint Surg Br,* 85**,** 223-30.

BERGMANN, G., GRAICHEN, F. & ROHLMANN, A. (1993) Hip joint loading during walking and running, measured in two patients. *J Biomech,* 26**,** 969-90.

BERGMANN, G., GRAICHEN, F. & ROHLMANN, A. (1999) Hip joint forces in sheep. *J Biomech,* 32**,** 769-777.

BERGMANN, G., GRAICHEN, F. & ROHLMANN, A. (2004) Hip joint contact forces during stumbling. *Langenbecks Arch Surg,* 389**,** 53-9.

BERGMANN, G., SIRAKY, J., ROHLMANN, A. & KOELBEL, R. (1984) A Comparison of Hip-Joint Forces in Sheep, Dog and Man. *J Biomech,* 17**,** 907-21.

BERRY, D. J., HARMSEN, W. S., CABANELA, M. E. & MORREY, B. F. (2002) Twenty-five-year survivorship of two thousand consecutive primary Charnley total hip replacements: factors affecting survivorship of acetabular and femoral components. *J Bone Joint Surg Am,* 84-A**,** 171-7.

BHUSHAN, B. (2002) *Introduction to tribology,* New York ; [Chichester], Wiley.

BIAN, L., LIMA, E. G., ANGIONE, S. L., NG, K. W., WILLIAMS, D. Y., XU, D., STOKER, A. M., COOK, J. L., ATESHIAN, G. A. & HUNG, C. T. (2008) Mechanical and biochemical characterization of cartilage explants in serum-free culture. *J Biomech,* 41**,** 1153-9.

BLACK, J., LEVINE, B. & JACOBS, J. (2007) Biomaterials Overview. IN CALLAGHAN, J. J., ROSENBERG, A. G. & RUBASH, H. E. (Eds.) *The Adult Hip.* 2nd ed. Philadelphia, PA, USA, Lippincott Williams & Wilkins.

BRINCKMANN, P., FROBIN, W. & HIERHOLZER, E. (1981) Stress on the articular surface of the hip joint in healthy adults and persons with idiopathic osteoarthrosis of the hip joint. *J Biomech,* 14**,** 149-56.

BRITTBERG, M. & WINALSKI, C. S. (2003) Evaluation of cartilage injuries and repair. *J Bone Joint Surg Am,* 85A**,** 58-69.

BROCKETT, C., WILLIAMS, S., JIN, Z., ISAAC, G. & FISHER, J. (2007) Friction of total hip replacements with different bearings and loading conditions. *J Biomed Mater Res B Appl Biomater,* 81**,** 508-15.

BRUYERE, O. & REGINSTER, J. Y. (2007) Glucosamine and chondroitin sulfate as therapeutic agents for knee and hip osteoarthritis. *Drugs Aging,* 24**,** 573-80.

BUCKWALTER, J. A. & MOW, V. C. (1992) Cartilage repair in osteoarthritis. IN MOSKOWITZ, R., HOWELL, D. S., GOLDBERG, V. M. & MANKIN, H. J. (Eds.) *Osteoarthritis: Diagnosis and Management.* 2 ed. Philadelphia, Saunders.

BULLOUGH, P. G. & DICARLO, E. F. (1990) Subchondral avascular necrosis: a common cause of arthritis. *Ann Rheum Dis,* 49**,** 412-20.

CARROLL, C., STEVENSON, M., SCOPE, A., EVANS, P. & BUCKLEY, S. (2011) Hemiarthroplasty and total hip arthroplasty for treating primary intracapsular fracture of the hip: a systematic review and cost-effectiveness analysis. *Health Technol Assess,* 15**,** 1-74.

CATANI, F., HODGE, A., MANN, R. W., ENSINI, A. & GIANNINI, S. (1995) The role of muscular co-contraction of the hip during movement. *Chir Organi Mov,* 80**,** 227-36.

COLEMAN, S. H. (2007) Hip Mobility and Hip Arthroscopy: A Patient's Guide to Correcting Femoro-acetabular Impingement. Accessed in Cited in: [http://www.hss.edu/conditions_Hip-Mobility-Arthroscopy-Patient's-Guide-Femoro-Acetabular-Impingement.asp]

COOK, S. D., THOMAS, K. A. & KESTER, M. A. (1989) Wear Characteristics of the Canine Acetabulum against Different Femoral Prostheses. *J Bone Joint Surg Br,* 71**,** 189-197.

CUI, T. & XIONG, D. S. (2009) Biotribological Properties of Natural Swine Joint Cartilage. *Advanced Tribology: Proceedings of CIST2008***,** 81-83.

DALLDORF, P. G., BANAS, M. P., HICKS, D. G. & PELLEGRINI, V. D., JR. (1995) Rate of degeneration of human acetabular cartilage after hemiarthroplasty. *J Bone Joint Surg Am,* 77**,** 877-82.

DENNISON, E., MOHAMED, M. A. & COOPER, C. (2006) Epidemiology of osteoporosis. *Rheumatic Disease Clinics of North America,* 32**,** 617-29.

DOUGADOS, M., AYRAL, X., LISTRAT, V., GUEGUEN, A., BAHUAUD, J., BEAUFILS, P., BEGUIN, J., BONVARLET, J. P., BOYER, T., COUDANE, H., DELAUNAY, C., DORFMANN, H., DUBOS, J. P., FRANK, A., KEMPF, J. F., LOCKER, B., PRUDHON, J. L. & THIERY, J. (1993) The Sfa System for Assessing Articular-Cartilage Lesions at Arthroscopy of the Knee. *Arthritis and Rheumatism,* 36**,** S207-S207.

DOUGADOS, M., AYRAL, X., LISTRAT, V., GUEGUEN, A., BAHUAUD, J., BEAUFILS, P., BEGUIN, J. A., BONVARLET, J. P., BOYER, T., COUDANE, H., DELAUNAY, C., DORFMANN, H., DUBOS, J. P., FRANK, A., KEMPF, J. F., LOCKER, B., PRUDHON, J. L. & THIERY, J. (1994) The Sfa System for Assessing Articular-Cartilage Lesions at Arthroscopy of the Knee. *Arthroscopy,* 10**,** 69-77.

DOWSON, D., FISHER, J., JIN, Z. M., AUGER, D. D. & JOBBINS, B. (1991) Design considerations for cushion form bearings in artificial hip joints. *Proc Inst Mech Eng [H],* 205**,** 59-68.

DOWSON, D. & WRIGHT, V. (1981) *An introduction to the bio-mechanics of joints and joint replacement,* London, Mechanical Engineering Publications.

DUMONT, J., IONESCU, M., REINER, A., POOLE, A. R., TRAN-KHANH, N., HOEMANN, C. D., MCKEE, M. D. & BUSCHMANN, M. D. (1999) Mature full-thickness articular cartilage explants attached to bone are physiologically stable over long-term culture in serum-free media. *Connect Tissue Res,* 40**,** 259-72.

DUNHAM, J., CHAMBERS, M. G., JASANI, M. K., BITENSKY, L. & CHAYEN, J. (1990) Changes in the orientation of proteoglycans during the early development of natural murine osteoarthritis. *J Orthop Res,* 8**,** 101-4.

DYTHAM, C. (2002) *Choosing and using statistics : a biologist's guide,* Oxford, Blackwell Science.

EHRLICH, M. G., HOULE, P. A., VIGLIANI, G. & MANKIN, H. J. (1978) Correlation between articular cartilage collagenase activity and osteoarthritis. *Arthritis Rheum,* 21**,** 761-6.

EHRLICH, M. G., MANKIN, H. J., JONES, H., WRIGHT, R., CRISPEN, C. & VIGLIANI, G. (1977) Collagenase and collagenase inhibitors in osteoarthritic and normal cartilage. *J Clin Invest,* 59**,** 226-33.

FEIN, R. S. (1967) Are synovial joints squeeze film lubricated? *Proc. Instn Mech. Engrs.,* 181**,** 125-128.

FLANNERY, C. R., ZOLLNER, R., CORCORAN, C., JONES, A. R., ROOT, A., RIVERA-BERMUDEZ, M. A., BLANCHET, T., GLEGHORN, J. P., BONASSAR, L. J., BENDELE, A. M., MORRIS, E. A. & GLASSON, S. S. (2009) Prevention of Cartilage Degeneration in a Rat Model of Osteoarthritis by Intraarticular Treatment With Recombinant Lubricin. *Arthritis and Rheumatism,* 60**,** 840-847.

FORSTER, H. & FISHER, J. (1996) The influence of loading time and lubricant on the friction of articular cartilage. *Proc Inst Mech Eng [H],* 210**,** 109-19.

FORSTER, H. & FISHER, J. (1999) The influence of continuous sliding and subsequent surface wear on the friction of articular cartilage. *Proc Inst Mech Eng [H],* 213**,** 329-345.

FOY, J. R., WILLIAMS, P. F., POWELL, G. L., ISHIHARA, K., NAKABAYASHI, N. & LABERGE, M. (1999) Effect of phospholipidic boundary lubrication in rigid and compliant hemiarthroplasty models. *Proc Inst Mech Eng [H],* 213**,** 5-18.

FRAMPTON, J. E. & KEATING, G. M. (2007) Celecoxib: a review of its use in the management of arthritis and acute pain. *Drugs,* 67**,** 2433-72.

FREEMAN, M. A. (1975) The fatigue of cartilage in the pathogenesis of osteoarthrosis. *Acta Orthop Scand,* 46**,** 323-8.

FREEMONT, A. J. & HOYLAND, J. A. (2007) Morphology, mechanisms and pathology of musculoskeletal ageing. *J Pathol,* 211**,** 252-9.

GAHUNIA, H. K., BABYN, P., LEMAIRE, C., KESSLER, M. J. & PRITZKER, K. P. (1995) Osteoarthritis staging: comparison between magnetic resonance imaging, gross pathology and histopathology in the rhesus macaque. *Osteoarthritis Cartilage,* 3**,** 169-80.

GANZ, R., PARVIZI, J., BECK, M., LEUNIG, M., NOTZLI, H. & SIEBENROCK, K. A. (2003) Femoroacetabular impingement - A cause for osteoarthritis of the hip. *Clin Orthop Relat Res***,** 112-120.

GOSSEC, L. & DOUGADOS, M. (2006) Do intra-articular therapies work and who will benefit most? *Best Pract Res Clin Rheumatol,* 20**,** 131-44.

GRAINDORGE, S., FERRANDEZ, W., INGHAM, E., JIN, Z., TWIGG, P. & FISHER, J. (2006) The role of the surface amorphous layer of articular cartilage in joint lubrication. *Proc Inst Mech Eng [H],* 220**,** 597-607.

HAMILL, J. & KNUTZEN, K. M. (1995) *Biomechanical basis of human movement.,* Malvern, Pa; London, Williams & Wilkins.

HARRIS, M. D., ANDERSON, A. E., HENAK, C. R., ELLIS, B. J., PETERS, C. L. & WEISS, J. A. (2012) Finite element prediction of cartilage contact stresses in normal human hips. *J Orthop Res,* [In Press].

HARRIS, W. H., RUSHFELDT, P. D., CARLSON, D. E., SCHOLLER, J. M. & MANN, R. W. (1975) Pressure distribution in the hip and selection of hemiarthroplasty. *Proc. Hip Soc.,* 3**,** 93-102.

HASEGAWA, M., SUDO, A. & UCHIDA, A. (2004) Disassembly of bipolar cup with self-centering system: a report of seven cases. *Clin Orthop Relat Res,* 425**,** 163-7.

HIGAKI, H., MURAKAMI, T., NAKANISHI, Y., MIURA, H., MAWATARI, T. & IWAMOTO, Y. (1998) The lubricating ability of biomembrane models with dipalmitoyl phosphatidylcholine and gamma-globulin. *Proc Inst Mech Eng [H],* 212**,** 337-346.

HILLS, B. A. & BUTLER, B. D. (1984) Surfactants identified in synovial fluid and their ability to act as boundary lubricants. *Ann Rheum Dis,* 43**,** 641-8.

HODGE, W. A., CARLSON, K. L., FIJAN, R. S., BURGESS, R. G., RILEY, P. O., HARRIS, W. H. & MANN, R. W. (1989) Contact Pressures from an Instrumented Hip Endoprosthesis. *J Bone Joint Surg Am,* 71A**,** 1378-1386.

HOLMES, M. H., LAI, W. M. & MOW, V. C. (1985) Singular Perturbation Analysis of the Nonlinear, Flow-Dependent Compressive Stress-Relaxation Behavior of Articular-Cartilage. *Journal of Biomechanical Engineering-Transactions of the Asme,* 107**,** 206-218.

IPAVEC, M., BRAND, R. A., PEDERSEN, D. R., MAVCIC, B., KRALJ-IGLIC, V. & IGLIC, A. (1999) Mathematical modelling of stress in the hip during gait. *J Biomech,* 32**,** 1229-35.

ISOTALO, K., RANTANEN, J., AARIMAA, V. & GULLICHSEN, E. (2002) The long-term results of Lubinus interplanta hemiarthroplasty in 228 acute femoral neck fractures. A retrospective six-year follow-up. *Scand J Surg,* 91**,** 357-60.

JAY, G. D. (1992) Characterization of a Bovine Synovial-Fluid Lubricating Factor .1. Chemical, Surface-Activity and Lubricating Properties. *Connective Tissue Research,* 28**,** 71-88.

JAY, G. D. & HONG, B. S. (1992) Characterization of a Bovine Synovial-Fluid Lubricating Factor .2. Comparison with Purified Ocular and Salivary Mucin. *Connective Tissue Research,* 28**,** 89-98.

JEFFERY, J. A. & ONG, T. J. (2000) Femoral head measurement in hemiarthroplasty: assessment of interobserver error using 3 measuring systems. *Injury-International Journal of the Care of the Injured,* 31**,** 135-138.

JOHNELL, O. & KANIS, J. A. (2006) An estimate of the worldwide prevalence and disability associated with osteoporotic fractures. *Osteoporosis International,* 17**,** 1726-1733.

JOHNSTON, C. E., RIPLEY, L. P., BRAY, C. B., SHAFFER, L. W., STRONG, T. E., HENNING, G. D. & PRUNER, R. A. (1982) Primary endoprosthetic replacement for acute femoral neck fractures. A review of 150 cases. *Clin Orthop Relat Res,* 167**,** 123-30.

JOHNSTON, R. C. & SMIDT, G. L. (1969) Measurement of hip-joint motion during walking. Evaluation of an electrogoniometric method. *J Bone Joint Surg Am,* 51A**,** 1083.

JOHNSTON, R. C. & SMIDT, G. L. (1970) Hip motion measurements for selected activities of daily living. *Clin Orthop Relat Res,* 72**,** 205-15.

JONES, A. S. (1936) Joint Lubrication. *The Lancet,* 227**,** 987-1046.

JUBB, R. W., PIVA, S., BEINAT, L., DACRE, J. & GISHEN, P. (2003) A one-year, randomised, placebo (saline) controlled clinical trial of 500-730 kDa sodium hyaluronate (Hyalgan) on the radiological change in osteoarthritis of the knee. *Int J Clin Pract,* 57**,** 467-74.

JUNQUEIRA, L. C. U. A. & CARNEIRO, J. (2005) *Basic histology : text & atlas,* New York ; London, McGraw-Hill Medical.

JURVELIN, J., KIVIRANTA, I., SAAMANEN, A. M., TAMMI, M. & HELMINEN, H. J. (1990) Indentation Stiffness of Young Canine Knee Articular-Cartilage - Influence of Strenuous Joint Loading. *J Biomech,* 23**,** 1239-1246.

JURVELIN, J. S., BUSCHMANN, M. D. & HUNZIKER, E. B. (1997) Optical and mechanical determination of Poisson's ratio of adult bovine humeral articular cartilage. *J Biomech,* 30**,** 235-241.

KANTOMAA, T. & HALL, B. K. (1988) Organ culture providing an articulating function for the temporomandibular joint. *J Anat,* 161**,** 195-201.

KAPLAN, E. (1958) Nonparametric estimation from incomplete observations. IN KOTZ, S. & JOHNSON, N. L. (Eds.) *Breakthroughs in Statistics.* New York, Springer.

KARATAN, E. & WATNICK, P. (2009) Signals, Regulatory Networks, and Materials That Build and Break Bacterial Biofilms. *Microbiology and Molecular Biology Reviews,* 73**,** 310-47.

KARLSSON, J., SJOGREN, L. S. & LOHMANDER, L. S. (2002) Comparison of two hyaluronan drugs and placebo in patients with knee osteoarthritis. A controlled, randomized, double-blind, parallel-design multicentre study. *Rheumatology (Oxford),* 41**,** 1240-8.

KATTA, J. (2007) Self-assembling Peptide Networks for Treatment of Cartilage Degenerative Diseases. *School of Mechanical Engineering.* Leeds, University of Leeds.

KATTA, J., JIN, Z., INGHAM, E. & FISHER, J. (2008) Friction and wear of native and GAG deficient articular cartilage. *World Biomaterials Congress.* Amsterdam, The Netherlands.

KATTA, J., PAWASKAR, S. S., JIN, Z. M., INGHAM, E. & FISHER, J. (2007) Effect of load variation on the friction properties of articular cartilage. *Proc Inst Mech Eng [H],* 221**,** 175-181.

KEENAN, K. E., KOURTIS, L. C., BESIER, T. F., LINDSEY, D. P., GOLD, G. E., DELP, S. L. & BEAUPRE, G. S. (2009) New resource for the computation of cartilage biphasic material properties with the interpolant response surface

method. *Computer Methods in Biomechanics and Biomedical Engineering,* 12**,** 415-422.

KEMPSON, G. E. (1991) Age-Related-Changes in the Tensile Properties of Human Articular-Cartilage - a Comparative-Study between the Femoral-Head of the Hip-Joint and the Talus of the Ankle Joint. *Biochimica Et Biophysica Acta,* 1075**,** 223-230.

KEMPSON, G. E., FREEMAN, M. A. R. & SWANSON, S. A. V. (1971) Determination of a Creep Modulus for Articular Cartilage from Indentation Tests on Human Femoral Head. *J Biomech,* 4**,** 239-50.

KERIN, A. J., COLEMAN, A., WISNOM, M. R. & ADAMS, M. A. (2003) Propagation of surface fissures in articular cartilage in response to cyclic loading in vitro. *Clinical Biomechanics,* 18**,** 960-968.

KING, R. G. (1966) A rheological measurement of three synovial fluids. *Rheological Acta,* 5**,** 41.

KLASHMAN, D., IKE, R., MORELAND, L., SKOVRON, M. L. & KALUNIAN, K. (1995) Validation of an Osteoarthritis Data Report Form for Knee Arthroscopy. *Arthritis and Rheumatism,* 38**,** 154-154.

KONRATH, G. A., HAMEL, A. J., GUERIN, J., OLSON, S. A., BAY, B. & SHARKEY, N. A. (1999) Biomechanical evaluation of impaction fractures of the femoral head. *J Orthop Trauma,* 13**,** 407-13.

KOOPMAN, W. J. & MORELAND, L. W. (2005) *Arthritis and allied conditions : a textbook of rheumatology,* Philadelphia, Pa. ; London, Lippincott Williams & Wilkins.

KOSASHVILI, Y., BACKSTEIN, D., SAFIR, O., RAN, Y., LOEBENBERG, M. I. & BAR ZIV, Y. (2008) Hemiarthroplasty of the hip for fracture - What is the appropriate sized femoral head.? *Injury-International Journal of the Care of the Injured,* 39**,** 232-237.

KREBS, D. E., ROBBINS, C. E., LAVINE, L. & MANN, R. W. (1998) Hip biomechanics during gait. *J Orthop Sports Phys Ther,* 28**,** 51-9.

KRISHNAN, R., KOPACZ, M. & ATESHIAN, G. A. (2004) Experimental verification of the role of interstitial fluid pressurization in cartilage lubrication. *J Orthop Res,* 22**,** 565-70.

KUSTER, M. S. (2002) Exercise recommendations after total joint replacement: a review of the current literature and proposal of scientifically based guidelines. *Sports Med,* 32**,** 433-45.

LABERGE, M., BOBYN, J. D., DROUIN, G. & RIVARD, C. H. (1992) Evaluation of Metallic Personalized Hemiarthroplasty - a Canine Patellofemoral Model. *Journal of Biomedical Materials Research,* 26**,** 239-254.

LAI, W. M., HOU, J. S. & MOW, V. C. (1989a) Applicaton of triphasic theory to the study of transient behaviour of cartilage. *Adv. Bioeng. Trans,* 15**,** 101-102.

LAI, W. M., HOU, J. S. & MOW, V. C. (1989b) Triphasic theory for articular cartilage swelling. *Proc. Biomech. Symp. Trans,* 98**,** 33-36.

LAI, W. M. & MOW, V. C. (1980) Drag-Induced Compression of Articular-Cartilage during a Permeation Experiment. *Biorheology,* 17**,** 111-123.

LAI, W. M., MOW, V. C. & ROTH, V. (1981) Effects of Non-Linear Strain-Dependent Permeability and Rate of Compression on the Stress Behavior of Articular-Cartilage. *Journal of Biomechanical Engineering-Transactions of the Asme,* 103**,** 61-66.

LEE, C., GRAD, S., WIMMER, M. & ALINI, M. (2006) The Influence of Mechanical Stimuli on Articular Cartilage Tissue Engineering. IN ASHAMMAKHI, N. & REIS, R. L. (Eds.) *Topics in Tissue Engineering.* Davos Platz, Switzerland, Expertissues.

LEE, H. H., LO, Y. C., LIN, L. C. & WU, S. S. (2008) Disassembly and dislocation of a bipolar hip prosthesis. *J Formos Med Assoc,* 107**,** 84-8.

LEOPOLD, S. S., REDD, B. B., WARME, W. J., WEHRLE, P. A., PETTIS, P. D. & SHOTT, S. (2003) Corticosteroid compared with hyaluronic acid injections for the treatment of osteoarthritis of the knee. A prospective, randomized trial. *J Bone Joint Surg Am,* 85-A**,** 1197-203.

LEUNIG, M. & GANZ, R. (2011) Evolution of technique and indications for the Bernese periacetabular osteotomy. *Bull NYU Hosp Jt Dis,* 69 Suppl 1**,** S42-6.

LEVINE, B. R., MEERE, P. A., DI CESARE, P. E. & ZUCHERMAN, J. D. (2007) Hip Fractures Treated by Arthroplasty. IN CALLAGHAN, J. J., ROSENBERG, A. G. & RUBASH, H. E. (Eds.) *The Adult Hip.* 2nd ed. Philadelphia, Lippincott Williams & Wilkins.

LEWIS, P. R. & MCCUTCHEN, C. W. (1959) Experimental evidence for weeping lubrication in mammalian joints. *Nature,* 184**,** 1285.

LIPSHITZ, H., ETHEREDGE, R., 3RD & GLIMCHER, M. J. (1975) In vitro wear of articular cartilage. *J Bone Joint Surg Am,* 57**,** 527-34.

LIPSHITZ, H. & GLIMCHER, M. J. (1979) In Vitro Studies of the Wear of Articular Cartilage II. *Wear,* 52**,** 297-339.

LIZHANG, J. (2010) Tribology of Hemiarthroplasty. *School of Mechanical Engineering.* Leeds, University of Leeds.

LO, I. K. Y., THORTON, G., MINIACI, A., FRANK, C. B., RATTNER, J. B. & BRAY, R. C. (2002) Structure and Function of Diarthroidal Joints. IN MCGINTY, J. B., BURKHART, S. S., JACKSON, R. W., JOHNSON, D. H. & RICHMOND, J. C. (Eds.) *Operative Arthroscopy* 3rd ed., Lippincott Williams and Wilkins.

LU, X. L., SUN, D. D. N., GUO, X. E., CHEN, F. H., LAI, W. M. & MOW, V. C. (2004) Indentation determined mechanoelectrochemical properties and fixed charge density of articular cartilage. *Annals of Biomedical Engineering,* 32**,** 370-379.

MACIROWSKI, T., TEPIC, S. & MANN, R. W. (1994) Cartilage stresses in the human hip joint. *J Biomech Eng,* 116**,** 10-8.

MALCOM, L. L. (1976) An experimental investigation of the frictional and deformational responses of articular cartilage interfaces to static and dynamic loading. San Diego, University of California.

MALININ, T. & OUELLETTE, E. A. (2000) Articular cartilage nutrition is mediated by subchondral bone: a long-term autograft study in baboons. *Osteoarthritis Cartilage,* 8**,** 483-491.

MANKIN, H. J., DORFMAN, H., LIPPIELLO, L. & ZARINS, A. (1971) Biochemical and metabolic abnormalities in articular cartilage from osteo-arthritic human hips. II. Correlation of morphology with biochemical and metabolic data. *J Bone Joint Surg Am,* 53**,** 523-37.

MANKIN, H. J. & THRASHER, A. Z. (1975) Water content and binding in normal and osteoarthritic human cartilage. *J Bone Joint Surg Am,* 57**,** 76-80.

MARTEL-PELLETIER, J., BOILEAU, C., PELLETIER, J. P. & ROUGHLEY, P. J. (2008) Cartilage in normal and osteoarthritis conditions. *Best Pract Res Clin Rheumatol,* 22**,** 351-84.

MARTIN, J. A. & BUCKWALTER, J. A. (2002) Aging, articular cartilage chondrocyte senescence and osteoarthritis. *Biogerontology,* 3**,** 257-64.

MATS, B., A. PAOLO, G. RALPH, H. LASZLO, J.H. HANS, P.J. ROLAND, L. DAVID, L. STEFAN, R.M. BERT, P. LARS & HANS-ULRICH, S. (2000) ICRS Cartilage Injury Evaluation Package.

MATTHEWS, J. N., ALTMAN, D. G., CAMPBELL, M. J. & ROYSTON, P. (1990) Analysis of serial measurements in medical research. *BMJ,* 300**,** 230-5.

MCCANN, L. (2009) Tribological Investigation of Articular Cartilage Substitution in the Medial Compartmental Knee. *School of Mechanical Engineering.* Leeds, University of Leeds.

MCCANN, L., INGHAM, E., JIN, Z. & FISHER, J. (2009a) Influence of the meniscus on friction and degradation of cartilage in the natural knee joint. *Osteoarthritis Cartilage,* 17**,** 995-1000.

MCCANN, L., INGHAM, E., JIN, Z. & FISHER, J. (2009b) An investigation of the effect of conformity of knee hemiarthroplasty designs on contact stress, friction and degeneration of articular cartilage: a tribological study. *J Biomech,* 42**,** 1326-31.

MCDONNELL, G. & RUSSELL, A. D. (1999) Antiseptics and disinfectants: activity, action, and resistance. *Clin Microbiol Rev,* 12**,** 147-79.

MCGILL, K. C., BUSH-JOSEPH, C. A. & NHO, S. J. (2010) Hip Microfracture: Indications, Technique, and Outcomes. *Cartilage,* 1**,** 127-136.

MELTON, L. J. (2003) Epidemiology worldwide. *Endocrinology and Metabolism Clinics of North America,* 32**,** 1-13.

MICHAELI, D. A., MURPHY, S. B. & HIPP, J. A. (1997) Comparison of predicted and measured contact pressures in normal and dysplastic hips. *Med Eng Phys,* 19**,** 180-6.

MONT, M. A. & HUNGERFORD, D. S. (1995) Non-traumatic avascular necrosis of the femoral head. *J Bone Joint Surg Am,* 77**,** 459-74.

MOORE, K. & AGUR, A. (2002) *Essential clinical anatomy,* Philadelphia, Lippincott Williams & Wilkins.

MORITA, Y., TOMITA, N., AOKI, H., SONOBE, M., WAKITANI, S., TAMADA, Y., SUGURO, T. & IKEUCHI, K. (2006) Frictional properties of regenerated cartilage in vitro. *J Biomech,* 39**,** 103-109.

MOW, V. C. & ATESHIAN, G. A. (1997) Lubrication and Wear of Diarthrodial Joints. IN MOW, V. C. & HAYES, W. C. (Eds.) *Basic Orthopaedic Biomechanics.* 2nd ed. Philadelphia, Lippincott-Raven Publishers.

MOW, V. C., GIBBS, M. C., LAI, W. M., ZHU, W. B. & ATHANASIOU, K. A. (1989) Biphasic indentation of articular cartilage--II. A numerical algorithm and an experimental study. *J Biomech,* 22**,** 853-61.

MOW, V. C., GU, W. Y. & CHEN, F. H. (2005) Structure and Function of Articular Cartilage and Meniscus. IN MOW, V. C. & HUISKES, R. (Eds.) *Basic Orthopaedic Biomechanics and Mechano-Biology*. 3rd ed. Philadelphia, Lippincott Williams and Wilkins.

MOW, V. C. & HAYES, W. C. (1997) *Basic orthopaedic biomechanics*, Philadelphia, Lippincott-Raven.

MOW, V. C., HOLMES, M. H. & LAI, W. M. (1984) Fluid Transport and Mechanical-Properties of Articular-Cartilage - a Review. *J Biomech*, 17**,** 377-394.

MOW, V. C. & HUISKES, R. (2005) *Basic orthopaedic biomechanics & mechano-biology*, Philadelphia, Pa. ; London, Lippincott Williams & Wilkins.

MOW, V. C. & HUNG, C. T. (2001) Biomechanics of Articular Cartilage. IN NORDIN, M. & FRANKEL, V. H. (Eds.) *Basic Biomechanics of the Musculoskeletal System* 3rd ed. Philadelphia, Lippincott Williams & Wilkins.

MOW, V. C., KUEI, S. C., LAI, W. M. & ARMSTRONG, C. G. (1980) Biphasic creep and stress relaxation of articular cartilage in compression? Theory and experiments. *J Biomech Eng*, 102**,** 73-84.

MOW, V. C. & LAI, W. M. (1980) Recent Developments in Synovial Joint Biomechanics. *SI A M Rev*, 22**,** 275-317.

MOW, V. C. & RATCLIFFE, A. (1997) Structure and Function of Articular Cartilage and Meniscus. IN MOW, V. C. & HAYES, W. C. (Eds.) *Basic Orthopaedic Biomechanics.* 2 ed. Philadelphia, PA, Lippincott Williams & Wilkins.

MOW, V. C., RATCLIFFE, A. & POOLE, A. R. (1992) Cartilage and Diarthrodial Joints as Paradigms for Hierarchical Materials and Structures. *Biomaterials*, 13**,** 67-97.

MULLER, L. P., DEGREIF, J., RUDIG, L., MEHLER, D., HELY, H. & ROMMENS, P. M. (2004) Friction of ceramic and metal hip hemi-endoprostheses against cadaveric acetabula. *Arch Orthop Trauma Surg*, 124**,** 681-687.

MURRAY, M. P. (1967) Gait as a total pattern of movement. *Am J Phy Med*, 46**,** 290.

NAKA, M. H., MORITA, Y. & IKEUCHI, K. (2005) Influence of proteoglycan contents and of tissue hydration on the frictional characteristics of articular cartilage. *Proc Inst Mech Eng [H]*, 219**,** 175-182.

NORDIN, M. & FRANKEL, V. H. (2001) *Basic Biomechanics of the Musculoskeletal System*, Lippincott Williams & Wilkins.

NORRISH, A. R., RAO, J. & PARKER, M. J. (2006) Prosthesis survivorship and clinical outcome of the Austin Moore hemiarthroplasty: An 8-year mean follow-up of a consecutive series of 500 patients. *Injury,* 37**,** 734-9.

NORTHWOOD, E., FISHER, J. & KOWALSKI, R. (2007) Investigation of the friction and surface degradation of innovative chondroplasty materials against articular cartilage. *Proc Inst Mech Eng [H],* 221**,** 263-279.

ORTHOPAEDICS (2007) Developmental dysplasia of the hip. in Orthopaedics. Accessed in 19/03/2007. Cited in: [http://www.lpch.org/DiseaseHealthInfo/HealthLibrary/orthopaedics/ddh.html,]

ORTHOPOD (2002) Hemiarthroplasty of the Hip. Accessed in Cited in: [http://www.eorthopod.com/public/patient_education/6500/hemiarthroplasty_of_the_hip.html]

OZKAYA, N. & NORDIN, M. (1998) *Fundamentals of biomechanics : equilibrium, motion, and deformation,* New York, Springer.

OZTURK, H. E., STOFFEL, K., JONES, C. F. & STACHOWIAK, G. W. (2004) The effect of surface-active phospholipids on the lubrication of osteoarthritic sheep knee joints. *Friction Tribal Lett* 16**,** 283-9.

PARK, S., COSTA, K. D. & ATESHIAN, G. A. (2004) Microscale frictional response of bovine articular cartilage from atomic force microscopy. *J Biomech,* 37**,** 1679-1687.

PARKKINEN, J. J., LAMMI, M. J., HELMINEN, H. J. & TAMMI, M. (1992) Local stimulation of proteoglycan synthesis in articular cartilage explants by dynamic compression in vitro. *J Orthop Res,* 10**,** 610-20.

PAUL, J. P. (1967) Forces transmitted by joints in the human body. *Proc Inst Mech Eng [H],* 181**,** 8-15.

PAVELKA, D., GATTEROVA, J. & OLEJAROVA, M. (2002) Glucosamin sulfate use and delay of progression of knee osteoarthritis: a 3-year, randomized, placebo-controlled, double-blind study. *Arch Intern Med,* 162**,** 2113–2123.

PAWASKAR, S. S. (2010) Joint Contact Modelling of Articular Cartilage in Synovial Joints. *Institute of Medical and Biological Engineering, School of Mechanical Engineering.* Leeds, UK, University of Leeds.

PAWASKAR, S. S., GROSLAND, N. M., INGHAM, E., FISHER, J. & JIN, Z. (2011a) Hemiarthroplasty of Hip Joint: An Experimental Validation using Porcine Acetabulum *J Biomech,* 44**,** 1536-1542.

PAWASKAR, S. S., INGHAM, E., FISHER, J. & JIN, Z. (2011b) Fluid load support and contact mechanics of hemiarthroplasty in the natural hip joint. *Med Eng Phys,* 33**,** 96-105.

PELTIER, F. L. (2007) A History of Hip Surgery. IN CALLAGHAN, J. J., ROSENBERG, A. G. & RUBASH, H. E. (Eds.) *The Adult Hip.* 2 ed. Philadelphia, Lippincott Williams & Wilkins.

PETERFY, C. G. & GENANT, H. K. (1996) Emerging applications of magnetic resonance imaging in the evaluation of articular cartilage. *Radiol Clin North Am,* 34**,** 195-213, ix.

PETERSON, L., MINAS, T., BRITTBERG, M., NILSSON, A., SJOGREN-JANSSON, E. & LINDAHL, A. (2000) Two- to 9-year outcome after autologous chondrocyte transplantation of the knee. *Clin Orthop Relat Res,* 374**,** 212-34.

PICKARD, J., FISHER, J., INGHAM, E., EGAN, J. & HALLETT, J. (2000) Investigation into the tribological condition of acetabular tissue after bipolar joint replacement hip surgery. *Proc Inst Mech Eng [H],* 214**,** 361-370.

PICKARD, J., INGHAM, E., EGAN, J. & FISHER, J. (1998) Investigation into the effect of proteoglycan molecules on the tribological properties of cartilage joint tissues. *Proc Inst Mech Eng [H],* 212**,** 177-182.

PLAINFOSSE, M., HATTON, P. V., CRAWFORD, A., JIN, Z. M. & FISHER, J. (2007) Influence of the extracellular matrix on the frictional properties of tissue-engineered cartilage. *Biochemical Society Transactions,* 35**,** 677-679.

POOLE, C. A., FLINT, M. H. & BEAUMONT, B. W. (1987) Chondrons in Cartilage - Ultrastructural Analysis of the Pericellular Microenvironment in Adult Human Articular Cartilages. *J Orthop Res,* 5**,** 509-522.

QIAN, S. H. & GE, S. R. (2009) Friction behavior of coupling motion for natural articular cartilage by reciprocating rotation. *Chinese Science Bulletin,* 54**,** 576-583.

QUINN, G. & KEOUGH, M. (2002) *Experimental design and data analysis for biologists,* Cambridge, Cambridge University Press.

QUINN, P. J. (2002) *Veterinary microbiology and microbial diseases,* Oxford, Blackwell Science.

RADIN, E. L., SWANN, D. A. & WEISSER, P. A. (1970) Separation of a hyaluronate-free lubricating fraction from synovial fluid. *Nature,* 228**,** 377-8.

REGINSTER, J. Y., BRUYERE, O., FRAIKIN, G. & HENROTIN, Y. (2005) Current concepts in the therapeutic management of osteoarthritis with glucosamine. *Bull Hosp Jt Dis,* 63**,** 31-6.

REGINSTER, J. Y., BRUYERE, O. & NEUPREZ, A. (2007) Current role of glucosamine in the treatment of osteoarthritis. *Rheumatology (Oxford),* 46**,** 731-5.

RHEE, D. K., MARCELINO, J., BAKER, M. A., GONG, Y. Q., SMITS, P., LEFEBVRE, V., JAY, G. D., STEWART, M., WANG, H. W., WARMAN, M. L. & CARPTEN, J. D. (2005) The secreted glycoprotein lubricin protects cartilage surfaces and inhibits synovial cell overgrowth. *Journal of Clinical Investigation,* 115**,** 622-631.

ROEMHILDT, M. L., COUGHLIN, K. M., PEURA, G. D., FLEMING, B. C. & BEYNNON, B. D. (2006) Material properties of articular cartilage in the rabbit tibial plateau. *J Biomech,* 39**,** 2331-7.

RUSHFELDT, P. D., MANN, R. W. & HARRIS, W. H. (1981) Improved techniques for measuring in vitro the geometry and pressure distribution in the human acetabulum. II Instrumented endoprosthesis measurement of articular surface pressure distribution. *J Biomech,* 14**,** 315-23.

RYDELL, N. (1965) Forces in the hip-joint: Part (ii) intravital measurements. IN KENEDI, R. M. (Ed.) *Proceedings of a Symposium on Biomechanics and Related Bio-Engineering Topics.* Glasgow, Symposium Publications Division, Pergamon Press, Oxford.

SAMOTO, N., TOMARI, S., AKIYAMA, T. & TOKUHISA, T. (2008) Acetabular diameter measurement determines proper prosthetic head size in hemiarthroplasty for femoral head osteonecrosis. *J Arthroplasty,* 23**,** 263-5.

SANDELL, L. J. & AIGNER, T. (2001) Articular cartilage and changes in arthritis - An introduction: Cell biology of osteoarthritis. *Arthritis Research,* 3**,** 107-113.

SAUDEK, D. M. & KAY, J. (2003) Advanced glycation endproducts and osteoarthritis. *Curr Rheumatol Rep,* 5**,** 33-40.

SCANZELLO, C. R., MOSKOWITZ, N. K. & GIBOFSKY, A. (2008) The post-NSAID era: what to use now for the pharmacologic treatment of pain and inflammation in osteoarthritis. *Curr Rheumatol Rep,* 10**,** 49-56.

SCHMIDT, M. B., MOW, V. C., CHUN, L. E. & EYRE, D. R. (1990) Effects of proteoglycan extraction on the tensile behavior of articular cartilage. *J Orthop Res,* 8**,** 353-63.

SCHMIDT, T. A., GASTELUM, N. S., NGUYEN, Q. T., SCHUMACHER, B. L. & SAH, R. L. (2007) Boundary lubrication of articular cartilage: role of synovial fluid constituents. *Arthritis Rheum,* 56**,** 882-91.

SCHURMAN, D. J. & SMITH, R. L. (2004) Osteoarthritis: current treatment and future prospects for surgical, medical, and biologic intervention. *Clin Orthop Relat Res,* 427 Suppl**,** S183-9.

SETTON, L. A., MOW, V. C., MULLER, F. J., PITA, J. C. & HOWELL, D. S. (1994) Mechanical properties of canine articular cartilage are significantly altered following transection of the anterior cruciate ligament. *J Orthop Res,* 12**,** 451-63.

SHANBHAG, A. S., SETHI, M. K. & RUBASH, H. E. (2007) Biological Response to Wear Debris: Cellular Interactions Causing Osteolysis. IN CALLAGHAN, J. J., ROSENBERG, A. G. & RUBASH, H. E. (Eds.) *The Adult Hip.* 2nd ed. Philadelphia, PA, USA, Lippincott Williams & Wilkins.

SHARIF, K. M. & PARKER, M. J. (2002) Austin Moore hemiarthroplasty: technical aspects and their effects on outcome, in patients with fractures of the neck of femur. *Injury,* 33**,** 419-22.

SHEPHERD, D. E. & SEEDHOM, B. B. (1999) Thickness of human articular cartilage in joints of the lower limb. *Ann Rheum Dis,* 58**,** 27-34.

SHLOPOV, B. V., GUMANOVSKAYA, M. L. & HASTY, K. A. (2000) Autocrine regulation of collagenase 3 (matrix metalloproteinase 13) during osteoarthritis. *Arthritis Rheum,* 43**,** 195-205.

SIMON, W. H. (1971) Scale effects in animal joints. II. Thickness and elasticity in the deformability of articular cartilage. *Arthritis Rheum,* 14**,** 493-502.

SMITH, G. D., TAYLOR, J., ALMQVIST, K. F., ERGGELET, C., KNUTSEN, G., GARCIA PORTABELLA, M., SMITH, T. & RICHARDSON, J. B. (2005) Arthroscopic assessment of cartilage repair: a validation study of 2 scoring systems. *Arthroscopy,* 21**,** 1462-7.

SOUZA, J. C. M., HENRIQUES, M., OLIVEIRA, R., TEUGHELS, W., CELIS, J. P. & ROCHA, L. A. (2010) Biofilms Inducing Ultra-low Friction on Titanium. *Journal of Dental Research,* 89**,** 1470-1475.

STOCKLEY, C. (1986) *The Usborne illustrated dictionary of biology.*, London, Usborne.

STREHL, R., TALLHEDEN, T., SJOGREN-JANSSON, E., MINUTH, W. W. & LINDAHL, A. (2005) Long-term maintenance of human articular cartilage in culture for biomaterial testing. *Biomaterials,* 26**,** 4540-9.

SUTHERLAND, I. W. (2001) The biofilm matrix - an immobilized but dynamic microbial environment. *Trends in Microbiology,* 9**,** 222-227.

SWANN, D. A., HENDREN, R. B., RADIN, E. L., SOTMAN, S. L. & DUDA, E. A. (1981a) The Lubricating Activity of Synovial-Fluid Glycoproteins. *Arthritis and Rheumatism,* 24**,** 22-30.

SWANN, D. A., RADIN, E. L., NAZIMIEC, M., WEISSER, P. A., CURRAN, N. & LEWINNEK, G. (1974) Role of Hyaluronic-Acid in Joint Lubrication. *Ann Rheum Dis,* 33**,** 318-326.

SWANN, D. A., SLAYTER, H. S. & SILVER, F. H. (1981b) The Molecular-Structure of Lubricating Glycoprotein-I, the Boundary Lubricant for Articular-Cartilage. *J Bio Chem,* 256**,** 5921-5925.

TETLOW, L. C., ADLAM, D. J. & WOOLLEY, D. E. (2001) Matrix metalloproteinase and proinflammatory cytokine production by chondrocytes of human osteoarthritic cartilage: associations with degenerative changes. *Arthritis Rheum,* 44**,** 585-94.

TOWNEND, J. (2002) *Practical statistics for environmental and biological scientists,* Chichester, Wiley.

TROUSDALE, R. T. & WENGER, D. (2007) Osteotomy: Overview. IN CALLAGHAN, J. J., ROSENBERG, A. G. & RUBASH, H. E. (Eds.) *The Adult Hip.* 2 ed. Philadelphia, Lippincott Williams & Wilkins.

UNSWORTH, A. (1991) Tribology of human and artificial joints. *Proc Inst Mech Eng [H],* 205**,** 163-72.

VAN DEN BEKEROM, M. P., HILVERDINK, E. F. & SIEREVELT, I. N. (2011) A comparison of hemiarthroplasty with total hip replacement for displaced intracapsular fracture of the femoral neck: a randomised controlled multicentre trial in patients aged 70 years and over (vol 92, pg 1422, 2010). *J Bone Joint Surg Br,* 93B**,** 140-140.

VAN DER MEULEN, M. C. H., BEAUPRE, G. S., SMITH, R. L., GIDDINGS, V. L., ALLEN, W. A., ATHANASIOU, K. A., ZHU, C. F., MANDELL, J. A., SONG, Y., POSER, R. D. & GOODMAN, S. B. (2002) Factors influencing changes in articular cartilage following hemiarthroplasty in sheep. *J Orthop Res,* 20**,** 669-675.

VAN DER SLUIJS, J. A., GEESINK, R. G., VAN DER LINDEN, A. J., BULSTRA, S. K., KUYER, R. & DRUKKER, J. (1992) The reliability of the Mankin score for osteoarthritis. *J Orthop Res,* 10**,** 58-61.

VERZIJL, N., DEGROOT, J., BEN ZAKEN, C., BRAUN-BENJAMIN, O., MAROUDAS, A., BANK, R. A., MIZRAHI, J., SCHALKWIJK, C. G., THORPE, S. R., BAYNES, J. W., BIJLSMA, J. W. J., LAFEBER, F. P. J. G. & TEKOPPELE, J. M. (2002) Crosslinking by advanced glycation end products increases the stiffness of the collagen network in human articular cartilage - A possible mechanism through which age is a risk factor for osteoarthritis. *Arthritis and Rheumatism,* 46**,** 114-123.

VERZIJL, N., DEGROOT, J., OLDEHINKEL, E., BANK, R. A., THORPE, S. R., BAYNES, J. W., BAYLISS, M. T., BIJLSMA, J. W. J., LAFEBER, F. P. J. G. & TEKOPPELE, J. M. (2000) Age-related accumulation of Maillard reaction products in human articular cartilage collagen. *Biochem J,* 350**,** 381-387.

VINCENT, W. J. (2005) *Statistics in kinesiology,* Champaign, Ill. ; Leeds, Human Kinetics.

VON EISENHART-ROTHE, R., ECKSTEIN, F., MULLER-GERBL, M., LANDGRAF, J., ROCK, C. & PUTZ, R. (1997) Direct comparison of contact areas, contact stress and subchondral mineralization in human hip joint specimens. *Anat Embryol (Berl),* 195**,** 279-88.

WALDSCHMIDT, J. G., RILLING, R. J., KAJDACSY-BALLA, A. A., BOYNTON, M. D. & ERICKSON, S. J. (1997) In vitro and in vivo MR imaging of hyaline cartilage: zonal anatomy, imaging pitfalls, and pathologic conditions. *Radiographics,* 17**,** 1387-402.

WALKER, P. S., DOWSON, D., LONGFIEL.MD & WRIGHT, V. (1968a) Boosted Lubrication in Synovial Joints by Fluid Entrapment and Enrichment. *Ann Rheum Dis,* 27**,** 512-20.

WALKER, P. S., DOWSON, D., LONGFIELD, M. D. & WRIGHT, V. (1968b) "Boosted lubrication" in synovial joints by fluid entrapment and enrichment. *Ann Rheum Dis,* 27**,** 512-20.

WALKER, P. S., UNSWORTH, A., DOWSON, D., SIKORSKI, J. & WRIGHT, V. (1970) Mode of aggregation of hyaluronic acid protein complex on the surface of articular cartilage. *Ann Rheum Dis,* 29**,** 591-602.

WANG, A., ESSNER, A., POLINENI, V. K., STARK, C. & DUMBLETON, J. H. (1998) Lubrication and wear of ultra-high molecular weight polyethylene in total joint replacements. *Tribology International,* 31**,** 17-33.

WANG, H. & ATESHIAN, G. A. (1997) The normal stress effect and equilibrium friction coefficient of articular cartilage under steady frictional shear. *J Biomech,* 30**,** 771-6.

WANG, M., MCCANN, L., RADJENOVIC, S., TANNER, S., RIES, M., FISHER, J. & JIN, Z. (2008) MRI Quantitative Study of Cartilage Tribology. *2nd Annual Workshop on Imaging Based Measures of Osteoarthritis.* Boston, MA USA.

WARRINGTON, P.D., (2001) Animal Weights and Their Food and Water Requirements, Environment and Resource Division, Ministry of Environment April 2012 Cited in: [http://www.env.gov.bc.ca]

WELLS, T., DAVIDSON, C., MORGELIN, M., BIRD, J. L., BAYLISS, M. T. & DUDHIA, J. (2003) Age-related changes in the composition, the molecular stoichiometry and the stability of proteoglycan aggregates extracted from human articular cartilage. *Biochem J,* 370**,** 69-79.

WHEATER, C. P. & COOK, P. A. (2000) *Using statistics to understand the environment,* London, Routledge.

WIMMER, M., PACIONE, C. A., SHEKHAWAT, V. K., BERGGREEN, P., J.J., J. & CHUBINSKAYA, S. (2008) In Vitro Testing of Living Cartilage Tissue. *54th Annual Meeting of the Orthopaedic Research Society.* San Francisco, CA, Orthopaedic Research Society.

WRIGHT, V. & DOWSON, D. (1976) Lubrication and cartilage. *J Anat,* 121**,** 107-18.

YAMAGATA, M., CHAO, E. Y., ILSTRUP, D. M., MELTON, L. J., 3RD, COVENTRY, M. B. & STAUFFER, R. N. (1987) Fixed-head and bipolar hip endoprostheses. A retrospective clinical and roentgenographic study. *J Arthroplasty,* 2**,** 327-41.

YOCHUM, T. R., ROWE, L. J. & MAOLA, C. J. (2005) Trauma. IN YOCHUM, T. R. & ROWE, L. J. (Eds.) *Essentials of skeletal radiology.* 3rd ed. ed., Philadelphia, Pa. ; Lippincott Williams & Wilkins.

ZHU, W. B., MOW, V. C., KOOB, T. J. & EYRE, D. R. (1993) Viscoelastic Shear Properties of Articular-Cartilage and the Effects of Glycosidase Treatments. *J Orthop Res,* 11**,** 771-781.